Understanding the Role of the Complement System in Ebola Virus and SARS-CoV-2 Pathogenesis

University of Liverpool

Institute of Infection, Veterinary and Ecological Sciences,
Department of Infection and Microbiomes

Thesis submitted in accordance with the requirements of the University of Liverpool for the degree of Doctor in Philosophy

Jack Mellors

May 2022

TABLE OF CONTENTS

Understanding the Role of the Complement System in Ebola Virus and SARS-CoV-2 Pathogenesis

Jack Mellors

Abstract

The role of the complement system in viral infections is often complex, with significant implications for pathogenesis and disease. The complement system can form part of the early innate immune response through the binding of glycosylated viral proteins, or through spontaneous activation on viral surfaces. The complement system can also be activated by antibodies in complex with viral antigens. These mechanisms have the potential to inhibit virus interactions with host proteins, mediate opsonisation, promote inflammation and chemotaxis, cause the agglutination of virions, lyse virions, and lyse virus-infected cells. Despite the diverse and significant roles of the complement system in viral infection, it is a relatively under-researched aspect of antiviral immunity. The complement system has been associated with more severe symptoms and fatal outcomes of Ebola virus (EBOV) disease (EVD) and Coronavirus disease (COVID)-19. However, the underlying mechanisms of the complement system in response to EBOV and SARS-CoV-2 (the causative agent of COVID-19), and the wider implications for immunity, are poorly understood. We first investigated the antibody-independent mechanisms of the complement system in response to *Ebolavirus* and *Coronavirus* glycoproteins (GPs), to better understand the underlying mechanisms of complement activation in the early stages of infection. Using novel ELISAs and western blot assays, we identified MBL binding to a range of *Ebolavirus* and *Coronavirus* GPs, and demonstrated their potential to activate the complement system, eventuating in formation of the membrane attack complex (MAC). We also utilised PCR assays, next-generation sequencing, and LC-MS/MS, to identify potential differences in the structure and expression of complement proteins in EVD survivors. We found broad diversity in the SNPs of several complement proteins but were restricted by the sample size to determine significance. These findings showed potential mechanisms for antibody-

independent complement activation that could influence the pathogenesis of EBOV and SARS-CoV-2 in the early stages of infection. Next, we evaluated the antibody-dependent mechanisms of the complement system. We developed novel flow cytometry assays to assess the ability of EVD convalescent, COVID-19 convalescent, and SARS-CoV-2 vaccinated plasma to mediate antibody-dependent complement deposition (ADCD) in response to the respective *Ebolavirus* and *Coronavirus* GPs. We found a differential response in ADCD between EVD plasma that was influenced by neutralisation titre, IgG titre, and/or the *Ebolavirus* GP present. For SARS-CoV-2, we found that ChAdOx1 nCoV-19 vaccine-induced antibodies could mediate ADCD, and that levels of ADCD correlated with disease severity in COVID-19 convalescent individuals. These findings are important for understanding the variability of responses in mediating the complement system, with particular relevance to recrudescence, re-infection, infection post-vaccination, and cross-reactivity. Lastly, we evaluated the significance of these antibody-independent and antibody-dependent complement mechanisms on wild-type EBOV and SARS-CoV-2 neutralisation. Independent of antibodies, the complement system did not influence virus neutralisation. However, in the presence of low-neutralising, virus-specific antibodies, we observed an enhancement in neutralisation of both EBOV and SARS-CoV-2 when the complement system was present. Neutralisation assays are a fundamental aspect of identifying therapeutic antibodies and determining correlates of protection, with further implications for vaccine licensure. Our observed effect of the complement system on neutralisation has implications for the initial assessments of therapeutic candidates, evaluating vaccine-induced immune responses, defining correlates of protection, and could be a consideration for the therapeutic use of complement inhibitors.

Publications

Chapter 1 of this thesis was partly based on my following lead-author and co-author publications:

Mellors, J., Tipton, T., Longet, S. and Carroll, M., 2020. Viral Evasion of the Complement System and Its Importance for Vaccines and Therapeutics. *Frontiers in Immunology* [Online], 11.

For this publication, I conducted the literature review, wrote the manuscript, and created the tables and figures.

Longet, S., **Mellors, J**., Carroll, M.W. and Tipton, T., 2021. Ebolavirus: Comparison of Survivor Immunology and Animal Models in the Search for a Correlate of Protection. *Frontiers in Immunology* [Online], 11, p.3871.

For this publication, I assisted with the overall writing of the manuscript and created a table for the comparison of animal models of EBOV infection.

Thom, R., Tipton, T., Strecker, T., Hall, Y., Akoi Bore, J., Maes, P., Raymond Koundouno, F., Fehling, S.K., Krähling, V., Steeds, K., Varghese, A., Bailey, G., Matheson, M., Kouyate, Saidou, Coné, M., Moussa Keita, B., Kouyate, Sekou, Richard Ablam, A., Laenen, L., Vergote, V., Guiver, M., Timothy, J., Atkinson, B., Ottowell, L., Richards, K.S., Bosworth, A., Longet, S., **Mellors, J**., Pannetier, D., Duraffour, S., Muñoz-Fontela, C., Sow, O., Koivogui, L., Newman, E., Becker, S., Sprecher, A., Raoul, H., Hiscox, J., Henao-Restrepo, A.M., Sakoba, K., Magassouba, N., Günther, S., Kader Konde, M. and Carroll, M.W., 2021. Longitudinal antibody and T cell responses in Ebola virus disease survivors and contacts: an observational cohort study. *The Lancet Infectious Diseases* [Online], 21(4), pp.507–516.

For this publication, I participated in the collection of West African plasma samples and assisted with the IFNγ T cell ELISpots in the year 2018, and used this knowledge to assist with the primary writing of the manuscript.

Tipton, T.R.W., Hall, Y., Bore, J.A., White, A., Sibley, L.S., Sarfas, C., Yuki, Y., Martin, M., Longet, S., **Mellors, J**., Ewer, K., Günther, S., Carrington, M., Kondé, M.K. and Carroll, M.W., 2021. Characterisation of the T-cell response to Ebola virus glycoprotein amongst survivors of the 2013–16 West Africa epidemic. *Nature Communications* [Online], 12(1), p.1153.

For this publication, I participated in the collection of West African plasma samples and assisted with the IFNγ T cell ELISpots in the year 2018, and used this knowledge to assist with the primary writing of the manuscript.

Hargreaves, A., Brady, C., **Mellors, J**., Tipton, T., Carroll, M.W. and Longet, S., 2021. Filovirus Neutralising Antibodies: Mechanisms of Action and Therapeutic Application. *Pathogens* [Online], 10(9), p.1201.

For this publication, I revised the manuscript for scientific accuracy and clarity, and suggested various language edits.

Chapter 3 of this thesis was partly based on my following lead-author and co-author publications and manuscript submissions:

Mellors, J., Tipton, T., Fehling, S.K., Akoi Bore, J., Koundouno, F.R., Hall, Y., Hudson, J., Alexander, F., Longet, S., Taylor, S., Gorringe, A., Magassouba, N., Konde, M.K., Hiscox, J., Strecker, T. and Carroll, M., 2022. Complement-Mediated Neutralisation Identified in Ebola Virus Disease Survivor Plasma: Implications for Protection and Pathogenesis. *Frontiers in Immunology* [Online], 13.

For this publication, I developed the antibody-dependent complement deposition assays, conducted all of the flow cytometry experiments, analysed the data, and wrote the manuscript with input from the other authors.

Barrett, J.R., Belij-Rammerstorfer, S., Dold, C., Ewer, K.J., Folegatti, P.M., Gilbride, C., Halkerston, R., Hill, J., Jenkin, D., Stockdale, L., Verheul, M.K., Aley, P.K., Angus, B., Bellamy, D., Berrie, E., Bibi, S., Bittaye, M., Carroll, M.W., Cavell, B., Clutterbuck, E.A., Edwards, N., Flaxman, A., Fuskova, M., Gorringe, A., Hallis, B., Kerridge, S., Lawrie, A.M., Linder, A., Liu, X., Madhavan, M., Makinson, R., **Mellors, J**., Minassian, A., Moore, M., Mujadidi, Y., Plested, E., Poulton, I., Ramasamy, M.N., Robinson, H., Rollier, C.S., Song, R., Snape, M.D., Tarrant, R., Taylor, S., Thomas, K.M., Voysey, M., Watson, M.E.E., Wright, D., Douglas, A.D., Green, C.M., Hill, A.V.S., Lambe, T., Gilbert, S. and Pollard, A.J., 2020. Phase 1/2 trial of SARS-CoV-2 vaccine ChAdOx1 nCoV-19 with a booster dose induces multifunctional antibody responses. *Nature Medicine* [Online], pp.1–10.

For this publication, I worked in collaboration with the Pathogen Immunology Group at UKHSA to adapt the antibody-dependent complement deposition assays I developed during my PhD project, to assess Fc-mediated IgG functions of plasma from recipients of the ChAdOx1 nCoV-19 vaccine.

Tomic, A., Skelly, D.T., Ogbe, A., O'Connor, D., Pace, M., Adland, E., Alexander, F., Ali, M., Allott, K., Azim Ansari, M., Belij-Rammerstorfer, S., Bibi, S., Blackwell, L., Brown, A., Brown, H., Cavell, B., Clutterbuck, E.A., de Silva, T., Eyre, D., Lumley, S., Flaxman, A., Grist, J., Hackstein, C.-P., Halkerston, R., Harding, A.C., Hill, J., James, T., Jay, C., Johnson, S.A., Kronsteiner, B., Lie, Y., Linder, A., Longet, S., Marinou, S., Matthews, P.C., **Mellors, J**., Petropoulos, C., Rongkard, P., Sedik, C., Silva-Reyes, L., Smith, H., Stockdale, L., Taylor, S., Thomas, S., Tipoe, T., Turtle, L., Vieira, V.A., Wrin, T., Pollard, A.J., Lambe, T., Conlon, C.P., Jeffery, K.,

Travis, S., Goulder, P., Frater, J., Mentzer, A.J., Stafford, L., Carroll, M.W., James, W.S., Klenerman, P., Barnes, E., Dold, C. and Dunachie, S.J., 2022. Divergent trajectories of antiviral memory after SARS-CoV-2 infection. *Nature Communications* [Online], 13(1), p.1251.

For this publication, I worked in collaboration with the Pathogen Immunology Group at UKHSA to adapt the antibody-dependent complement deposition assay I developed during my PhD project, to assess disease trajectories following natural SARS-CoV-2 infection.

Marchevsky, N.G., Li, G., Aley, P., Clemens, S.A.C., Belij-Rammerstorfer, S., Bibi, S., Dold, C., Flaxman, A., Folegatti, P., Jenkin, D., Gilbert, S., Hill, J., Kelly, S., Lambe, T., Plested, E., Ramasamy, M., Singh, N., Taylor, S., Weckx, L., Pollard, A.J., Voysey, M., **Oxford COVID Vaccine Trial Group**. Sex-differences in response to ChAdOx1 nCoV-19 (ACD1222) vaccine. A pre-specified subgroup analysis of randomised controlled trials. *Manuscript submitted*.

For this publication, I worked in collaboration with the Pathogen Immunology Group at UKHSA to adapt the antibody-dependent complement deposition assay I developed during my PhD project, to investigate sex-differences in response to the ChAdOx1 nCoV-19 vaccine.

Chapter 4 of this thesis was associated with the following (and aforementioned) lead-author publication:

Mellors, J., Tipton, T., Fehling, S.K., Akoi Bore, J., Koundouno, F.R., Hall, Y., Hudson, J., Alexander, F., Longet, S., Taylor, S., Gorringe, A., Magassouba, N., Konde, M.K., Hiscox, J., Strecker, T. and Carroll, M., 2022. Complement-Mediated Neutralisation Identified in Ebola Virus Disease Survivor Plasma: Implications for Protection and Pathogenesis. *Frontiers in Immunology* [Online], 13.

For this publication, I developed the antibody-dependent complement deposition assays, conducted all of the flow cytometry experiments, analysed the data, and wrote the manuscript with input from the other authors.

Acknowledgements

I would like to thank my supervisor, **Professor Miles Carroll**, for his ongoing support and guidance throughout this PhD. He established the foundations for this project, facilitated my development as a scientist throughout, and granted me the opportunity to bring this project to fruition. I would like to thank **Dr. Tom Tipton** for his support, encouragement, and technical advice throughout this project. I would like to thank **Dr. Yper Hall** for her constant professional, academic, and personal support. I would like to thank all members of the **Carroll Group: High Consequence Emerging Viruses Group** for providing an excellent learning environment with constant support and encouragement. I would like to extend this gratitude with a special mention to **Cillian Gartlan**, **Hannah Klim**, **Dr. Stephen Laidlaw**, **Dr. Stephanie Longet**, and **Dr. Dung Nguyen** for their advice and expertise at various stages of this project.

I would like to thank **Professor Julian Hiscox** for his collaboration and support with this project. I would like to extend this thanks to all members of the Hiscox Group, with special mentions to **Dr. Stuart Armstrong**, **Dr. Xiaofeng Dong**, **Dr. Abbie Harrison**, **Ben Jones**, **Dr. Rebekah Penrice-Randal**, and **Yan Ryan** for their help and for always making me feel welcome on my visits to Liverpool. I would like to thank all members of the **Pathogen Immunology Group**, with a special acknowledgment of the contributions made by **Steve Taylor** to the foundations and development of this PhD project, and to **Frances Alexander**, **Breeze Cavell**, **Rachel Halkerston**, and **Steve Thomas** for their technical support and collaboration. This project was funded by the **UKHSA** (formerly **Public Health England**) and was completed in collaboration with **Porton Down** and the **University of Oxford** - **Wellcome Centre for Human Genetics**.

I would like to thank **Jean Balchin**, **Rowan Curtis**, **Dr. Julia de Romémont**, and **Dr. Bethany White** for their help and support in academia and beyond. And to thank **Sonnya**, **Colin**, **Maddie**, and **Leighton** for their kindness and encouragement. Lastly, I would like to thank **Mum**, **Dad**, **Sarah**, and **Will** for their endless love, support, and belief in me; I could not have accomplished this without them.

List of Figures

List of Tables

List of Abbreviations

Ab	Antibody
ACE	Angiotensin converting enzyme
ADCD	Antibody-dependent complement deposition
ADE	Antibody-dependent enhancement
ALT	Alanine aminotransferase
AP	Alkaline phosphatase
ARDS	Acute respiratory distress syndrome
AST	Aspartate aminotransferase
BDBV	Bundibugyo virus
BOMV	Bombali
BSL	Biosafety level
C1-INH	C1-inhibitor
C4bp	C4 binding protein
C8bp	C8 binding protein
CCHFV	Crimean-Congo haemorrhagic fever virus
CDC	Centers for Disease Control and Prevention
CFR	Case fatality rate
CHIKV	Chikungunya virus
CoV	Coronavirus
COVID-19	Coronavirus disease-19
CPE	Cytopathic effect
CPN	Carboxypeptidase-N
CR	Complement receptor
CRP	C-reactive protein
Ct	Cycle threshold
DAF	Decay accelerating factor
DC	Dendritic cell
DENV	Dengue virus
DIC	Disseminated intravascular coagulation
DNA	Deoxyribonucleic acid
DRC	Democratic Republic of the Congo
DTT	Dithiothreitol
E	Envelope protein
EBOV	Ebola virus
ECL	Enhanced chemiluminescence
EDTA	Ethylenediaminetetraacetic acid
ELISA	Enzyme-linked immunosorbent assay
ELISpot	Enzyme-linked immunosorbent spot
ER	Endoplasmic reticulum
ERGIC	Endoplasmic reticulum - Golgi intermediate compartment
EVD	Ebola virus disease
Fc	Fragment crystallisable
FCN	Ficolin

FCS	Fetal calf serum
FDC	Follicular dendritic cell
GALT	Gut-associated lymphoid tissue
GI	Gastrointestinal tract
GP	Glycoprotein
HBSS	Hanks balanced salt solution
HCMV	Human cytomegalovirus
hCoV	Human coronavirus
HCV	Hepatitis C virus
HEK	Human embryonic kidney
HIV	Human immunodeficiency virus
HRP	Horseradish peroxidase
HSV	Herpes simplex virus
HUJV	Huángjiāo
IC50	Half maximal inhibitory concentration
IFN	Interferon
Ig	Immunoglobulin
IL	Interleukin
LC	Liquid chromatography
LLOV	Lloviu
M	Membrane protein
MAC	Membrane attack complex
MA-EBOV	Mouse-adapted Ebola virus
MAF	Minor allele frequency
MALV	Měnglà virus
MARV	Marburg Virus
MASP	Mannose-binding lectin-associated serine proteases
MBL	Mannose binding lectin
MCP	Membrane cofactor protein
MERS	Middle eastern respiratory syndrome
MS	Mass spectrometry
MSD	Meso Scale Discovery
MuV	Mumps virus
MVA	Modified Vaccinia Ankara
N	Nucleocapsid
NGS	Next generation sequencing
NHP	Non-human primate
NiV	Nipah virus
NK	Natural killer
NP	Nucleoprotein
NPC	Niemann Pick
PAMP	Pathogen associated molecular pattern
PBMC	Peripheral blood mononuclear cell
PBS	Phosphate buffered saline
PCA	Principle component analysis

PCR	Polymerase chain reaction
PHP	Pooled human plasma
PRM	Patter recognition molecule
PRR	Pattern recognition receptor
RAVV	Ravn virus
RBD	Receptor binding domain
RNA	Ribonucleic acid
RT	Room temperature
S	Spike protein
SARS	Severe acute respiratory syndrome
SDS	Sodium dodecyl sulfate
SDS-PAGE	Sodium dodecyl sulfate - polyacrylamide gel electrophoresis
SNP	Single nucleotide polymorphism
SUDV	Sudan virus
SV5	Simian virus 5
TAFV	Taï Forest virus
TED	Thioester domain
Th	T helper
TLR	Toll-like receptor
TMPRSS2	Transmembrane serine protease
VP	Viral protein
WHO	World Health Organization
WNV	West Nile virus
XILV	Xīlǎng virus
YFV	Yellow fever virus
YMH	Yambuku Mission Hospital
ZIKV	Zika virus

Chapter 1: Introduction

The complement system can have both complex and significant implications for viral pathogenesis, yet its antiviral role in innate immunity is relatively under-researched. From the opsonisation and lysis of viruses, to the enhancement of antibody-mediated neutralisation, to the development of a robust adaptive immune response, the complement system orchestrates a broad area of immunity against viral pathogens (1). Whilst the Ebola virus (EBOV) and severe acute respiratory syndrome coronavirus (SARS-CoV)-2 are distinct in many of their characteristics such as transmission, morphology, and virulence, both of these viruses activate the complement system with profound implications for pathogenesis and disease. This thesis explores the underlying molecular mechanisms of complement activation with EBOV and SARS-CoV-2 proteins; the variability of complement-mediated immune responses in convalescent and vaccinee plasma; and the implications of these mechanisms on viral pathogenesis in the context of virus neutralisation.

The primary focus of this project was on EBOV, but I was able to repurpose many of my research assays in response to the COVID-19 pandemic to support the global research efforts towards understanding SARS-CoV-2 pathogenesis. For this reason, the emphasis of this thesis will be on the complement system and EBOV, with the appropriate references to my SARS-CoV-2 research where relevant.

1.1 Complement System Overview

This section will provide a general overview of the complement system, followed by its impact on pathogenesis and disease for a range of viruses.

The complement system is a heat-labile component of plasma involving both extracellular and cell surface membrane-associated proteins to form a major constituent of the innate immune response. The system comprises over 30 proteins which have the potential to react *via* an enzymatic cascade in response to various stimuli, such as pathogen-associated molecular patterns (PAMPs) and abnormal or damaged host cells. Activation of the complement system occurs *via* three distinct

target recognition pathways (the classical, lectin, and alternative pathways) which converge at a single point: the cleavage of complement component C3. Each pathway has its own unique protease zymogens which recognise and respond to different antigens, but all pathways primarily work to: lyse pathogens through formation of the membrane attack complex (MAC); promote inflammation and chemotaxis through the production of anaphylatoxins (C3a and C5a); opsonise pathogens for phagocytosis; clear soluble immune complexes from the circulation; and enhance the development of adaptive immunity (1–5).

The importance of each pathway during infection can vary depending on the types of PAMPs presented by the pathogen (6–8), the complement evasion mechanisms exhibited by the pathogen (9–11), and the presence or absence of IgM/IgG-specific antibodies to activate the classical pathway (12,13).

1.1.1 Classical Complement Pathway

The classical complement pathway is typically activated when hexameric C1q proteins bind to the fragment crystallisable (FC) CH2-domains of antigen-bound IgM and/or IgG immune complexes (5,12,14). The binding affinity of C1q to IgG is dependent on the IgG isotype. C1q has the greatest affinity for IgG-3, followed by IgG-1, with only a weak association with IgG-2, and no interaction with IgG-4 (15). C1q is a versatile pattern recognition receptor (PRR) and in rare instances can activate the complement system in the absence of antibodies by directly binding apoptotic cells (16,17), viral proteins (18–20), or host plasma proteins such as C-reactive protein (21,22), fibronectin (23,24), decorin (25), lactoferrin (26), pentraxin-3 (13), and serum amyloid P component (27).

The C1q molecule is an assembly of six heterotrimers, each containing three chains (C1qA, C1qB, and C1qC) with a central collagenous stem and a globular head at the C-terminus. The C1q molecule forms a calcium-dependent complex with two C1r and two C1s serine proteases to form the C1q complex (28). Ligand recognition and binding *via* the C1q molecule in the C1 complex induces a conformational change and

autoactivation of the $C1r_2s_2$ tetramer to activate the classical complement pathway (5,14). The activated C1s cleaves complement proteins C4 and C2 into active fragments C4b and C2a, along with two small inactive fragments (C4a and C2b). Non-covalent binding of C4b and C2a forms the classical pathway C3 convertase, C4bC2a, responsible for the cleavage of C3 into C3a (anaphylatoxin) and C3b (active component of the convertase). The newly formed complex, C4bC2aC3b, is a C5 convertase which can be formed from either the classical or lectin complement pathway and cleaves the C5 molecule into C5a (anaphylatoxin) and C5b (active component of the convertase). C5 proteolysis and the successive steps are then the same for each of the three complement pathways, resulting in the deposition of C5b onto the activating surface and subsequent irreversible binding of C6, C7, C8, and multiple copies of C9 to form the MAC capable of penetrating lipid membranes (**Figure 1**) (1,5,14,29).

1.1.2 Lectin Complement Pathway

The lectin complement pathway follows the same enzymatic cascade as the classical pathway but is distinct in the antigens and proteases required for its activation. The lectin pathway is typically activated *via* the direct binding of PAMPs by lectins complexed with mannose-binding lectin-associated serine proteases (MASPs)-1/2/3. These activators include mannose-binding lectin (MBL), ficolin-1 (FCN-1, M-ficolin), ficolin-2 (FCN-2, L-ficolin), ficolin-3 (FCN-3, H-ficolin), and collectin-11 (CL-11) (30–33). In humans, MBL is typically present as a trimer, tetramer, pentamer, or hexamer and these oligomeric structures influence its carbohydrate binding properties (34,35). Each monomeric subunit in the complex is a homotrimer with each polypeptide containing a cysteine-rich region at the N-terminus, followed by a collagen-like domain, a neck region, and a carbohydrate recognition domain capable of binding specific sugars present on pathogenic surfaces, i.e. *N*-acetyl-D-glucosamine and D-mannose (36,37).

Similar to MBL, multimeric ficolin complexes are assembled through homotrimer subunits with cysteine-rich N-terminal segments which form interchain disulphide

bonds followed by collagen-like regions, but they are unique in their ability to bind distinct carbohydrates *via* their C-terminal fibrinogen-like domains (38,39). The functional activity of the three ficolins can vary, but they all complex with MASP-2 to activate the lectin complement pathway (40). FCN-1 is predominantly synthesised in monocytes and granulocytes where it can be found present on their surface or extracellularly in native human plasma. FCN-2 is synthesised in the liver and secreted into the bloodstream where it can bind to various acetylated structures and sugars *via* three inner binding sites (41). FCN-3 is synthesised in the liver and lungs and is present in plasma at a higher concentration than FCN-1/2, although less is known about its functional capabilities (42). CL-11 can form heterotrimeric complexes with collectin liver 1 (CL-10) in serum and can associate with MASPs to activate the lectin complement pathway (43).

Once a lectin is in complex with MASP-2 and has bound its target, MASP-2 then cleaves C4 and C2 to form the C3 convertase (C4bC2a complex). Following the proteolytic cleavage of C3, the lectin complement pathway follows the same catalytic process as the classical complement pathway (**Figure 1**) (44). The roles of MASP-1 and MASP-3 in this pathway are relatively ambiguous (31,45). MASP-1 is capable of cleaving complement component C2 and, to a much lower extent, components C3 and C4 (31,46), whilst MASP-3 may have a negative regulatory role of the lectin pathway through the downregulation of MASP-2 cleaving activity (1,47,48).

1.1.3 Alternative Complement Pathway

The alternative pathway does not require the specific protein-protein or protein-carbohydrate interactions seen with the other two pathways. Under normal physiological conditions, ~1% of complement component C3 per hour undergoes spontaneous hydrolysis to produce C3(H_2O). Factor-B can then associate with C3(H_2O) to induce a conformational change which enables factor-D mediated cleavage of factor-B into two components: Ba (which dissociates from the complex) and Bb (which remains bound in the complex). The protein complex C3bBb is the alternative pathway C3 convertase, which is stabilised through the binding of

properdin to produce C3bBbP, and can cleave further C3 molecules through the serine protease activity of fragment Bb. The alternative pathway therefore has the potential to both activate and enhance complement activity through an amplification loop: cleaved C3 components produce C3 convertases which cleave further C3 molecules (49). Cleavage of C3 also yields C3a and C3b, where C3b remains bound in the complex to form the alternative pathway C5 convertase, C3bBbPC5b, and C3a acts as an anaphylatoxin; the rest of the complement cascade is then identical for all pathways (**Figure 1**) (1,50,51).

The activity of the alternative pathway is relatively non-specific and must be controlled through complement regulatory proteins expressed extracellularly or on cell surface membranes. Therefore, this mechanism can effectively target various pathogens which lack specific complement proteins (52), but the absence of such regulatory proteins on host cells may predispose individuals to certain autoimmune diseases (53,54). A less conventional means of alternative pathway activation *via* the direct binding of properdin to pathogens (55,56) and apoptotic and necrotic cells (57,58) has also been reported.

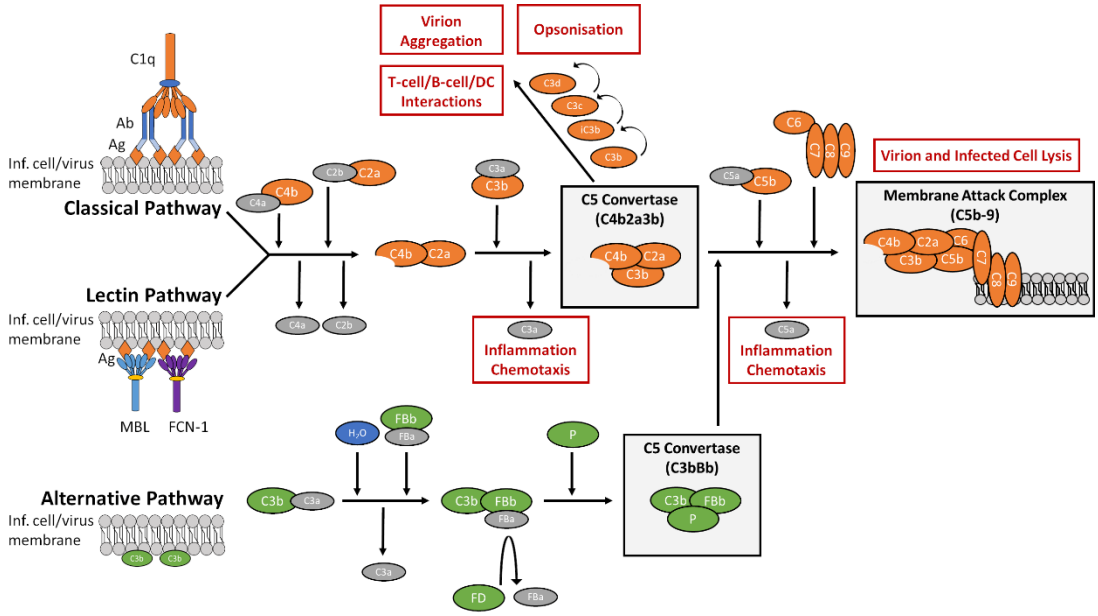

Figure 1: An overview of the complement system

The complement system is a collection of plasma and membrane-bound proteins that form part of the innate immune response against viruses. The system can be divided into three pathways: classical, lectin, and alternative. The classical pathway is typically antibody-mediated and requires the binding of the C1q protein. The lectin pathway is antibody-independent and is activated by the binding of lectins such as mannose-binding lectin (MBL) or ficolin-1 (FCN-1) to viral glycoproteins. The alternative pathway is spontaneously activated through hydrolysis of the C3 protein. Once activated, the complement system results in the formation of the membrane attack complex through a proteolytic cascade, and the formation of anaphylatoxins (C3a and C5a). This figure was previously published by Mellors et al., 2022. Abbreviations: Ag = antigen; Ab = antibody; DC = dendritic cells; FB = factor B; FD = Factor D; FCN-1 = ficolin-1; Inf = infected; MBL = mannose-binding lectin; P = properdin.

1.1.4 Complement Protein Expression and Regulation

Most complement proteins are primarily synthesised in the liver and secreted into the bloodstream. Complement proteins can also be produced by epithelial cells (59–61), endothelial cells (62,63), and circulating immune cells such as granulocytes, monocytes, macrophages, and dendritic cells (64,65). The plasma concentrations and functionality of these proteins may vary greatly between individuals; influenced by factors such as age, gender, and genetics (66–68). Such genetic variances often occur in the form of single nucleotide polymorphisms (SNPs) in the promoter and structural regions, which influence protein expression and functionality, respectively. The

frequency of such SNPs can vary significantly between ethnic groups and can influence an individual's susceptibility to infection and disease severity (66–70). Functional SNPs, such as those identified in the *MBL* gene, are reportedly common in certain populations (7,71,72) and can increase susceptibility to certain pathogens (69,70,72–76), although these associations are not always consistent in other studies (70) (77). Similarly, functional SNPs in the *FCN-1* gene have been shown to influence the functional activity and serum levels of FCN-1 (78), and have been associated with fatal outcomes for patients with systemic inflammation (79).

During infection, complement proteins are rapidly upregulated to try and control/eliminate the invading pathogen (80). Excessive activation of the complement system or lack of regulatory molecules can cause damage to the host through: excessive/chronic inflammation; recruitment of other pro-inflammatory immune cells; immune complex and cell debris accumulation; and autoimmunity (66,81–83). Alternatively, lack of stimulation of the complement system can increase susceptibility to certain pathogens (84–86). Multiple regulation points exist within the complement system in the form of extracellular proteins and cell-surface membrane receptors to either promote or impede the proteolytic cascade (**Table 1**). The complement system can influence multiple aspects of the immune response and must therefore be tightly regulated (**Figure 2**).

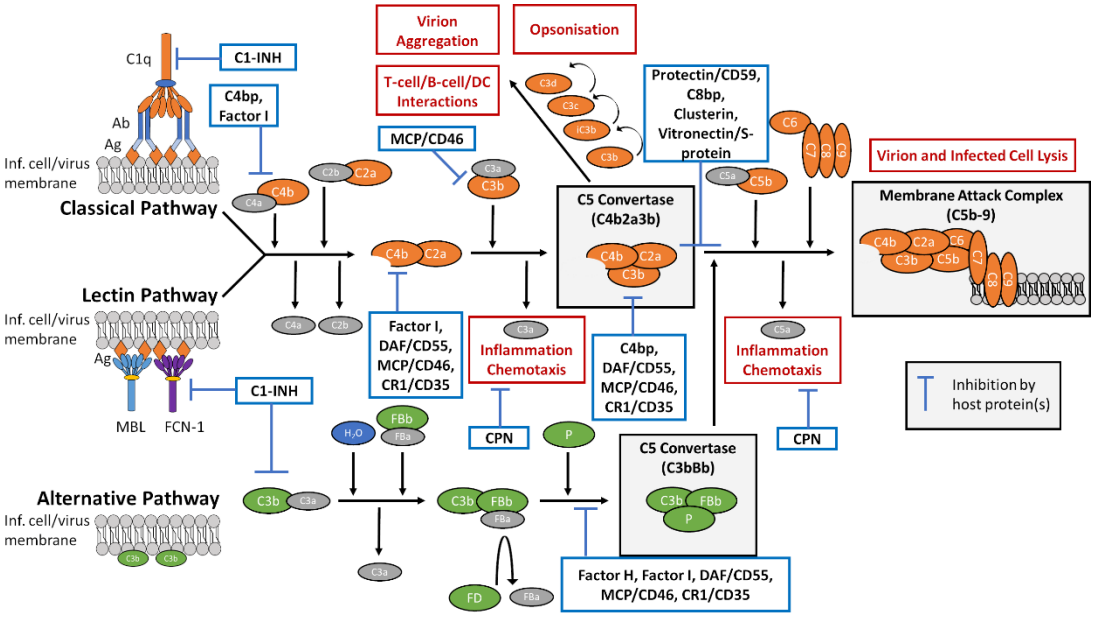

Figure 2: Complement system overview with regulatory proteins and receptors

Overview of the complement system and the regulatory points mediated by host membrane-bound and soluble proteins (blue boxes). Abbreviations: C1-inhibitor (C1-INH); C4-binding protein (C4bp); C8-binding protein (C8bp); carboxypeptidase-N (CPN); complement receptor 1 (CR1); decay-accelerating factor (DAF); membrane cofactor protein (MCP). This figure was adapted from previously published figures by Mellors et al., 2020 and Mellors et al., 2022.

Complement Receptors				
Complement Receptors	**Presentation on Circulating Cells**	**Host Target Complement Protein(s)**	**Role(s) in the Complement System**	**References**
$A_2\beta_1$ integrin	Mast cells	C1q	1) Mast cell activation and cytokine secretion	(87)
cC1qR/CR or calreticulin	Most cell types excluding erythrocytes	C1q collagen-like region, CD91	1) Complex with CD91 to enhance phagocytosis of C1q-coated particles	(88–91)
CD91 (LRP-1) or α2 macroglobulin receptor	Monocytes, astrocytes, fibroblasts, dendritic intestinal cells	C1q and cC1qR/CR (calreticulin)	1) Complex with cC1qR/CR (calreticulin) to enhance phagocytosis of C1q-coated particles	(89,92,93)
gC1qR	Mast cells, neutrophils, platelets, B cells, immature DCs	C1q globular heads	1) Mediate neutrophil and immature DC chemotaxis	(94–96)
C1q-Rp or C1qR1 or CD93	Monocytes, neutrophils, DCs	C1q	1) Potentially modulate C1q-dependent phagocytosis	(97–99)
CR1 or CD35	B cells, basophils, follicular dendritic cells, erythrocytes, monocytes, neutrophils, renal epithelium,	C1q, C3b, C4b	1) Bind opsonised C3b particles to enhance phagocytosis 2) Removal of immune complexes *via* erythrocytes	(100–108)

	CD4+ and CD8+ T cells		3) Enhance B-cell activation, production of antigen-specific antibodies proliferation, and 4) Protect host epithelial cells from complement activity	
CR2 or CD21	B cells, T cells, follicular dendritic cells	Polymerized iC3b, C3dg, C3d	1) Enhance B-cell maturation through recognition of C3d-coated antigens and co-ligation with B-cell receptors	(109–111)
CR3 or CD11b/18	Basophils, macrophages, monocytes, neutrophils, dendritic cells, NK cells	iC3b	1) Mediate phagocytosis of C3b-bound targets 2) Supress dendritic cell stimulation	(105,111–113)
CR4 or CD11c/18	Basophils, macrophages, neutrophils, monocytes, dendritic cells	iC3b	1) Mediate phagocytosis of C3b-bound targets	(105,111,113)
C3aR	Astrocytes, basophils, dendritic cells, eosinophils, mast cells, monocytes, neutrophils	C3a	1) Enable broad biological functions of C3a	(114–120)

C5aR or CD88	Basophils, dendritic cells, eosinophils, mast cells, monocytes, neutrophils	C5a	1) Enable broad biological functions of C5a	(105,115–117,121)
GPR77 or C5L2	Leukocytes, adipose tissue	C5a	1) Generally considered to be a non-signalling receptor	(122)
CRIg	Kupffer cells	C3b, iC3b	1) Phagocytosis of C3-opsonised particles in circulation	(123)
Complement regulators				
Complement regulators	**Location**	**Host target complement protein(s)**	**Role(s) in the complement system**	**References**
Membrane cofactor protein (MCP) or CD46	All major peripheral blood cells except erythrocytes	C3, C3b, and C4b	1) Cofactor for factor-I mediated C3b and C4b inactivation 2) Possible protection against unwanted C3 activation 3) Inhibit C3b deposition	(105,124–126)
Decay-accelerating factor or CD55	All major peripheral blood cells and endothelial and epithelial cells	C3b, C4b, CD97 (EMR1)	1) Destabilise C3 and C5 convertases 2) Negatively regulate T cell immunity	(127–131)
CD59 or protectin	Erythrocytes, leukocytes, and broad	C5b-8 and C9	1) Prevent MAC formation	(132–137)

	tissue expression		2) Signal transduction molecule to disrupt T cell activation and proliferation	
C8 binding protein	Peripheral blood cells and muscle cells of myocardial tissue	C8	1) Prevent MAC formation	(138)
C1-inhibitor	Plasma	C1r, C1s, MASP-1, MASP-2, C3b	1) Inhibit C1r and C1s of the classical pathway 2) Inactivate MASP-1 and MASP-2 of the lectin pathway 3) Bind C3b to inhibit factor B binding 4) Regulate coagulation factors and plasma kallikrein	(45,139)
Factor H	Plasma	C3b	1) Accelerates decay of alternative pathway C3 convertase (C3bBb) 2) Factor I cofactor for cleavage and inactivation of C3b 3) Prevents further C3b	(140–142)

			deposition on cell surface membranes	
Factor I	Plasma	C3b, iC3b, and C4b	1) Cleavage of C3b and C4b components	(143,144)
Properdin	Plasma	C3bBb, some microbial surfaces	1) Stabilise alternative pathway C3 convertase (C3bBb) 2) Pattern recognition molecule from complement activation	(55,145)
C4-binding protein	Plasma	C4b and C-reactive protein	1) Bind and sequester C4b 2) Accelerate the decay of the classical C3 convertase 3) Act as a cofactor for factor I inactivation of C4b	(140,146,147)
Clusterin	Plasma	C7, C8, C9	1) Prevent lytic activity of the MAC	(148)
Vitronectin or S protein	Plasma	C5b-7	1) Block membrane binding of C5b-7 2) Prevent C9 polymerization	(149)
α(2) macroglobulin	Plasma	MBL, MASP-1, MASP-2	1) Inhibit MASP-1/2	(150)
Carboxypeptidase-N/R	Plasma	C3a, C5a	1) Inhibit C3a and C5a through cleavage of	(151)

			carboxy-terminal arginine residues	

Table 1: Overview of the key complement regulatory proteins and receptors

A summary of the functions and locations of key complement regulatory proteins and receptors. Table previously published by Mellors et al., 2020.

1.1.5 Antiviral Activity of the Complement System

One primary function of the complement system is to assist in the killing and containment of invading pathogens, including bacteria (152), fungi (153), protozoa (154), and viruses (155). In turn, many viruses have developed mechanisms to manipulate or evade this system (**Figure 3**). Knowledge of this interplay enables a better understanding of the viral pathogenesis which can be exploited for the development of antivirals, therapeutics, and vaccines (1).

Complement activity can achieve virus neutralisation through various immune mechanisms which work together. I have divided these mechanisms into four main discussion points to highlight the complement-virus interplay. Initially, complement proteins may bind or be deposited onto virions to prevent host-cell receptor interactions, to aggregate virus particles, or to induce an antiviral state if internalised (156–158). Complement deposition may then progress to the formation of the MAC. The MAC can lyse the lipid membranes of infected host-cells expressing viral antigens (159) or the lipid membranes of enveloped viruses (160). Activation of the complement system also produces pro-inflammatory anaphylatoxins (C3a and C5a) which can promote chemotaxis and phagocytosis, and even contribute to disease pathology (161). Finally, activation of the complement system can play an important role in the development of adaptive immunity against a virus, including: promotion of the Th1 response (162); modulation of the Treg and Th17 responses (163); extension of B-cell memory; and enabling a drastic increase in antigen-specific antibody titres (164).

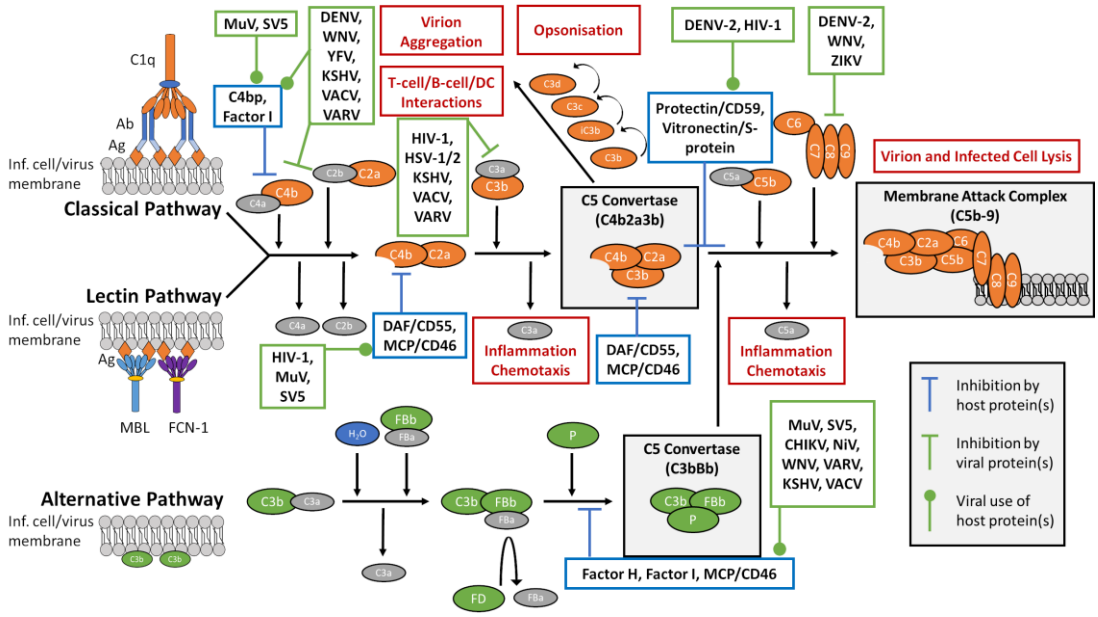

Figure 3: Overview of the complement system and the points of manipulation by viruses

Overview of the complement system and the target points for viral manipulation (green boxes), either through the expression of viral proteins or the acquisition of host proteins. Abbreviations: chikungunya virus (CHIKV); dengue virus (DENV); hepatitis C virus (HCV); human immunodeficiency virus-1 (HIV-1); herpes simplex virus-1/2 (HSV-1/2); Kaposi's sarcoma-associated herpesvirus (KSHV); mumps virus (MuV); simian virus 5 (SV5); vaccinia virus (VACV); variola virus (VARV); West Nile virus (WNV); yellow fever virus (YFV); Zika virus (ZIKV). This figure was adapted from previously published figures by Mellors et al., 2020 and Mellors et al., 2022.

1.1.5.1 Complement Opsonisation and Deposition

Complement opsonisation and deposition can occur on virions following activation *via* the classical, lectin, and alternative complement pathways. These mechanisms can supress or enhance viral infection depending on the composition of complement proteins, the viral evasion mechanisms, and the virus tropism.

MBL is capable of directly binding glycoproteins on the surface of virions to promote virus opsonisation and/or prevent their interactions with host cell receptors for cell entry, which has previously been shown for HIV-1 (155,165) and SARS-CoV-1 (77,166). The binding of MBL can also activate the complement system *via* the lectin

pathway, resulting in complement deposition. The deposition of complement proteins on a viral surface can assist neutralisation in a MAC-independent process, through the aggregation of virions and restriction of their interactions with host cells (6,20,167,168). Alternatively, the complement components deposited on a viral surface can promote viral infection by providing an alternative cell-entry mechanism using host cell complement receptors, as described for HIV (169) and herpes simplex virus (HSV)-2 infection of dendritic cells (DCs) (170). Some viruses, such as Kaposi's sarcoma virus (171), vaccinia virus (172), and variola virus (173), encode viral proteins which inhibit complement activation through the accelerated decay of C3 and use of host protein factor I.

Once the virion has been internalised by the host cell, complement proteins deposited on the viral surface can exhibit intracellular functions (158). This effect has only been described for non-enveloped viruses where complement deposition on the viral capsid can prevent viral entry into the cytosol (174), trigger proteasomal virion degradation, and induce an antiviral state in uninfected cells (158). Therefore, some viruses have evolved evasion mechanisms to promote their survival. For example, rhinoviruses and polioviruses produce a 3C protease which cleaves C3. In turn, the antiviral drug Rupintrivir inhibits the action of viral 3C protease which renders the virus susceptible to intracellular complement sensing again (158). For enveloped viruses, these intracellular complement mechanisms are likely avoided as the cell entry processes such as membrane fusion or endocytosis involves the removal of the lipid membrane, preventing it from interacting with intracellular host proteins (158).

1.1.5.2 Complement-Mediated Lysis

As the complement system progresses, complement deposition can eventuate in the formation of the MAC. The MAC has been shown to reduce viral load *in vitro via* lysis of lipid membranes on enveloped viruses and/or the infected host cell expressing viral antigens (19,159,160,175). Formation of the MAC begins with the cleavage of C5 to release the C5b thioester domain (TED) and the 'C1r/C1s, Uegf, Bmp1' domains which extend along the protein scaffold. C6 then wraps around the TED to facilitate

C7 binding, which anchors the C5b6 complex to the lipid bilayer and reduces the energy required for the membrane to bend. The heterotrimeric C8 complex (C8α, C8β, C8γ) is then incorporated into the membrane-bound assembly, and the β-hairpin structures of the C8 molecules interact with the lipid membrane, bending and piercing the bilayer to create an arc pore. The C8γ subunit then facilitates the oligomerisation of eighteen C9 molecules to the C5b8 complex and insertion into the lipid membrane, causing the membrane to stiffen. The final MAC is a flexible, asymmetric pore that resembles a 'split-washer' formation (29,176,177).

Formation of the MAC on a virion surface can neutralise some viruses, as demonstrated for HIV-1 (178) and ZIKV (19) *in vitro*. Various viral evasion mechanisms therefore exist to evade this immune response. The NS1 protein of some Flaviviruses regulates complement activity through the recruitment of host proteins (C4 binding protein (179), factor H (180) and vitronectin (11)) and the direct binding and antagonism of C4 (9). Other viruses such as Nipah virus (NiV) and Chikungunya virus (CHIKV) exhibit factor I-like activity to cleave C3b into iC3b and prevent complement-mediated neutralisation (181,182). Evasion of the MAC has also been described for MuV, SV5, and HIV-1 through the acquisition of host membrane-bound regulatory proteins into the viral lipid membrane during the budding process (183,184).

Virus-infected host cells which express viral antigens may also be neutralised *via* complement dependent cytotoxicity. Broadly neutralising antibodies can recognise viral proteins on the surface of infected cells and initiate complement deposition to prevent viral dissemination (185) or lyse the virus-infected cell (159). Some viruses protect infected cells from complement activation. For example, HSV-1 and HSV-2 express the viral glycoprotein C-1 which interacts with deposited C3, C3b, and C3c to prevent subsequent binding of properdin and C5 (175,186).

1.1.5.3 Inflammation and Chemotaxis

Activation of the complement system results in the production of C3a and C5a anaphylatoxins which mediate chemotaxis and inflammation (187). This response

helps to coordinate the immune response against invading pathogens (188,189). However, excessive or sustained complement activation in response to viral infections (including DENV, Ross River virus, SARS-CoV-1, MERS-CoV-1) is often associated with more severe disease symptoms and pathology (190–196).

SARS-CoV-1 infection studies in mice have shown that wild-type mice experience a loss in respiratory function and weight, and a greater level of lung pathology and inflammatory chemokines and cytokines compared to C3-deficient mice (195). In humans, SARS-CoV-1 patients show an elevated acute-phase response and complement activation compared to non-SARS-CoV-1 patients (197). Similarly, MERS-CoV infection of hDPP4-transgenic mice resulted in elevated levels of C5a (in sera) and C5b-9 (in lung tissue). Lung and tissue damage could be alleviated with the use of a C5aR inhibitor to reduce local and systemic inflammation (196). These studies show that sustained or heightened activation of the complement system during viral infection is associated with more severe disease pathology. By preventing complement-mediated anaphylatoxin activity using gene knockouts or protein inhibitors, pathology was reduced, demonstrating a direct mechanism of C3a/C5a activity and disease severity.

1.1.5.4 Complement and Adaptive Immunity

The complement system bridges the gap between innate and adaptive immune responses that are important for the clearance of, and protection against, viral infections. This activity is most commonly mediated by intracellular complement components, the local production of complement proteins, and the activation of complement receptors on immune cells.

Immune and non-immune cells can internalise and process C3(H_20) from the extracellular space, of which ~80% is recycled back to the cell exterior, and together with TCR and CD46 activated T cells, can alter cytokine production and increase IL-6 production (198). T cells also contain intracellular and endosomal stores of C3 which are cleaved by cathepsin L in active T cells to produce C3a and C3b. These products

are shuttled to the cell surface and C3aR is upregulated. C3a and C3b can then engage the receptors C3aR and CD46/MCP respectively, to promote T cell survival, enhance cell viability, and promote IFNγ secretion (199,200). C3aR/C5aR signalling also promotes $CD4^+$ T cell expansion (201), prevents T cell switching to $Foxp3^+$ induced regulatory T cells (202), and is required for proliferation, survival, and Th1 differentiation (203,204). The presence of C3 and the stimulation of C5aR is important for T cell production, priming, migration, and clearance of Influenza virus infections in mice (205,206). T-cell complement activity is inhibited by the HCV core protein during infection, as it disrupts C9 promoter activity internally through T-cell factor-4 transcription factor inhibition (10) and interacts with the complement receptor gC1qR to reduce IFN-γ and IL-2 production and proliferation (207).

C3 and C3 cleavage products deposited on a virion surface also interact with the B-cell receptor and B-cell co-receptor complex (CR2/CD21 ligated with CD19 and CD81) to reduce the activation threshold by several orders of magnitude. This response drastically increases antibody titres, modulates the proliferation of mature B cells, and protects the B cells from CD95-mediated elimination (164,208). The deposition of C3 and its cleavage products on immune complexes can also bind complement receptors on follicular DCs (FDCs), which are then presented to B cells in the germinal centre. This interaction can optimise B cell responses, including: antibody production; somatic hypermutation; class switching; and affinity maturation (107,209). The C3-coated complexes can then be retained by the FDCs within the lymphoid to promote memory B cell generation and survival (210). In the context of HCV infections, the core protein has been shown to interact with gC1qR on monocyte-derived DCs to inhibit IL-12 production and promote Th2 cytokine production, limiting their differentiation into Th1 cells (211).

In summary, the role of the complement system in antiviral immunity is complex, with significant implications for coordinating the innate immune response; promoting the opsonisation and neutralisation of viruses; and developing a robust adaptive immune response. However, some of these mechanisms can exacerbate the

severity of disease, which typically occur due to excessive and sustained complement-mediated inflammation. Before we begin to understand the role of the complement system in EBOV pathogenesis, I will provide an overview of the *Filoviridae* family.

1.2 Filovirus Overview

The *Filoviridae* family is comprised of five genera (*Ebolavirus*, *Marburgvirus*, *Cuevavirus*, *Striavirus*, and *Thamnovirus*) with the proposal of a sixth genus, *Dianlovirus* (Table 2) (212,213). The *Ebolavirus* genus contains five species and a putative sixth member, Bombali virus (BOMV). Four of the five officially accepted *Ebolavirus* species (Bundibugyo virus (BDBV), Ebola virus (EBOV), Sudan virus (SUDV), and Taï Forest virus (TAFV)) have been shown to cause disease in humans, where case fatality rates (CFR) reportedly range from 25 – 90% (214). The fifth member, Reston virus (RESTV), can infect humans but does not reportedly cause overt symptoms (215–217). The final member and latest proposed addition, BOMV, is capable of infecting human cell lines in a mechanism similar to other pathogenic *Ebolaviruses*, but whether it can infect humans *in vivo* and cause disease remains to be determined (218). The two viruses of the *Marburgvirus* genus (Marburg virus (MARV) and Ravn virus (RAVV)) demonstrate similar virulence in humans to the pathogenic *Ebolaviruses* with a CFR of approximately 50% (219). The most recently discovered Měnglà virus (MALV) of the *Dianlovirus* genus is genetically most similar to MARV and RAVV. MLAV demonstrates similar mechanisms of infection of human cell lines as *Ebolaviruses* and *Marburgviruses*, but like BOMV, its potential to infect humans and cause disease remains to be determined (220). Lastly, viruses of the *Cuevavirus* (Lloviu virus (LLOV)), *Striavirus* (Xīlǎng virus (XILV)), and *Thamnovirus* (Huángjiāo virus (HUJV)) genera do not reportedly cause disease in humans (221,222).

Genus	Species	Virus Name	Virus Abbreviation	Disease in Humans?	Year First Discovered
Cuevavirus	*Lloviu cuevavirus*	Lloviu virus	LLOV	No	[1]2002
*Dianlovirus**	*Mengla dianlovirus**	Měnglà virus	MLAV	N/D	[2]2018
Ebolavirus	*Bombali ebolavirus**	Bombali virus	BOMV	N/D	[3]2019
	Bundibugyo ebolavirus	Bundibugyo virus	BDBV	Yes	[4]2007
	Reston ebolavirus	Reston virus	RESTV	No	[5]1989
	Sudan ebolavirus	Sudan virus	SUDV	Yes	[6]1976
	Tai Forest ebolavirus	Taï Forest virus	TAFV	Yes	[7]1994
	Zaire ebolavirus	Ebola virus	EBOV	Yes	[8]1976
Marburgvirus	*Marburg marburgvirus*	Marburg virus	MARV	Yes	[9]1967
		Ravn virus	RAVV	Yes	[10]1987
Striavirus	*Xilang striavirus*	Xīlǎng virus	XILV	No	[11]2018

Thamnovirus	*Huangjiao thamnovirus*	Huángjiāo virus	HUJV	No	[11]2018

Table 2: Overview of Filovirus species

*The nomenclature for all known Filoviruses to date, according to (212). N/D = not determined. * = proposed names that have not been officially accepted. References: [1](221), [2](220), [3](218), [4](223), [5](224), [6](225), [7](226), [8](227), [9](228), [10](229), [11](222).*

Filoviruses contain a non-segmented, single-stranded, negative-sense RNA genome that is approximately 19 kilobases in length (**Figure 4**). The Filovirus genome encodes seven proteins: the nucleoprotein (NP), the viral proteins (VP) 35 and 40, the glycoprotein (GP), the VPs 30 and 24, and the RNA-dependent RNA polymerase (RdRp) (L) (230). During transcription, mRNA of the *GP* gene is edited to produce secreted GP (sGP), $GP_{1,2}$, and the small secreted GP (ssGP) for BDBV, EBOV, RESTV, SUDV, TAFV, and LLOV. This gene editing does not occur for MARV or RAVV, and is unlikely to occur for MLAV which lacks the transcription editing site within the *GP* gene (220).

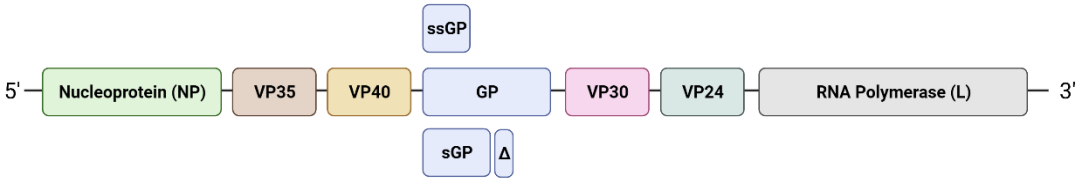

Figure 4: A schematic of the Filovirus genome

The negative-sense RNA genomes of Filoviruses are identical in transcription, with the exception of the glycoprotein (GP). The GP gene contains a transcriptional editing site for the production of GP, sGP, ssGP, and delta peptide (Δ) that is known to be absent from the Marburgvirus genome. This figure was created with BioRender.com.

The Filovirus proteins have primary roles in virus structure (**Figure 5**) and replication, with many of them moonlighting as antagonists of the host immune response, as summarised in **Table 3**. Briefly, the NP directly binds the viral RNA to form a helical

complex with other EBOV proteins (VP30, VP35, VP24) to protect the RNA from degradation (231). VP35 is a critical component for EBOV replication which forms part of the viral RdRp complex (232–234) and is required for nucleocapsid assembly (235,236). VP40, also known as the matrix protein, is responsible for virus morphology, assembly, and budding (231). The GP is responsible for binding to cellular receptors and virus entry into host cells, whilst other products of Ebolavirus and Cuevavirus *GP* transcriptional editing (sGP, ssGP, delta peptide) may function as antigen decoys (237). The VP30, also referred to as the minor nucleoprotein, binds viral RNA and associates with NP, VP35, and L to form the RNA synthesis machinery. VP35 is essential for, and initiates, EBOV genome transcription, but is not essential for MARV (238,239). Lastly, VP24 is required for nucleocapsid assembly and stability (along with NP, VP30, VP35) (231,235), and the polymerase is a key component of the RNA synthesis machinery for genome replication (231).

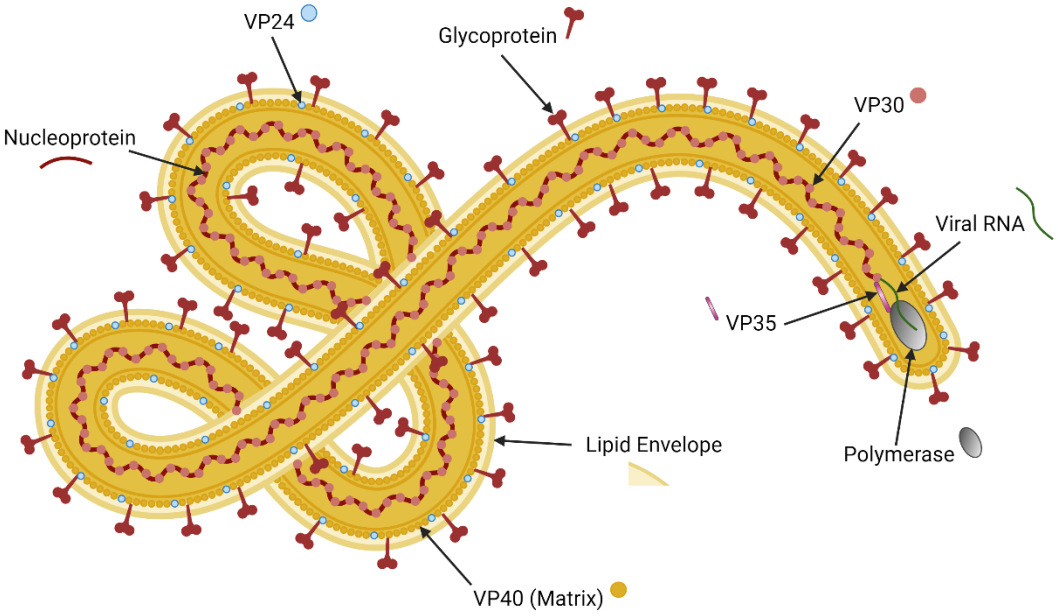

Figure 5: An overview of EBOV structure and proteins

A diagram of a mature EBOV virion and visualisation of the protein's structural roles. The nucleoprotein (along with VP30, VP35, VP24) directly binds to the viral RNA to form a helical nucleocapsid complex that protects the RNA from degradation. VP35 forms part of the nucleocapsid and the viral RNA-dependent RNA polymerase (RdRp). VP40 contributes to virus morphology, assembly, and budding. The GP is the only viral protein expressed on the surface of the virion and is required for cellular entry. VP30 forms part of the nucleocapsid and the viral RdRp. VP24 forms part of the nucleocapsid. Lastly, the polymerase protein is an essential component of the RdRp. This figure was adapted from the "Ebola (editable)" grouped icon from BioRender.com.

EBOV Protein	Major Function	Reference
Nucleoprotein	1) Primary component of the nucleocapsid which protects viral RNA from degradation	(235)
VP35	1) Binds nucleoprotein to form part of the nucleocapsid 2) Forms part of the replication machinery 3) Type-I IFN antagonist 4) siRNA antagonist	(234,240–242)
VP40	1) Primary role in virus assembly and budding 2) Exosome release and immune cell apoptosis 3) Regulates intracellular transcription 4) siRNA antagonist	(243–246)
GP	1) Virus attachment and cell entry 2) Immunosuppression of NK cells	(237,247,248)
sGP	1) Decoy molecule 2) Inhibition of pro-inflammatory cytokine production in macrophages	(249,250)
ssGP	Unknown function	(251)
Delta Peptide	1) Capable of inhibiting cell infection	(252)
VP30	1) Initiates EBOV transcription 2) Minor component of the nucleocapsid 3) siRNA antagonist	(238,239,244)
VP24	1) Inhibit IFN response 2) Nucleocapsid assembly and stability	(231,235)
L	3) Essential component of RdRp complex	(231)

Table 3: Overview of EBOV protein functions

A summary of the main functions of all EBOV proteins, which typically show both structural and immune regulatory roles.

1.2.1 Filovirus Disease

Filoviruses which cause disease in humans may result in EBOV disease (EVD), following infection with BDBV, EBOV, SUDV, and TAFV, or result in MARV disease (MVD) following infection with MARV or RAVV. Despite the different aetiologies, EVD and MVD are clinically similar (219). Following an incubation period of 2-21 days, symptoms can start to develop and the virus becomes transmissible from person-to-person *via* bodily fluids. The early stages of infection are typically sudden and non-

specific, with symptoms including fever, fatigue, muscle pain, headache, and sore throat. As the disease progresses, this may lead to vomiting, diarrhoea, rash, impaired kidney and liver function, and internal and external bleeding (214,219). Following recovery from EVD or MVD, the virus can remain latent within the body, potentially resulting in relapse or transmission to uninfected individuals. Early evidence shows the potential for MARV to persist in semen and to be sexually transmitted (253). MARV was also identified in aqueous fluid of the eye in a survivor of MVD (254), and according to the World Health Organization (WHO), MARV can persist in the placenta, amniotic fluid, and foetus of pregnant women, with the potential to persist in breast milk (219). During the 2013-2016 EBOV outbreak in West Africa, several novel observations were made regarding the potential latency of EBOV in EVD survivors. Similar to MARV, viable EBOV was detected in the ocular fluid of a convalescent EVD patient (255) and the viruses ability to persist in semen resulted in new chains of transmission, with evidence of infectious EBOV persistence in semen for at least 531 days after symptom onset (256). More recent evidence suggests that EBOV can remain latent in convalescent individuals with the potential for resurgence up to 5 years post-infection (257). EBOV was also identified in the cerebrospinal fluid of a convalescent patient suffering from meningoencephalitis nine months after EVD recovery (258), and EBOV persistence in the breast milk of an asymptomatic mother was a likely cause of infection to her infant (259).

After recovering from a Filovirus infection, patients often report ongoing symptoms. Some of these symptoms may be attributed to viral persistence, whereas the aetiology of others is less clear. Sequelae following *Ebolavirus* infection has been reported for EBOV, BDBV, SUDV, and TAFV with no obvious distinction between symptoms. Symptoms of relapse without re-infection have been attributed to viral latency and persistent viral replication in immune-privileged sites as previously discussed (255,258). A plethora of symptoms occur post-infection, ranging from abdominal (abdominal or pelvic pain, gastritis), musculoskeletal (neck pain, back pain, joint pain, myalgia), neurological (headaches, dizziness), ocular (ocular pain, vision problems, conjunctivitis, glaucoma, cataract, iridocyclitis, uveitis), and more

general symptoms such as fever, fatigue, anorexia, hearing loss, and hair loss which can persist for several years post-infection with no clear aetiology (260–264). In some instances, these sequelae have been associated with elevated levels of CD8+ and CD4+ T cell responses (265), psychological distress from bereavement, stress, stigma (266), Fc-mediated antibody functions (267), and persistent immune dysregulation (268). Reports of sequelae following MARV infection are markedly less compared to *Ebolaviruses* due to the significantly lower number of infected individuals. For MARV, patients in the recovery and convalescence stage following infection can suffer complications such as arthralgia, asthenia, hepatitis, myalgia, ocular disease, and psychosis (269), similar to the reports of *Ebolavirus* infection.

1.2.2 Filovirus Reservoirs and Spillovers

Filoviruses have a wide range of natural hosts. The *Thamnovirus*, HUJV, and *Striaviruses*, XILV, are only reported to infect fish (222). RNA of the *Dianlovirus*, MLAV, was isolated from *Rousettus* bats in China (220), and RNA of the *Cuevavirus*, LLOV, was detected in *Miniopterus schreibersii* bats in Europe (221,270). Of the *Marburgviruses,* MARV was successfully isolated from Egyptian fruit bats (*Rousettus aegyptiacus*) in Uganda (271) and this species of bat is considered to be its natural reservoir (228,272). Evidence of *Ebolavirus* infection is most extensively studied in relation to EBOV, where evidence of natural infection has been identified in dogs (273), duikers (274), non-human primates (NHPs) (275,276), humans (274), and lastly bats, which are the putative reservoir (277–279). RESTV is also capable of infecting pigs (280,281). Unlike MARV, bats have not been defined as the primary natural reservoir for *Ebolaviruses* despite evidence of antibodies (277,282–286) and viral RNA (277,279), and their ability to harbour virus without overt clinical disease and excrete the virus in their urine and faeces (277,287). Evidence of a consistent prevalence of active and past infection in bats and the ability to shed virus at levels sufficient to maintain circulation in the population have not been determined (278).

EBOV has also been shown to replicate efficiently in snake cell lines (288), and experimental infection of ferrets with EBOV can be lethal (289). EBOV is also capable

of infecting rodents, and serial passaging of the virus through certain rodents can generate strains lethal to mice (290), Syrian hamsters (291,292), and guinea pigs (293). Non-human primates (NHPs) are also susceptible to EBOV infection which results in severe disease. NHPs are a common link in the spillover of *Ebolaviruses* to humans. Of the known causes of index cases of *Ebolavirus* transmission to humans, the patients either had direct contact with infected fruit bats or in the handling and consumption of bushmeat (294). The hunting and consumption of bushmeat is widespread in tropical regions of Africa where pathogenic ebolaviruses (*Bundibugyo*, *Sudan*, and *Zaire* strains) are endemic. Although bushmeat is an important source of food and income for people within these regions, it increases the risk of ebolavirus transmission (295). Transmission rates from person-to-person may be exacerbated by practices such as traditional burial ceremonies, which involve the washing and bathing of the dead, or visiting traditional healers, where healthy individuals are exposed to infected patients or the recently deceased and their infectious bodily fluids without sufficient protective measures (296).

1.2.3 The Emergence of EBOV

In the beginning of September 1976, an acute viral haemorrhagic fever outbreak started to spread amongst residents of rural Yambuku in northwest Democratic Republic of the Congo (DRC; formerly Zaire), eventually affecting over 300 residents. The index case – entering the outpatient clinic of Yambuku Mission Hospital (YMH) on the 26th August with chills and fever – was first treated with chloroquine by parenteral injection for suspected malaria. The patient's fever diminished initially but soon returned. Their symptoms developed in severity which ultimately resulted in death. The routine use of parenteral injection and poor sterilisation methods is believed to be the major source of dissemination of the virus amongst patients, followed by contact with infected patients, as they reportedly presented with non-specific symptoms in the early stages of disease. Beyond day four, the symptoms increased in severity to include abdominal pain, a maculopapular rash, and internal bleeding primarily from the gastrointestinal tract (GI). Disease pathology included non-icteric hepatitis, acute pancreatitis, and disseminated intravascular coagulation.

The causative agent of this haemorrhagic fever outbreak was subsequently identified as EBOV, which had spread to a total of 318 individuals with a case fatality rate of 88% (227,297).

Individual cases, laboratory infections, and small outbreaks occurred sporadically in the following years, most notably an EBOV outbreak reportedly affecting 315 individuals in Kikwit, DRC in 1995; the first reported outbreak of EBOV in the Republic of the Congo in 2001 where several outbreaks would occur in the following years; the largest EBOV outbreak originating in Guinea, December 2013 where >28,000 individuals were infected; the second-largest EBOV outbreak in DRC in 2018 where >3,000 individuals were infected; and in 2021 where two separate persistent infections were the likely cause of resurgences in DRC and Guinea, from outbreaks which ended one year and five years prior, respectively (298). A summary of EBOV outbreaks in Africa since 1976 are shown in **Figure 6**.

1.2.4 The Emergence of SUDV

Following notification of the EBOV outbreak in the DRC, later investigations determined that in June of the same year (1976), patients in Nzara, Southern Sudan, were suffering with a haemorrhagic illness of unknown origin. Initially, three factory workers became ill with a severe febrile illness and haemorrhagic complications, where the infection was passed onto family members and close contacts. The only connection between the three cases appeared to be a cotton factory in the town centre of Nzara. Small pockets of infections developed around Nzara as a result of human-to-human transmission primarily through direct contact to those administering care for infected individuals. In the subsequent months, new cases arose in individuals where no direct contact with sick individuals was established. They did, however, all work at the same cotton factory later found to contain insectivorous bats, the putative EBOV reservoir. Infections were passed on to their families in remote areas which were consequently self-limiting. Over 100 km away in Maridi, a contact of one of the original factory workers had become ill and travelled from Nzara, their symptoms becoming so severe that they were admitted to the

Maridi hospital, where the infection spread. Shortly after, a second patient from Nzara was also admitted to the Maridi hospital, which introduced another case of infection and chain of transmission. The hospital became the main area of viral transmission in the outbreak, which eventually ended with a total of 284 cases and a CFR of 53% (225,297). This was the first discovery of SUDV in an outbreak that occurred simultaneously with, but was distinct from, EBOV. Several outbreaks of SUDV have occurred since its discovery, the largest being in Uganda in 2000, which affected 425 individuals. The last reported outbreaks of SUDV were in Uganda, 2012 (298). A summary of SUDV outbreaks in Africa since 1976 are shown in **Figure 6**.

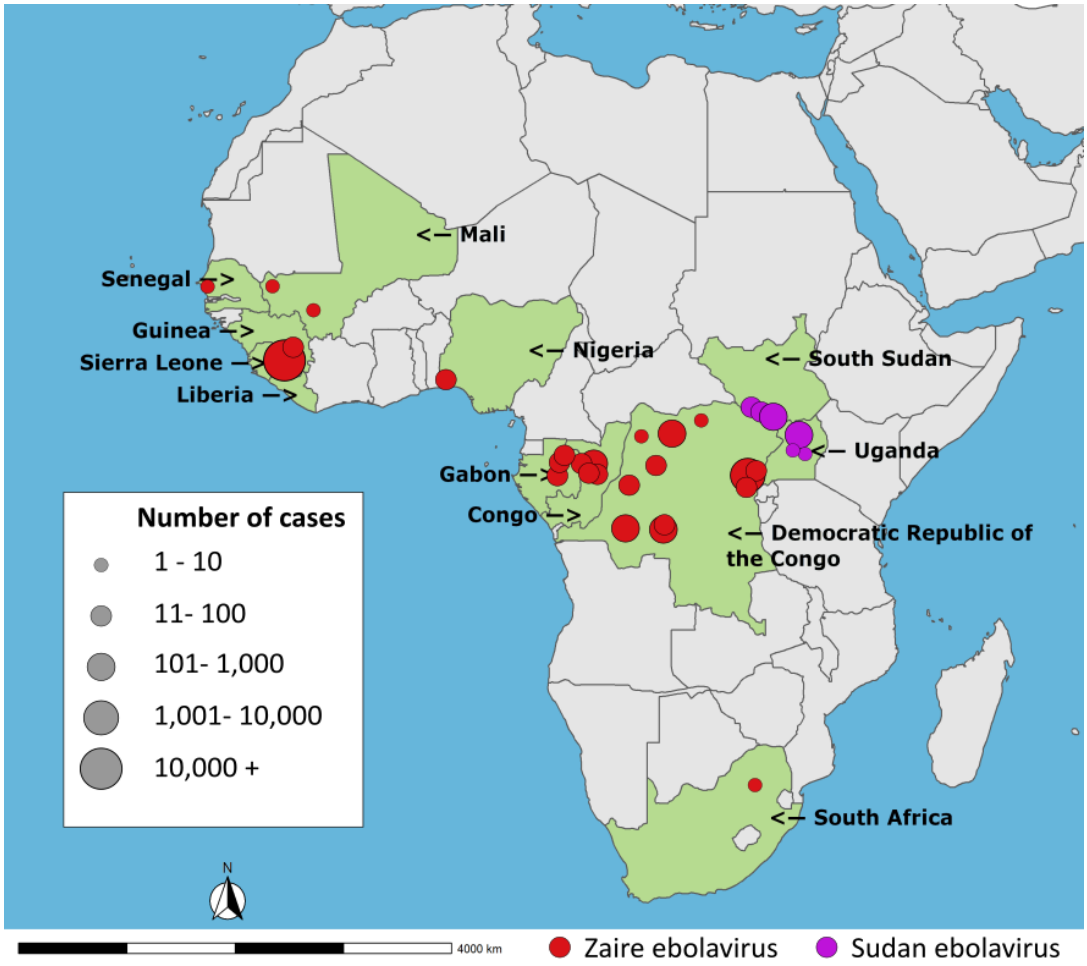

Figure 6: A Map of the Reported EBOV and SUDV Outbreaks in Africa

Reported outbreaks of EBOV and SUDV in Africa were plotted according to reports by the CDC. Each spot represents the location of an outbreak of EBOV (red) or SUDV (purple), and the size of each spot is roughly proportionate to the number of cases. The original map was created in R Studio with the following packages: ggplot2 (299)*, rnaturalearth* (300)*, rnaturalearthdata* (301)*, sf* (302)*, ggspatial* (303)*. The final image was then created using GNU Image Manipulation Program and Inkscape software.*

1.2.5 The Emergence of Other Clinically Relevant Filoviruses

1.2.5.1 Marburg Virus (MARV)

MARV was the first Filovirus to be discovered. In 1967, an outbreak of haemorrhagic fever occurred simultaneously in laboratories in Marburg and Frankfurt, Germany, and in Belgrade, Yugoslavia (now Serbia). The outbreak originated from African Green monkeys imported from Uganda, where thirty-one people became ill and seven

succumbed to infection. According to the Centers for Disease Control and Prevention (CDC), a further thirteen outbreaks of MARV have occurred since its discovery, including a single fatal case of human infection in Guéckédou, Guinea – the origin of the world's largest EBOV outbreak from 2013-2016 (228,304). The reservoir host for MARV is the African fruit bat, *Rousettus aegyptiacus*. Infected fruit bats do not show overt clinical symptoms, unlike NHPs and humans which can develop severe disease leading to mortality (271,305).

1.2.5.2 Reston Virus (RESTV)

RESTV first emerged in October 1989, when 100 cynomolgus monkeys were transported from Manila in the Philippines to a primate facility in Reston, Virginia. In November, four of these animals died inexplicably and were subsequently autopsied, which attributed the cause of death to infection with simian haemorrhagic fever virus (SHFV). Fourteen more animals succumbed to a similar illness within the next few days, with further isolates of SHFV along with a novel Filovirus, RESTV. Identical findings of RESTV in cynomolgus monkeys imported from three suppliers in the Philippines were made in Pennsylvania and Texas (224,306). Interestingly, twelve people (6%) exposed to cynomolgus monkeys from the Philippines were seropositive for RESTV with no reports of disease (215–217). RESTV-infected NHPs were again imported from the Philippines to other countries; Italy in 1992 and the US in 1996 (307). RESTV has also been identified domesticated pigs coinfected with porcine reproductive and respiratory syndrome virus in Manila, the Philippines (280) and in China (281). Again, six workers on pig farms or handlers of swine products were seropositive for RESTV with no reports of illness (280).

1.2.5.3 Côte d'Ivoire/ Taï Forest Virus (TAFV)

TAFV (formerly known as Côte d'Ivoire virus) first emerged in November 1994, when a team of animal behaviour researchers discovered and dissected several decomposed chimpanzee corpses in the Taï Forest National Park. Eleven days later, one of the researchers was admitted to a clinic with fever, chills, headache, and myalgia but physical examinations remained normal. Symptoms continued to

develop and included diarrhoea, nausea, vomiting, anorexia, a non-itching rash, and central nervous symptoms including temporary memory loss, anxiety, confusion, and irritability (226,260). Fifteen days after symptom onset, the patient was discharged and after six weeks made a full recovery but experienced hair loss for approximately three months, beginning one month after symptom onset. Serological and antigenic investigations of 74 contacts and other researchers within the team were negative for *Ebolavirus* antigens. TAFV was isolated from serum of the case patient on day three of symptom onset (260). Their IgG response was cross-reactive with all known *Ebolavirus* strains at the time (EBOV, SUDV, RESTV) and the newly isolated TAFV strain, whilst IgM reacted only with TAFV (226). No further cases of TAFV infection have since been reported.

1.2.5.4 Lloviu Virus (LLOV)

LLOV was first discovered in 2002 following a mass die-off of Schreiber's bats (*Miniopterus schreibersii*) in Spain. The genomic RNA was isolated from the bat carcasses and sequenced to reveal a genetically distinct Filovirus: the first to emerge in Europe (221). There were no further reports of the virus until 2016, when a similar mass die-off of Schreiber's bats occurred in Hungary and LLOV RNA was again detected in the bat carcasses (270). Investigations into LLOV serology amongst Schreiber's bats suggested that LLOV may be widespread within this species across Spain (308). Using recombinant LLOV (rLLOV) from minigenome systems, rLLOV was shown to infect hepatocytes and macrophages, but unlike EBOV, rLLOV infection of macrophages did not induce inflammatory responses that are characteristic of EVD (309). In a recent study, LLOV was isolated for the first time from Schreiber's bats in north-eastern Hungary. Blood samples were collected from 2016-2020 where various bats were seropositive. LLOV RNA was identified in bats that appeared healthy, and in their ectoparasites (*Nycteribiidae* and *Ixodidae* families). From one of these PCR positive bats, LLOV was successfully isolated for the first time and the viral isolate was capable of infecting both monkey and human cells (310), which suggests a possibility for human infection.

1.2.5.5 Bundibugyo Virus (BDBV)

In August 2007 in the Bundibugyo district of Uganda, a 26-year-old pregnant woman was hospitalised with symptoms of fever and general weakness, which progressed to diarrhoea and difficulty breathing. This patient is the putative index case, as six further contacts (the neonate, sister, mother, and two nieces of the index patient) became infected and succumbed to the disease. Wildlife in the surrounding national parks were protected and so the origins of the virus were never determined (223). In November 2007, cases of haemorrhagic fever amongst residents were reported and genomic sequencing of patient sera identified BDBV as the aetiological agent. Their clinical symptoms were typical of what had become recognised as EVD: fever, fatigue, headache, abdominal pain, vomiting, diarrhoea, and in some cases, haemorrhagic manifestations (214,223,311). The outbreak was concluded in February 2008, with 149 cases (93 putative and 56 laboratory-confirmed) and 37 deaths, with a final CFR of 25% (223,312). The second and last reported outbreak of BDBV occurred in the Isiro Health Region of the DRC in 2012. Advances in molecular techniques and increased awareness of EVD helped control the epidemic, which was concluded with 38 lab-confirmed cases and a CFR of 34% (313,314).

1.2.5.6 Bombali Virus (BOMV)

In Sierra Leone in 2016, 1,278 samples from 535 animals (244 bats, 46 rodent, 240 dogs, and 5 cats) were collected for molecular investigations to determine the *Ebolavirus* reservoir. Four insectivorous free-tailed bats within 20 km of each other inside human dwellings were positive for a novel Filovirus. Viral genomes which shared 99.1% sequence identity were isolated from two of the bats. The virus shared 55-59% nucleotide identity to other *Ebolaviruses* and was provisionally named BOMV. Recombinant vesicular stomatitis virus (VSV) encoding the BOMV *GP* gene is capable of infecting human (293FT) cells and Vero E6 cells in a Niemann-Pick type C1 (NPC1) dependent manner, consistent with other Filoviruses (218). This data highlights the possibility of infection in humans, but whether it is able to establish infection and cause disease is unknown. This finding also raises considerations regarding seroprevalence studies where spillover events from other pathogenic

Ebolaviruses may have occurred previously. Following the discovery of BOMV, RNA of the virus was later detected in free-tailed bats in N'Zerekore Prefecture, Guinea (315), and again in south-eastern Kenya (316).

1.2.5.7 Měnglà Virus (MALV)

The pathogenicity of the newly discovered Měnglà virus (MLAV) in the proposed *Dianlovirus* genus in humans remains to be determined. The discovery of MLAV was reported in 2018 following its isolation from *Rousettus* bats in the Yunnan Province of China. Whilst its potential to infect and cause disease in human remains undetermined, MLAV is genetically most closely related to MARV and RAVV, it is as equally efficient as EBOV and MARV at infecting HEK293 cells, and it exhibits a similarly broad tropism utilising the NPC1 protein for cellular entry (220).

1.3 The Ebola Virus

This section will elaborate on the pathogenesis of, and protective immune responses against, EBOV. I will then discuss the current literature regarding the complement system and EBOV pathogenesis, which formed the primary focus of this PhD project.

1.3.1 The 2013-2016 EBOV Outbreak

In December 2013, an 18-month-old boy believed to be infected with EBOV from contact with an insectivorous bat was the index case of the world's largest EBOV epidemic. The spillover occurred in Meliandou in the Guéckédou prefecture of Guinea. The infection spread to his four-year-old sister and pregnant mother. All three cases died within two weeks. On the night of her death, the mother suffered a spontaneous abortion and was cared for her by family members, local female healthcare volunteers, and a male local healthcare worker. All individuals subsequently developed EVD and four of them died. One of the family members and one of the healthcare volunteers attended district hospitals, resulting in further chains of transmission. Transmission was further exacerbated by funeral practices in Meliandou and surrounding local villages (Macenta, Nzérékoré, Kissidougou). On the first of February, an infected member of the index case's extended family was taken

to Conakry, the capital of Guinea, where they died four days later and the chain of transmission continued (317–320). For several months, EBOV spread undetected through the forested regions of Guinea and initial reports suggested a 100% CFR. A retrospective study using oral swab samples from Meliandou residents identified a further eight individuals that were seropositive for EBOV. This brought the CFR down to 55.6% and two of the eight individuals reported mild or asymptomatic forms of infection. By the time the EBOV epidemic was declared by the WHO in March, the virus had spread throughout multiple areas of Guinea and across the border to Sierra Leone and Liberia (318). By July 2014, EBOV had spread to the capitals of all three countries and for the first time was spreading through densely populated urban areas (321).

Efforts to bring the outbreak under control included accelerated vaccine developments (including the FDA licensure of the rVSV-ZEBOV vaccine), therapeutic developments, establishment of EBOV treatment centres, healthcare support, staff training, border and travel restrictions, viral surveillance, contact tracing, and laboratory testing including PCR and serology (321). Furthermore, the implementation of real-time genomic sequencing with the use of the portable MinION sequencer (Oxford Nanopore Technologies, Oxford, UK) in support of molecular epidemiology assisted the rapid identification and prevention of transmission chains (322). A further seven countries were also affected by the travel of infected individuals: Italy, Mali, Nigeria, Senegal, Spain, the United Kingdom, and the United States, with some secondary infections occurring predominantly in healthcare settings. Two and a half years since the index case, the epidemic ended with over 28,000 cases and over 11,000 deaths recorded (321).

Previous EBOV outbreaks were sporadic, short-lived, and in relatively remote areas. The 2013-2016 epidemic was the longest and largest EBOV outbreak and this led to multiple novel discoveries. For the first time, EBOV was found to persist in semen for at least 500 days before sexual transmission (264), could persist in the cerebrospinal fluid and cause recrudescence (258), and could persist in ocular fluid following

infection (255). The rVSV-ZEBOV (Ervebo®) vaccine was also utilised under compassionate use protocols during the outbreak and was eventually licensed by the EMA and FDA (323). The high number of cases and longitudinal studies which followed were an important foundation for this PhD project.

1.3.2 EBOV Pathogenesis

EBOV enters a human host through mucous membranes, breaks in the skin, or parenterally. From there, it primarily infects mononuclear phagocytic cells and DCs (324), with an even wider cell tropism for endothelial cells, fibroblasts, hepatocytes, adrenal cortical cells, and epithelial cells where the virus can replicate and cause the host cell to lyse (325,326). EBOV binds target cells using two types of relatively non-specific receptors: C-type lectins which interact with $GP_{1,2}$ residues, and phosphatidylserine receptors which interact with phosphatidylserine on the viral envelope (327). Internalisation of EBOV virions is primarily believed to occur *via* macropinocytosis (and to a lesser extent, clathrin-mediated endocytosis) but the mechanism triggering this uptake is unknown, and is not directly triggered by C-type lectins or phosphatidylserine receptor interactions. The EBOV virions are internalised into early endosomes and trafficked to late endosomes, where the mucin-like domain (MLD) and glycan cap of the GP1 subunit are cleaved by host low-pH-dependent cathepsins. The exposed RBD and GP1 subunit of the fusion-active GP binds to the host NPC1 receptor, and a GP2 hydrophobic fusion loop inserts into the late-endosome membrane to create a pore for the release of the ribonucleoprotein complex into the cytoplasm (327–329).

The negative-sense single-stranded EBOV RNA genome is first transcribed into seven monocistronic mRNAs by the ribonucleoprotein complex (NP, VP35, VP30, L) which are then translated into the viral proteins. The increase in protein levels (particularly NP) leads to the formation of inclusion bodies and a switch from genome translation to replication. The negative-sense EBOV RNA is used as a template for the synthesis of positive-sense EBOV RNA, which in turn acts as a template for negative-sense EBOV RNA. In the late stages of RNA synthesis, ribonucleoprotein complexes are condensed

into replication- and transcription-inactive nucleocapsids that are transported to the cell-surface membrane in an actin-dependent manner (327). VP40 is also transported to the cell surface by interacting with various cellular trafficking components: actin coordinates the movement and assembly of VP40 (330) and is incorporated into virus-like particles (331); VP40 associates with microtubules and enhances tubulin polymerisation (332); the host scaffolding protein, IQGAP1, interacts with VP40 and is required for the budding of EBOV VP40 virus-like particles (333); and Sec24C of the COPII transport system interacts with VP40 and is required for its transport to the plasma membrane (334). The GP is transported to the cell surface by the secretory pathway where O-linked and N-linked glycan post-translational modifications are added, and furin cleaves GP into GP1 and GP2 subunits. VP40 and various host factors then coordinate the assembly of the virions that bud from the cell and are released into the extracellular space, causing the host cell to lyse (327) (**Figure 7**).

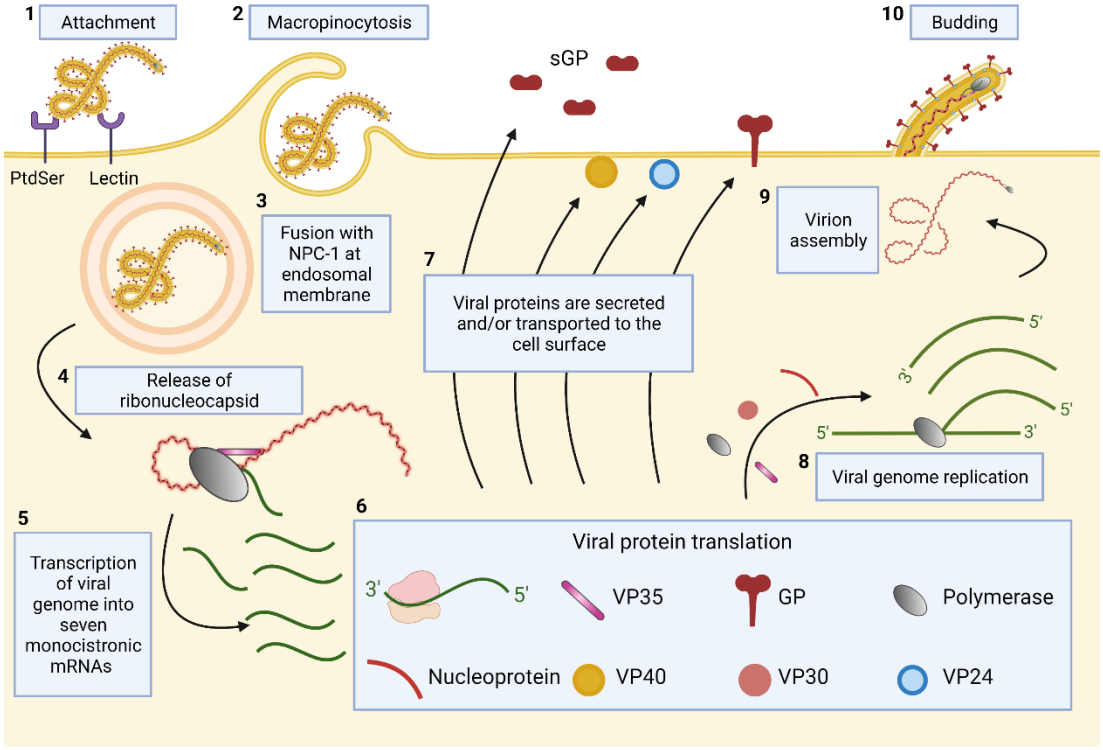

Figure 7: Overview of Ebola virus (EBOV) lifecycle

1) *The EBOV attaches to the host cell membrane through interactions with lectin or phosphatidylserine (PtdSer) receptors.* ***2)*** *The EBOV then enters the host cell via macropinocytosis.* ***3)*** *Acidification of the endosome activates low-pH host proteases, resulting in the cleavage of the EBOV glycoprotein (GP), which enables its interactions with the host Niemann-Pick C1 receptor.* ***4)*** *This interaction creates a pore in the endosome and the viral nucleocapsid is released into the cytoplasm.* ***5)*** *The negative-sense viral RNA is then transcribed into seven monocistronic mRNAs by the ribonucleoprotein complex (NP, VP35, VP30, L).* ***6)*** *The monocistronic mRNAs are then transcribed by host ribosomes into the viral proteins.* ***7)*** *Products of transcriptional editing of the GP gene (such as sGP) are secreted from the host cell. VP40 and VP24 are trafficked to the cell surface membrane, and the* $GP_{1,2}$ *is incorporated into the host cell membrane.* ***8)*** *Following an accumulation of NP, there is a switch from translation to transcription. The negative-sense viral RNA is transcribed into a positive-sense genome, which is used as a template for RNA synthesis.* ***9)*** *The negative-sense RNA genome and viral proteins are assembled and packaged.* ***10)*** *The virion then buds from the host cell, enveloping itself in the host cell membrane with EBOV-GP on the surface. This figure was created with BioRender.com using the "Ebola (editable)" grouped icon.*

Investigations using NHPs and isolated human PBMCs shows that EBOV infection of monocytes and macrophages impairs their natural antiviral interferon mechanisms whilst the virus continues to replicate, eventually causing macrophage depletion. The pro-inflammatory cytokine signalling (including TNF-α, MIP-1 α, MCP-1, IL-1β, IL-6, IL-8) of the macrophages and monocytes in response to infection continues, leading to the recruitment of further target cells for EBOV, vasodilation, increased endothelial cell permeability, and increased expression of endothelial cell-surface adhesion molecules which ultimately aid viral dissemination *via* the blood to other organs (335–339). EBOV-infected macrophages also synthesise cell-surface tissue factor (TF) which triggers the extrinsic coagulation pathway by interacting with factors VIIa and X, leading to the deposition of fibrin – a protein involved in blood clotting – on the surface of infected cells. The deposition of fibrin contributes to disseminated intravascular coagulation (DIC): a severe condition of abnormal clotting in blood vessels that is associated with EVD. Therefore, the dysregulation of the coagulation system seen in EVD may be partly attributed to this macrophage activity (340). *In vitro*, EBOV infection of human DCs was shown to prevent cytokine secretion (IFNα) and impair the otherwise normal development of adaptive immunity by preventing the expression of costimulatory molecules and MHC class I and II surface antigens. EBOV-infected DCs were also incapable of supporting T cell proliferation (341,342). Following the infection of macrophages and DCs, EBOV is able to disseminate into the lymph nodes and other organs (326).

In EBOV-infected patients, biomarkers that were pro-inflammatory and/or associated with coagulation dysfunction were higher in those that succumbed to infection (343,344) and such biomarkers (active prothrombin time and international normalised ratio) correlated with viraemia, indicating a direct role of EBOV and coagulation dysfunction (344). Investigations using NHPs suggests that the coagulation irregularities are associated with tissue factor expression from EBOV-infected macrophages/monocytes, mentioned previously (340). Liu *et al* also found that four of the most strongly differentially expressed genes were associated with the clotting pathway and were higher in those with a fatal outcome. As this was using

mRNA from peripheral blood, they concluded that this response was likely the result of liver pathology (345).

In humans infected with EVD, characteristics of early EBOV infection show leukopenia with lymphopenia, followed by neutrophilia, a left shift with atypical lymphocytes, and thrombocytopenia (346). Based on NHP studies, leukopenia does not appear to be the result of direct infection of these cells (335). There is also an eventual decline in natural killer (NK) cell frequency (345,347), which may be the result of EBOV-GP on the cell-surface membrane of infected cells directly interacting with NK cell receptors to suppress their function (247,248).

EBOV may spread to the liver (348), where clinical biomarkers of liver damage are associated with fatal EVD outcomes (344,349,350). *In vitro* studies using human hepatocytes have shown that EBOV infection leads to the suppression of antiviral responses including TLR-, IFN regulatory factor 3-, and protein kinase R- mediated pathways. The IFN response is largely supressed during EBOV infection and this effect is most pronounced with EBOV compared to RESTV, which suggests an association between IFN suppression and Filovirus virulence (351). EBOV-infected hepatocytes also show an upregulation of TGFβ secretion and induced characteristics typical of epithelium-to-mesenchyme-like transition (352). Markers of liver damage, aspartate aminotransferase (AST) and alanine aminotransferase (ALT), often correlate with levels of viraemia in patients with EVD and the liver damage is believed to partly be the result of viral replication (344). Damage to the liver can exacerbate other clinical aspects of EVD as it is the primary site of synthesis for many proteins, including those involved in the coagulation pathway. Coagulation pathway dysfunction is strongly associated with a fatal outcome and biomarkers of this dysregulation correlate with viraemia (340,343,344).

Continued spread of EBOV can also cause acute kidney injury, which is strongly associated with mortality (349). However, kidney damage does not appear to be a direct result of virus replication. Lanini *et al* report that biomarkers of kidney damage

(creatinine and blood urea nitrogen) in acute EVD patients showed no biological correlation with levels of viraemia, but did correlate with a fatal clinical outcome. They concluded that kidney damage is likely a secondary multifactorial effect such as rhabdomyolysis, dehydration, or acidosis (344). This concept is supported by other studies where viable EBOV can be found in the urine of convalescent patients that do not present with symptoms (353,354).

EBOV can infect endothelial cells of the GI tract which was a commonly reported symptom in patients of the 2013-2016 EBOV outbreak (349), and gut-associated lymphoid tissue (GALT) is significantly affected in terminal disease of EBOV-infected NHPs. The transport of infected monocytes, macrophages, and DCs to the GALT *via* the bloodstream induces apoptosis of lymphocytes and NK cells as previously mentioned. Direct damage from EBOV replication in the endothelial cells and the pro-inflammatory responses from infected immune cells leads to increased vascular permeability and necrosis (355).

EBOV replication is also believed to play a direct role in the damage of muscle tissue, as levels of viraemia have been shown to correlate with biomarkers of muscle tissue damage (lactate dehydrogenase and AST) in EBOV patients (344). Rhabdomyolysis appears to be more common in EVD than other viral infections (356). EBOV can also infect adrenal cortical cells and is capable of inducing their congestion, degeneration, and necrosis, as reported in experimental infections of NHPs (324,357,358). Transcriptional analysis of EBOV-infected NHPs revealed significant damage to the adrenal glands, with an early downregulation of genes involved in metabolism, coagulation, hormone synthesis, and angiogenesis, and an upregulation of genes associated with inflammation (359). NHP studies show lymphoblasts and considerable histological changes in the spleen following EBOV infection (324,360).

1.3.3 EBOV Protection

A correlate of protection for EBOV has not yet been defined. However, there are various factors that are significantly associated with clinical outcome. Levels of

viraemia at the point of diagnosis, as determined by cycle threshold (Ct) values from real-time quantitative PCR (RT-qPCR), are often associated with clinical severity and patient outcome (249,343,344,349,350). Other factors associated with survival include the generation of early and robust antibody responses (361–364), the presence of neutralising antibodies (276,365–368), Fc-mediated antibody functions (369), T cell profiles (345,370–372), and NK-cell subtypes (345,347,366,373).

EVD Survival - Cell-Mediated

Generally, the development of a robust immune response to EBOV infection in humans is associated with survival. Baize *et al* compared the immune responses of those that succumbed to, or survived, EBOV infection during the Gabon outbreak in 1996. Fatal infections were characterised by an absence of IgG, considerably low levels of IgM, and extensive apoptosis of T cells, in contrast to the survival group (361). Later studies also found correlations between the patients that succumbed to EVD and massive lymphocyte apoptosis, contrary to survivors (363,374,375). Ruibal *et al* found that fatal cases of EVD in humans from the 2013-2016 outbreak showed similar overall T cell activation compared to survivors, but there were variations within the T cell subsets activated. CD4+ and CD8+ T cells in those that succumbed to infection had a significantly higher expression of inhibitory molecules CTLA-4 and PD-1 which correlated with elevated inflammatory markers and viral load, whilst survivors had significantly lower expression of CTLA-4 and PD-1 with reduced inflammation (371). However, the enhanced expression of PD-1, along with impaired IFNγ production, has been reported in a small study with two EVD survivors. During the course of infection, there was an overall decline in functional lymphocytes and an inversion of CD4+ and CD8+ T cell ratios, which was reverted during the recovery period and may be indicative of a critical point in the course of infection (370). Using digital cell quantification (DCQ) on the peripheral blood of acute EBOV patients, Liu *et al* predicted a decrease in CD4+ T cells for both survivors and fatalities compared to EBOV convalescent controls, whilst CD8+ significantly increased for survivors only (345). EBOV-specific T cell responses were sustained after infection and the dominant CD8+ phenotype amongst survivors (IFNγ+, TNF+, IL-2-) was the same T cell

population associated with survival in NHP studies (372). Whilst there are some discrepancies between studies, overall it seems that a robust and sustained lymphocyte response increases the chances of survival from EBOV infection.

NK cells have generally been shown to have a protective role in EBOV infection, although most of the evidence comes from the use of animal models and so the responses in humans may differ. Warfield *et al* found that the injection of mice with non-replicating EBOV VLPs (expressing the *GP* and *VP40* genes) conferred protection and enhanced NK cell numbers in lymphoid tissues, whilst NK cell-deficient mice would succumb to infection in spite of vaccination. Subsequently, the adoptive transfer of NK cells treated with VLPs could restore protection. Unlike live EBOV infection, the treatment of NK cells with VLPs enhanced cytokine secretion and cytolytic activity (366). Similarly, Williams *et al* found that post-exposure treatment of mouse-adapted (MA)-EBOV-infected mice with VSVΔG/EBOV-GP significantly enhanced NK cell cytotoxicity and IFNγ secretion (373). Following vaccination with the Ad26.ZEBOV and MVA-BN-Filo vaccine regimen, NK cells of human participants showed increased proliferation and activation (376). However, *in vitro* investigations using human PBMCs have shown potential immune-suppressing functions of the EBOV-GP. The EBOV-GP can directly interact with various receptors on NK cells and the expression of EBOV-GP on mammalian cells can reduce NK cell-mediated lysis, degranulation, and cytokine secretion (247,248). Lastly, investigations of patients with acute EBOV infection have revealed an overall decrease in NK cell frequency, with lower levels of NK cells being associated with fatal EVD outcomes compared to survivors (345,347). These studies suggest that the function of NK cells can confer some level of protection against EBOV infection, but these cells may be suppressed during the course of infection. Lastly, a possible contribution of NK cells to viral pathogenicity has been shown in mice, where mice challenged with MA-EBOV showed a reduction in circulating NK cells, but an accumulation in virus replication sites which correlated with enhanced EVD progression in specific conditions (377).

Whilst maintaining a robust T cell and NK cell response is associated with survival, elevated pro-inflammatory cytokine signalling and acute-phase responses have been more commonly associated with a fatal outcome (345). At first, the observations of a robust IFN response during EBOV infection seemed counter-intuitive given the immunosuppressive nature of the virus. However, transcriptomic analysis of peripheral blood from acute stage EBOV-infected patients firstly showed that for both survival and fatal outcome groups, there was a significant enrichment of genes associated with IFN signalling, the complement system, the coagulation pathway, hormone receptors, and acute-phase signalling. For fatal compared to survival outcomes, genes associated with IFN signalling and acute phase responses were the most significantly upregulated (345), with similar findings for EBOV-infected NHPs (378). The authors suggest that the role of EBOV as an IFN antagonist may only act locally rather than systemically, which is in part supported by the absence of EBOV infection in lymphocytes, and so an overall difference in IFN responses is still observed. Elevated levels of C-reactive protein (CRP) were significantly higher during the acute phase in those that eventually succumbed to infection, supporting the notion of elevated acute-phase signalling being associated with poor clinical outcome (350). Vernet *et al* also identified an elevation of the pro-inflammatory marker IL-6 in those that eventually succumbed to infection, although other studies have not been able to distinguish IL-6 between survival or fatal outcomes (345,350).

EVD Survival - Antibody-Mediated

The generation of robust and early antibody responses has repeatedly been reported for those that survive EVD compared to those that succumb to infection (361–363,379). One study found that these antibody responses can persist for up to 40 years post-infection (364). However, EVD survivors produce a wide spectrum of antibody responses and so antibody titre alone does not determine protection. A major focus of interest for protective antibodies is their capacity for neutralisation. Similar to total antibody titres, neutralising antibody titres are often associated with protection and are therefore favoured in initial screenings for therapeutic development (276,365–368). The use of concentrated polyclonal IgG antibodies from

vaccinated and challenged NHPs was shown to have virus-neutralising activity and was capable of conferring complete protection in NHPs starting from 48 hrs post-infection (380). However, not all neutralising antibodies are able to confer protection *in vivo*. One of the earliest, well-characterised EBOV-GP monoclonal antibodies (KZ52) demonstrated strong neutralisation *in vitro* (381) and even protection in mice and guinea pigs (382), but its passive transfer failed to protective NHPs from lethal EBOV infection. The lack of protection was not the result of mutagenic escape nor low circulating concentrations of KZ52 at the time of challenge (383).

Future therapeutic developments utilised a cocktail of neutralising antibodies. ZMAb contains three neutralising antibodies and was shown to be protective from lethal EBOV infection in mice and guinea pig models (384) and cynomolgus macaques (385). Another antibody cocktail, MB-003, was comprised of three monoclonal antibodies, except they only had a low neutralising potential based on *in vitro* assays and relied partially upon immune effector functions. This cocktail could confer protection to rhesus macaques infected with EBOV (386,387). A new antibody cocktail, ZMapp, then utilised a mixture of antibodies from ZMAb and MB-003 with changes in the Fc structure and glycosylation that could rescue NHPs from lethal EBOV infection (388). ZMapp was trialled for effectiveness in human populations to treat EBOV, and while its use appeared to be beneficial, it did not meet the statistical threshold for efficacy (389). Currently, only two antibody-based EVD therapeutics have been approved by the FDA (390). The first approved was Inmazeb™, which is a combination of three monoclonal antibodies (atoltivimab, maftivimab, odesivimab). All three proteins bind the EBOV-GP to neutralise the virus and/or utilise antibody effector functions: maftivimab helps neutralise, odesivimab relies on immune effector functions, and atoltivimab relies on both neutralisation and immune functions (391). The second FDA-approved therapeutic was Ebanga™, which utilises a single monoclonal antibody (ansuvimab) that inhibits virus entry by binding the RBD of the GP-1 subunit, preventing EBOV-GP from binding to the NPC-1 receptor (392). However, in a recent study using NHPs, EBOV-challenged rhesus macaques that survived infection following monoclonal antibody treatment showed EBOV persistence in macrophages

infiltrating the brain ventricular system. This persistence was associated with fatal disease recrudescence including severe tissue damage, inflammation, and meningoencephalitis (393).

The effectiveness of the rVSV-ZEBOV vaccine was attributed to the development of antibodies for protection in NHPs (394) and mice (395) which depended on CD4+ T cells, whilst the role of CD8+ T cells was minimal. In humans, the rVSV-ZEBOV vaccine is capable of inducing strong humoral and cell-mediated responses including the induction of neutralising antibodies (396,397). Its use in ring vaccination studies where 2,119 individuals were vaccinated showed 100% efficacy from ten days post-vaccination (398). However, the exact efficacy was later disputed due to a bias in the methodology which may have influenced a change in behaviour of vaccinated participants, thus reducing their exposure to EBOV and infected individuals (399). The two-dose heterologous regimen with Ad26.ZEBOV and MVA-BN-Filo was also found to induce a strong humoral response in both adults (400) and children (401), supporting its implementation as a prophylaxis for EBOV infection.

1.3.4 Complement and Ebola Virus Disease

The complement system has been implicated in EVD outcome and EBOV pathogenesis in various ways, but there are still many questions to be answered. During the acute phase of EBOV infection, transcriptomic analysis revealed that individuals who eventually succumbed to infection had a significant upregulation of gene sets associated with interferon signalling, the complement system, the coagulation pathway, hormone receptors, and acute phase signalling, compared to convalescent controls (345). These findings suggest that a strong innate immune response to EBOV may not always be beneficial. Similar gene expression profiles have been reported for survivors of EVD with a median of 23 months post-discharge from treatment centres. These survivors showed a long-lasting immune dysfunction and a significant enrichment of genes associated with interferon signalling, the complement system, PRRs, and acute phase signalling (268). It is important to note

that an upregulation of the complement system may be a non-specific response to other disease factors, such as an increase in viral load.

Investigations of the underlying mechanisms for complement activation and how it may interact with EBOV can give further insight into the role of complement in EBOV pathogenesis and its implications for protection. In this discussion, the mechanisms of complement in EBOV pathogenesis have been divided into antibody-dependent and antibody-independent mechanisms.

1.3.5 Antibody-Dependent Mechanisms of Complement in EBOV Pathogenesis

Some of the early investigations regarding antibody-dependent mechanisms of complement in EBOV pathogenesis were from Takada *et al*. They first showed that antisera from the immunisation of mice with a plasmid encoding the EBOV-GP could mediate ADE of VSV pseudotyped with EBOV-GP infection into human kidney 293 cells. ADE was then enhanced with the use of EGTA and heat-inactivation of the plasma samples (402). It was later identified that EBOV-GP antibodies from EBOV convalescent human plasma could enhance wild-type EBOV infection of primate kidney cells. This effect was enhanced with the addition of C1q and could be enhanced further in the presence of EGTA, which suggests the ADE was independent of complement activation and was a direct result of the C1q protein binding (403). Finally, the C1q-mediated ADE was shown to be dependent on four distinct epitopes bound by certain monoclonal antibodies (404).

As discussed previously, interactions with the complement system can enhance antibody-mediated virus neutralisation. This has been reported for some antibodies against HCMV (405), CCHFV (406), Influenza A virus (159), MuV and SiV5 (167), and EBOV (407). For EBOV, Wilson *et al* demonstrated that certain monoclonal antibodies were only capable of virus neutralisation in the presence of complement, *in vitro*. They also demonstrated that the protection of mice from EBOV infection through the administration of monoclonal antibodies was most optimal with the murine IgG2a

subclass, which shows the greatest efficiency for mediating complement activation (407). Interestingly, this effect was not observed in a different study that investigated the potential for guinea pig complement to enhance neutralisation of EBOV with convalescent human plasma from the 1976 EBOV outbreak in Yambuku (364). There are some key differences between these two studies which may account for these observations. Firstly, the use of human plasma instead of purified monoclonal antibodies would likely reduce the complement-mediated enhancement of neutralisation, as only certain monoclonal antibodies in the vast polyclonal response will benefit from the addition of complement. Secondly, guinea pig complement demonstrates some functional differences to human complement which may account for some variation (408–410). Lastly, the works by Rimoin *et al* were investigating antibody responses in convalescent survivors forty years after infection. It has been reported that isotype switching to the non-complement activating IgG-4 isotype starts developing 1-2 years post-EBOV infection which may explain the lack of enhancement (411).

In survivors of the 2007 BDBV outbreak, robust polyfunctional antibody profiles remained 2 years post infection. The survivors with antibody functions capable of mediating antibody-dependent cellular phagocytosis, activating NK cells, or mediating antibody-dependent complement deposition (ADCD), had a significantly lower chance of developing hearing loss – a common sequelae of BDBV infection (267).

1.3.6 Antibody-Independent Mechanisms of Complement in EBOV Pathogenesis

Antibody-independent mechanisms of the complement system which influence EBOV pathogenesis have been described for the lectin pathway. MBL was first shown to bind the EBOV-GP (and MARV-GP) incorporated into the membrane of pseudotyped HIV particles. The binding of MBL to lectins on the EBOV-GP prevented its interactions with the host-receptor DC-SIGN, thus neutralising the pseudotyped virus. Neutralisation was significantly reduced with the use of MBL-deficient plasma

and neutralisation was replenished with the addition of MBL (157). MBL was later shown to have some therapeutic benefit against EBOV infection. Mice were administered with a lethal dose (100 PFU) of MA-EBOV either 12 hours before or 1 hour after treatment with recombinant MBL. MBL was administered at doses corresponding to 7- to 24-fold higher than average human plasma concentrations, every 12 hours for 10 days, which successfully rescued 40% of mice. This response was dependent on complement activation, as C3-deficient mice did not survive infection irrespective of MBL administration (412). As discussed previously, the EBOV-sGP is the primary transcript of the *GP* gene and is actively secreted from cells during EBOV infection. MBL reportedly binds to the EBOV-sGP. The treatment of EBOV-sGP with human sera prevented EBOV-sGP interactions with DC-SIGN and macrophages. Cytokine release and the expression of co-stimulatory molecules were subsequently inhibited. This effect was abolished with the use of MBL-deficient sera (413).

Whilst the majority of these studies show a protective effect of MBL against EBOV, one study has shown an MBL-mediated enhancement of EBOV infection under certain conditions. Using pseudotyped lentivirus with EBOV-GP, the addition of recombinant MBL enhanced infection of HEK 293F cells and primary human macrophages in a dose-dependent manner, *in vitro*. At low serum concentrations (< 10%), a similar enhancement of EBOV infection was also observed. However, when serum concentrations were increased above 10%, the enhancement of EBOV infection started to reverse. The proposed mechanism for this enhancement was *via* MBL-mediated lipid-raft-dependent macropinocytosis that preferentially utilised microtubules rather than microtubules and actin as seen in the canonical EBOV pathway (7). A similar enhancement of EBOV infection was observed for FCN-1, an alternative activator of the lectin pathway. FCN-1 was shown to bind sialylated moieties of the EBOV-GP MLD and, based on competition studies, likely uses a common host receptor for the mechanism of enhancement. The addition of FCN-1 showed a dose-dependent response in the enhancement of both EBOV-GP pseudo-typed viruses and wild-type EBOV infection into Vero E6 cells and human monocyte-

derived macrophages, irrespective of other complement proteins in serum (8). When the complement system can progress uninhibited however, its activation does not appear to play a role in ADE of EBOV infection (414).

In summary, there are many gaps in our knowledge and understanding of the complement system in EBOV pathogenesis. Whilst some aspects such as the binding of MBL appear to be protective, under certain conditions these have been shown to exacerbate infection. Similarly, whilst the C1q protein of the complement system has been associated with ADE, the presence of complement has been shown to enhance antibody-mediated neutralisation. In each study, the effects of the complement system are profound, but there is an overall disagreement in whether its involvement would be beneficial or detrimental.

1.4 Coronavirus Overview

The emergence of SARS-CoV-2 and the ongoing coronavirus disease (COVID)-19 pandemic has applied severe pressure on health infrastructures, devastated economies worldwide, resulted in over 6 million deaths across the globe, and continues to pose future threats with the emergence of new variants. I will begin this section with a brief overview of Coronaviruses, before focusing on SARS-CoV-2 and the relevance of the complement system to its pathogenesis.

1.4.1 Coronavirus Structure

Coronaviruses (CoVs) are enveloped, non-segmented, positive-sense RNA viruses, capable of infecting a range of animals and mammals to cause a broad scope of disease. The coronavirus group is subdivided *via* phylogenetic clustering into four genera: *Alphacoronaviruses*, *Betacoronaviruses*, *Gammacoronaviruses*, and *Deltacoronaviruses* (415). Alpha and beta CoVs infect mammals, gamma-CoVs infect avian species, and delta-CoVs infect both mammalian and avian species (416). Viruses in the *Coronavirus* genus contain relatively large genomes (26 - 32kb) (416), with two-thirds occupied by the open-reading frames (ORF)-1a and ORF-1b encoding non-structural proteins, and the remaining third encoding structural and accessory

proteins. The accessory proteins are generally nonessential for replication but do have roles in viral pathogenesis and are interspersed within structural genes at the 3' end. The overall genome organisation is 5'-ORF1a-ORF1b-spike(S)-envelope(E)-membrane(M)-nucleocapsid(N)-3' (415). Seven coronaviruses are known to be pathogenic to humans (HCoV), many of which cause mild symptoms (HCoV-NL63, HCoV-229E, HCoV-OC43, HCoV-HKU1), whilst others can cause more severe respiratory illnesses potentially resulting in death: SARS-CoV-1, SARS-CoV-2, and Middle Eastern respiratory syndrome (MERS)-CoV (416). The three HCoVs which cause the most severe disease in humans and are the most clinically relevant belong to the *Betacoronavirus* genus.

1.4.1 Coronavirus Lifecycle

For coronavirus infection of a host cell, the class I fusion spike protein must first bind the cell entry receptor. Specificity of the spike protein determines the viral tropism, such as the human aminopeptidase N (HCoV-229E), the angiotensin converting enzyme 2 (ACE2; HCoV-NL63, SARS-CoV-1, SARS-CoV-2), or the dipeptidyl peptidase 4 (MERS-CoV) (417). Host cell proteases such as the transmembrane serine protease 2 (TMPRSS2) or cathepsin B are then required for the cleavage of the spike protein. The virus enters the host cell through clathrin or non-clathrin mediated endocytosis, where the acidification of the endosome activates host proteases that promote viral fusion with the endosomal membrane and the release of viral RNA into the cytoplasm. Alternatively, fusion may occur at the cell-surface membrane (418,419). The genome is then translated to produce the viral replication-transcription complex (RTC). The RTC transcribes the genome into negative-sense RNA, followed by the translation of positive sense subgenomic mRNAs (sgmRNA). Viral structural proteins are translated from the sgmRNA by host ribosomes and are inserted into the endoplasmic reticulum (ER) membrane (spike, envelope, and membrane proteins) before translocating to the ER-Golgi intermediate compartment (ERGIC), or they remain in the cytoplasm (nucleocapsid protein). Viral RNA is then packaged into helical structures by the nucleocapsid protein, which interacts with the membrane

protein for virion assembly. The virions then bud from the ERGIC membranes and leave the cell *via* the exocytic pathway (415) (**Figure 8**).

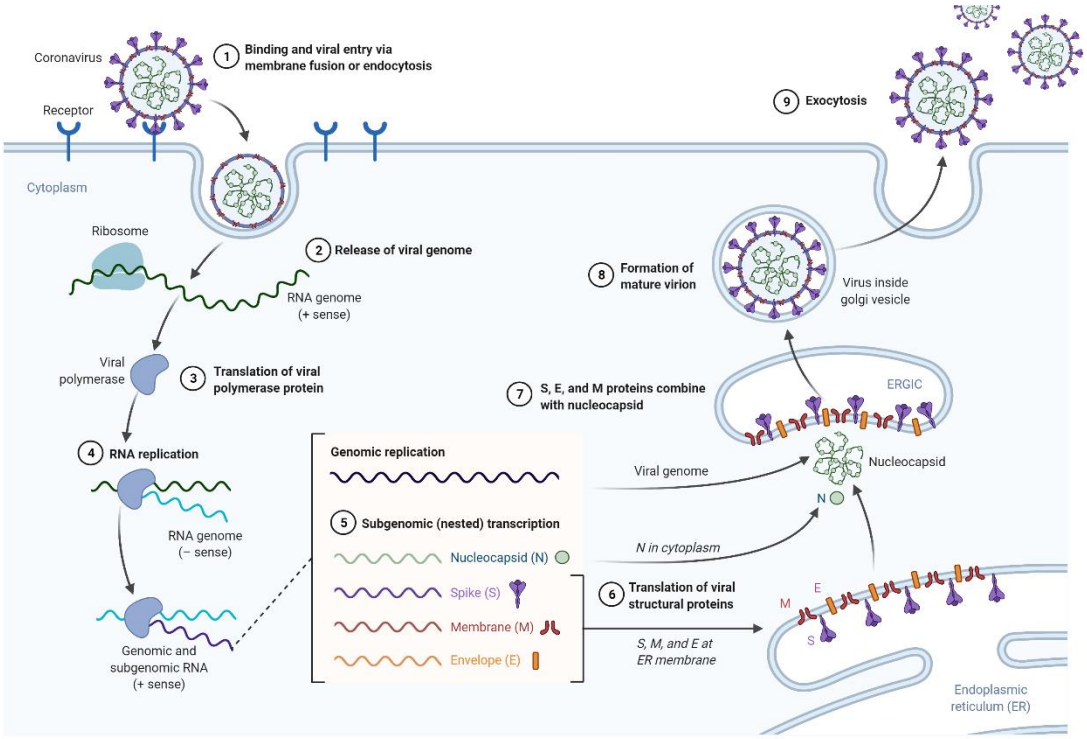

Figure 8: Lifecycle of Coronaviruses

1) *The virus first binds to the host receptor via its spike protein and enters the cell via membrane fusion or clathrin-mediated endocytosis.* ***2)*** *After entry, the viral genome is released into the cytoplasm and translated to produce the polyproteins pp1a and pp1ab.* ***3)*** *The polyproteins are processed further to produce the viral replication-transcription complex (RTC).* ***4)*** *The viral genome is then replicated by the RTC to produce negative-sense RNA.* ***5)*** *Positive-sense subgenomic mRNAs (sgmRNA) encoding the structural proteins are produced from the negative-sense RNA.* ***6)*** *sgmRNA is then translated to produce the structural proteins S, E, and M by host ribosomes on the endoplasmic reticulum (ER), which are inserted into the ER membrane, and move to the ER-Golgi intermediate compartment (ERGIC). The N protein is synthesised in the cytoplasm.* ***7)*** *The N protein packages viral RNA into helical structures and interacts with the M protein in the ERGIC for virion assembly.* ***8)*** *Virus particles move through the golgi apparatus towards the membrane surface.* ***9)*** *The virus then leaves the cell via exocytosis. This figure was adapted from the "Lifecycle of Coronavirus" template, by BioRender.com (2022). Retrieved from https://app.biorender.com/biorender-templates.*

1.4.1 *Betacoronaviruses*

The five viruses of the *Betacoronavirus* genus are: HCoV-OC43, HCoV-HKU1, SARS-CoV-1, MERS-CoV, and SARS-CoV-2. HCoV-OC43 was first identified in the 1960s and typically causes upper respiratory tract infections and symptoms consistent with the common cold, with very rare instances of progression to more severe lower respiratory tract infections (420–422). HCoV-HKU1 was first identified in 2005 and is one of the four endemic coronaviruses associated with common colds in humans, causing mild-to-moderate upper-respiratory tract illness (423,424). SARS-CoV-1 first emerged in the Guangdong Province of China in 2002 as the aetiological agent of severe atypical pneumonia in patients (425–427). Within three months, the SARS outbreak had spread to two Hong Kong hospitals, Singapore, Toronto, and Hanoi (425,426). The emergence of SARS-CoV-1 was associated with a live-animal retail market, where subsequent investigations found a SARS-CoV-1 related virus (sharing 99.8% sequence homology to SARS-CoV-1) in civet cats (*Paguma larvata*) and a raccoon dog (*Nyctereutes procyonoides*). Market workers also had neutralising antibodies to the isolated virus (428). Civet cats were the suspected natural reservoir host. However experimental SARS-CoV-1 infection of civet cats produced overt clinical symptoms (429) and the seroprevalence of SARS-CoV-1 in civet cats in surrounding areas shortly after the outbreak were remarkably low (430). The first SARS-CoV-1 outbreak was contained in July 2003 after a reported >8,000 cases and 774 deaths across >25 countries (431,432). MERS-CoV was first identified in the Kingdom of Saudi Arabia (KSA) in June 2012 following the hospitalisation of a man with respiratory and renal failure. Retrospective analysis showed the first known cases of MERS appeared in Jordan in April 2012, and the virus has since spread to 27 other countries (all incidences involve travel from the Arabian Peninsula) with over 2,500 known deaths and a CFR ~35% (433–435). The dromedary camel is a major viral host for transfer to humans, and bats are potentially the main mammalian reservoir (436).

1.5 SARS-CoV-2

The emergence of the fifth *Betacoronavirus* came in December of 2019, when a cluster of atypical pneumonia cases were reported in the Wuhan province of China. These cases were some of the clinical presentations first identified for the respiratory disease COVID-19, which led to the identification of a novel coronavirus, SARS-CoV-2, as the aetiological agent. The early cases were believed to originate from wild animals at a wholesale seafood market in the city of Huanan. The virus rapidly began to spread through China and to the rest of the world, affecting over 200 countries, and reaching pandemic status in March 2020 (437). The pandemic continues to date, and as of March 2022, the worldwide reported cases to the WHO have exceeded 460 million with over 6 million deaths (438).

SARS-CoV-2 belongs to the beta-CoV genus and the wild-type strain shares a similar genome (82%) and structural protein (>90%) sequence identity to SARS-CoV-1 and MERS-CoV within the same genus. An important difference between these Coronaviruses is the spike protein sequences which influence the host entry mechanisms. The MERS-CoV spike protein recognises the host dipeptidyl peptidase 4 receptor, whereas SARS-CoV-1 and SARS-CoV-2 spike proteins recognise the host angiotensin-converting enzyme (ACE)2 receptor (416). The origins of SARS-COV-2 are still unknown. The virus with the highest genome similarity (96.2%) to SARS-CoV-2 is the RaTG13-CoV, isolated from a bat in Yunnan in 2013 (439). The sequence similarity is enough to indicate a close ancestry but not the result of a direct spillover (440). Further evidence leans towards a possible recombination event leading to SARS-CoV-2 between RaTG13 and a Pangolin-CoV, with the latter showing greater RBD similarity, which could suggest a spillover directly from pangolins to humans (441).

The ~29.9kb genome of SARS-CoV-2 (**Figure 9**) is single-stranded positive-sense RNA which encodes four structural proteins (S, E, M, N) and sixteen non-structural proteins (NSP 1 – 16). The structural proteins are essential for the formation of the virion (**Figure 10**) whilst the functions of non-structural proteins include: RNA processing and replication, modulating host cell responses, modification of host cell

membranes, and modulation of protein trafficking (442). The spike protein is responsible for host cell receptor binding, attachment, and cellular entry using the ACE2 receptor and host enzymes including TMPRSS2 and furin (443,444). The envelope protein is a small integral membrane protein which contributes to virion assembly, maturation, and budding (443,445,446). The membrane protein coordinates the trafficking and assembly of virions, with a further role in pathogenesis as an IFN antagonist (443,446,447). The nucleocapsid protein directly binds the viral RNA to improve stability and to compact the genome for packaging, whilst its C-terminal domain recognises viral transcriptional regulatory sequences to regulate gene transcription (448–450) (**Table 4**).

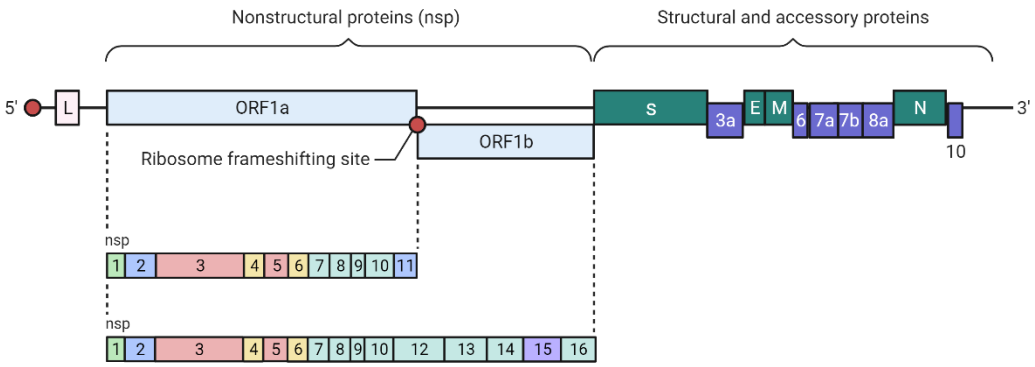

Figure 9: Overview of SARS-CoV-2 genome

The positive-sense SARS-CoV-2 RNA genome contains a leader sequence (L) at the 5' end, followed by two open-reading frames (ORF1a and ORF1b) which encode the polyproteins (PP) pp1a and pp1ab. The pp1a and pp1ab sequences are further cleaved into 16 non-structural proteins (NSPs). Towards the 3' end, are the structural and accessory proteins including the Spike (S), Envelope (E), Membrane (M), and Nucleocapsid (N) proteins. This figure was adapted from the "Genome Organization of SARS-CoV" template, by BioRender.com (2022). Retrieved from https://app.biorender.com/biorender-templates.

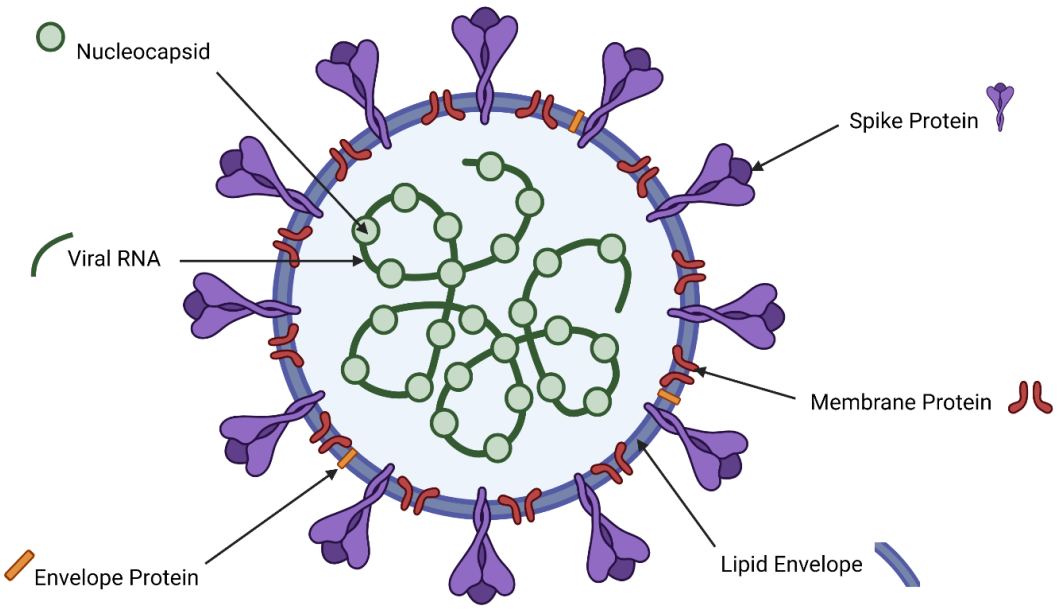

Figure 10: A schematic of the SARS-CoV-2 virion

This schematic shows the location of each SARS-CoV-2 structural protein, important for the formation of the virion. The spike protein is expressed on the surface of the virion and is required for cell entry. The envelope protein enables virion assembly, production, maturation, and budding. The membrane protein coordinates the trafficking and assembly of the virion. Lastly, the nucleocapsid protein directly binds and stabilises the viral RNA. This figure was adapted from the "Human Coronavirus Structure" template, by BioRender.com (2022). Retrieved from https://app.biorender.com/biorender-templates.

Structural Proteins	Function	Reference
Spike Protein	1) Host cell receptor binding, cell attachment, and cell entry	(443)
Envelope Protein	1) Viroporin ion channel across the endoplasmic reticulum-Golgi intermediate compartment membrane 2) Regulate intracellular trafficking and processing of the spike protein 3) Contributes to virion assembly, production, maturation, and budding	(443,445,446)
Membrane Protein	1) Coordinate virion assembly through interactions with all structural proteins 2) IFN antagonist 3) Regulate intracellular trafficking and processing of the spike protein	(443,446,447)
Nucleocapsid Protein	1) Directly binds viral RNA for stability, compaction, and regulation of gene transcription	(448–450)

Table 4: Overview of SARS-CoV-2 structural protein functions

A summary of the SARS-CoV-2 structural proteins and their primary functions.

1.5.1 Coronavirus Disease 2019 (COVID-19)

The symptoms of COVID-19 are broad and our understanding of the symptoms continue to evolve. Following an incubation period of 2-14 days, symptoms typically include but are not limited to: fever or chills; cough; fatigue; headache; sore throat; loss of taste or smell; shortness of breath or difficulty breathing; nausea or vomiting; diarrhoea. Illness can range from asymptomatic to severe. Symptoms of more severe illness include difficulty breathing, persistent pain or pressure in the chest, inability to stay awake or wake, confusion, and pale or discoloured skin. More severe illness can affect anyone but is more common in older adults with underlying health conditions such as diabetes or heart disease (451).

The emergence of new variants resulted in greater transmissibility of the virus, but a generally milder version of COVID-19, particularly for the Omicron variant. Despite the small percentage of cases requiring hospitalisation from infection, much of the pressure on healthcare systems came from the high volume of cases (452). The emergence of new variants also contributed to the number of cases of re-infection (453). Further complications may arise in the form of long COVID, where symptoms persist after infection. The symptoms of long COVID are broad and are currently known to affect respiratory, cardiovascular, neurological, GI, and musculoskeletal systems. One study has shown that the recovery time for the majority of COVID-19 patients exceeds 35 weeks (454) and the development of long COVID was not associated with the severity of acute illness (455).

Severe complications of COVID-19 include the development of acute respiratory distress syndrome (ARDS) and lung failure. ARDS is a life-threatening form of respiratory failure which causes diffuse alveolar damage in the lungs, characterised by the acute onset of bilateral infiltrates, severe hypoxemia, and lung oedema. Severe illness typically manifests approximately 1 week after symptom onset, where patients most commonly develop dyspnoea and hypoxemia, and progressive respiratory failure can develop. Other severe symptoms include lymphopenia; thromboembolic complications; central or peripheral nervous system disorders; acute kidney, cardiac, or liver injury; cardiac arrhythmias; rhabdomyolysis; coagulopathy; and shock (456).

1.5.2 SARS-CoV-2 Pathogenesis

The virus may enter the respiratory tract by inhalation of respiratory droplets from an infected person. From there, the primary target cells of infection are ciliated cells which induce type I and III IFN responses, IL-6 production, and activation of IFN stimulated genes in both infected and bystander cell populations (457,458). These observations by Ravindra *et al* extended to basal cells and club cells, although Fiege *et al* found that basal cells were relatively resistant to SARS-CoV-2 infection, which is likely the result of its near-absent expression of TMPRSS2 (459). The infection spreads

to secretory cells where the virus continues to replicate along with IL-6 upregulation (457,459,460). SARS-CoV-2 infection of ciliated and secretory cells causes cytopathic effects (CPE) in cell culture and morphological changes including cell fusion, apoptosis, destruction of epithelium integrity, cilium shrinking, and beaded changes (457). The mechanism of these host cells to then mediate mucociliary clearance is impaired. The virus can then continue to spread along the respiratory tract to the alveolar compartment where the tropism changes to targeting alveolar type II cells. Severe morbidity and mortality are sometimes caused by infection of alveolar type II cells of the distal lung and associated inflammation (461). Some differences between the alveolar region and the nasal passages may account for the more severe symptoms associated with type II alveolar infection. Alveolar infection results in the robust activation of pro-inflammatory cytokines with potential involvement of complement components secreted by alveolar epithelial cells (59). The alveolar compartment is less capable of clearing debris by mucociliary clearance and coughing, and much of the debris is phagocytosed by macrophages locally and transported to draining lymph nodes. Lastly, type II cells are the primary progenitor cells for alveolar epithelium and are susceptible to SARS-CoV-2 infection, whereas basal cells are the progenitor cells for the conducting airways and are not susceptible to SARS-CoV-2 infection (462).

SARS-CoV-2 may spread to the GI tract. The host receptors ACE2 and TMPRSS2 required for SARS-CoV-2 entry are highly expressed in absorptive enterocytes from the ileum and colon (463), and intestinal epithelium has been shown to support SARS-CoV-2 replication (464). Lehmann *et al* analysed biopsies of the small intestine from the early stages of infection in SARS-CoV-2 patients with mild to moderate diseases. They identified SARS-CoV-2 RNA and N protein in the duodenal mucosa and the activation of intraepithelial CD8+ T cells in infected intestinal epithelial cells, along with epithelial apoptosis (465).

The ACE2 receptor is primarily expressed on epithelial cells of the lung and intestine but is readily detectable in pericytes and the endothelium of coronary arteries

(466,467), podocytes and tubular epithelium in human kidneys (468,469), and the ovaries, uterus, vagina, and placenta (470). The function of the spike protein also relies on cleavage by host proteins including TMPRSS2 and furin, to enable viral fusion (471). As part of the normal endocytic process, cytosolic Ca^{2+} ions are released from the endosomal environment *via* NAADP and a two-pore channel (TPC2). The acidic late-endosomal environment triggers fusion of the virion and endosomal cell membrane, leading to nucleocapsid release into the cytoplasm (472,473).

1.5.3 SARS-CoV-2 Protection

The development of high IgG antibody titres and neutralising IgG antibody titres show a strong association with vaccine efficacy, protection from infection/re-infection, and/or protection from severe COVID-19. The generation of SARS-CoV-2 antibodies from either vaccination or infection have been shown to offer at least temporary protection to individuals from becoming re-infected. The majority of reports show that this protection lasts for at least six months, although there is some decay in antibody titres (474–483).

Another major focus of protection against SARS-CoV-2 infection and severe COVID-19 is the development of specific and robust T cell responses. Firstly, the development of SARS-CoV-2 spike-specific CD4+ T cell responses in COVID-19 convalescent patients has been shown to correlate with SARS-CoV-2 IgG and IgA titres (484). SARS-CoV-2-specific CD4+ T cells were also identified in unexposed individuals, which suggests possible cross-reactivity from other circulating coronaviruses to SARS-CoV-2 (484). Tan *et al* observed that the early induction of functional IFN-γ-secreting T cells specific to SARS-CoV-2 was associated with rapid viral clearance and reduced disease severity (485). The notion that certain functional T cells may be protective is supported by Le Bert *et al*, as they found that T cell frequencies between asymptomatic and symptomatic individuals infected with SARS-CoV-2 were similar, but the former showed an increase in IFN-γ and IL-2 production, which suggests that asymptomatic cases appear to have a more robust cell-mediated immune response (486). However, the variance within these subsets is an important consideration, as

proliferating CD4+ and CD8+ T cells have been associated with severe COVID-19, whilst CD4+ T cells expressing *IL22* and CD8+ effector memory T cells were enriched in individuals with asymptomatic and mild infections within the same study (487). CD8+ lymphopenia in the peripheral blood has been reported for patients with severe COVID-19, which might suggest that a protective role in infection, as their decline is associated with an increase in systemic inflammation (488). Lastly, as the pandemic continues and new variants of concern continue to arise, T cells may be especially important as in some instances, they have been shown to target more conserved epitopes of SARS-CoV-2 variants of concern compared to antibody responses which lose neutralisation potency (489).

1.5.4 Complement and COVID-19

A characteristic marker of severe COVID-19 pathology is excessive inflammation which is in part attributed to activation of the complement system. Serum complement concentrations and markers of complement activity are shown to be elevated in COVID-19 patients compared to healthy or recovered controls, and with an increase with disease severity (490). A significant reduction in C3 (491–493), an increase in C3a (494,495), and an increase in C5a (494,496,497) have been associated with COVID-19 patients compared to healthy controls or patients with milder COVID-19 symptoms. Studies which interpret these results of COVID-19 patients compared to healthy controls should be interpreted with caution, as complement activity typically increases in response to infection and may be non-specific. For example, the development of more severe COVID-19 symptoms has been associated with a cytokine storm. De Nooijer *et al* showed that whilst markers of complement activation (C3a, C3c, C5b-9) were higher in COVID-19 patients compared to healthy controls, patients with COVID-19 and ARDS had a less profound increase in complement markers compared to patients with bacterial sepsis. However, complement markers were still associated with disease severity and mortality (495).

In many cases, the complement system has been associated with more severe COVID-19 symptoms. In lung tissue biopsies from patients that succumbed to COVID-19,

complement components C5b-9, C4d, and MASP-2 were deposited in the microvasculature (498). Ma *et al* measured markers of complement activation in COVID-19 patients that were admitted to ICU compared to hospitalised patients with influenza. Circulating markers of complement activation were significantly higher in the COVID-19 cohort, in particular the enhanced activation of the alterative pathway (499). Similarly, Charitos *et al* found an association between overactivation of the alternative pathway and severe COVID-19. COVID-19 patients that required invasive ventilation had a significant reduction in activity of the alternative pathway due to excessive activation and eventual complement consumption, compared to other COVID-19 patients. No significant difference was observed in the lectin pathway activity (500). A comparison of hospitalised COVID-19 patients compared to out-patients also found that uncontrolled complement activity and eventual consumption was associated with disease severity (501).

A retrospective study of 6,398 patients with SARS-CoV-2 infection showed that a history of macular degeneration (a proxy for complement activation disorders) and coagulation disorders were risk factors for COVID-19 morbidity and mortality, independent of age, sex, or history of smoking. Transcriptional profiling showed robust engagement and activation of the complement and coagulation pathways. Gene association studies showed that severe COVID-19 was associated with genetic variants in critical regulators of the complement and coagulation pathways. Hyperactive complement and coagulative genetic variations predisposed individuals to adverse outcomes with SARS-CoV-2 infection (502).

In summary, the majority of findings regarding the complement system and COVID-19 show its involvement is associated with adverse outcomes. However, a balance between its activation, without overactivation, may be beneficial to protection, particularly in the earlier stages of infection.

1.5.5 Antibody-Dependent Mechanisms of Complement in SARS-CoV-2 Pathogenesis

The IgG binding of COVID-19 convalescent plasma to the RBD of the spike protein was predominantly bound by the most efficient complement-activating subclasses, IgG-1 and IgG-3. The resulting complement deposition was found to correlate with IgG titre and disease severity, which suggests that complement activation may be more prominent in those with severe disease and/or higher IgG titres (503). However, it is worth noting that this mechanism would be less relevant during the initial stages of infection of a naïve individual, as the IgG response would not develop until later in infection. The chimpanzee adenovirus-vectored vaccine, ChAdOx1 nCoV-19, induced antibodies that were protective and capable of eliciting multiple immune effector functions including complement activation, which correlated with IgG titre. The significance of this complement activity on immunity is not clear (504).

1.5.6 Antibody-Independent Mechanisms of Complement in SARS-CoV-2 Pathogenesis

The spike and nucleocapsid proteins of SARS-CoV-2 have been shown to bind MBL, FCN-2, and CL-11 of the lectin pathway to promote complement deposition. HEK 293 T cells expressing the SARS-CoV-2 spike protein were more susceptible to C3b deposition and this process was impaired with the use of a MASP-2 inhibitor. Furthermore, the N protein is capable of directly binding the MASP-2 enzyme to activate the complement pathway (505), and the spike protein is capable of directly activating the alternative pathway (506). These observations show possible mechanisms of complement activation during SARS-CoV-2 infection of both naïve and previously exposed individuals.

In summary, there are many reports which associate high levels of complement activation with severe COVID-19. However, there is very little evidence which shows the underlying mechanisms of this complement activation and why this process is heightened for some individuals.

1.7 Research Aims

This PhD project utilised a combination of biochemical, molecular, and virology techniques in an attempt to improve our understanding of the role of complement in EBOV and SARS-CoV-2 pathogenesis. I first explored the antibody-independent interactions of complement with EBOV and SARS-CoV-2 proteins to understand how, and to what extent, the complement system is activated. I then investigated these interactions in the presence of antibodies using convalescent and/or vaccinee plasma, to understand the variability of complement-mediated responses following infection. Lastly, I explored the significance of both the antibody-dependent and antibody-independent mechanisms of complement for wild-type EBOV and SARS-CoV-2 neutralisation, to understand how these mechanisms might influence viral pathogenesis.

Chapter 2: Antibody-independent complement deposition

Aim: To determine the role of the lectin/alternative (antibody-independent) complement pathways in EBOV and SARS-CoV-2 pathogenesis.

Hypotheses:

- Differences in complement proteins at the genomic and/or proteomic level would be associated with EVD outcome.
- MBL of the lectin pathway would bind to all *Ebolavirus* and *Coronavirus* proteins of interest.
- The *Ebolavirus* and *Coronavirus* proteins of interest would activate the complement system to completion, independent of antibodies.

Goals (EBOV):

- Investigate potential differences in complement proteins at the genomic and proteomic levels of convalescent EBOV plasma that may have contributed to their survival.

- Develop novel ELISAs and western blot assays to determine whether MBL is capable of binding, and to what extent, to the EBOV-GP, EBOV-sGP, and SUDV-GP.
- Develop novel ELISAs to determine whether the complement system is activated to completion following stimulation from EBOV-GP, EBOV-sGP, and SUDV-GP, independent of antibodies.

Goals (SARS-CoV-2):

- Re-purpose novel ELISAs to assess whether MBL is able to bind the SARS-CoV-2 spike protein.
- Re-purpose novel ELISAs to assess whether the SARS-CoV-2 spike protein is capable of activating the complement system to completion, independent of antibodies.

Chapter 3: Antibody-dependent complement deposition

Aim: To investigate the differential responses of ADCD in response to EBOV and SARS-CoV-2 glycoproteins using convalescent and/or vaccinee plasma.

Hypotheses:

- Low-neutralising, convalescent EVD plasma would be capable of mediating ADCD as a possible Fc-mediated function for protection.
- Vaccine-induced SARS-CoV-2 spike antibodies would be capable of mediating ADCD as a possible Fc-mediated function for protection.
- The potential for SARS-CoV-2 convalescent plasma to mediate ADCD would be associated with disease severity.

Goals (EBOV):

- Design and develop novel flow cytometry assays to assess the extent of ADCD with convalescent EBOV plasma in response to EBOV-GP, EBOV-sGP, and SUDV-GP.

Goals (SARS-CoV-2):

- Re-purpose ADCD flow cytometry assays to assess immune effector functions of ChAdOX1 nCoV-19 vaccinee plasma and SARS-CoV-2 convalescent plasma. This work was conducted in collaboration with the University of Oxford and the Pathogen Immunology Group at the United Kingdom Health Security Agency (UKHSA).

Chapter 4: Complement-mediated neutralisation

Aim: Considering the evidence collected in Chapters 2 and 3, determine whether the complement system has any influence on EBOV and SARS-CoV-2 neutralisation.

Hypotheses:

- Independent of antibodies, the complement system would be able to influence EBOV and SARS-CoV-2 neutralisation.
- The complement system would enhance the neutralisation of low-neutralising antibodies against wild-type EBOV and SARS-CoV-2.

Goals (EBOV):

- Supplement wild-type EBOV neutralisation assays with exogenous human plasma as a source of complement to determine whether: **A)** the complement system can neutralise EBOV, and **B)** does the complement system enhance the neutralisation of low-neutralising EBOV-GP antibodies.

Goals (SARS-CoV-2):

- Supplement wild-type SARS-CoV-2 neutralisation assays with exogenous human plasma as a source of complement to determine whether: **A)** the complement system can neutralise SARS-CoV-2 and **B)** does the complement system enhance the neutralisation of low-neutralising SARS-CoV-2 S antibodies.
- Investigate the effects of recombinant MBL on SARS-CoV-2 neutralisation following the evidence collected in Chapter 2.

Chapter 2: Antibody-Independent Complement Deposition

2.1 Introduction

The complement system is a component of innate immunity found in a wide array of species including bats (507), cows (508), deer (509), pigs (510), rabbits (511), and rats (511). It can form one of the first lines of defence against viruses and its impact on disease progression can persist after viral clearance (1). Bloodborne pathogens, such as EBOV, and even respiratory pathogens such as SARS-CoV-2, would encounter the complement system during the course of infection of their mammalian hosts. In this chapter, I explored the antibody-independent components of the complement system in response to a range of *Ebolavirus* and *Coronavirus* glycoproteins (GPs) to understand the mechanisms involved in their pathogenesis, before the development of an adaptive immune response.

The lectin and alternative complement pathways can function independently of antibodies. Typically, proteins of the lectin pathway, such as mannose-binding lectin (MBL) or ficolin-1 (FCN-1), bind to the glycosylated regions of viral proteins and activate the complement system. The alternative pathway can then augment the lectin (and classical) pathways, or the alternative pathway can activate spontaneously on microbial surfaces *via* the hydrolysis of C3. The plasma concentrations and functionality of complement proteins within these pathways can vary greatly between individuals, and this is reflected in their genome and proteome (74,79,82,512–517). Single nucleotide polymorphisms (SNPs), such as those seen for MBL and FCN-1, are reportedly common within certain ethnic populations and can significantly influence an individual's resistance to infection and/or the severity of disease (69,70,72–76). Three SNPs within the *MBL2* promoter region have been shown to significantly alter promoter activity and MBL transcription levels: L/H (rs11003125), Y/X (rs7096206), and P/Q (rs7095891) (514). Three SNPs in exon 1 of *MBL2* are often implicated in disease and have been shown to impact protein function and expression, located at: codon 52 (rs5030737) (513), codon 54 (rs1800450) (512), and codon 57 (rs1800451) (516). Similarly, SNPs in the *FCN1* gene at locations rs10120023 and rs10117466 significantly impact circulating levels of FCN-

1 (79,517). For SARS-CoV-2, *MBL* SNPs have been associated with increased COVID-19 severity (518). Variations in the plasma concentration and function of MBL and FCN-1 could also be important for EBOV pathogenesis, as both proteins have been shown to influence EBOV infection and disease outcome (7,8,157,412,413).

As discussed in **Chapter 1**, both MBL and FCN-1 have been shown to influence EBOV infection. MBL has been shown to limit EBOV infection *in vitro* by preventing the interactions of the EBOV-GP and EBOV-sGP with DC-SIGN (157,413). Recombinant MBL also showed therapeutic potential *in vivo* by rescuing 40% of mice infected with a lethal dose of MA-EBOV (412). However, both MBL and FCN-1 have shown a dose-dependent enhancement of EBOV infection *in vitro* (7,8). Therefore, it seems plausible that *MBL* and *FCN1* SNPs which influence the function and expression of these proteins, may also influence EBOV infection. This is an aspect of potential EBOV immunity which has not previously been explored.

Whilst these studies of the genome and proteome are useful for finding associations with disease and/or protection, they do not confirm causal relationships. The previous studies which show the potential role of lectins in EBOV pathogenesis do not show the downstream effects of complement activation beyond the cleavage of C4 (7), nor the implications of this. As previously discussed, multiple regulation points exist within the complement system that can be manipulated by viral proteins to down-regulate or inhibit its activity, such as the factor I-like activity exhibited by Chikungunya virus and Nipah virus to destabilise the complement system at the cleavage of C3 (181,182). So, although the EBOV-GP and EBOV-sGP can bind MBL to induce the cleavage of C4, the effect on the downstream mechanisms important for inflammation, chemotaxis, and lysis, are unknown. These responses could be important, as high levels of inflammation are a hallmark of EVD that is significantly associated with disease severity and fatal outcomes (345,519,520). Chemotaxis includes the recruitment of DCs and macrophages, but this mechanism can lead to a more systemic spread of EBOV as they are the primary target cells for infection (335–339). Complement-mediated lysis could provide some level of protection against

EBOV, as it has been shown to lyse infected cells and target virions in other viral infections (19,159,160,175).

In this chapter, we wanted to determine the role of the lectin/alternative (antibody-independent) complement pathways in EBOV pathogenesis. We hypothesised that genomic and proteomic differences in complement proteins would be associated with EVD survival; that MBL would bind to all *Ebolavirus* glycoproteins of interest; and that these *Ebolavirus* glycoproteins would activate the complement system to completion, independent of antibodies. I first utilised a genomic (polymerase chain reaction [PCR] and next-generation sequencing [NGS]) and proteomic approach (liquid chromatography – mass spectrometry/ mass spectrometry [LC-MS/MS]) to investigate *MBL* and *FCN-1* SNPs, and possible variations in the levels of circulating plasma proteins, between EVD survivors and EVD naïve controls. We observed large diversity in the SNPs within our Guinean population but did not observe any significant differences between cohorts. We also developed novel ELISAs to investigate the potential for MBL binding and complement deposition in response to a range of *Ebolavirus* glycoproteins, to determine which proteins could activate the complement system, and whether this led to the final formation of the membrane attack complex (MAC).

Following the emergence of SARS-CoV-2, early observations of patients with severe COVID-19 showed significantly higher levels of complement proteins and inflammation compared to healthy individuals and patients with milder COVID-19 symptoms (491–497). At the time of this study, no viral mechanism to explain this complement activation, nor to what extent the complement system was activated, had been determined. We hypothesised that MBL would bind to the SARS-CoV-2 spike protein, and that the spike protein would activate the complement system to completion, independent of antibodies. I was able to modify my MBL binding and C5b-9 deposition ELISAs developed within this chapter, to address these hypotheses.

2.2 Methods

2.2.1 Sample Collection and Ethics

West African plasma samples from survivors of the 2013-2016 EBOV outbreak, and negative individuals from the same region who did not come into contact with known EBOV-infected patients, nor did they present with EVD symptoms, were collected as part of a longitudinal study from 2015-2017 (372). Ethical approval for the collection and uses of this plasma was obtained from the National Ethics Committee for Health Research, Guinea (33/CNERS/15) and from the National Research Ethics Service, UK. All volunteers were informed of the study procedures and purposes, and only consenting participants with written and informed consent were included.

Pooled human plasma (PHP) was collected as previously described (521) and used as the exogenous source of complement. Venous human blood was collected using butterfly cannulas and 50 ml syringes and immediately decanted into polypropylene centrifuge tubes containing 0.04 mg/ml Hirudin, on ice. The tubes were inverted to mix the blood and Hirudin. The tubes were then centrifuged at 3,000 x g for 10 min with no brake to separate the red blood cells and plasma. The plasma was then aliquoted into 0.2 ml or 0.5 ml polypropylene tubes and stored at -80^{0}C to be thawed and used immediately when required. During the course of this project, a total of three different batches of PHP were used. All batches were prepared in the same way and varied only in the number of donors, using either: 20 UK donors; 40 UK donors; or 5 UK donors. In this chapter, we used the PHP from 20 UK donors collected and processed by the Pathogen Immunology Group at the UKHSA.

2.2.2 Viral Proteins

All of the viral proteins used in this study were sourced externally and were expressed in HEK 293 cell lines to maintain consistency in protein glycosylation patterns (**Table 5**).

Protein	Strain (GenBank Accession number)	Company
EBOV-GP	Makona (AHX24649.1)	Nuffield Department of Medicine, University of Oxford
EBOV-sGP	Mayinga (AHC70242.1)	Integrated BioTherapeutics
HIV gp120	HIV-1 (ABL67444.1)	Abcam
SARS-CoV-1 Spike	Beijing02 (AY278487)	Immune Technologies
SARS-CoV-2 Spike	Wuhan (NA)	Lake Pharma
SUDV-GP	Gulu (YP_138523.1)	Sino Biological

Table 5: Viral proteins for ELISAs

All recombinant viral proteins used for the ELISAs were expressed in HEK 293 cells and were sourced from a range of suppliers. Abbreviations: not available (NA).

2.2.3 West African Plasma Isolation

Blood samples were collected in EDTA tubes and processed in the field (Conakry, Guinea) to isolate the plasma and peripheral blood mononuclear cells (PBMCs). First, Leucosep tubes with 15mL of ficoll were centrifuged at 800 xg for 15 min with no brake. The plasma was transferred to a clean 15 ml tube and centrifuged at 1,500 xg for 10 min before aliquoting and storing at -80^{o}C. PBMCs were also isolated and used for other research purposes (372,522) beyond the scope of this PhD project.

2.2.4 PCR Amplification of *MBL* and *FCN1* SNPs in West African Plasma Samples

Ten EBOV-GP IgG positive and five EBOV-GP IgG negative Guinean plasma samples were selected for SNP analysis. Two genomic regions containing six *MBL* or two *FCN1* SNPs known to influence protein expression and/or function were amplified *via* PCR. The *MBL* reverse primer (5' -CCAGGCAGTTTCCTCTGGAAGG- 3') was obtained from Kalia *et al* (523) and a novel forward primer (5' - TGGGAGGAGGATTCAAGGCAAGT- 3') was designed using DNASTAR (Version 14.0) and the Single Nucleotide Polymorphism Database to capture all six *MBL* SNPs. Forward (5' -GTCCACAGCGTGGCCTG- 3') and reverse primers (5' -CTTGTGCCACAGTTTCTCAAC- 3') for individual *FCN-1* SNPs (79)

were combined to capture all targets in a single assay, and their compatibility was assessed using the OligoEvaluator software (Merck).

The final 25 µl reaction volume consisted of 5 µl template DNA (1.5 - 2.0 ng/µl) or 5 µl PCR-grade water as a negative template control (NTC), and a 20 µl mastermix comprised of: 5 µl PCR-grade water, 1.25 µl of forward primer (10 µM), 1.25 µl of reverse primer (10 µM), and 12.5 µl of Q5® Hot Start High-Fidelity 2x Master Mix (New England Biolabs). The PCR cycling conditions using the Applied Biosystems Veriti Thermal Cycler were as follows: 1 cycle of 98°C for 2 min, 35 cycles of 98°C denaturation for 10 s, annealing for 30 s at 65°C (*FCN-1*) or 68°C (*MBL*), and extension at 72°C for 30 sec, followed by a final extension step at 72°C for 2 min.

2.2.5 DNA Purification and NGS of *MBL* and *FCN-1* SNPs

Following PCR amplification, the 25 µl PCR reaction mixture was mixed with 4.2 µl of Gel Loading Dye, Purple (6x, New England BioLabs), and loaded onto a 1% agarose gel with SYBR safe. The positive DNA fragments, along with the NTC and TrackIt™ 1kb Plus DNA ladder (New England Biolabs), were separated *via* gel electrophoresis and the desired DNA amplicons were isolated using the QIAquick Gel Extraction Kit (QIAGEN), according to the manufacturer's instructions. Samples were quantified *via* NanoDrop™ and diluted to 1 – 100 ng/µl with a minimum volume of 60 µl for MiSEQ NGS analysis at the UKHSA – Colindale. Consensus sequences from the raw NGS data were generated by Daniel Carter in the Genomics Group at the UKHSA – Porton Down.

The consensus sequences were then aligned to the reference genomes (FCN-1: NG_046982.2 and MBL: NG_008196.1) using DNASTAR (Version 14.0) to identify the SNPs of interest. The minor allele frequencies (MAFs) were calculated for each cohort and compared using Fisher's exact test (significance = P value < 0.05) to obtain significance values. The statistical power was then calculated using the observed MAFs as described by Chow *et al* (524).

2.2.6 LC-MS/MS of West African Plasma Samples

An initial categorisation of Guinean plasma samples was made for "survivors" (EBOV PCR positive), "contacts" (no confirmed EBOV PCR), and "negatives" (no contact with known EBOV-infected individuals). Ten samples were selected from each category for proteomic analysis *via* LC-MS/MS using previously published methods (525,526). Plasma protein concentrations were measured using the Pierce™ Coomassie (Bradford) Protein Assay Kit (ThermoFisher Scientific), according to the manufacturer's instructions. Eight volumes of 15% (w/v) trichloroacetic acid (TCA) in acetone were added to a plasma volume equivalent to 100 µg of protein and incubated overnight at -20°C. The samples were then centrifuged for 10 min at 14,000 rpm, 4°C. The pellets were washed with 200 µl of acetone and centrifuged for 1 min at 14,000 rpm. The acetone was then removed and the pellets air-dried. The pellets were then resuspended in 10 µl of 1% (w/v) RapiGest (Waters) and 150 µl of 50 mM ammonium bicarbonate, and incubated for 10 min at 80°C. The proteins were then reduced with the addition of 10 µl of 60 mM dithiothreitol (DTT, Sigma) and incubated for 10 min at 60°C. The samples were then alkylated with the addition of 10 µl of 180 mM iodoacetamide (Sigma) and incubated for 30 min at RT, in the dark. A further 10 µl of 60 mM DTT was then added and the samples were incubated for 10 min at RT. Proteomic-grade trypsin (Sigma-Aldrich) was added to the proteins at a protein:trypsin ratio of 50:1 for digestion, and the samples were incubated at 37°C overnight. Protein digestion was confirmed *via* SDS-PAGE. Trifluoroacetic acid was added at a final concentration of 0.5% (v/v) to the peptide samples before centrifugation for 30 min at 14,000 rpm. Peptides were analysed by on-line nanoflow LC using the Ultimate 3000 nano system (Dionex/Thermo Fisher Scientific).

The raw data was acquired by Stuart Armstrong at the Institute of Infection, Veterinary and Ecological Sciences, at the University of Liverpool, UK. Proteomics analysis was similar to that described by Aljabr *et al* (2019) (526). Thermo RAW files were imported into Progenesis LC–MS (version 4.1, Nonlinear Dynamics). Default settings were used for time alignment and peak selection, which were filtered to include only peaks with a charge state between +2 and +7. Spectral data were

analysed using the PEAKS studio X software (Bioinformatics Solutions Inc., Waterloo, ON, Canada, Bin Ma *et al*). Tandem MS data were searched against the *Homo sapiens* reference genome sequence (Uniprot, UP000189706) with a false discovery rate set at 1%. Search results were imported into Progenesis LC–MS as pepXML files. Peptide intensities were normalised against the reference run by Progenesis LC-MS to highlight relative differences in protein expression between sample groups. Only proteins with two or more identified peptides were included in quantitative analysis. Statistical analysis (ANOVA) of the data was performed using Progenesis LC-MS to identify significantly ($q \leq 0.05$, relative fold change ≥ 2) differentially expressed proteins.

A principle component analysis (PCA) was then performed using GraphPad prism software (version 9) to identify potential clusters within the samples and omit any outliers. A k-means cluster analysis in R studio (packages: tidyverse (527); readxl (528); FactoMineR (529); factoextra (530)) was also performed for a non-biased approach to determine possible sample clusters. Lastly, a cluster heatmap was performed in R studio (packages: ggplot2 (299); tidyverse (527); cluster (531)) with the normalised abundances to identify possible clusters between samples.

2.2.7 MBL Binding ELISA

MaxiSorp™ ELISA plates were coated in triplicate with 50 µl of viral antigen (HIV-1 gp120, EBOV-GP, EBOV-sGP, SUDV-GP, SARS-CoV-1, SARS-CoV-2) in Hanks Balanced Salt Solution with calcium and magnesium (HBSS) at a concentration of 4 µg/ml, or coated with HBSS only, then incubated overnight at 4°C. The plates were then washed four times with 200 µl of HBSS and blocked with 200 µl of HBSS containing 5% Fetal Calf Serum (FCS) and incubated at 37°C for 2 hrs, 900 rpm. All subsequent dilutions were made using HBSS with 2% FCS, and all subsequent wash steps used 200 µl of HBSS with 0.05% tween-20, four times. Plates were washed and incubated with 50 µl of MBL (R&D Systems) at four protein concentrations in a 1:2 dilution series, for 1 hr at RT, 900 rpm. Protein concentrations were adjusted for each viral protein to obtain a signal within the linear range of the standard cure, and varied from 4 µg/ml down

to 0.0156 µg/ml. The ELISA plates were then washed and incubated with 1 µg/ml (100 µl) of goat anti-MBL antibody (R&D Systems) at RT for 1 hr, 450 rpm. ELISA plates were washed and incubated with 1 µg/ml (100 µl) of a HRP-conjugated, cross-adsorbed anti-goat antibody (Life Technologies) at RT for 1 hr, 450 rpm. The plates were washed again before developing in 100 µl of One-Step Turbo TMB (ThermoFisher Scientific) for 10 min and stopped with 100 µl of 1 M sulfuric acid. The O.D. was determined at 450 nm using SoftMax® Pro 7 software and analysed using GraphPad Prism software (version 9). All assays were performed in duplicate.

As a negative control for each protein, 10 mM of EDTA was added during the incubation step with the highest concentration of MBL. Each plate also included HBSS-coated controls with the addition of 4 µg/ml MBL, two QC samples coated in triplicate with mannan, and a blank well which was subtracted from all values before analysis. The negative cut-off was determined using average of the HBSS-coated controls with 4 µg/ml MBL for all plates, plus three SDs. Each plate was then tested in duplicate with an intra-assay variation < 15% CV and an inter-assay variation ≤ 25% CV. All replicates were then averaged and two dilution points were used for interpolation from the standard curve using mannan, before averaging. Samples were then reported as the ability to bind MBL, relative to mannan.

2.2.8 SDS-PAGE to Assess Protein Purity

Viral proteins were deglycosylated using the PNGase F Glycan Cleavage Kit (ThermoFisher Scientific) according to the manufacturer's instructions. Both native and deglycosylated protein samples were diluted to a final concentration of 25 µg/ml in Laemmli lysis buffer (Merck) and incubated at 95°C for 10 min. Novex™ Sharp Pre-Stained Protein Standard (ThermoFisher Scientific) and MagicMark™ XP Western Protein Standard (ThermoFisher Scientific) were mixed with a 1:1 ratio for the final protein standard. Each sample was then loaded onto NuPAGE™ 4-12% Bis-Tris gels (ThermoFisher Scientific) at a concentration of 0.5 µg (or 10 µl of protein standard) and separated *via* gel electrophoresis with NuPAGE MOPS SDS buffer (Life Technology) and 500 µl of NuPAGE antioxidant (Life Technology) at 175 volts for 1 hr.

The gels were then stained with SimplyBlue™ SafeStain (ThermoFisher Scientific) according to the manufacturer's instructions and visualised using the ChemiDoc™ MP Imaging System (BioRad). The final images were then annotated using Inkscape software.

2.2.9 Western Blot Assays for MBL Binding

Both native and deglycosylated proteins were diluted in Laemmli lysis buffer (Merck) and loaded onto NuPAGE™ 4-12% Bis-Tris gels (ThermoFisher Scientific) at a final protein concentration of 0.250 µg (HIV gp120), 0.500 µg (EBOV-GP, SARS-CoV-1 spike), 2.000 µg (EBOV-sGP, SARS-CoV-2 spike), or 3.125 µg (SUDV-GP). Novex™ Sharp Pre-Stained Protein Standard (ThermoFisher Scientific) and MagicMark™ XP Western Protein Standard (ThermoFisher Scientific) were mixed in a 1:1 ratio for the protein standard, using 10 µl per well. Samples were separated *via* gel electrophoresis with NuPAGE MOPS SDS buffer (Life Technology) and 500 µl of NuPAGE antioxidant (Life Technology) at 175 volts for 1 hr and transferred to polyvinylidene difluoride (PVDF) membranes using the iBlot™ Transfer Stack (ThermoFisher Scientific), according to the manufacturer's instructions. PVDF membranes were then blocked using HBSS containing 5% skim milk and 0.05% tween-20, overnight at 4°C. The membranes were then incubated with 5 µg of MBL (R&D Systems) for 1 hr at RT. The membranes were then washed five times for 5 min with wash buffer (HBSS containing 0.05% tween-20) and incubated with 0.5 µg of goat anti-MBL antibody (R&D Systems) for 1 hr at RT. The membranes were then washed five times for 5 min with wash buffer and incubated with 0.5 µg of an HRP-conjugated, cross-adsorbed anti-goat antibody (Life Technologies) for 1 hr at RT. The membranes were then washed five times for 5 min with wash buffer and developed with Amersham ECL Prime (Cytiva) according to the manufacturer's instructions, for 5 min in the dark. The samples were then visualised using the ChemiDoc™ MP Imaging System (BioRad) and the final images were annotated using Inkscape software.

2.2.10 PHP IgG ELISA

IgG ELISAs were developed to verify that the preparations of PHP in this study did not contain antibodies to the viral proteins tested: HIV-1 gp120, EBOV-GP, EBOV-sGP, SUDV-GP, SARS-CoV-1, and SARS-CoV-2. MaxiSorp™ ELISA plates were coated in triplicate with 1 µg/ml of viral antigen (50 µl) in PBS and incubated overnight at 4°C. All subsequent dilutions were made with Blocker™ Casein in PBS (ThermoFisher Scientific) and all subsequent wash steps used 200 µl of PBS containing 0.05% Tween-20, six times. The plates were washed and blocked with 100 µl of Blocker™ Casein in PBS for 1 hr at RT. The plates were then washed, 50 µl of PHP or positive control sample (diluted 1:500 in PBS casein, listed below) was added, and the plates were incubated for 2 hrs at RT. The plates were washed again and 50 µl of anti-human IgG conjugated to alkaline phosphatase (1:1000 in PBS casein, Merck) was added to each well and incubated for 1 hr at RT. The plates were washed and developed with 100µl of 20 mg 4-nitrophenyl phosphate disodium salt hexahydrate (Merck) in Pierce™ Diethanolamine Substrate Buffer (ThermoFisher Scientific) for 20 min at RT, in the dark. The O.D. was measured at 405 nm and the data was analysed using GraphPad Prism software (version 9).

The samples tested were: the three unique batches of PHP, one UK EBOV-GP IgG negative plasma sample, and a pool of three West African EBOV-GP negative plasma samples. The positive control material was either seropositive plasma (HIV gp120, EBOV-GP, EBOV-sGP, SARS-CoV-2), seropositive EBOV-GP IgG plasma with known cross reactivity (SUDV-GP), or 0.5 µg/ml of monoclonal antibody (SARS-CoV-1). A blank well with substrate-only was subtracted from all values. A QC of EBOV-GP IgG positive plasma (1:500) with EBOV-GP coated wells was used for each assay. The intra-assay and inter-assay variations were < 25% CV.

2.2.11 C5b-9 Deposition ELISA

MaxiSorp™ ELISA plates were coated in triplicate with 50 µl of viral antigen (HIV-1 gp120, EBOV-GP, EBOV-sGP, SUDV-GP, SARS-CoV-1, SARS-CoV-2) in HBSS at a concentration of 10 µg/ml, or coated with HBSS only, and incubated overnight at 4°C.

The plates were then washed four times in 200 µl of HBSS and blocked with 200 µl of HBSS containing 5% FCS, incubated at 37°C for 2 hrs, 900 rpm. All subsequent dilutions were made using HBSS with 2% FCS, and all subsequent wash steps used 200 µl of HBSS with 0.05% tween-20, four times. The plates were washed and incubated with 50 µl of PHP at four dilutions in a 2:3 dilution series, for 1 hr at 37°C, 900 rpm. PHP dilutions were adjusted for each viral protein to obtain a signal within the linear range of the standard cure, and varied from 40% down to 1.48%. The plates were then washed and incubated with 100 µl of a mouse C5b-9 monoclonal antibody (SantaCruz Biotechnology) at a concentration of 2 µg/ml, for 1 hr at RT, 450 rpm. The plates were then washed and incubated with 100 µl of HRP-conjugated anti-mouse antibody (ThermoFisher Scientific) at a concentration of 2 µg/ml, for 1 hr at RT, 450 rpm. The plates were washed again before developing in 100 µl of One-Step Turbo TMB (ThermoFisher Scientific) for 10 min and stopped with 100 µl of 1 M sulfuric acid. The O.D. was measured at 450 nm using SoftMax® Pro 7 software and analysed using GraphPad Prism software (version 9). All assays were performed in duplicate.

As a negative control for each protein, 10mM of EDTA was added during the incubation with the highest concentration of PHP. Each plate also included HBSS-coated controls with the addition of 20% PHP, two QC samples coated in triplicate with mannan, and a blank well which was subtracted from all values before analysis. The negative cut-off was determined using the average of the HBSS-coated controls with 20% PHP for all plates, plus three SDs. Each plate was then tested in duplicate. All assays were then normalised using the percentage difference of the two QCs across all plates, with intra-assay and inter-assay variations < 25% for samples above the negative threshold (0.1 O.D.). All replicates were then averaged and two dilution points were used for interpolation from the standard curve using mannan, before averaging. Samples were then reported as the ability to mediate complement deposition, relative to mannan.

2.3 Results

2.3.1 PCR Amplification of *MBL* and *FCN1* SNPs

A combination of commercial and custom PCR primers were used to amplify the desired regions containing known SNPs of the *MBL* and *FCN1* genes, which influence protein function and plasma concentrations. PCR amplicons were successfully amplified for each of these regions in ten EBOV survivor samples and five EBOV naïve samples. The amplicons were separated *via* gel electrophoresis (**Figure 11**) and prepared for NGS.

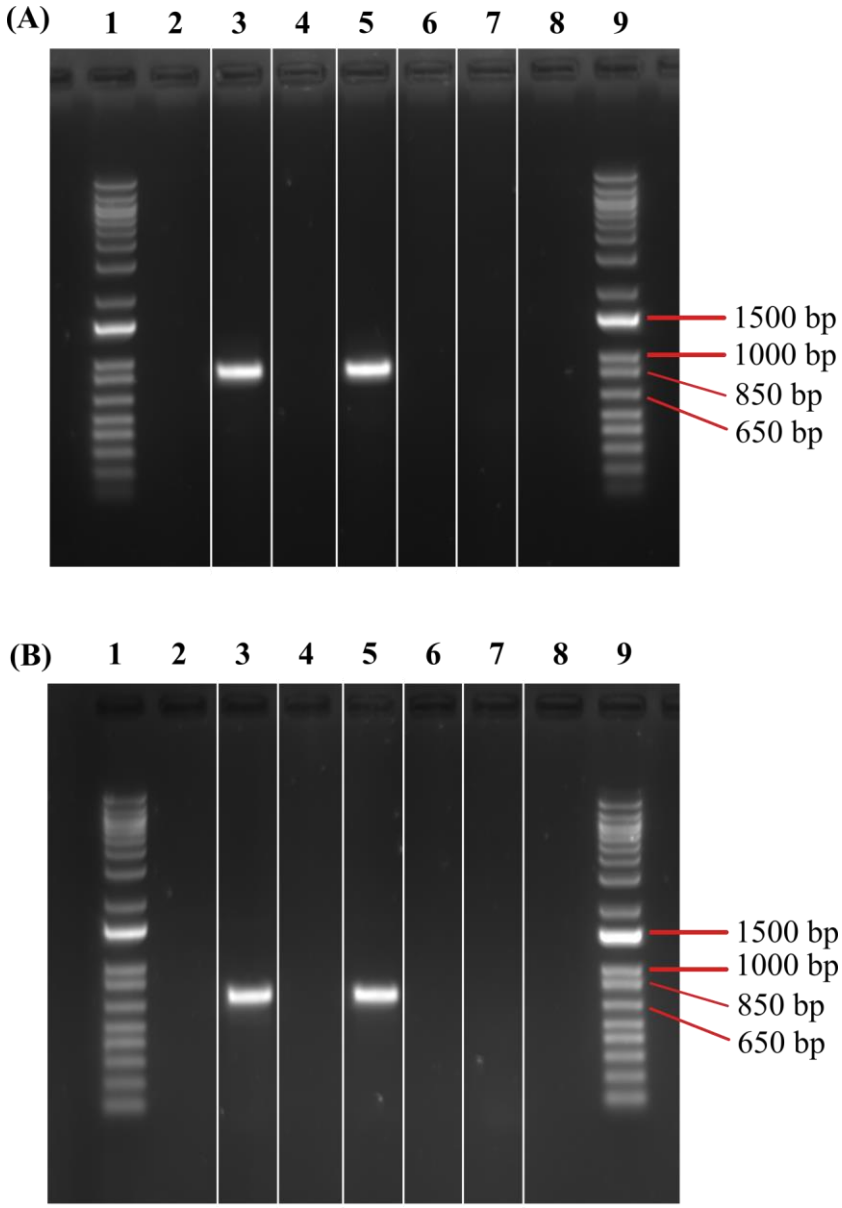

Figure 11: Gel electrophoresis of *MBL* and *FCN1* PCR amplicons

Example data of gel electrophoresis using two West African plasma sample PCR amplicons and a negative template control. ***A)*** *Lanes 1 and 9 show the 1kb DNA ladder. Lanes 3 and 5 show the PCR amplicon from the MBL gene at the expected size (842bp). Lane 7 was a negative template control. Lanes 2, 4, 6, and 8 were empty.* ***(B)*** *Lanes 1 and 9 show the 1kb DNA ladder. Lanes 3 and 5 show the PCR amplicon from the FCN-1 gene at the expected size (699bp). Lane 7 was a negative template control. Lanes 2, 4, 6, and 8 were empty.*

2.3.2 MBL and FCN-1 Genotypes of EBOV Convalescent Plasma

Following the PCR amplification and NGS of *MBL* and *FCN-1* SNPs, the consensus NGS sequences were aligned to reference genomes (*MBL*: GenBank accession number: NG_008196.1, *FCN1*: GenBank accession number: NG_046982.2) to identify the SNPs of interest. A mixture of homozygous and heterozygous variants were identified for the majority of the SNPs. MAFs were calculated for each of the variants to determine the frequency of the mutant allele within our sample cohort. The Fisher's exact test revealed no significant difference (significance = $P < 0.05$) in the MAFs between the cohorts. However, calculation of the statistical power of this pilot study, factoring in our results from the MAFs within our cohort, shows that the statistical analysis of only one SNP (rs101174) provides over > 80% confidence of avoiding a type II error (**Table 6**). Based on the results from this pilot study, we observed large variation in functional *MBL* and *FCN1* SNPs and based on the MAF, we could calculate the approximate sample number required to achieve a statistical power > 80% for calculating statistical significance. Unfortunately, the required number of samples to achieve this level of statistical power was not deemed suitable for this study.

MBL				
SNP ID	**Survivor MAF (N = 20)**	**Negative MAF (N = 10)**	**Fisher's Test (P value)**	**Power**
rs11003125	0.15	0.10	> 0.999	0.108
rs7096206	0.10	0.30	0.300	0.584
rs7095891	0.45	0.40	> 0.999	0.074
rs5030737	0.00	0.00	> 0.999	NA
rs1800450	0.00	0.00	> 0.999	NA
rs1800451	0.15	0.10	> 0.999	0.108
FCN-1				
SNP ID	**Survivor MAF (N = 20)**	**Negative MAF (N = 10)**	**Fisher's Test (P value)**	**Power**
rs101200	0.40	0.20	0.480	0.545
rs101174	0.35	0.10	0.210	0.859

Table 6: Pilot study of *MBL* and *FCN1* SNPs in Guinean plasma samples

A summary of the next generation sequencing analysis from ten EBOV survivors and five EBOV naïve plasma samples. No significant difference was observed in the minor allele frequencies (MAFs) between the two cohorts using a Fisher's exact test (significance = P < 0.05). Calculation of the statistical power based on MAFs suggests that only one sample was above > 80% confidence of avoiding a type II error, and that a much higher sample number would be required to determine significant differences. Abbreviations: minor allele frequency (MAF); not applicable (NA); single nucleotide polymorphism (SNP).

2.3.3 LC-MS/MS Data Analysis

Whilst there was no significant difference observed for the SNPs between EBOV convalescent and naïve (negative) plasma, variations could still exist at the protein level. Initial investigations using commercial ELISAs to determine plasma levels of MBL, FCN-1, and C1q did not show any significant difference between EBOV convalescent and negative samples (Appendix I, **Figure 23**). To broaden these investigations, an LC-MS/MS approach was adopted for thirty plasma samples: 10 survivors, 10 contacts, and 10 negatives. Although we were able to identify various complement proteins in this analysis, no significant difference was observed between the cohorts following the ANOVA (significance = P < 0.05) and Mann Whitney tests with the Benjamini Hochberg correction (1%). A PCA was then used to try and

determine potential clusters between the samples (**Figure 12**). Sample S2 was identified as an outlier and excluded from further analysis (Appendix I, **Figure 24**).

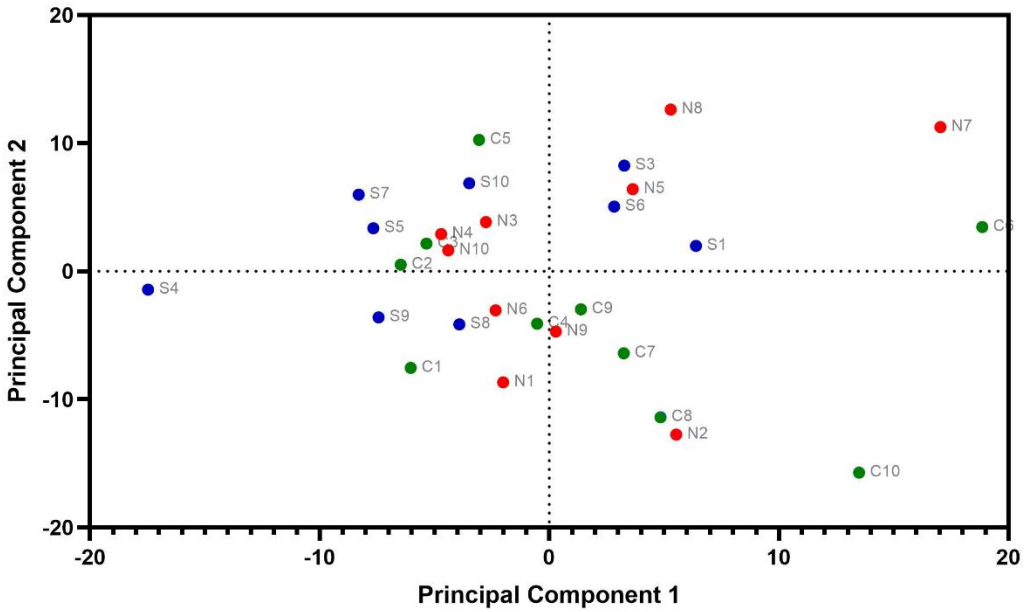

Figure 12: PCA of LC-MS/MS samples

The PCA of all samples (excluding S2) did not show any obvious clustering of samples. The PCA was calculated using GraphPad Prism software (version 9) and the graphs were overlaid using the GNU Image Manipulation Program (version 2.10.30). Each dot represents a sample from a survivor (S) in blue, a contact (C) in red, or a negative (N) individual in green.

A K-means clustering analysis was used as an unbiased approach to visualise potential clusters between the samples (**Figure 13**), but did not reveal any clear distinction between the cohorts.

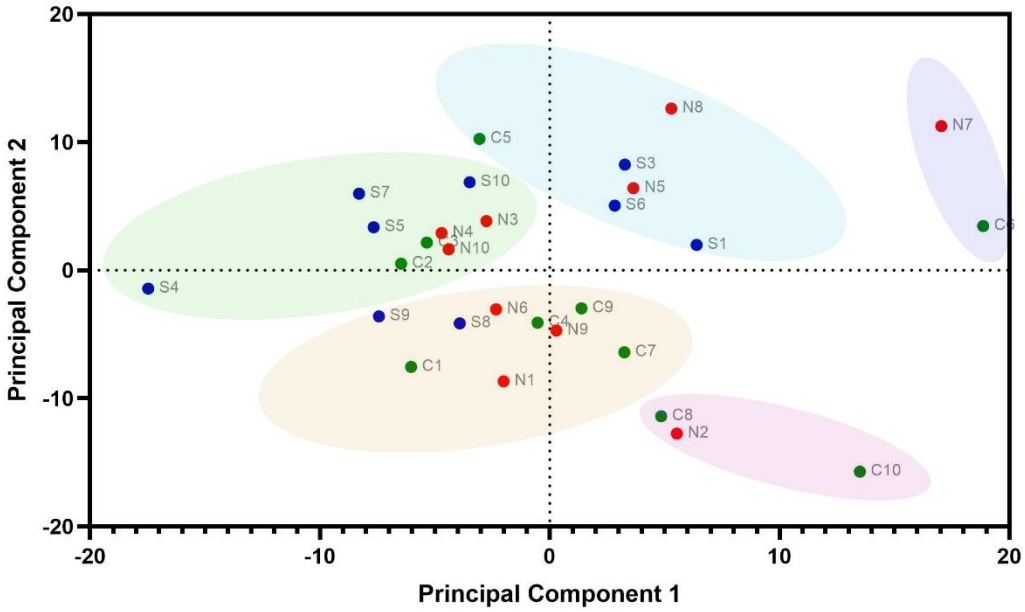

Figure 13: K-means clustering of PCA groups

A K-means clustering analysis of the PCA clusters was performed using R Studio with the following packages: tidyverse; readxl; FactoMineR; factoextra. There was no clear difference between the cohorts following the k-means cluster analysis. The original PCA was performed using GraphPad Prism software (version 9) and the image overlaid in the GNU Image Manipulation Program (version 2.10.30). Each dot represents a sample from a survivor (S) in blue, a contact (C) in red, or a negative (N) in green. Each coloured oval represents a cluster determined by the K-means analysis.

Lastly, a clustered heatmap was used to identify possible variations between the samples with all of the LC-MS/MS data collected (**Figure 14**). Again, there were no clear differences between the samples tested.

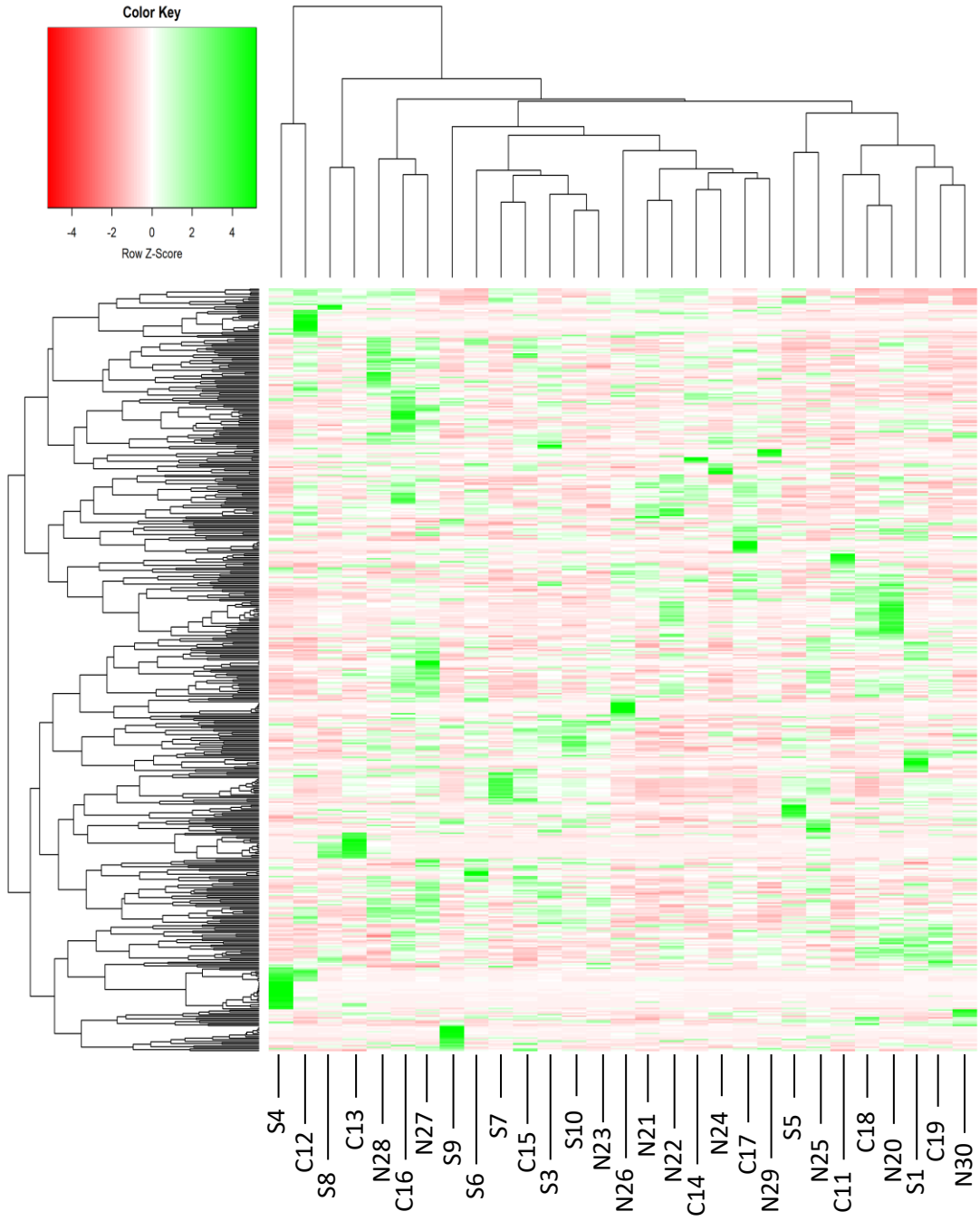

Figure 14: Heatmap of LC-MS/MS samples

The cluster heatmap was performed for all samples (excluding S2) using R Studio with the following packages: ggplot2; tidyverse; cluster. Each column represents a sample from a survivor (S), contact (C), or negative (N) individual and the hierarchical clustering for sample similarity is shown with the horizontal dendrogram. Each row shows the normalised values for each protein detected by the LC-MS/MS, with high expression in green and low expression in red. The hierarchical clustering of protein expression is shown with the vertical dendrogram. There was no clear difference in clustering between the cohorts.

2.3.4 MBL Binding ELISA with Viral Proteins

The genomic and proteomic pilot studies did not provide sufficient evidence to warrant continuation of this approach, although significant differences may be observed with larger sample numbers. Instead, a more practical approach was adopted to resolve unanswered questions regarding MBL interactions with *Ebolavirus* and *Coronavirus* proteins, and the downstream effects on complement activation.

We developed novel ELISAs to measure the binding capability of recombinant MBL to the *Ebolavirus* (EBOV-GP, EBOV-sGP, SUDV-GP) and *Coronavirus* (SARS-CoV-1 spike, SARS-CoV-2 spike) proteins of interest, with the additional use of mannan and HIVgp120 as positive controls. This was an important pre-requisite to determine activation of the lectin pathway and to identify potentially novel interactions of MBL with the SUDV-GP and SARS-CoV-2 spike protein. MBL bound to all of the viral proteins of interest and this binding was abolished with the addition of EDTA (which chelates the calcium ions essential for the formation of the MBL complex) at the MBL binding stage (Appendix I, **Figure 31**), or with the use of HBSS-only coated wells. A broad dilution of recombinant MBL was required to obtain an O.D. within the linear range for all of the proteins used (**Figure 15**, **(A)**), so that the results could be interpolated from the standard curve (Appendix I, **Figure 30**) and presented as the efficiency of MBL binding relative to mannan (**Figure 15**, **(B)**). The HIV gp120 protein and the mannan carbohydrate were known to bind MBL and showed a strong capacity for MBL binding in this assay. The EBOV-GP and EBOV-sGP (Mayinga variants) were also known to bind MBL and we confirmed this in our assays, but using the Makona variant of the EBOV-GP. Our observations of MBL binding to the SUDV-GP were novel, and we observed a significant (Mann Whitney test at 1 µg/ml MBL, $P = 0.002$) 4.2-fold reduction in MBL binding compared to the EBOV-GP. We also confirmed the binding of MBL to the SARS-CoV-1 spike protein, which was observed previously in two out of three studies (77,166,532). Lastly, we were able to determine MBL binding to the SARS-CoV-2 spike protein, which was significantly lower (Mann

Whitney test at 1 µg/ml MBL, P = 0.002) with a 1.42-fold change reduction in MBL binding compared to the SARS-CoV-1 spike protein.

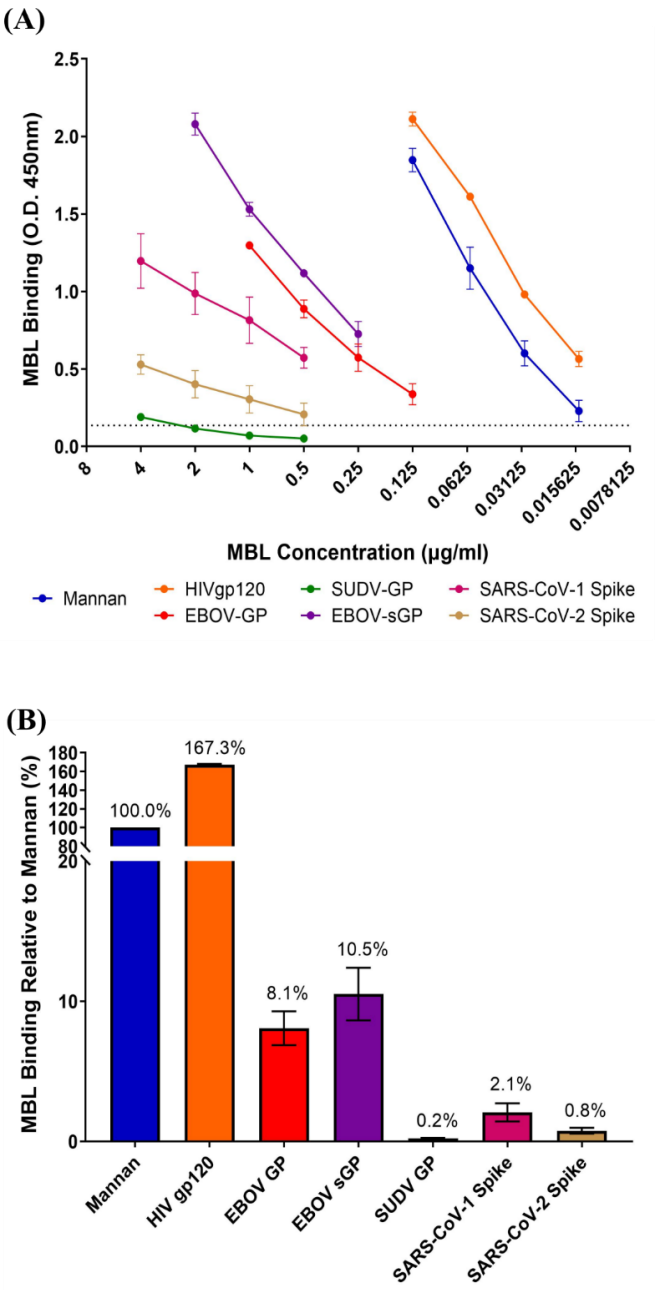

Figure 15: MBL binding ELISA

MBL binding ELISAs were performed on all viral proteins with mannan and HIV gp120 as positive controls. ***(A)*** *MBL was titrated against each protein to determine a linear range of MBL binding for interpolation. A negative cut-off (grey dotted line) was determined using HBSS-only wells incubated with 4 µg/ml of MBL plus three SDs. Each dot represents the mean value of triplicate samples across duplicate assays (total n =*

6) with error bars to show the variation. ***(B)*** *Two dilution points from the MBL titration for each protein were then used for interpolation from the standard curve (**Figure 30**), and then averaged to determine the relative efficiency of MBL binding compared to mannan. The error bars represent the variation of the two dilution points after interpolation. All samples were analysed using GraphPad Prism software (version 9).*

2.3.5 SDS-PAGE Analysis of Viral Proteins

After the confirmation of MBL binding to the *Ebolavirus* and *Coronavirus* glycoproteins *via* ELISA, SDS-PAGE assays were used to check for impurities within the protein samples that could influence the results, and to check the protein integrity following deglycosylation with PNGase F. All native proteins appeared at the expected positions on the gel relative to their molecular weight, with no unexpected bands visible that would suggest sample impurity. Proteins treated with the PNGase F enzyme migrated faster through the gel which indicated the removal of the N-linked glycans, and the PNGase F enzyme was visible on the gel at a molecular weight between 30 – 40 kDa, which is in concordance with its reported molecular weight of 36 kDa. Despite the final concentration of 200 mM DTT in each protein sample, the proteins appeared denatured but not reduced, as only single bands were observed for each protein at its total molecular weight (**Figure 16** and **Figure 17**).

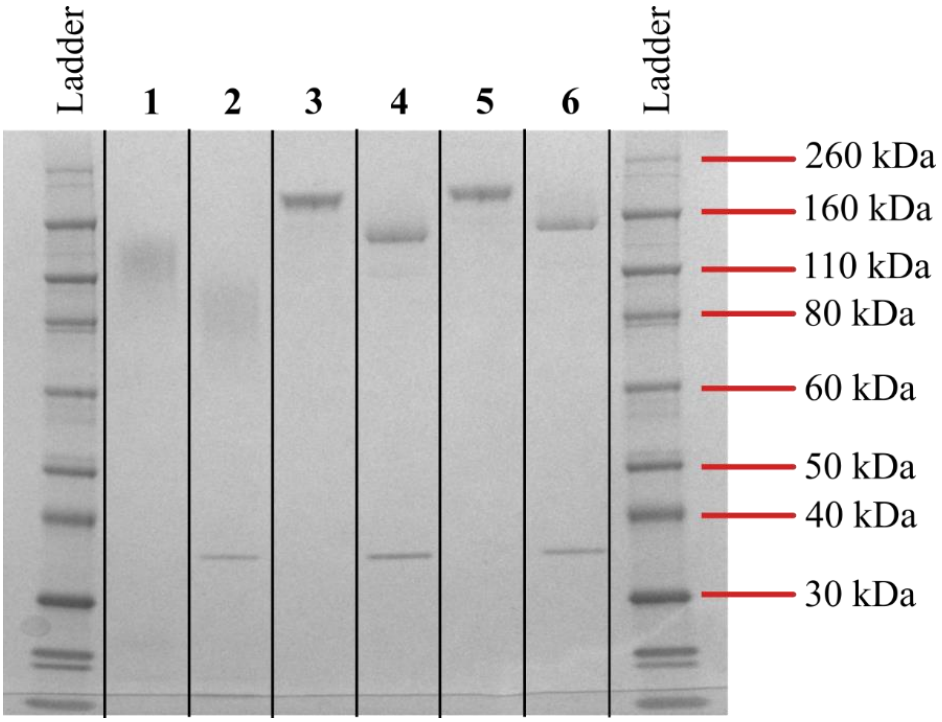

Figure 16: SDS-PAGE of SUDV-GP, SARS-CoV-1 spike, and SARS-CoV-2 spike

1: *SUDV-GP,* ***2:*** *PNGase F-treated SUDV-GP,* ***3:*** *SARS-CoV-1 spike,* ***4:*** *PNGase F-treated SARS-CoV-1 spike,* ***5:*** *SARS-CoV-2 spike,* ***6:*** *PNGase F-treated SARS-CoV-2 spike. All samples were loaded with 0.5 µg of protein and stained with SimplyBlue™ SafeStain (ThermoFisher Scientific). The image was taken using the ChemiDoc™ MP Imaging System (BioRad) and annotated using Inkscape software. All native proteins migrated relative to their approximate molecular weight whilst the deglycosylated proteins migrated through the gel at a faster rate. All proteins were tested at a concentration of 0.5 µg. Abbreviations: kilodalton = kDa.*

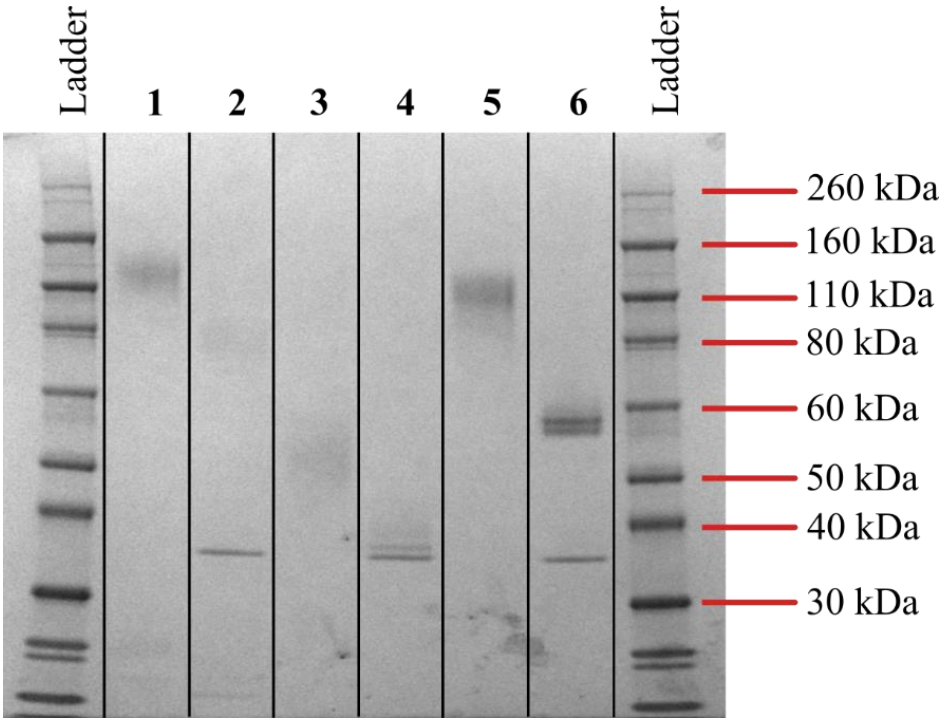

Figure 17: SDS-PAGE of EBOV-GP, EBOV-sGP, and HIV gp120

1: *EBOV-GP,* ***2:*** *PNGase F-treated EBOV-GP,* ***3:*** *EBOV-sGP,* ***4:*** *PNGase F-treated EBOV-sGP,* ***5:*** *HIV gp120,* ***6:*** *PNGase F-treated HIV gp120. All samples were loaded with 0.5 µg of protein and stained with SimplyBlue™ SafeStain (ThermoFisher Scientific). The image was taken using the ChemiDoc™ MP Imaging System (BioRad) and annotated using Inkscape software. All native proteins migrated relative to their approximate molecular weight whilst the deglycosylated proteins migrated through the gel at a faster rate. All proteins were tested at a concentration of 0.5 µg. Abbreviations: kilodalton = kDa.*

2.3.6 Western Blot MBL Detection

We showed that MBL could bind to the *Ebolavirus* and *Coronavirus* glycoproteins *via* ELISA (**Figure 15**), and we confirmed the deglycosylation of these proteins with PNGase F, using SDS-PAGE assays (**Figure 16** and **Figure 17**). We next used western blot assays to confirm that the MBL binding was dependent on the N-linked glycans of these viral proteins. We first confirmed the binding of MBL to the EBOV-GP and HIV gp120 N-linked glycans. MBL binding to the EBOV-sGP was not detected in this particular assay when using 0.5 µg of EBOV-sGP (**Figure 18**), but was later confirmed using a higher protein concentration of 2 µg (**Figure 20**).

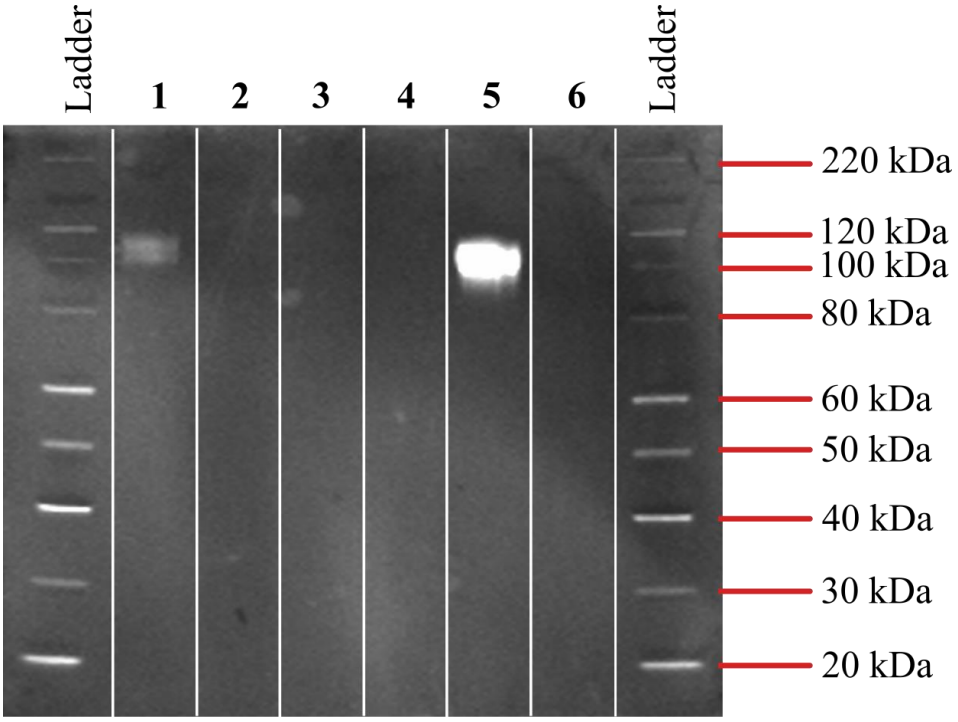

Figure 18: Western blot of MBL binding to EBOV-GP and HIV gp120

1: *EBOV-GP,* ***2:*** *PNGase F-treated EBOV-GP,* ***3:*** *EBOV-sGP,* ***4:*** *PNGase F-treated EBOV-sGP,* ***5:*** *HIV gp120,* ***6:*** *PNGase F-treated HIV gp120. MBL binding was detected for the EBOV-GP and HIV gp120, and this signal was lost following treatment with the PNGase F enzyme. A signal for MBL binding to the EBOV-sGP was not detected in this particular assay, but was later confirmed using a higher concentration of EBOV-sGP (****Figure 20****). Bands which show MBL binding were visible for EBOV-GP (****1****) and HIV gp120 (****5****) between 110-120 kilodaltons (kDa).*

MBL was also shown to bind to the N-linked glycans of SARS-CoV-1 and SARS-CoV-2 spike proteins *via* western blot (**Figure 19**).

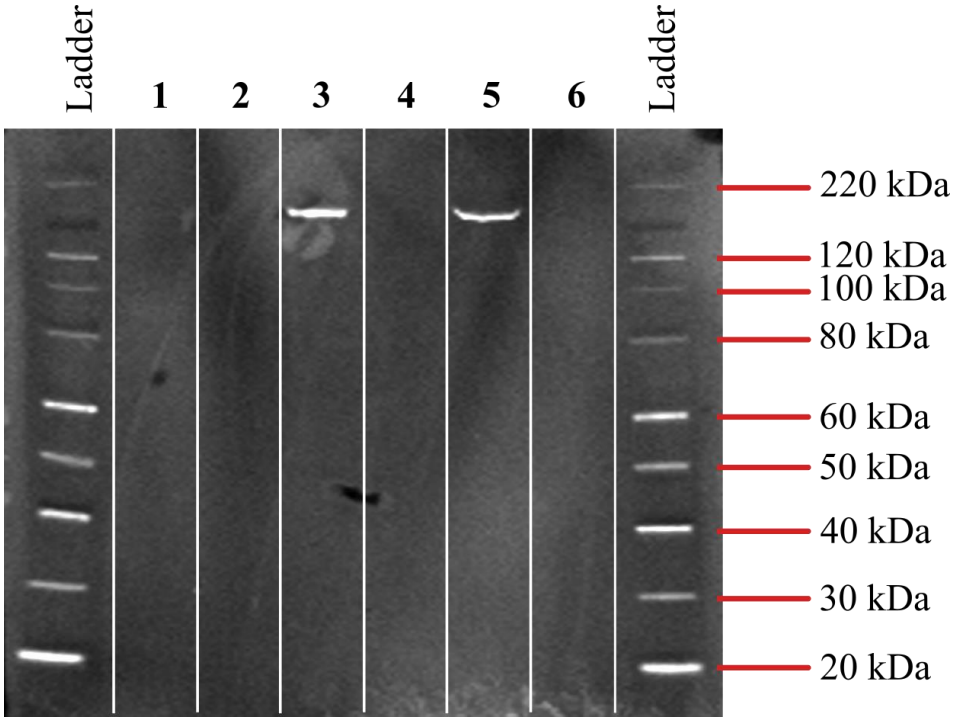

Figure 19: Western blot of MBL binding to SARS-CoV-1/2 spike proteins

1: *SUDV-GP,* ***2:*** *PNGase F-treated SUDV-GP,* ***3:*** *SARS-CoV-1 spike,* ***4:*** *PNGase F-treated SARS-CoV-1 spike,* ***5:*** *SARS-CoV-2 spike,* ***6:*** *PNGase F-treated SARS-CoV-2 spike. MBL binding was detected for the SARS-CoV-1 and SARS-CoV-2 spike proteins, and this signal was lost following treatment with the PNGase F enzyme. Bands which show MBL binding were visible for SARS-CoV-1 (**3**) and SARS-CoV-2 (**5**) spike proteins between 120-220 kilodaltons (kDa). No signal was detected for the SUDV-GP.*

Lastly, MBL binding to the EBOV-sGP was detected *via* western blot when the concentration of EBOV-sGP was increased to 2 µg (**Figure 20**). MBL binding to the SUDV-GP still could not be detected despite increasing the protein concentration to 3.125 µg. This was the maximum concentration that could be used for this protein considering the stock concentration (250 µg/ml) and maximum well volume of the gel (25 µl).

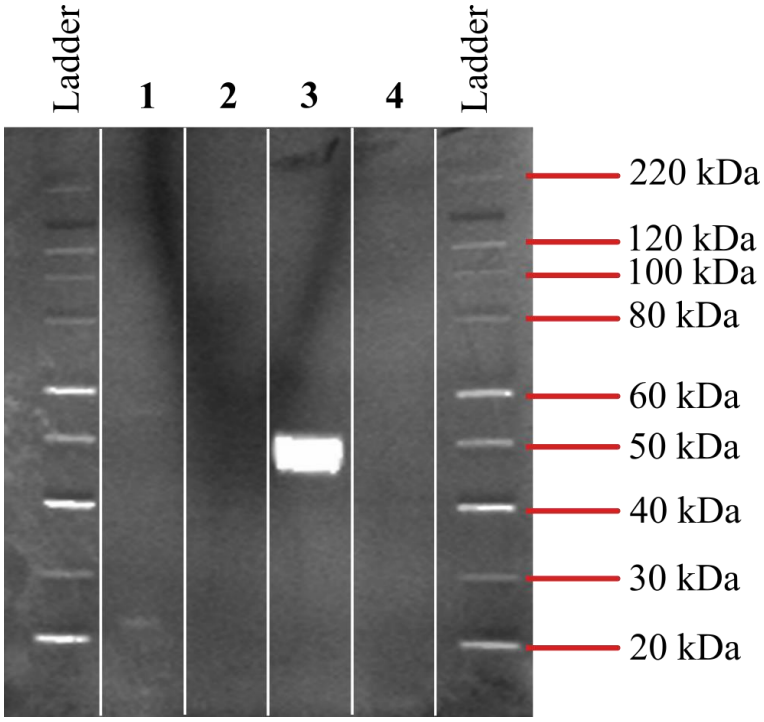

Figure 20: Western blot of MBL binding to the EBOV-sGP

***1:** SUDV-GP, **2:** PNGase F-treated SUDV-GP, **3:** EBOV-sGP, **4:** PNGase F-treated EBOV-sGP. MBL binding was detected for the EBOV-sGP, and this signal was lost following treatment with the PNGase F enzyme. Bands which show MBL binding were visible for the EBOV-sGP (**3**) between 40-50 kilodaltons (kDa). No signal was detected for the SUDV-GP.*

2.3.7 IgG Titres of PHP

ELISAs were developed for the detection of IgG antibodies against all of the viral proteins used throughout this project (**Figure 21**). These ELISAs were then used to screen each of the PHP batches to ensure that no virus-specific IgG antibodies were present that would confound the antibody-independent investigations. For all viral proteins except the EBOV-sGP, the O.D.s for the negative and PHP samples were too low (O.D. ≤ 0.07) for any statistical analyses (Mann Whitney test) to be valid and thus were concluded as negative. For the EBOV-sGP, the O.D.s for all three PHP samples were within three standard deviations of the average of the two negative plasma samples and were also concluded as negative. We were further reassured that these samples were absent for IgG against the viral proteins tested based on their history

of illnesses, vaccination history, travel history, and area of residence. The PHP was collected before the emergence of SARS-CoV-2.

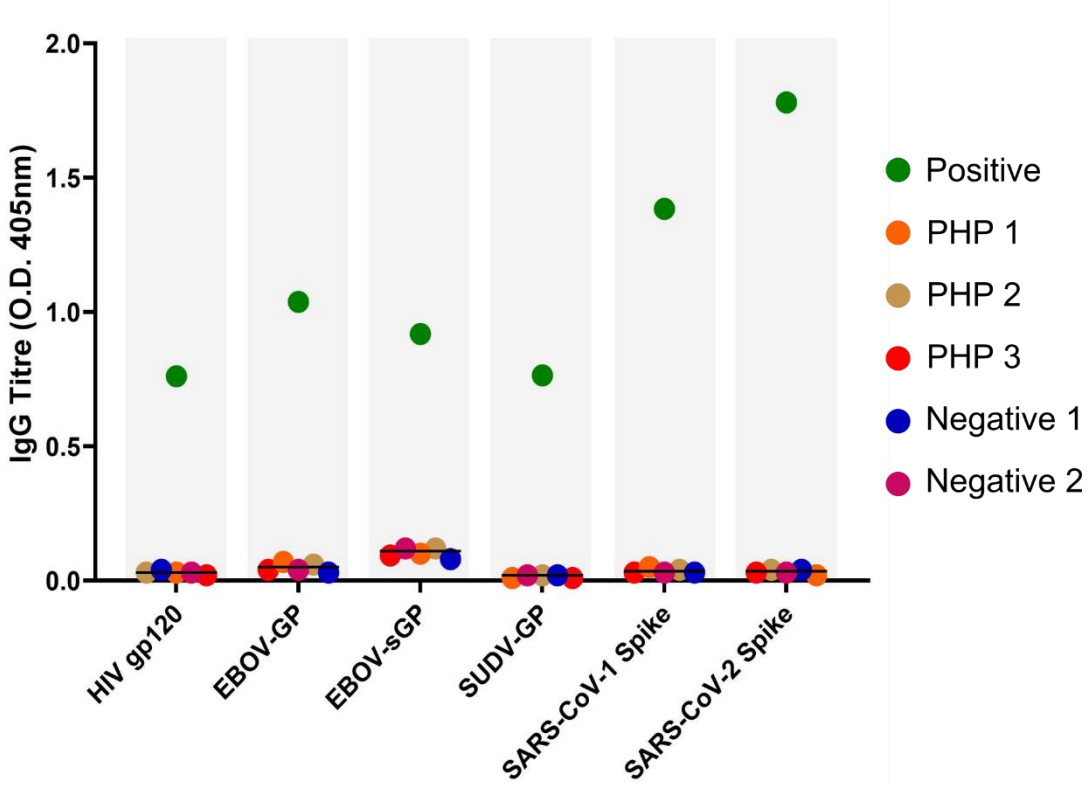

Figure 21: IgG screen of PHP against viral proteins

All pooled human plasma (PHP) samples were negative for IgG binding to the viral proteins tested. Grey shaded areas represent each assay and horizontal black bars show the median value for all PHP and negative samples. Each dot represents the mean value of triplicate samples at a 1:500 dilution. Details of the samples used are as follows: positive (either seropositive plasma [HIV gp120, EBOV-GP, EBOV-sGP, SARS-CoV-2 spike], cross-reactive EBOV-GP IgG plasma [SUDV-GP], or a monoclonal antibody [SARS-CoV-1 spike]); PHP 1 (pool from 5 UK donors); PHP 2 (pool from 20 UK volunteers); PHP 3 (pool from 40 UK volunteers); Negative 1 (single UK donor); Negative 2 (pool from 3 Guinean donors).

2.3.8 C5b-9 Deposition on Viral Proteins

Following the confirmation of MBL binding, C5b-9 deposition ELISAs were developed using the same viral proteins from the MBL ELISA. PHP was used to determine whether the viral proteins could activate the complement system to completion i.e.

formation of the MAC (**Figure 22**), based on the detection of a C9 neoepitope. We observed a similar trend in C5b-9 deposition to the results from our MBL ELISAs. HIV gp120 and mannan were used as positive controls for complement deposition and demonstrated the highest complement activating activity. We made the novel observation that the EBOV-GP and the EBOV-sGP were capable of activating the complement system in the absence of antibodies, which then proceeded uninhibited to the formation of the MAC. Similar to the result for MBL binding, the SUDV-GP showed capacity for mediating complement deposition but this activity was significantly reduced (Mann Whitney test, P = 0.002) by 2.46-fold compared to the EBOV-GP. Similarly, we observed complement deposition against the SARS-CoV-1 and SARS-CoV-2 spike proteins, with a significant (Mann Whitney test, P = 0.002) 1.90-fold reduction in deposition against the latter. Again, the levels of complement deposition followed a similar trend to the levels of MBL binding observed previously (**Figure 15**).

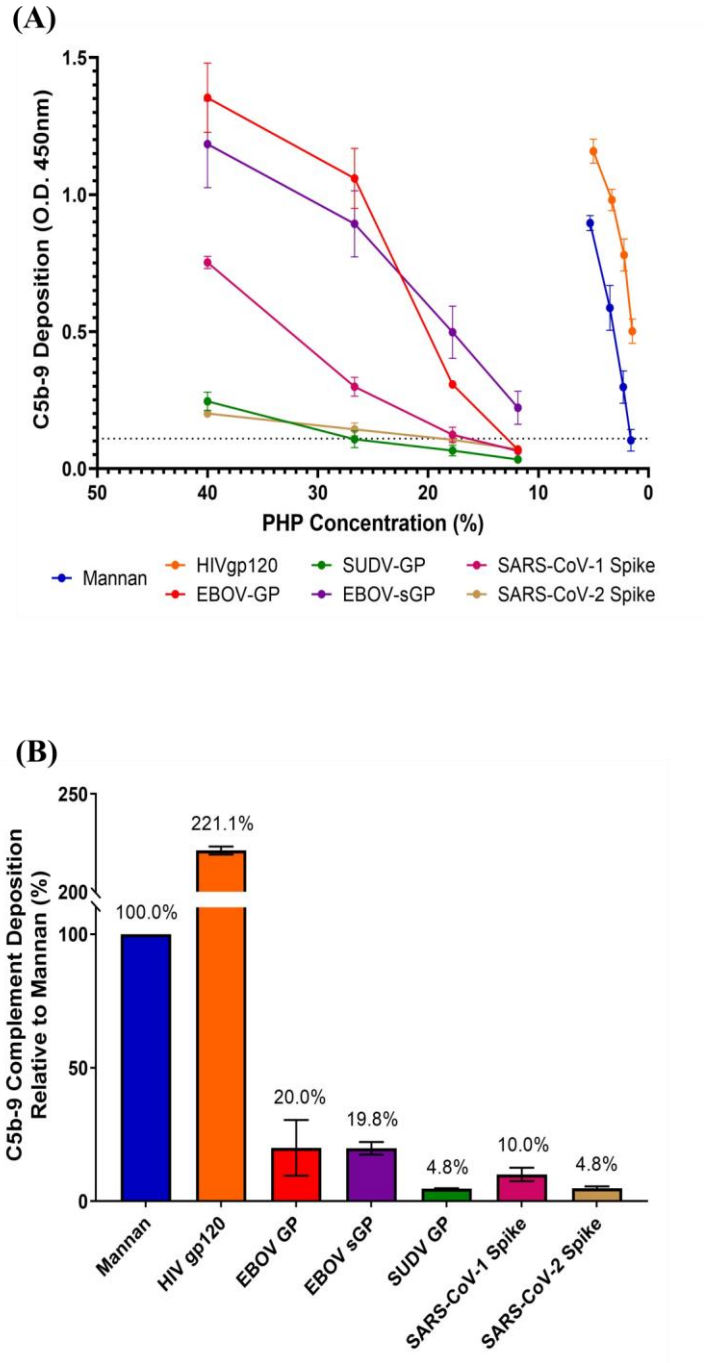

Figure 22: C5b-9 deposition ELISA with viral proteins

C5b-9 deposition ELISAs were performed on all viral proteins with mannan and HIV gp120 as positive controls. ***(A)*** *PHP was titrated against each protein to determine a linear range of C5b-9 deposition for interpolation. A negative cut-off (grey dotted line) was determined using HBSS-only wells incubated with 20% PHP plus three SDs. Each dot represents the mean value of triplicate samples across duplicate assays (total n = 6) with error bars to show the variation.* ***(B)*** *Two points from the PHP titration were then used for interpolation from the standard curve, and then averaged to determine the efficiency of mediating complement deposition relative to mannan. The error bars*

represent the variation of the two dilution points after interpolation. All samples were analysed using GraphPad Prism software (version 9).

2.4 Discussion

This chapter first demonstrated the broad variability of SNPs within the *MBL* and *FCN1* genes that may impact protein function and expression. However, we did not observe any significant differences in the MAFs between survivor and negative cohorts in our pilot study. Similarly, proteomic analysis *via* LC-MS/MS could not distinguish any significant differential protein expression or clustering between the selected cohorts. Novel ELISAs were developed to assess MBL binding and complement deposition in response to viral glycoproteins. We confirmed the binding of MBL to the EBOV-GP (Makona variant) and EBOV-sGP, with the novel observation of MBL binding to the SUDV-GP. We also confirmed MBL binding to the SARS-CoV-1 spike protein, and observed MBL binding to the SARS-CoV-2 spike protein which was novel at the time of the study. Lastly, we observed the formation of the MAC in response to all viral proteins tested, with significant variations in the level of deposition that followed a similar trend to the level of MBL binding.

The frequency of *MBL* and *FCN1* SNPs vary extensively between some ethnic populations (513,514). Whilst we observed large variability in the MAFs of our Guinean cohort, there were no significant differences between EBOV survivors and EBOV naïve individuals (**Table 6**). Using these MAFs, we calculated the statistical power and determined that sample numbers > 200 would be required to confidently determine statistical significance. The real sample number would likely exceed this, as we were unable to acquire DNA from individuals that succumbed to EVD; our selection of EBOV naïve samples would likely contain individuals capable of surviving infection if challenged. Therefore, the NGS approach was not deemed practical for this study, but the information regarding MAF in a Guinean population could inform future study designs. A recent study has shown that these *MBL* SNPs may be risk factors for severe COVID-19 symptoms and the development of a cytokine storm (533). Similarly, we did not observe any significant (significance = $P < 0.05$) differences

or clusters between our Guinean cohorts using LC-MS/MS (**Figure 12**, **Figure 13**, **Figure 14**). This analysis was performed on convalescent plasma samples in absence of infection rather than their response to infection, where proteomic differences may become apparent. A proteomic approach for studying EBOV infection in human samples is limited by the requirement of biosafety level (BSL)-4 facilities and the common methods used to inactivate EBOV, such as the use of Trizol©, that would interfere with the downstream LC-MS/MS analysis. A recent study used a proteomic approach, which included LC-MS/MS, on gamma irradiated samples from twelve EVD patients: eight survivors and four fatalities. They identified unique proteome signatures for each outcome and amongst these differentially expressed proteins, complement proteins C5, C2, and factor H-related protein 1 were significantly upregulated in the fatal outcome group. They also note that regardless of outcome, there is an increase in complement cascade components and other inflammatory markers (534).

Using novel ELISAs, we were able to determine the relative efficiency of MBL binding for a range of viral glycoproteins (**Figure 15**). For the *Ebolavirus* glycoproteins, we firstly identified MBL binding to the Makona variant of the EBOV-GP where previous evidence is for the Mayinga variant only. Given the sequence similarity between these variants (535) this result was expected, but together with the use of EBOV-sGP, provided useful controls and reference points for the assay. We also made the novel observation of MBL binding to the SUDV-GP, which was significantly lower (Mann Whitney test at 1 µg/ml MBL, $P = 0.002$) with a 4.2-fold reduction compared to the EBOV-GP. As discussed previously, MBL can significantly influence EBOV infection *in vitro* and *in vivo* (7,157,412), and SUDV typically has a lower mortality rate than EBOV (298). Whilst more evidence would be required, it is interesting to hypothesise the possible effects this reduced MBL binding may have on SUDV pathogenesis.

MBL binds to the mannose residues of N-linked glycans. N-linked glycosylation occurs on the amide nitrogen of asparagine (N) residues in the amino acid sequences N-X-S/T, where X is any amino acid except proline (536). The reduced MBL binding to the

SUDV-GP compared to the EBOV-GP may in part be explained by the reduced number of N-X-S/T sequence motifs. Using the NetNGlyc – 1.0 software, the EBOV-GP (GenBank accession: AHX24649.1) has seventeen of these motifs (in agreement with published data (537)), whilst the SUDV-GP (YP_138523.1) has twelve. It is also important to consider the different types of N-linked glycosylation that can occur at these sites as they contain different concentrations of D-mannose (high-mannose, complex, and hybrid) (538), and that the sequence motif alone is not sufficient criteria for N-linked glycosylation to occur (536). Whilst the EBOV-GP and SUDV-GP were of a similar size and purity, direct comparisons between the proteins in our ELISAs should be interpreted with caution, as coating concentrations were calculated using μg/ml instead of molarity.

One previous study could not detect MBL binding to the SARS-CoV-1 spike protein (532), whilst two other studies identified MBL binding to immobilised SARS-CoV-1 (77) or the SARS-CoV-1 spike protein (166). Our results were in concordance with the majority, as we identified MBL binding to the spike protein. We also identified MBL binding to the SARS-CoV-2 spike protein which was a novel observation at the time of the study, but has since been published elsewhere (505,518). We observed a significant 1.42-fold reduction (Mann Whitney test at 1 μg/ml MBL, $P = 0.002$) in the level of MBL binding to the spike protein of SARS-CoV-2 compared to SARS-CoV-1. This may partly be reflected in the number of predicted N-linked glycosylation sites reported for the spike proteins of SARS-CoV-1 compared to SARS-CoV-2, which are 29 and 22 respectively (539,540). Whilst this number is greater than the N-linked sites reported for the EBOV-GP, this was not reflected in the signals for MBL binding. As mentioned previously, results should be interpreted with caution when comparing proteins of different sizes, and the type of N-glycans present should also be considered. Of note, N-glycan compositions have only been reported for HIV gp120 (56 – 73% of the ~25 N-linked glycans are of the high-mannose type) (541,542) and the SARS-CoV-2 spike protein (55% complex, 17% hybrid, and 28% high mannose) (540) out of the proteins used in this study. Cell culture environments can also cause variations in glycosylation. Whilst all the proteins used were of a similar level of purity

and were produced in mammalian HEK 293 cells, there could be some minor inherent variations in their glycosylation influenced by different cell culture environments (543).

We confirmed that our observations of MBL binding *via* ELISA were protein and N-glycan specific by treating each protein with PNGase F, then analysing the native and deglycosylated proteins *via* SDS-PAGE and western blot. The SDS-PAGE firstly verified the removal of the N-glycans, as the deglycosylated proteins were a lower molecular weight compared to the native proteins (**Figure 16** and **Figure 17**). The molecular weights *via* SDS-PAGE were then used as a reference point for the western blots. MBL was shown to bind all native proteins except for the SUDV-GP, and MBL binding to all native proteins was lost following the removal of N-linked glycans (**Figure 18**, **Figure 19**, and **Figure 20**). The absence of MBL binding to the native SUDV-GP *via* western blot may be explained by a sensitivity issue. SUDV-GP showed the lowest capacity for MBL binding *via* ELISA, followed by the SARS-CoV-2 spike protein (**Figure 15**). In the western blots, 2 µg of the SARS-CoV-2 spike protein was required for a positive signal and the maximum concentration of SUDV-GP that could be used was 3.125 µg, due to limitations of protein stock concentration (250 µg/ml), the maximum well loading volume (25 µl), and the requirement of diluting with 2x Laemmli buffer (Merck).

Independent of antibodies, we observed complement deposition against all viral proteins tested. There were large discrepancies in the amount of complement deposition between proteins, which followed a similar trend to the amount of MBL binding (Pearson correlation, $r = 0.9997$, $P < 0.0001$). We show for the first time that the complement system is activated to completion (formation of the MAC) following stimulation with the EBOV-GP, EBOV-sGP, and SUDV-GP, with a 5.4-fold reduction in complement deposition on the SUDV-GP compared to the EBOV-GP (Mann Whitney test at 40% PHP, $P = 0.002$). It is possible that our detection of the C9 neoepitope is also indicative of surface-tethered soluble MAC (sMAC). sMAC is formed from MAC assembly precursors, together with the extracellular regulatory proteins clusterin and vitronectin, to form a partial MAC with up to three C9 molecules instead of the

full eighteen (544,545). The observation of GP-mediated complement deposition suggests that EBOV virions and EBOV-infected cells could be susceptible to complement deposition and formation of the MAC. However, EBOV successfully infects humans and other species with functional complement systems, which leaves several possibilities regarding its pathogenesis.

Firstly, our results rule out the likelihood of complement regulation by the EBOV-GP, as we observed formation of the MAC and/or sMAC. Secondly, complement deposition may actually enhance viral infection in ways previously described for HIV-1 (169) and HSV-2 (170), which could explain the association between excessive complement activation and fatal EVD outcomes (546). Thirdly, host complement regulatory proteins (CD46, CD55, CD59) may be incorporated into the EBOV lipid membrane during the budding process to protect the virion from complement-mediated lysis, which has been observed for MuV, SV5, and HIV-1 (183,184). Fourthly, other viral proteins such as the VP40 – which is reportedly secreted into the extracellular space – may be responsible for complement regulation (547). Lastly, our observations of complement deposition in response to the EBOV-sGP could suggest a potential decoy mechanism leading to complement consumption and diversion from the virion: a mechanism that has been described for other pathogens (548,549). The EBOV-sGP is the primary transcript of the *GP* gene (550) which is actively secreted from infected host cells during infection at levels detectable in the blood of acutely infected patients (551). The EBOV-sGP has previously been proposed as an antigen decoy mechanism from the neutralising antibody response (237,552), and it is therefore plausible that a similar mechanism exists for the complement system. Again, this is particularly interesting when considering the excessive complement activation associated with fatal EVD outcomes (534,546).

We also observed C5b-9 deposition in response to the SARS-CoV-1 spike protein, which was previously only shown to result in the cleavage of C4, and complement has been shown to neutralise VSV pseudotyped with the SARS-CoV-1 spike protein (77). Lastly, we identified C5b-9 deposition in response to the SARS-CoV-2 spike protein

which was novel at the time of this study, but has recently been published elsewhere (518). This provides a potential mechanism through which complement activation occurs in COVID-19 patients, which is particularly important in those with severe COVID-19 where excessive complement-mediated inflammation contributes to severe disease outcome (490–497,499–501). Unlike the previous studies, we were able to draw some comparison between the SARS-CoV-1/2 spike proteins and observed a significant 1.42-fold reduction (Mann Whitney test at 1 µg/ml MBL, P = 0.002) in MBL binding and a 3.75-fold reduction (Mann Whitney test at 40% PHP, P = 0.002) in complement deposition in response to the SARS-CoV-2 spike protein.

In summary, we identified a variety of *MBL* and *FCN1* SNPs within a Guinean cohort and the MAF can be used to inform sample numbers for future genomic studies. We found a significant reduction in MBL binding to the SUDV-GP compared to the EBOV-GP and EBOV-sGP, which was consistent with our observations of C5b-9 deposition. This shows the potential for *Ebolavirus* proteins to activate the complement system to completion. Similarly, we confirmed MBL binding to the spike proteins of SARS-CoV-1 and SARS-CoV-2, with a significant difference between these proteins that was consistent with our observations for complement deposition. These findings demonstrate a possible mechanism for complement activation during EBOV and SARS-CoV-2 infections, independent of antibodies, with implications for viral pathogenesis and neutralisation.

2.5 Appendix I

2.5.1 ELISAs to Determine MBL, FCN-1, and C1q Titres in Convalescent EVD Plasma Samples

Commercial ELISAs were used for the detection and quantification of MBL, FCN-1, and C1q in EBOV-GP IgG positive and EBOV-GP IgG negative plasma samples to ascertain whether there were variations in concentration at the proteomic level.

Methods

MBL (MBL Oligomer ELISA Kit, bioporto), FCN-1 (Human FCN-1/M-ficolin ELISA Kit, abcam), and C1q (C1q Human ELISA Kit, ThermoFisher Scientific) ELISAs were performed on EBOV-GP IgG positive and EBOV-GP IgG negative plasma samples from Guinea. All samples were tested in duplicate in accordance with the manufacturer's instructions and samples with a CV > 20% were excluded from the analysis. A Mann Whitney test was performed to determine significance values (significance = $P < 0.05$) between the positive and negative plasma cohorts using GraphPad Prism software (version 9).

Results

The plasma concentration of all three proteins demonstrated large variations between individuals of the same cohort, but did not significantly differ (significance = $P < 0.05$) between the survivor and negative cohorts (**Figure 23**).

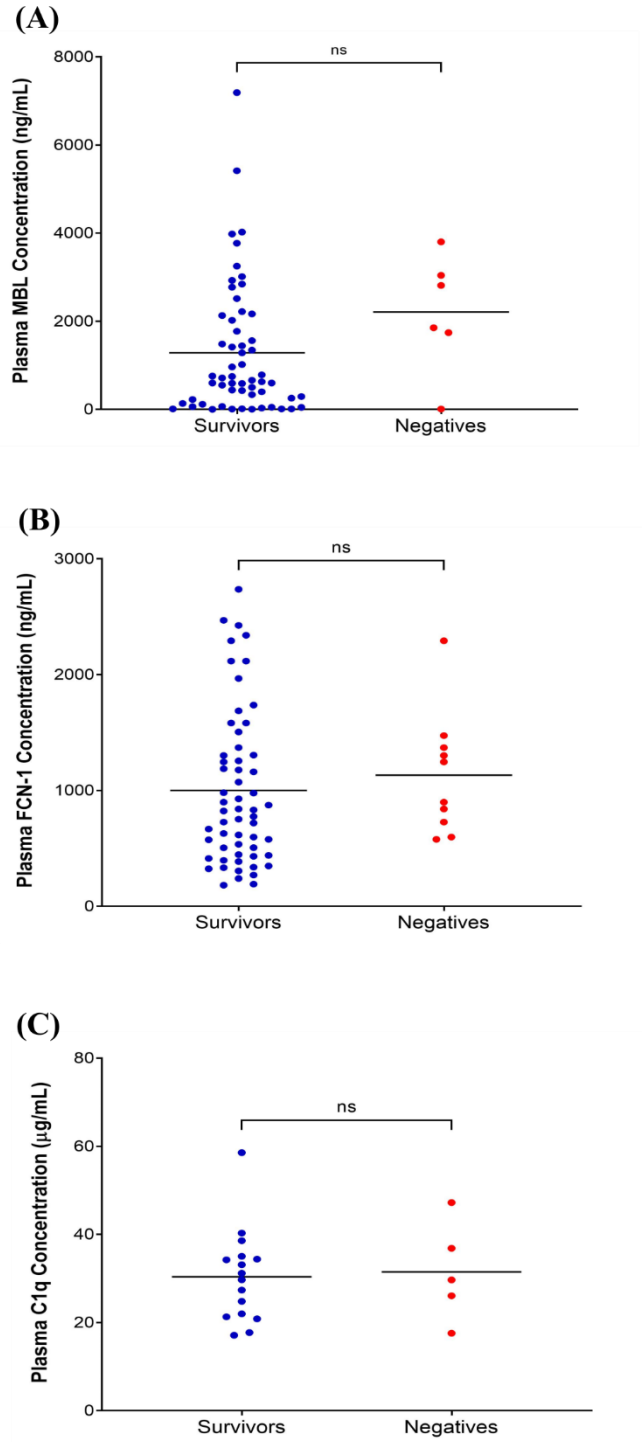

Figure 23: ELISAs to determine MBL, FCN-1, and C1q concentrations in West African plasma samples

*No significant differences were observed between the EBOV survivor (**(A)** MBL: n = 57; **(B)** FCN-1: n = 58; **(C)** C1q: n = 16) and negative cohorts (**(A)**MBL: n = 6; **(B)** FCN-1: n = 10; **(C)** C1q: n = 5) for any of the proteins tested. Each dot represents the mean value of the sample replicates (n = 2) for survivors (blue) and negatives (red). A Mann Whitney test was performed to calculate significance values (significance = P < 0.05). Abbreviations: Ficolin-1 = FCN-1; mannose-binding lectin = MBL; not significant = ns.*

2.5.2 PCA of LC-MS/MS Results Including the S2 Outlier

Based on the PCA, sample S2 was a clear outlier and subsequently excluded from further analysis (**Figure 24**).

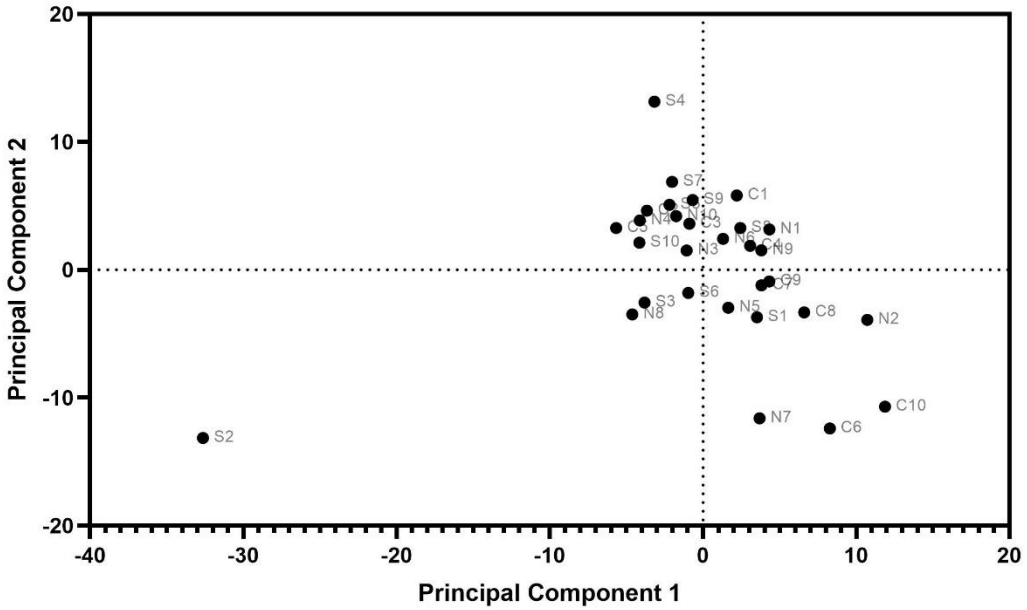

Figure 24: PCA of LC-MS/MS samples including S2 outlier

The PCA was calculated using GraphPad Prism software (version 9) with the LC-MS/MS data for all samples and shows that sample S2 was a clear outlier. Each dot represents a sample from a survivor (S), a contact (C), or a negative (N).

2.5.3 FCN-1 ELISA Development

We attempted to design an ELISA that could detect the binding of FCN-1 to the viral proteins of interest, as it was previously shown to bind to the EBOV-GP (8). However, the development was unsuccessful as recombinant FCN-1 from two different suppliers failed to show any binding ability.

2.5.3.1 FCN-1 ELISA: The Binding of FCN-1 to Target Proteins

ELISAs were first developed to detect FCN-1 binding to the EBOV-GP adsorbed onto MaxiSorp™ ELISA plates, with human fetuin as a positive control.

Methods

MaxiSorp™ ELISA plates were coated in duplicate with 100 µl of EBOV-GP (Nuffield Department of Medicine, University of Oxford, Oxford, UK), Fetuin-A (Merck), or BSA (Merck) in HBSS at a concentration of 3 µg/ml and incubated overnight at 4°C. The plates were then washed six times in 200 µl of wash buffer (HBSS with 0.1% tween-20) and blocked using 200 µl of 5% skim milk in HBSS, at RT for 1 hr. The plates were washed six times in 200 µl of wash buffer and 100 µl of recombinant FCN-1 (SinoBiological and R&D Systems) was added at a concentration of 3 µg/ml and incubated at RT for 1 hr. The plates were washed six times in 200 µl of wash buffer and the samples were incubated with 100 µl of 6x-His tag monoclonal antibody (ThermoFisher Scientific) at a concentration of 2 µg/ml for 1 hr at RT. The plates were washed six times in 200 µl of wash buffer and the samples were incubated with 100 µl of HRP-conjugated anti-mouse IgG antibody at a concentration of 2 µg/ml for 1 hr at RT. The plates were washed a final time before developing with ABTS (Merck) for 10 min in the dark. The O.D.s were measured at 405 nm and the data was analysed using GraphPad Prism software (version 9).

Results

Two recombinant FCN-1 proteins were obtained from different suppliers (SinoBiological and R&D Systems). Both proteins could be detected using an anti-His tag antibody when adsorbed to the ELISA plate, but no signal was detected for FCN-1 binding to EBOV-GP or fetuin-A (**Figure 25**).

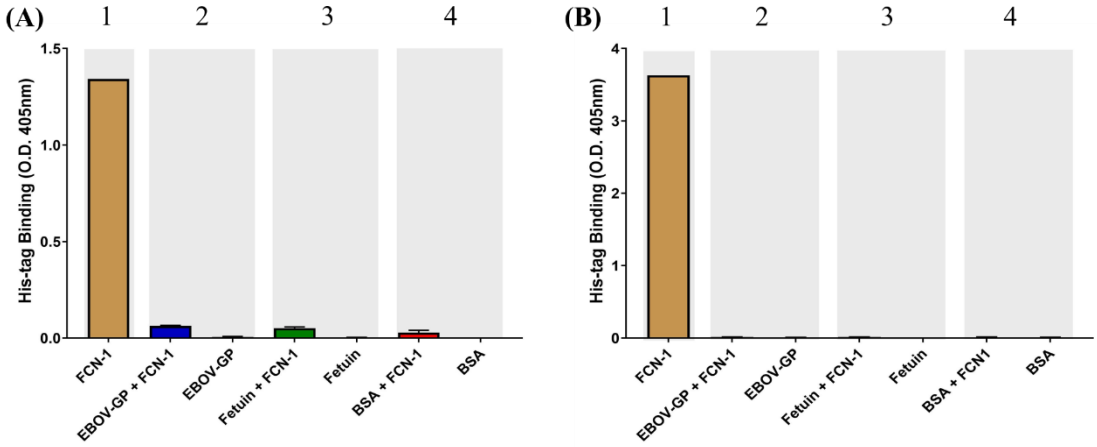

Condition	Coating Protein	Binding Protein	Primary Antibody	Secondary Antibody
1	FCN-1	-	His-tag antibody	HRP-conjugated anti-mouse IgG antibody
2	EBOV-GP	FCN-1		
	EBOV-GP	-		
3	Fetuin-A	FCN-1		
	Fetuin-A	-		
4	BSA	FCN-1		
	BSA	-		

Figure 25: FCN-1 ELISA: FCN-1 binding to EBOV-GP, fetuin-A, and BSA

*FCN-1 proteins from R&D Systems **(A)** and SinoBiological **(B)** were unable to bind the EBOV-GP and fetuin-A, which are known antigens for FCN-1. A positive signal was observed when adsorbing both FCN-1 proteins to the ELISA plate. Grey shaded areas show unique conditions for the assay which are numbered and described in the table. Error bars show the variation of replicates (n = 2) from the mean. All data were analysed using GraphPad Prism software (version 9).*

2.5.3.2 FCN-1 ELISA: EBOV-GP Binding to FCN-1

To determine whether the lack of FCN-1 binding was due to epitope availability of the adsorbed proteins, we instead tried coating with FCN-1 and using EBOV-GP to detect binding.

Methods

MaxiSorp™ ELISA plates were coated in duplicate with 100 µl of FCN-1 (SinoBiological and R&D Systems) in HBSS at a concentration of 3 µg/ml and incubated overnight at 4°C. The plates were then washed six times in 200 µl of wash buffer (HBSS with 0.1%

tween-20) and blocked in 200 µl of 5% skim milk in HBSS, at RT for 1 hr. The plates were washed six times in 200 µl of wash buffer and 100 µl EBOV-GP (Nuffield Department of Medicine, University of Oxford, Oxford, UK) was added at a concentration of 3 µg/ml, then incubated at RT for 1 hr. The plates were washed six times in 200 µl of wash buffer and the samples were incubated with 100 µl of KZ52 (2 µg/ml), EBOV-GP polyclonal antibody (2 µg/ml, ThermoFisher Scientific), or 1:100 EBOV-GP IgG positive plasma for 1 hr at RT. The plates were washed six times in 200 µl of wash buffer and the samples were incubated with 100 µl of HRP-conjugated anti-human IgG antibody (Merck) diluted 1:5000, for 1 hr at RT. The plates were washed a final time before developing with ABTS (Merck) for 10 min in the dark. The O.D.s were measured at 405 nm and the data was analysed using GraphPad Prism software (version 9).

Results

We were unable to detect any binding of the EBOV-GP to FCN-1 from either SinoBiological or R&D Systems. Various means of detecting EBOV-GP binding were used to ensure that the lack of signal was not due to restricted epitopes in the binding process (**Figure 26**).

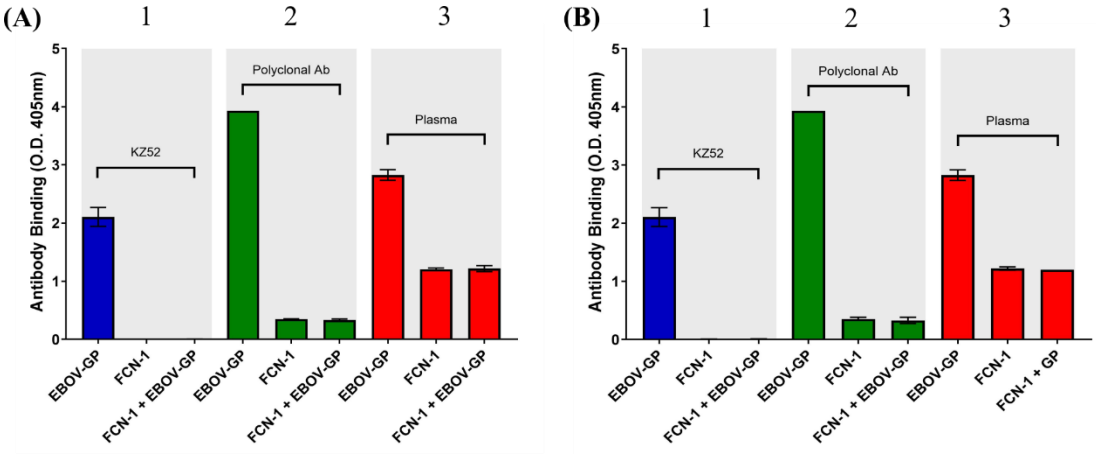

Condition	Coating Protein	Binding Protein	Primary Antibody	Secondary Antibody
1	EBOV-GP	-	KZ52 antibody	HRP-conjugated anti-human IgG
	FCN-1	-		
	FCN-1	EBOV-GP		
2	EBOV-GP	-	Polyclonal anti-EBOV-GP antibody	HRP-conjugated anti-rabbit IgG
	FCN-1	-		
	FCN-1	EBOV-GP		
3	EBOV-GP	-	EBOV-GP IgG positive plasma	HRP-conjugated anti-human IgG
	FCN-1	-		
	FCN-1	EBOV-GP		

Figure 26: EBOV-GP binding to ficolin-1

*The EBOV-GP was not shown to bind FCN-1 from either **(A)** R&D Systems or **(B)** SinoBiological, in the conditions tested. Grey shaded areas show unique conditions for the assay which are numbered and described in the table. Error bars show the variation of replicates (n = 2) from the mean. All data were analysed using GraphPad Prism software (version 9).*

2.5.4 MBL ELISA Optimisation

MBL ELISA parameters were optimised using mannan as a positive control. Coating concentration, MBL concentration, and antibody concentrations were optimised to improve assay sensitivity and signal-to-noise ratios.

2.5.4.1 MBL ELISA: Coating Titration

Mannan was titrated to determine an approximate range for coating concentrations and to conclude that the ELISA signal was dependent on mannan.

Methods

The methods are as described in Methods Section **2.2.7**, with the following modifications: mannan was coated using a 1:2 dilution series from 2.000 µg/ml – 0.016 µg/ml, and MBL was added at a concentration of 1 µg/ml.

Results

The assay began to saturate with the use of mannan at a concentration of 2 µg/ml and the signal noticeably decreased with each 1:2 dilution (**Figure 27**).

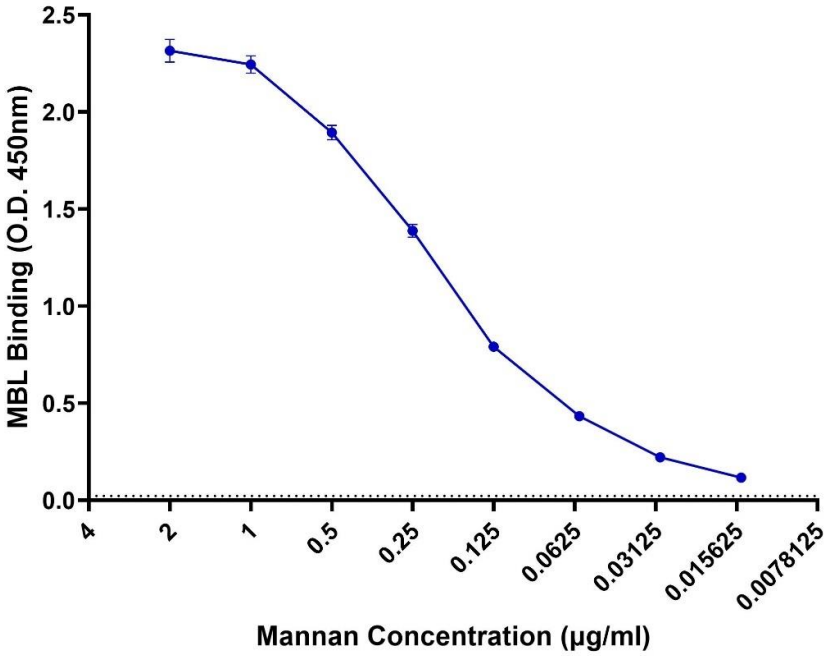

Figure 27: MBL ELISA coating titration with mannan

The level of MBL binding was reduced with decreasing concentrations of mannan. Each dot represents the mean value of all replicates (n = 3) for each concentration of mannan. The dotted line represents the O.D. for HBSS-coated wells with 1 µg/ml of MBL as a negative control. All data were analysed using GraphPad Prism software (version 9).

2.5.4.2 MBL ELISA: MBL Titration

MBL was titrated against mannan to determine an approximate range required for MBL concentrations and to conclude that the ELISA signal was dependent on the addition of MBL.

Methods

The methods are as described in Methods Section **2.2.7**, with the following modifications: mannan was coated at a concentration of 1 µg/ml and MBL was added using a 1:2 dilution series from 2.000 µg/ml – 0.016 µg/ml.

Results

The signal noticeably decreased with each 1:2 dilution of MBL in the wells coated with mannan, whilst the low background signal with HBSS remained constant (**Figure 28**).

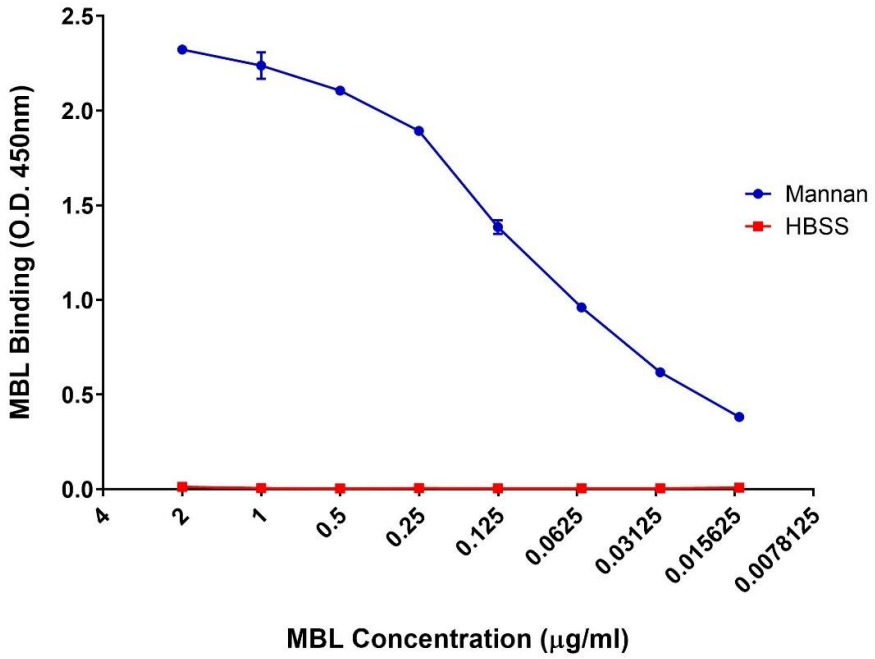

Figure 28: MBL ELISA: titration of MBL

The background signal for wells coated with HBSS did not increase with increasing MBL concentrations, whilst the wells coated with mannan increased as expected. Each dot represents the mean value of all replicates (n = 3) for a particular concentration of MBL. All data were analysed using GraphPad Prism software (version 9).

2.5.4.3 MBL ELISA: Antibody Optimisation

The optimal antibody concentrations for the MBL ELISA were determined using a chequerboard screening method with the primary and secondary antibodies.

Methods

The methods are as described in Methods Section **2.2.7**, with the following modifications: mannan was coated at a concentration of 1 µg/ml; MBL was added at a concentration of 1 µg/ml; antibody concentrations were tested in combination with 1, 2, and 3 µg/ml.

Results

Only minor changes in the signal-to-noise ratio were observed with changes in the antibody concentrations (**Figure 29**).

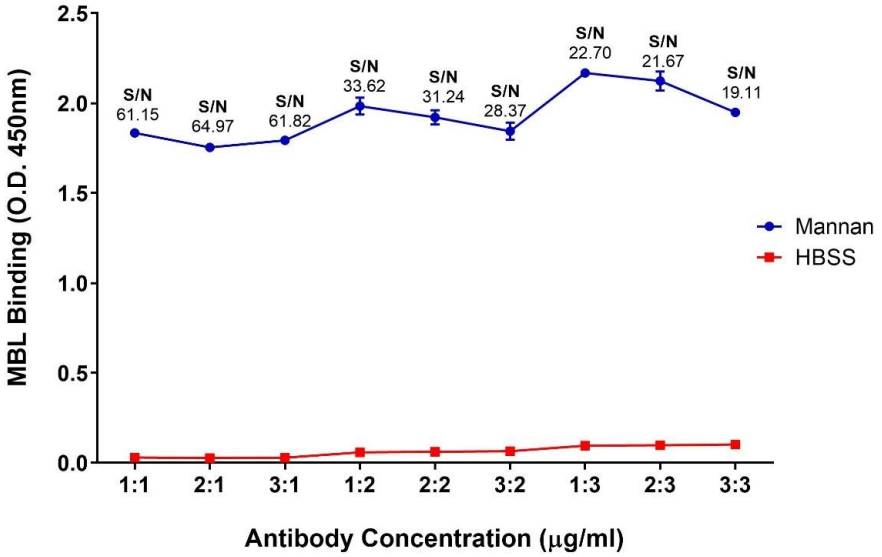

Figure 29: MBL ELISA antibody optimisation

The signal-to-noise ratio (S/N) was not improved with increasing antibody concentrations, as both the mannan and HBSS coated wells showed an increase in signal. Each dot represents the mean value of all replicates (n = 3). The ratio of primary:secondary antibody concentrations varied between 1, 2, and 3 µg/ml whilst mannan and MBL were fixed at a concentration of 1 µg/ml. All data were analysed using GraphPad Prism software (version 9).

2.5.4.4 MBL ELISA: Standard Curve

A standard curve was generated using mannan-coated wells and a titration of MBL for the interpolation of data.

Methods

The methods are as described in Methods Section **2.2.7**, with the following modifications: MBL was added at a concentration of 1.000 µg/ml – 0.002 µg/ml.

Results

A sigmoid curve was obtained with the titration of MBL against mannan and fitted with a 4-parameter logistic curve (**Figure 30**).

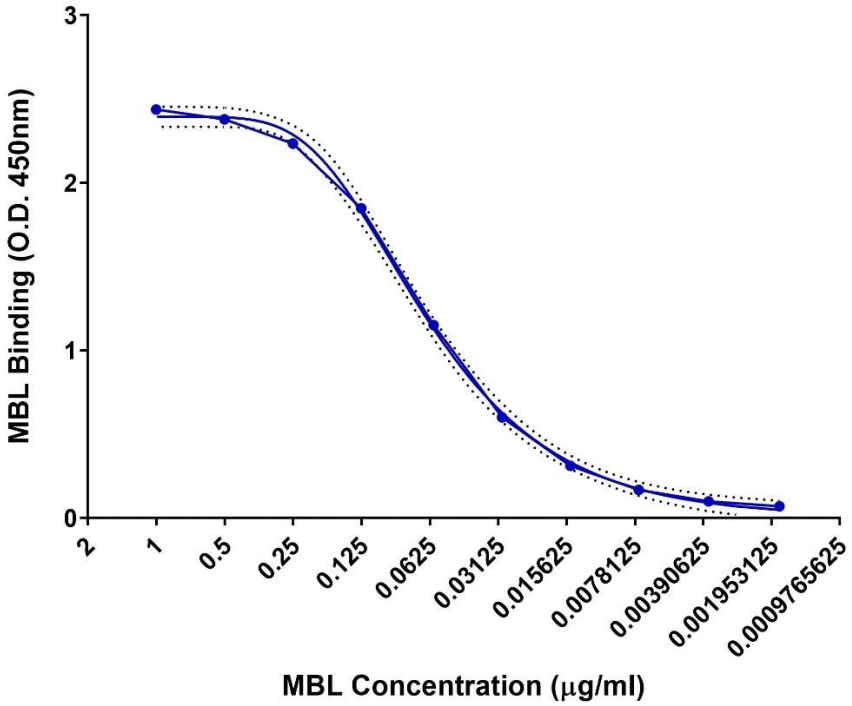

Figure 30: MBL ELISA standard curve

The standard curve of MBL binding to mannan was fitted with a 4-parameter logistic (4PL) curve (blue line without dots) and used for interpolation of MBL binding to viral proteins. The dotted lines represent the error bars for the 4PL mean. Each blue dot represents the mean value of all replicates (n = 3). All data were analysed using GraphPad Prism software (version 9).

2.5.4.5 MBL ELISA: EDTA Controls

EDTA was included with the highest concentration of MBL used for each viral protein as a negative control.

Methods

The methods are as described in section **2.2.7** for the MBL binding ELISA with no modifications.

Results

The addition of 10 mM EDTA at the MBL incubation stage reduced all positive signals below the negative threshold (**Figure 31**).

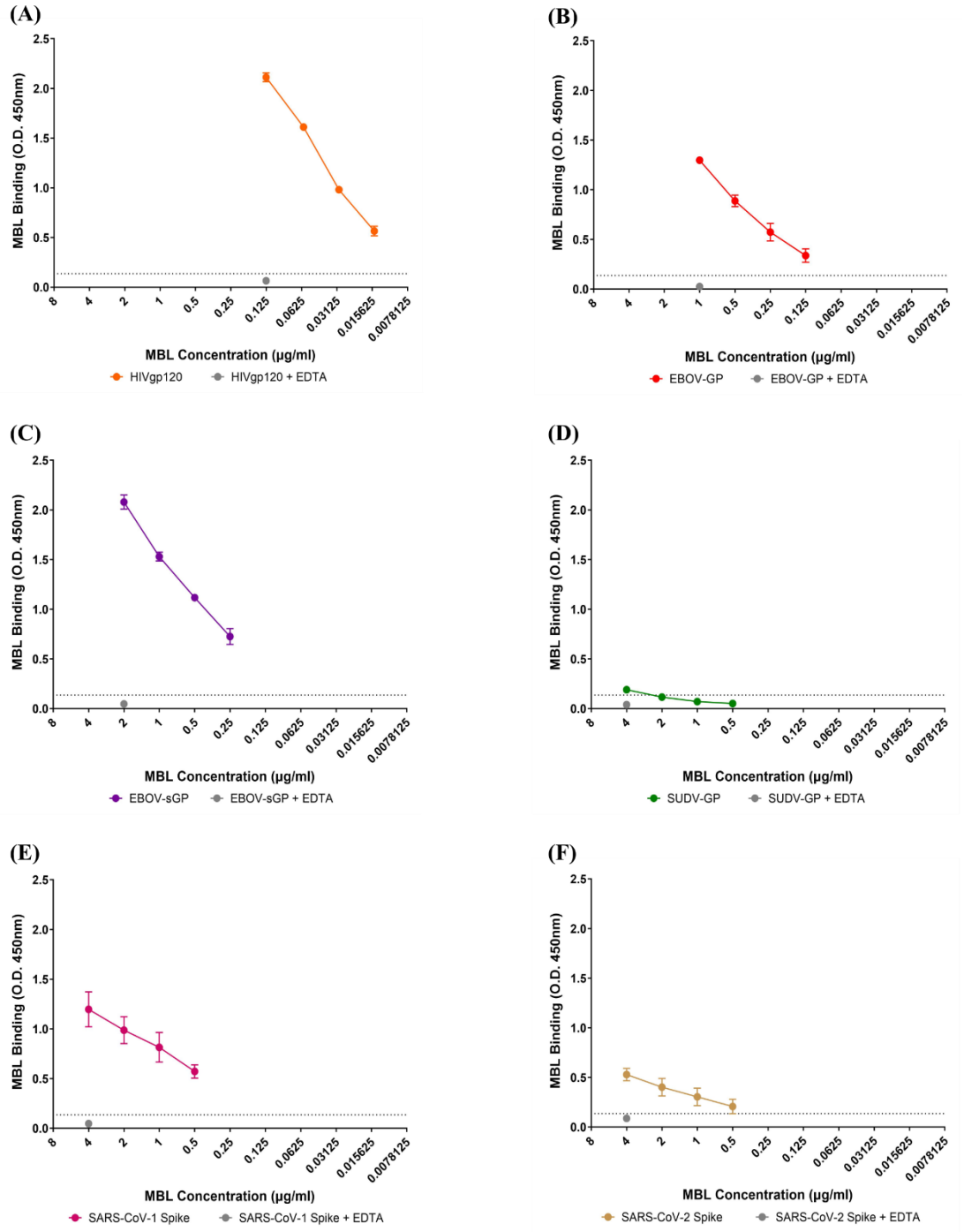

Figure 31: MBL ELISA with EDTA controls

MBL binding ELISAs were performed on all viral proteins with mannan as a positive control. A negative cut-off (grey dotted line) was determined using HBSS-only wells incubated with 4 µg/ml of MBL plus three SDs. Each dot represents the mean value of triplicate samples across duplicate assays (total n = 6) with error bars to show the variation. ***(A)*** *HIV gp120 MBL titration with EDTA control,* ***(B)*** *EBOV-GP MBL titration with EDTA control,* ***(C)*** *EBOV-sGP MBL titration with EDTA control,* ***(D)*** *SUDV-GP MBL*

titration with EDTA control, ***(E)*** *SARS-CoV-1 spike protein MBL titration with EDTA control,* ***(F)*** *SARS-CoV-2 spike protein MBL titration with EDTA control. Each EDTA control is represented as a single grey dot for each protein. All samples were analysed using GraphPad Prism software (version 9).*

2.5.5 C3c ELISA Development

This section highlights some of the key experiments for the development of the complement deposition ELISAs. The complement deposition ELISAs were originally developed to target C3c of the complement pathway. After the development and optimisation of the C3c deposition assay, the background signal with HBSS-only wells was too high to accurately determine complement deposition for some of the viral proteins. The detection antibody was eventually changed to target the neoantigen of C9 on the C5b-9 complex, and used as described in section **2.2.11**.

2.5.5.1 C3c ELISA: Blocking Optimisation

A range of blocking buffers were tested to minimise the amount of background signal and prevent non-specific complement deposition.

Methods

Specific conditions for each optimisation are detailed in the table below each figure (**Figure 32**, **Figure 33**, **Figure 34**, **Figure 35**). Briefly, MaxiSorp™ ELISA plates were coated in duplicate with 100 µl of "Coating Protein" (see table) in HBSS overnight at 4°C. The plates were washed six times with 200 µl of wash buffer (HBSS containing 0.01% tween-20) and blocked with "Blocking Buffer" (see table). The plates were washed six times with 200 µl of wash buffer and PHP was added at a concentration of 5%, and incubated at 37°C for 30 min, 900 rpm. The plates were washed again and incubated with 100 µl of anti-C3c monoclonal antibody (ThermoFisher Scientific), or HRP-conjugated C3c polyclonal antibody (abcam), at RT for 1 hr, 500 rpm. If detection of the monoclonal antibody was required, the plates were washed and incubated with 100 µl of HRP-conjugated anti-mouse secondary antibody (ThermoFisher Scientific) at RT for 1 hr. The plates were washed again and developed using 100 µl

of ABTS (Merck) for 10 min in the dark. The O.D.s were read at 405 nm and the data analysed using GraphPad Prism software (version 9).

Results

Various blocking buffers were incubated overnight at 4^{o}C to determine whether the increased contact time could reduce the non-specific complement deposition with the HBSS-only wells. None of the blocking buffers were deemed suitable at these conditions (**Figure 32**).

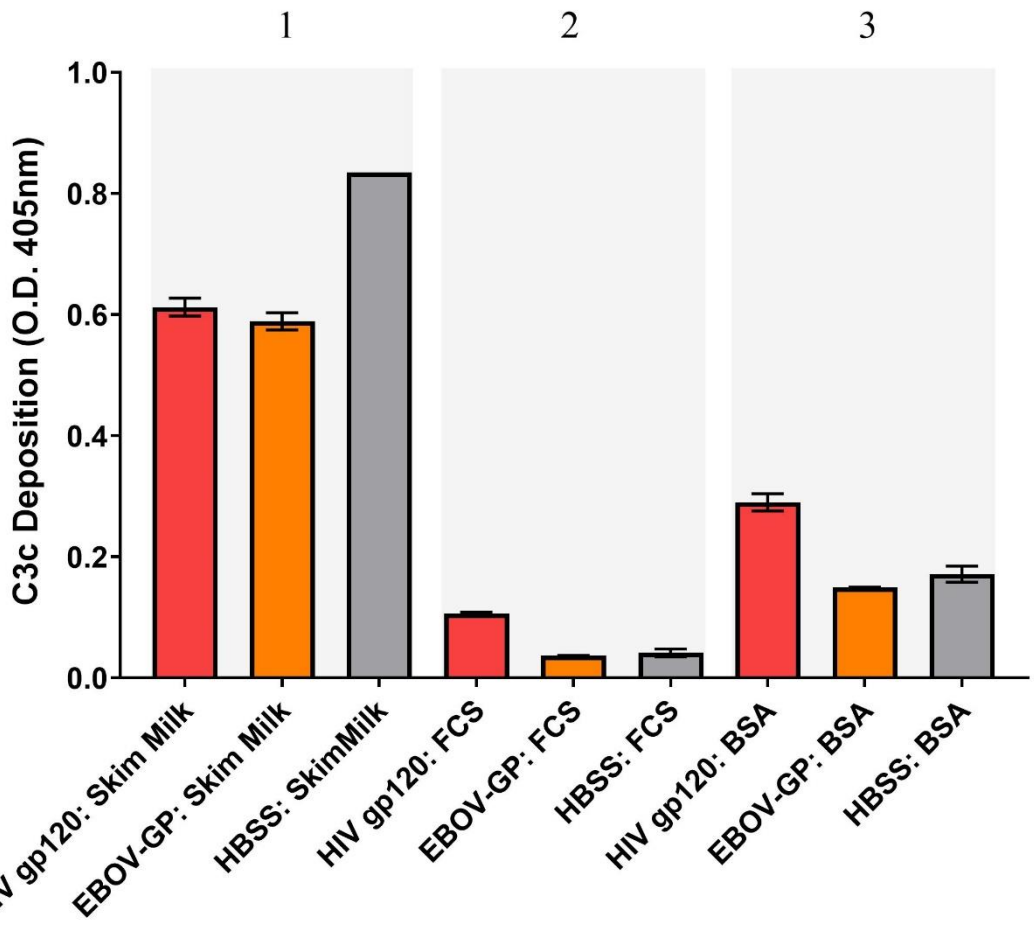

Blocking Overnight at 4°C				
Condition	**Coating Protein (1 µg/ml)**	**Blocking Buffer (200 µl)**	**Primary Antibody (1 µg/ml)**	**Secondary Antibody (1 µg/ml)**
1	HIV gp120	5% Skim milk	Anti-C3c monoclonal	HRP-conjugated anti-mouse IgG polyclonal
	EBOV-GP			
	HBSS			
2	HIV gp120	5% FCS		
	EBOV-GP			
	HBSS			
3	HIV gp120	5% BSA		
	EBOV-GP			
	HBSS			

Figure 32: C3c deposition ELISA: blocking overnight at 4°C

HIV gp120 and EBOV-GP were used as positive controls and HBSS was used as a negative control. The X-axis labels describe the coat:block conditions. None of the blocking buffers suitably blocked non-specific C3c deposition in the HBSS-coated wells at the conditions tested. Grey shaded areas show unique conditions for the assay which are numbered and described in the table. Error bars show the variation of replicates (n = 2) from the mean. All data were analysed using GraphPad Prism software (version 9).

A range of blocking buffers were incubated at RT for 1 hr in an attempt to reduce the non-specific complement-deposition in the HBSS-only wells. None of the blocking buffers were suitable in these conditions (**Figure 33**).

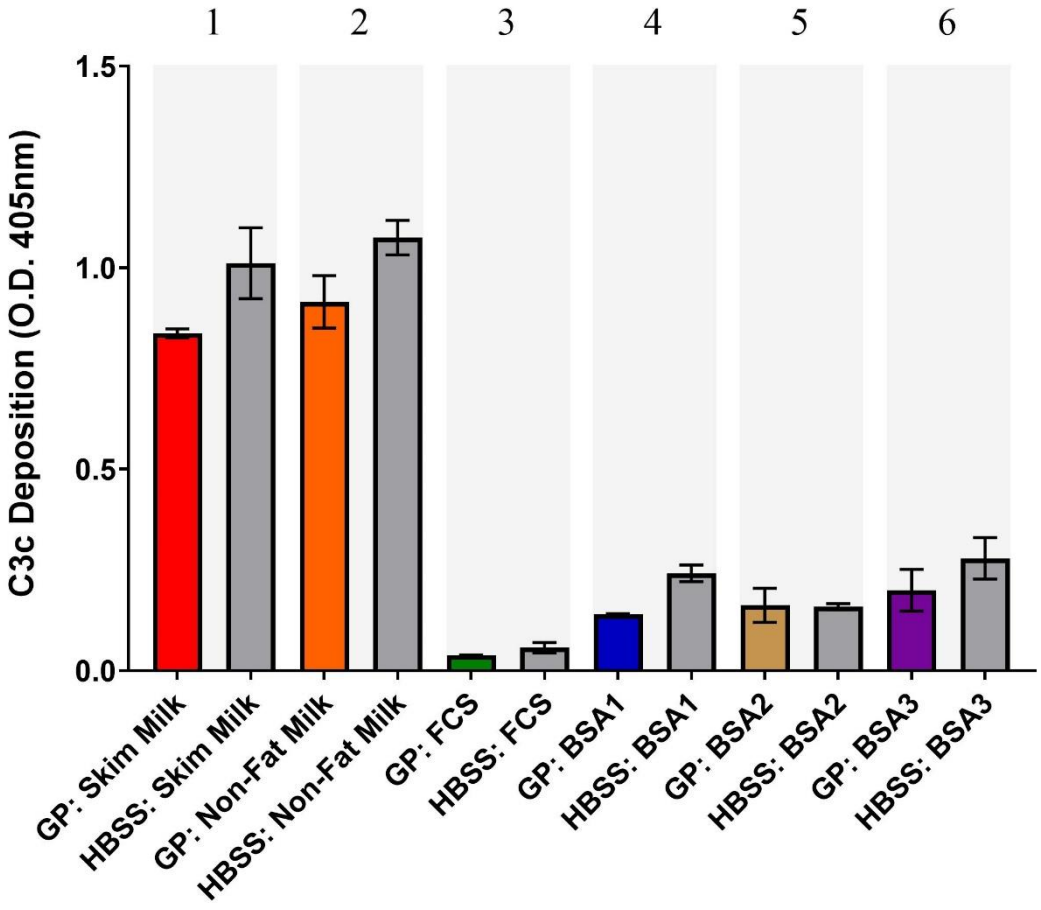

Blocking at RT for 1 hr				
Condition	**Coating Protein (1 µg/ml)**	**Blocking Buffer (200 µl)**	**Primary Antibody (1 µg/ml)**	**Secondary Antibody (1 µg/ml)**
1	EBOV-GP	5% Skim milk	Anti-C3c monoclonal	HRP-conjugated anti-mouse IgG polyclonal
	HBSS			
2	EBOV-GP	5% Non-fat milk		
	HBSS			
3	EBOV-GP	5% FCS		
	HBSS			
4	EBOV-GP	5% BSA 1		
	HBSS			
5	EBOV-GP	5% BSA 2		
	HBSS			
6	EBOV-GP	5% BSA 3		
	HBSS			

Figure 33: C3c deposition ELISA: blocking at room temperature

EBOV-GP was used as a positive control and HBSS was used as a negative control. The X-axis labels describe the coat:block conditions. None of the blocking buffers suitably blocked non-specific C3c deposition in the conditions tested. Grey shaded areas show unique conditions for the assay which are numbered and described in the table. Error bars show the variation of replicates (n = 2) from the mean. All data were analysed using GraphPad Prism software (version 9).

A range of blocking buffers were incubated at 37°C to reduce non-specific complement deposition with HBSS-only wells. Both BSA and FCS sufficiently blocked the ELISA plates at these conditions, with the best results observed for FCS (**Figure 34**).

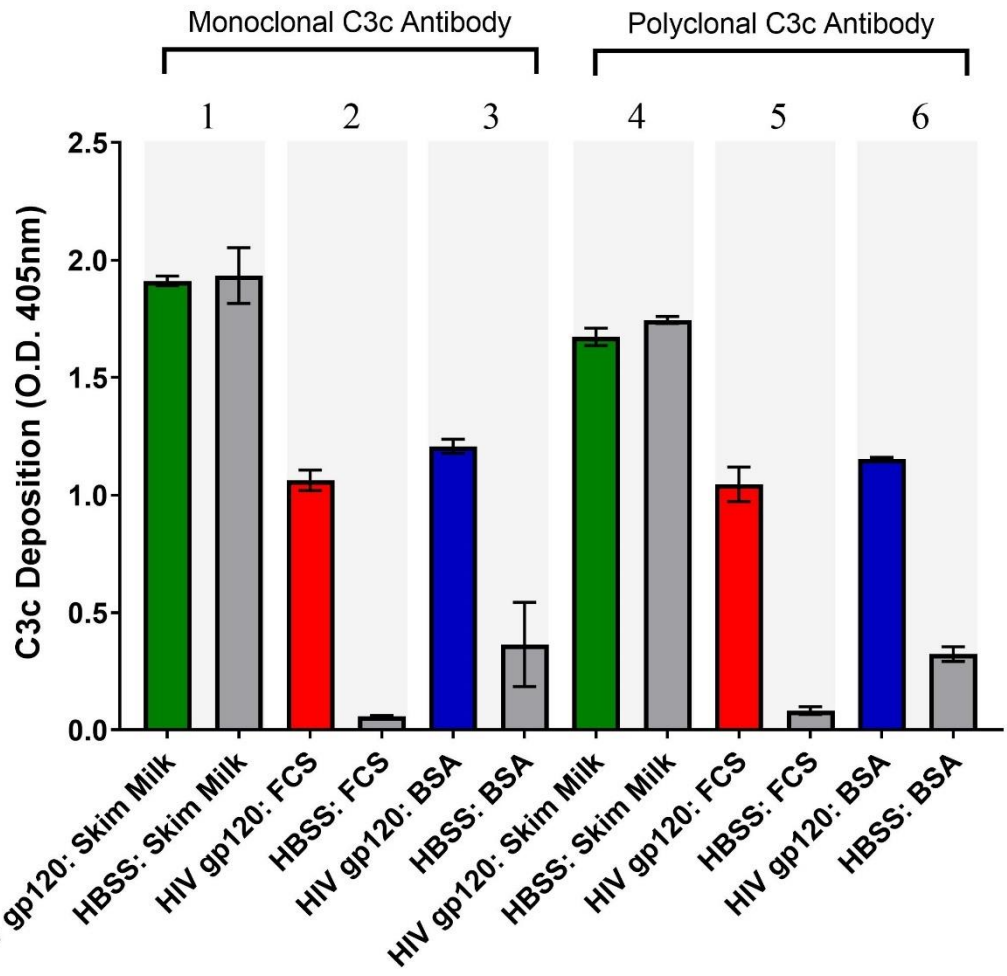

Blocking at 37°C for 1 hr				
Condition	**Coating Protein (3 µg/ml)**	**Blocking Buffer (200 µl)**	**Primary Antibody (2 µg/ml)**	**Secondary Antibody (2 µg/ml)**
1	HIV gp120	5% Skim milk	C3c monoclonal Antibody	HRP-conjugated anti-mouse IgG polyclonal antibody
	HBSS			
2	HIV gp120	5% FCS		
	HBSS			
3	HIV gp120	5% BSA		
	HBSS			
4	HIV gp120	5% Skim milk	HRP-conjugated C3c polyclonal antibody	NA
	HBSS			
5	HIV gp120	5% FCS		
	HBSS			
6	HIV gp120	5% BSA		
	HBSS			

Figure 34: C3c deposition ELISA: blocking at 37°C

HIV gp120 was used as a positive control and HBSS was used as a negative control. The X-axis labels describe the coat:block conditions. FCS and BSA blocking buffers suitably blocked non-specific C3c deposition in HBSS-coated wells at 37°C, with FCS showing the greatest reduction in background signal. Skim milk failed to prevent non-specific C3c deposition. There were no clear differences in assay signal between using the monoclonal or polyclonal anti-C3c antibody. Grey shaded areas show unique conditions for the assay which are numbered and described in the table. Error bars show the variation of replicates (n = 2) from the mean. All data were analysed using GraphPad Prism software (version 9). Abbreviations: NA = not applicable.

Once FCS at 37°C was determined to be the optimal condition for blocking the ELISA plates, different concentrations of FCS were tested against 2% and 10% PHP to determine suitable FCS concentrations (**Figure 35**). There was no further reduction in background signal with higher concentrations of FCS.

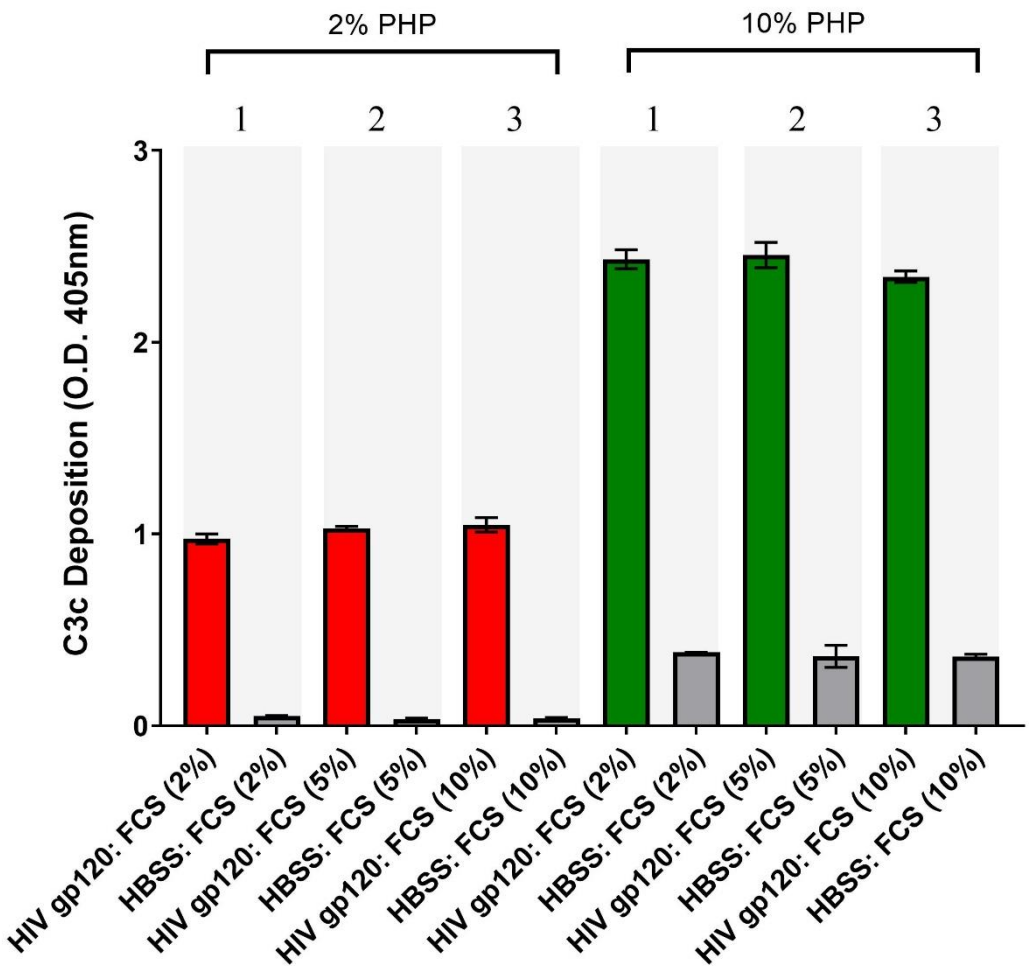
2% PHP
10% PHP
1
2
3
1
2
3
C3c Deposition (O.D. 405nm)
0
1
2
3
HIV gp120: FCS (2%)
HBSS: FCS (2%)
HIV gp120: FCS (5%)
HBSS: FCS (5%)
HIV gp120: FCS (10%)
HBSS: FCS (10%)
HIV gp120: FCS (2%)
HBSS: FCS (2%)
HIV gp120: FCS (5%)
HBSS: FCS (5%)
HIV gp120: FCS (10%)
HBSS: FCS (10%)

Blocking Test				
Condition	**Coating Protein (3 µg/ml)**	**Blocking Buffer (200 µl)**	**Primary Antibody (2 µg/ml)**	**Secondary Antibody (2 µg/ml)**
1	HIV gp120	2% FCS	C3c monoclonal antibody	HRP-conjugated anti-mouse IgG polyclonal antibody
	HBSS			
2	HIV gp120	5% FCS		
	HBSS			
3	HIV gp120	10% FCS		
	HBSS			

Figure 35: C3c deposition ELISA: assessment of FCS blocking agent

HIV gp120 was used as a positive control and HBSS was used as a negative control. The X-axis labels describe the coat:block conditions. There was no clear difference in the effectiveness of blocking with different concentrations of FCS. Both the positive and background signals increased with higher PHP concentrations. Grey shaded areas show unique conditions for the assay which are numbered and described in the table. Error bars show the variation of replicates (n = 2) from the mean. All data were analysed using GraphPad Prism software (version 9).

2.5.5.2 C3c ELISA: Antibody Optimisation

Primary and secondary antibody concentrations were optimised using a chequerboard approach to try and improve the signal-to-noise and reduce the background signal.

Methods

MaxiSorp™ ELISA plates were coated in duplicate with 100 µl of mannan (10 µg/ml) in HBSS and incubated overnight at 4°C. The plates were washed six times with 200 µl of wash buffer (HBSS containing 0.01% tween-20) and blocked with 200 µl of HBSS containing 5% FCS, at 37°C for 2 hrs, 400 rpm. The plates were washed six times with 200 µl of wash buffer and PHP was added at a concentration of 10% and incubated at 37°C for 30 min, 900 rpm. The plates were washed six times with 200 µl of wash buffer and incubated with 100 µl of anti-C3c monoclonal antibody (ThermoFisher Scientific) using 1 – 3 µg/ml concentrations, at RT for 1 hr. The plates were washed six times with 200 µl of wash buffer and incubated with 100 µl of HRP-conjugated

anti-mouse secondary antibody (ThermoFisher Scientific) using 1 – 3 µg/ml concentrations at RT for 1 hr. The plates were washed a final time and developed with 100 µl of One-Step Turbo TMB (ThermoFisher Scientific) substrate for 10 min in the dark. The O.D.s were measured at 450 nm and the data was analysed using GraphPad Prism software (version 9).

Result

There was no improvement in the signal-to-noise ratio with the use of higher antibody concentrations (**Figure 36**).

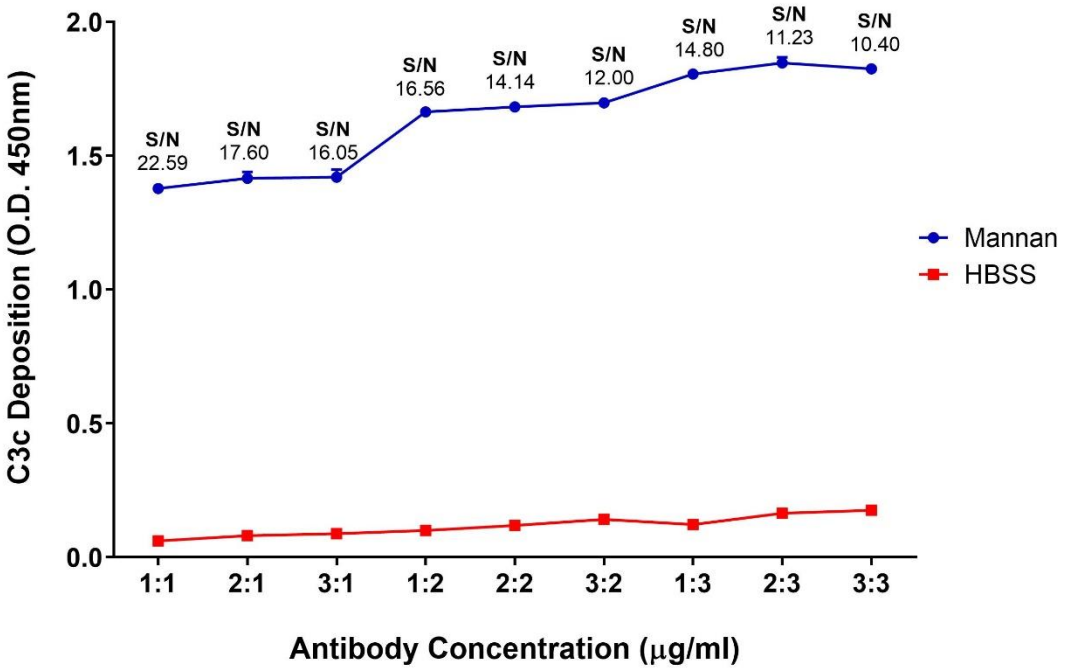

Figure 36: C3c deposition ELISA: antibody optimisation

An increase in antibody concentrations increased both the positive and background signals, resulting in a reduced signal-to-noise ratio (S/N) with higher concentrations. Each dot represents the mean value of all replicates (n = 2). The ratio of primary:secondary antibody concentrations varied between 1, 2, and 3 µg/ml whilst mannan (10 µg/ml) and PHP (10%) were at fixed concentrations. All data were analysed using GraphPad Prism software (version 9).

2.5.5.3 C3c ELISA: Coating and PHP Optimisation

Optimal concentrations of PHP and coating protein were determined using a chequerboard approach with the C3c deposition ELISAs.

Methods

MaxiSorp™ ELISA plates were coated in duplicate with 100 µl of antigen (mannan, HIV gp120, EBOV-GP, EBOV-sGP, SUDV-GP, SARS-CoV-1 spike, SARS-CoV-2 spike, HBSS) at 20, 10, and 5 µg/ml in HBSS and incubated overnight at 4°C. The plates were washed six times with 200 µl of wash buffer (HBSS containing 0.01% tween-20) and blocked with 200 µl of HBSS containing 5% FCS, at 37°C for 2 hrs, 400 rpm. The plates were washed six times with 200 µl of wash buffer and PHP was added at a concentration of 20%, 10%, and 5% in 100 µl of HBSS containing 5% FCS, and incubated at 37°C for 30 min, 900 rpm. The plates were washed six times with 200 µl of wash buffer and incubated with 100 µl of anti-C3c monoclonal antibody (ThermoFisher Scientific) at a concentration of 1 µg/ml, at RT for 1 hr. The plates were washed six times with 200 µl of wash buffer and incubated with 100 µl of HRP-conjugated anti-mouse secondary antibody (ThermoFisher Scientific) at a concentration of 1 µg/ml, at RT for 1 hr. The plates were washed a final time and developed using 100 µl of One-Step Turbo TMB (ThermoFisher Scientific) substrate for 10 min in the dark. The O.D.s were measured at 450 nm and analysed using GraphPad Prism software (version 9).

Results

The assay signal for C3c deposition was dependent on both coating concentrations and PHP concentrations, to varying extents for each protein. The use of 50 µl of protein at a concentration of 20 µg/ml for coating the ELISAs was used to determine assay limitations but would be too expensive to repeat in further assays with the desired number of replicates. Therefore, 10 µg/ml of protein was deemed optimal (**Figure 37**).

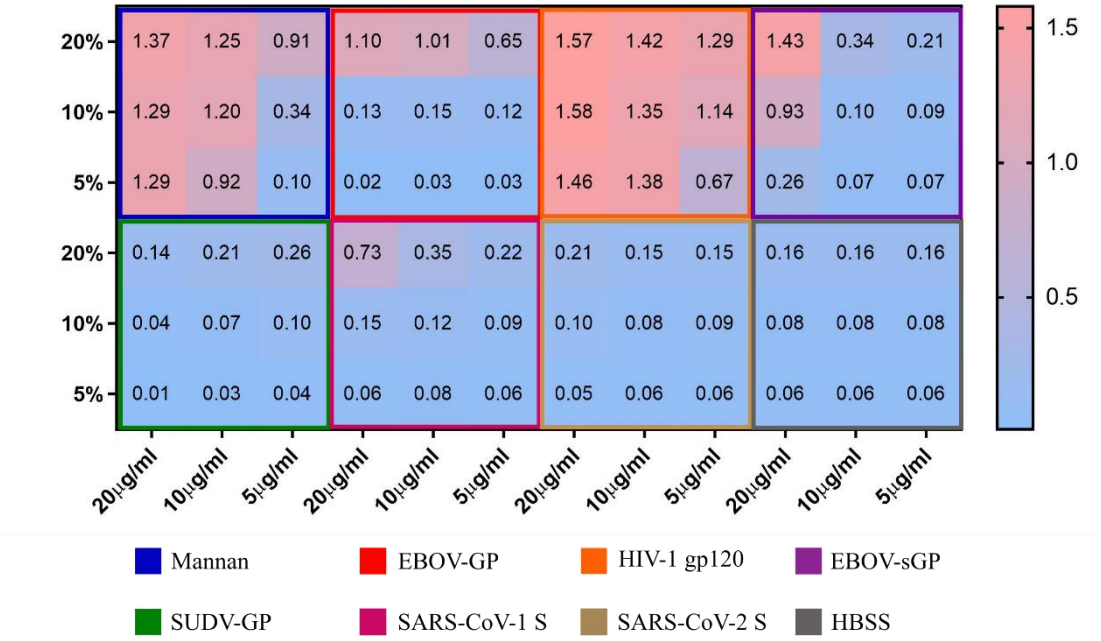

Figure 37: C3c deposition ELISA: coating optimisation

Both the coating concentration and the PHP concentration were important for the signal intensity of C3c complement deposition. C3c deposition ELISAs were performed on all viral proteins with mannan and HIV gp120 as positive controls, and HBSS as a negative control. The X axis shows the titration of the coating protein using 20 µg/ml, 10 µg/ml, and 5 µg/ml concentrations. The Y axis shows the titration of PHP using 20%, 10%, and 5% concentrations. The heatmap colours show the range of O.D. values from low (blue) to high (red), with the O.D. value labelled for each well. Single replicates were performed for all samples. All samples were analysed using GraphPad Prism software (version 9).

2.5.5.4 C3c ELISA: Initial Protein Screen

Following the optimisation of the C3c deposition ELISA, an initial screen was conducted using all viral proteins of interest to determine whether the assay was suitable for use.

Methods

MaxiSorp™ ELISA plates were coated in triplicate with 100 µl of antigen (mannan, HIV gp120, EBOV-GP, EBOV-sGP, SUDV-GP, SARS-CoV-1 spike, SARS-CoV-2 spike, HBSS) at a concentration of 10 µg/ml, or with HBSS-only, in HBSS and incubated

overnight at 4°C. The plates were washed six times with 200 µl of wash buffer (HBSS containing 0.01% tween-20) and blocked with 200 µl of HBSS containing 5% FCS, at 37°C for 2 hrs, 400 rpm. The plates were washed six times with 200 µl of wash buffer and PHP was added at a concentration of 10.00%, 5.00%, 2.50%, and 1.25% in 100 µl of HBSS containing 5% FCS, and incubated at 37°C for 30 min, 900 rpm. The plates were washed and incubated with 100 µl of anti-C3c monoclonal antibody (ThermoFisher Scientific) at a concentration of 1 µg/ml, at RT for 1 hr. The plates were washed and incubated with 100 µl of HRP-conjugated anti-mouse secondary antibody (ThermoFisher Scientific) at a concentration of 1 µg/ml, at RT for 1 hr. The plates were washed a final time and developed using 100 µl of One-Step Turbo TMB (ThermoFisher Scientific) substrate for 10 min in the dark. The O.D.s were measured at 450 nm and analysed using GraphPad Prism software (version 9). The negative cut-off was determined using the average of the HBSS-coated controls with 10% PHP for all plates, plus three SDs.

Results

Using a negative threshold of plus three SDs from the mean of HBSS-only wells with 10% PHP, mannan, HIV gp120, and the EBOV-sGP were clear positives. The SARS-CoV-1/2 spike proteins were very weak positives and the EBOV-GP and SUDV-GP fell below the threshold for a positive signal. Based on these results and the previous optimisation attempts, the background of the C3c deposition ELISA was still too high to obtain information regarding the potential for complement activation with all of the viral proteins tested (**Figure 38**). Eventually, the assay was modified to target C5b-9 instead of C3c using the methods described in section **2.2.11**, which suitably reduced the background signal and enabled a clear identification for antigen-specific complement deposition (**Figure 22**).

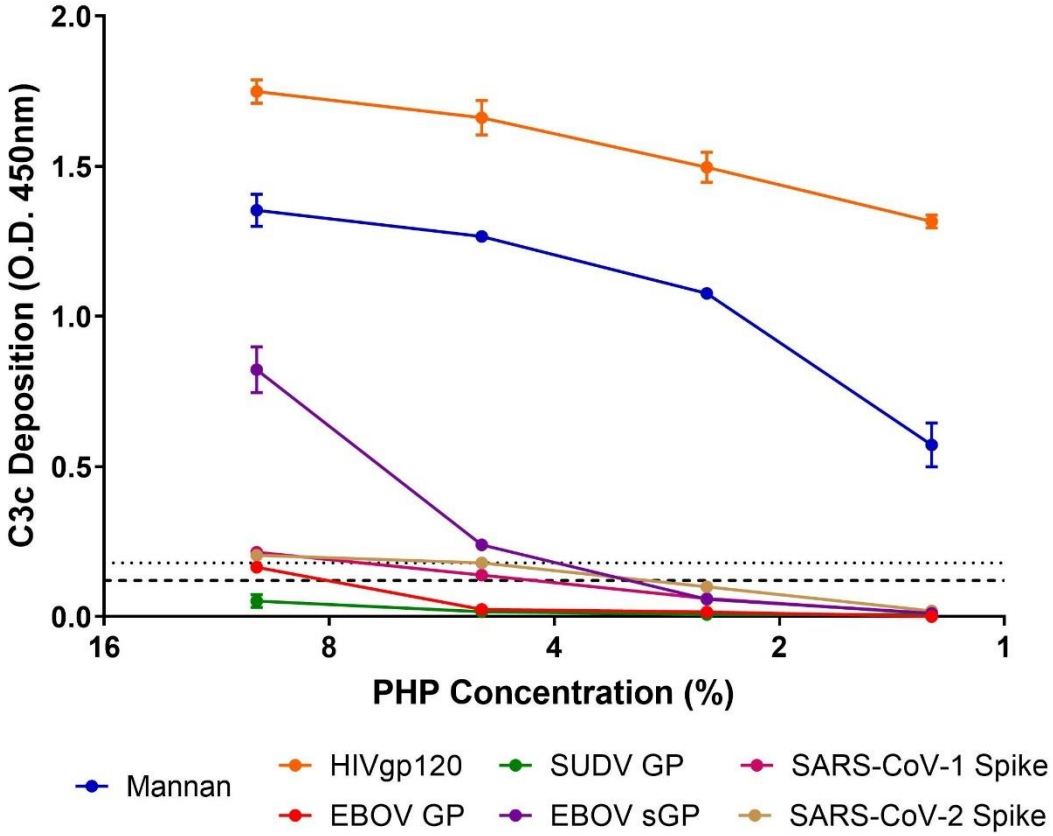

Figure 38: C3c deposition ELISA with viral proteins

C3c deposition ELISAs were performed on all viral proteins with mannan and HIV gp120 as a positive control. PHP was titrated for each protein to determine a linear range of C5b-9 deposition for interpolation. A negative cut-off (grey dotted line) was determined using HBSS-only wells incubated with 10% PHP plus three SDs. Each dot represents the mean value of triplicate samples with error bars to show the variation. The dashed line shows the mean value for all HBSS-only controls, and the dotted line shows the mean plus three SDs. All samples were analysed using GraphPad Prism software (version 9).

2.5.6 C5b-9 ELISA Development

The C3c deposition ELISA was modified to target a neoantigen of the C9 protein in the C5b-9 complex.

2.5.6.1 C5b-9 ELISA: Standard Curve

A standard curve was generated using mannan-coated wells and a titration of PHP for the interpolation of data.

Methods

The methods are as described in section **2.2.11** for the C5b-9 deposition ELISA with the following modifications: mannan was coated at a concentration of 10 µg/ml and PHP was titrated in a 2:3 dilution series from 40% - 0.5%.

Results

A sigmoid curve was obtained with the titration of PHP against mannan and fitted with a 4-parameter logistic curve (**Figure 39**).

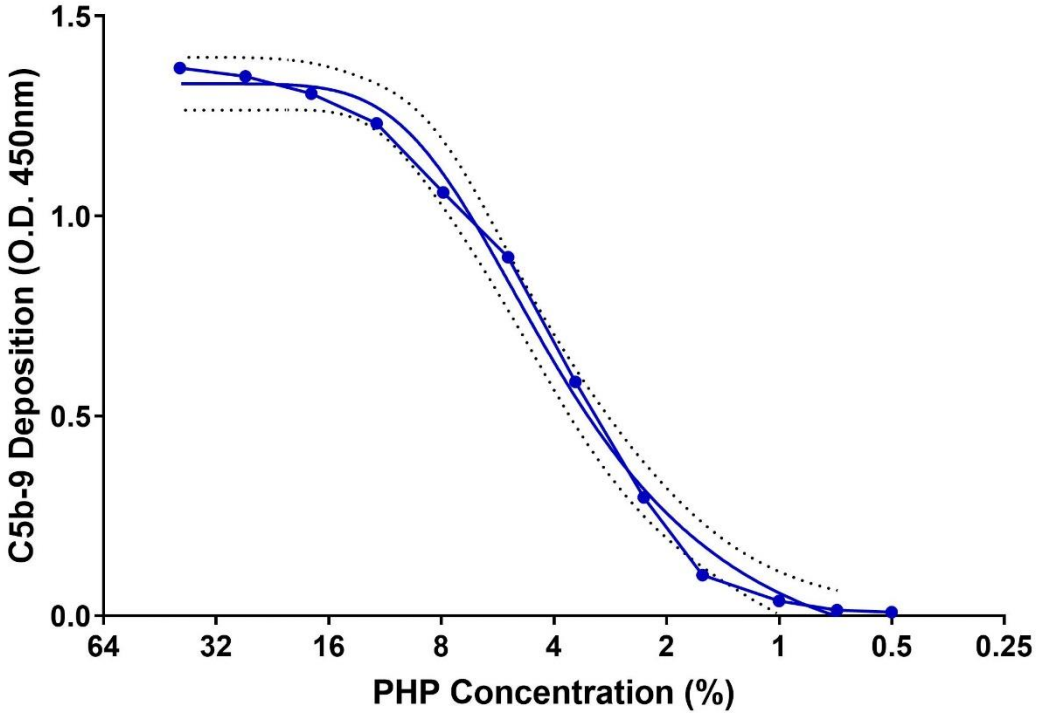

Figure 39: C5b-9 deposition ELISA standard curve

The standard curve of C5b-9 deposition against mannan was fitted with a 4-parameter logistic (4PL) curve (blue line without dots) and used for interpolation of MBL binding to viral proteins. The dotted lines represent the error bars for the 4PL mean. Each large dot represents the mean value of all replicates (n = 3). All data were analysed using GraphPad Prism software (version 9).

2.5.6.2 C5b-9 ELISA: EDTA Controls

EDTA was included with the highest concentration of PHP used for each viral protein as a negative control.

Methods

The methods are as described in section **2.2.11** for the C5b-9 deposition ELISA with no modifications.

Results

The addition of 10 mM EDTA at the PHP incubation stage reduced all positive signals below the negative threshold (**Figure 40**).

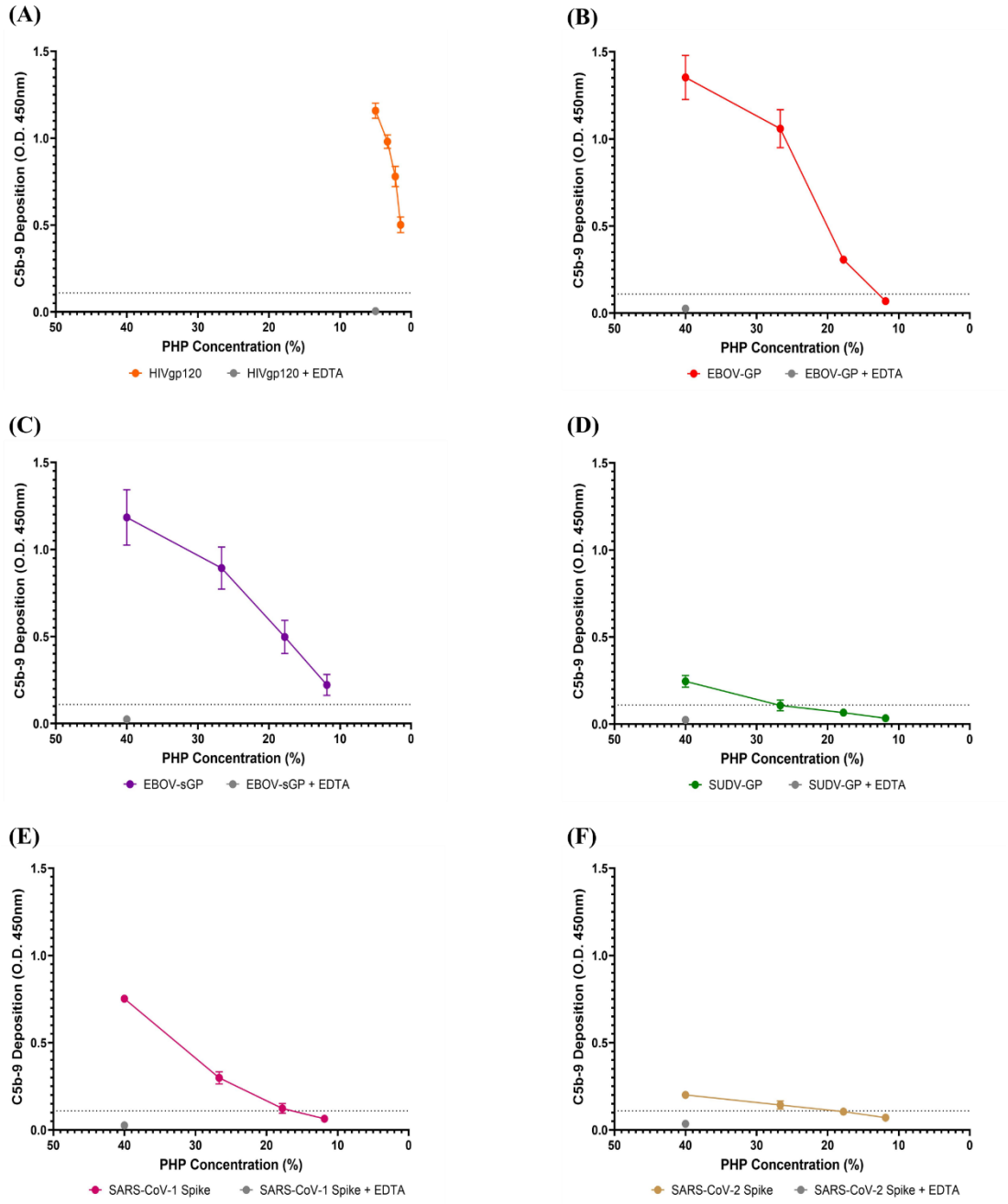

Figure 40: C5b-9 deposition ELISA with EDTA controls

C5b-9 deposition ELISAs were performed on all viral proteins with mannan as a positive control. A negative cut-off (grey dotted line) was determined using HBSS-only wells incubated with 20% PHP plus three SDs. Each dot represents the mean value of triplicate samples across duplicate assays (total n = 6) with error bars to show the variation. ***(A)*** *HIV gp120 PHP titration with EDTA control,* ***(B)*** *EBOV-GP PHP titration with EDTA control,* ***(C)*** *EBOV-sGP PHP titration with EDTA control,* ***(D)*** *SUDV-GP PHP titration with EDTA control,* ***(E)*** *SARS-CoV-1 spike protein PHP titration with EDTA*

control, ***(F)*** *SARS-CoV-2 spike protein PHP titration with EDTA control. Each EDTA control is represented as a single grey dot for each protein. All samples were analysed using GraphPad Prism software (version 9).*

Chapter 3: Antibody-Dependent Complement Deposition

3.1 Introduction

In the previous chapter, I demonstrated the potential for the complement system to be activated to completion (resulting in the formation of the membrane attack complex (MAC)), in response to a range of *Ebolavirus* and *Coronavirus* glycoproteins (GPs). This mechanism was antibody-independent and at least partially mediated by the binding of MBL. The complement system bridges the innate and adaptive immune responses, and the presence of antibodies can significantly alter complement activity. In this chapter, I investigated the potential for low-neutralising EBOV-convalescent plasma to mediate antibody-dependent complement deposition (ADCD) in response to the EBOV-GP, EBOV-sGP, and SUDV-GP, as a potential Fc-mediated component of EBOV immunity.

Initial investigations to determine the level of protection conferred by antibodies are often based on neutralisation assays. Whilst antibody neutralisation titres can be a good indicator of protection, other immune effector functions can be of equal importance and neutralisation alone does not always confer protection, as previously discussed for EBOV in **Chapter 1** (369,383). However, these immune effector functions are typically more complex to measure than neutralisation, and can often be overlooked, at least during the early investigations into correlates of protection. As discussed previously for EBOV, the importance of Fc-mediated antibody functions were recognised and included in the monoclonal antibody INMAZEB^{TM} formulation approved by the FDA (553). However, the emergence of new variants puts pressure on the use of monoclonal antibodies as therapeutics and creates a further need for new interventions. For SARS-CoV-2, new variants continue to emerge, whilst for *Ebolaviruses*, other pathogenic strains (SUDV and BDBV) currently have no licensed therapeutics and new EBOV outbreaks continue to arise. A deeper understanding of the influence of immune effector functions on these viruses may provide greater variety for the selection of therapeutic antibodies to expedite future therapeutic developments. The complement system, for example, is an Fc-mediated immune

effector function that is often excluded from immunoassays *via* heat-inactivation due to complications with cytotoxic effects against cultured cells.

ADCD is a measurement of complement deposition mediated by the antibody-dependent classical pathway. The ability to mediate ADCD varies greatly between antibodies, depending on factors such as epitope diversity (554–556) and antibody isotype (15,557,558). Gunn *et al* showed that ADCD was crucial for the complete protection of mice against MA-EBOV using engineered antibody Fc variants (559). Other antibody-mediated immune effector functions, independent from neutralisation, were shown to contribute to EBOV protection (560,561) and polyfunctional antibodies show a strong relationship with protection, similar to neutralisation (369,562). For BDBV, the presence of antibodies capable of mediating ADCD was associated with the absence of certain long-term sequelae (267). The effects of ADCD on immunity can include the promotion of inflammation and chemotaxis, signalling to other immune cells, opsonisation of virions, aggregation of virions, and formation of the MAC. Whilst ADCD has occasionally been acknowledged with regards to EBOV infection, it is an area which remains largely under-researched.

In this chapter, we hypothesised that low-neutralising, convalescent EVD plasma would be able to mediate ADCD in response to the *Ebolavirus* GPs as a potential Fc-mediated function for protection. We developed novel flow cytometry assays to determine the potential for EVD convalescent plasma from the 2013-2016 West African EBOV epidemic to mediate ADCD, and attempt to understand which factors influence this response. I first identified two cohorts from historical data collected during a longitudinal study (372) of EBOV survivor responses: one cohort with low EBOV-neutralisation titres relative to EBOV-GP IgG titres (LN cohort), and the other with a direct linear relationship between EBOV-neutralisation and EBOV-GP IgG titres (N cohort). We measured the ability to mediate ADCD between these cohorts in response to the EBOV-GP and EBOV-sGP as these proteins are the most likely to interact with antibodies and the complement system during EBOV infection, due to their expression on the surface of the virions and infected cells, or secretion from the

host cell, respectively. This work was then expanded using the SUDV-GP from the second-most virulent *Ebolavirus* species, to determine whether these mechanisms would occur with cross-reactive EBOV-GP antibodies, and to consider which factors might influence this relationship with ADCD. This was the first characterisation of EVD plasma for ADCD and is most relevant in the event of EBOV re-infection, recrudescence, and cross-reactivity, with implications for pathogenesis and protection.

Following the emergence of SARS-CoV-2, these ADCD flow cytometry assays were adapted for use with the SARS-CoV-2 spike protein. In collaboration with the Pathogen Immunology Group at the UKHSA and with the University of Oxford, these assays were first used to investigate multifunctional antibody responses (including ADCD) in recipients of the ChAdOx1 nCoV-19 vaccine. In this study, we hypothesised that vaccine-induced antibodies to the SARS-CoV-2 spike protein could mediate ADCD, which may be an Fc-mediated function important for survival. We showed that ADCD was induced following the prime dose, and was significantly increased in a dose-dependent response with a booster vaccine. This research supported the use of a two-dose vaccine regime for phase III clinical trials (504). The second research collaboration investigated the divergent trajectories of immune responses following natural infection with SARS-CoV-2. We hypothesised that ADCD would be associated with disease severity and could be protective. Using a machine-learning approach, ADCD was found to correlate with disease severity up to 180 days post-infection and was one of the most significant predictors of immune responses following infection (563). Lastly, the ADCD assays were used to investigate sex differences in response to the ChAdOx1-nCoV-19 vaccine (manuscript submitted). The SARS-CoV-2 ADCD research was a contribution to collaborative research that is now published. For this reason, the remainder of this section will be focussed on the EBOV work central to this PhD project.

3.2 Methods

3.2.1 Sample Collection and Ethics

West African plasma and pooled human plasma (PHP) as an exogenous source of complement from UK volunteers was collected and processed as described in section **2.2.1**. In this chapter, we used the PHP batch from 20 UK volunteers, collected and processed by the Pathogen Immunology Group at the UKHSA.

3.2.3 Sample Selection Criteria

EBOV convalescent and naïve plasma from the 2015-2017 longitudinal study (372) was utilised in wild-type EBOV neutralisation assays and EBOV-GP ELISAs prior to this PhD project. Using data from 145 plasma samples from 2017, I correlated EBOV-GP IgG titres with EBOV-neutralisation titres to identify two cohorts: one with low-neutralisation titres in relation to EBOV-GP IgG titres (LN cohort), and one with a direct linear relationship between neutralisation and EBOV-GP IgG titres (N cohort). The LN cohort was determined using a maximum neutralisation score cut-off of 130 GMT to identify samples with a low neutralisation titre, a minimum antibody titre cut-off of 0.35 optical density (O.D.) at 405 nm to ensure the presence of EBOV-GP IgG antibodies, and a maximum residual cut-off from the line of best fit of -100 GMT to select for low-neutralising antibodies. The N cohort was defined by a neutralisation score cut-off greater than 200 GMT and the closest possible residual to the line of best fit to obtain matching cohort numbers. Two additional plasma samples for each cohort were identified using the 2017 historical neutralisation data collected prior to this study, and the flow cytometry assays developed within this PhD project. Correlations were defined as follows: no correlation (R^2 = < 0.200 and P value > 0.050), weak correlation (R^2 = 0.210–0.400 and P value < 0.050), moderate correlation (R^2 = 0.410–0.700 and P value < 0.050), strong correlation (R^2 = 0.710–1.000 and P value < 0.050).

3.2.4 Fluorescent Bead Protein Conjugation

EBOV-GP (*Makona* strain, sourced from the Nuffield Department of Medicine, Oxford University, Oxford, UK. GenBank Accession: AHX24649.1) (372), EBOV-sGP (*Mayinga*

strain, sourced from IBT Bioservices. GenBank Accession: AHC70242.1), and SUDV-GP (*Gulu* strain, sourced from SinoBiological. GenBank Accession: YP_138523.1) were covalently coupled to SPHERO™ Magnetic Flow Cytometry Multiplex Bead Assay Particles (Spherotech) using a modification of a published protocol (564), with protein concentrations at saturation levels. Modifications were as follows: centrifuge steps were replaced with magnetic bead retention for >30 s using the EasyEights™ EasySep™ Magnet (STEMCELL Technologies), and the conjugated beads were blocked using phosphate-buffered saline (PBS) containing 2% Bovine Serum Albumin (BSA) and 0.05% sodium azide (pH 7.4). A known EBOV-GP IgG positive convalescent plasma sample with known reactivity to EBOV-GP, EBOV-sGP, and cross-reactivity to SUDV-GP based on my IgG ELISAs in results section **2.3.7**, was used for IgG detection to determine whether the conjugation was successful.

3.2.5 Flow Cytometry Data Acquisition

A minimum of 100 beads per sample were acquired with a CytoFLEX S flow cytometer (Beckman Coulter). Conjugated beads were first gated based on the forward scatter and violet side scatter. A histogram of the APC peak was then gated to select for the APC-fluorescent beads, and presented on either a FITC histogram (C3c deposition) or PE histogram (IgG, C1q, and C5b-9 deposition). The gating method is demonstrated in **Figure 41** . FlowJo software (version 10.8.0.) was then used to determine the median fluorescence intensity (MFI) values within the FITC and PE channels, and this data was finally presented using GraphPad Prism software (version 9).

3.2.6 Flow Cytometry IgG Binding Assays

Heat-inactivated plasma samples (heat block at 56^{o}C for 30 min) were diluted 1:50 in blocking buffer (Hank's Balanced Salt Solution (HBSS) containing 2% BSA) and titrated 1:2 for a 3-point dilution series in duplicate, transferring 20 µl. A further 20 µl of EBOV-GP, EBOV-sGP, or SUDV-GP conjugated beads (50 beads per µl) were added to each sample for a final plasma dilution of 1:100, 1:500, and 1:2500. Samples were incubated for 1 h at RT whilst shaking at 550 rpm, then washed twice in 200 µl of wash buffer (HBSS, 0.05% tween-20) and resuspended in 100 µl (0.5 µg/ml) of PE-

conjugated anti-human IgG (Cambridge Bioscience) in blocking buffer. Samples were again incubated for 1 h at RT whilst shaking at 550 rpm, washed twice in 200 µl of wash buffer, and resuspended in 50 µl HBSS. The samples were then acquired according to section **3.2.5**.

Quality controls (QCs) were included for all IgG assays, using three dilutions of the same plasma sample with the EBOV-GP conjugated beads, in duplicate. All replicates and QCs were below 30% CV (Appendix I, **Figure 51 (A)**). For the IgG assays using SUDV-GP and EBOV-sGP conjugated beads, further controls were included to monitor bead integrity using a single plasma dilution (Appendix I, **Figure 51 (B)**). All replicates were below 15% CV. The final results were reported using a single plasma dilution point which avoided assay saturation, with the negative sample value subtracted from the corresponding plate.

3.2.7 Flow Cytometry C1q Binding Assays

EBOV-GP, EBOV-sGP, or SUDV-GP conjugated beads were incubated with heat-inactivated EBOV-GP IgG positive plasma with known reactivity to EBOV-GP, EBOV-sGP, and SUDV-GP, or incubated with heat-inactivated (56^{o}C for 30 min) EBOV-GP negative plasma, at a final 1:20 plasma dilution, in duplicate. The samples were then incubated for 30 min at 25^{o}C whilst shaking at 900 rpm, washed twice in 200 µl of wash buffer (same method for all subsequent wash steps), and resuspended in 100 µl (5 µg/ml, 2.5 µg/ml, and 1.25 µg/ml) of purified C1q protein (Sigma Aldrich) or with blocking buffer only. The samples were then incubated at 25^{o}C for 1 h whilst shaking at 900 rpm, washed, and resuspended in 100 µl (1 µg/ml) of anti-C1q monoclonal antibody (Quidel). The samples were then incubated at 25^{o}C for 30 min whilst shaking at 900 rpm, washed, and resuspended in 100 µl (1 µg/ml) of PE-anti-mouse IgG (ThermoFisher Scientific). After a final incubation step at 25^{o}C for 30 min whilst shaking at 900 rpm, the samples were washed and resuspended in 50 µl of HBSS. The samples were then acquired according to section **3.2.5**. A negative cut-off was determined using an average of all bead and plasma controls which excluded the primary antibody step, plus three standard deviations.

3.2.8 Flow Cytometry C3c and C5b-9 Deposition Assays

Heat-inactivated EBOV-GP IgG positive plasma starting from a 1:10 (SUDV-GP) or 1:20 (EBOV-GP and EBOV-sGP) dilution was serially diluted 1:2 in duplicate and incubated with EBOV-GP, EBOV-sGP, or SUDV-GP conjugated beads (50 beads per µl) for 30 min at 25^{o}C whilst shaking at 900 rpm. The samples were washed twice in 200 µl of wash buffer (same method for all subsequent wash steps) and resuspended in 50 µl of PHP (1:10 in blocking buffer). The samples were then incubated at 37^{o}C for 15 min whilst shaking at 900 rpm and washed. For C3c detection, the samples were resuspended in 100 µl (1:500 dilution in blocking buffer) of FITC-conjugated rabbit anti-human C3c polyclonal antibody (Abcam) and incubated for 20 min in the dark. For C5b-9 detection, the samples were resuspended in 100 µl (1 µg/ml in blocking buffer) of a monoclonal C5b-9 antibody (SantaCruz Biotechnology) and incubated for 20 min in the dark. C5b-9 detection required a further wash step, resuspension in 100 µl (1 µg/ml) of PE-conjugated anti-mouse polyclonal antibody (ThermoFisher Scientific), and incubation for 20 min in the dark. For both the C3c and C5b-9 deposition assays, the beads were washed and re-suspended in 50 µl HBSS. The samples were then acquired according to section **3.2.5**.

Each plate included a heat-inactivated EBOV-GP IgG negative plasma control, a primary antibody-only control, a PHP-only control, and a plate QC using EBOV-GP beads with a fixed dilution of EBOV-GP IgG positive plasma (C3c: **Appendix I**, **Figure 52 (A)**, C5b-9: **Appendix I**, **Figure 53 (A)**). A further QC to monitor bead integrity was included, using either EBOV-GP, EBOV-sGP, or SUDV-GP beads at a fixed plasma dilution (C3c: **Appendix I**, **Figure 52 (B)**, C5b-9: **Appendix I**, **Figure 53 (B)**). All replicates and QCs were within 30% CV. Linear regression was used to predict the MFI from larger dilutions when plasma samples saturated the assay at the 1:10 or 1:20 dilution. Where new bead conjugations were required, the negative sample MFI on each plate was subtracted from the relevant samples to best normalise the data based on the QCs. All other assays used a single bead conjugation where the PHP-only control was subtracted, based on the QC data. Assays were certified fit for

purpose by using heat-inactivated 10% PHP with a range of EBOV-GP IgG positive plasma to confirm that a heat-labile plasma component (indicative of complement) was required for the positive signal, and with the use of a range of negative plasma to determine the background fluorescence.

3.3 Results

3.3.1 Gating Strategy and Confirmation of Protein Conjugation

An EBOV-GP IgG positive plasma sample with known reactivity to EBOV-GP, EBOV-sGP, and cross-reactivity to SUDV-GP based on my IgG ELISAs in results section **2.3.7**, along with an EBOV-GP IgG negative plasma sample, were used to confirm successful protein conjugation to the beads and determine the background fluorescence. The addition of EBOV-GP IgG positive plasma demonstrated an increase in MFI on the PE-A channel for IgG (**Figure 41 (C)**) and C5b-9 (**Figure 41 (D)**), and the FITC-A channel for C3c (**Figure 41 (E)**), as an indication of successful protein conjugation.

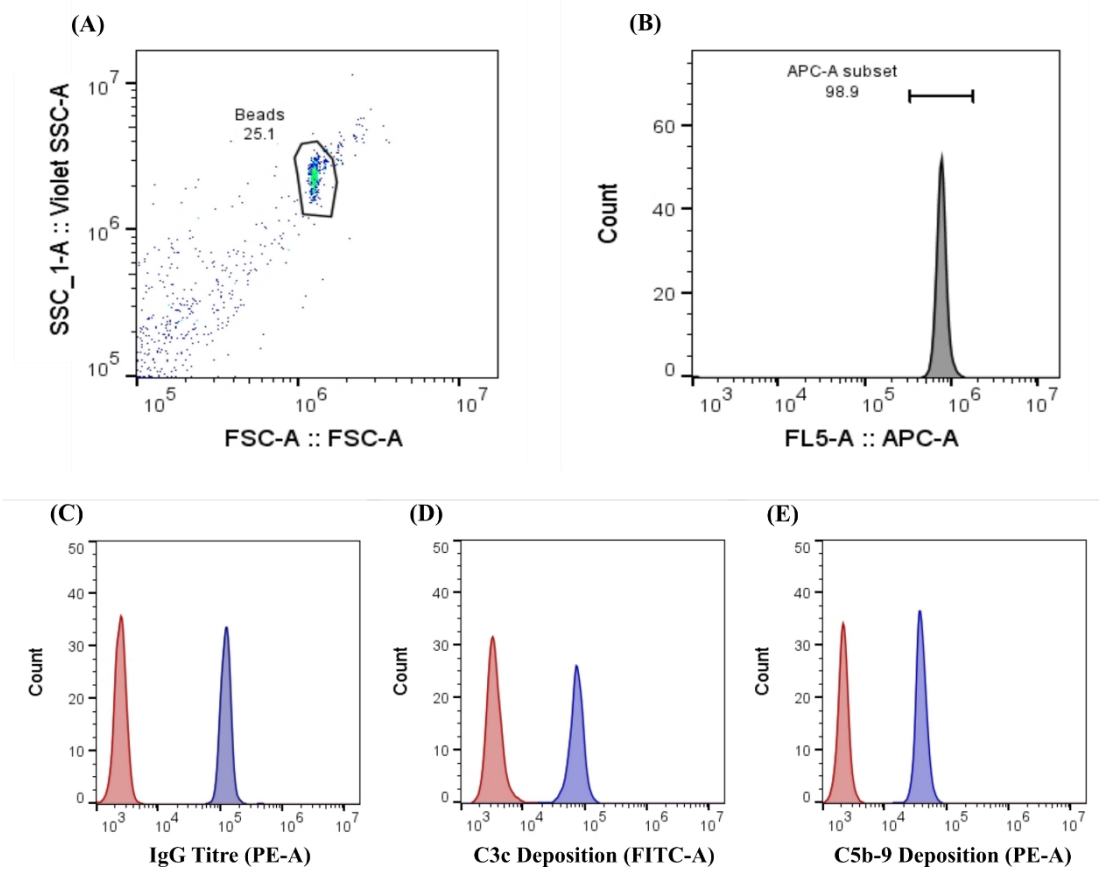

Figure 41: Gating strategy example for flow cytometry assays

The median fluorescence intensity (MFI) for all flow cytometry samples was determined using FlowJo software (Version 10.8.0). ***(A)*** *The forward-scatter versus violet side-scatter was used to create the first gate around the conjugated beads.* ***(B)*** *The second gate, specific to the APC-fluorescent beads, was created using the APC channel. Lastly, the MFI for* ***(C)*** *IgG binding,* ***(D)*** *C3c deposition, or* ***(E)*** *C5b-9 deposition could be determined via the FITC or PE channels. Example data shows an EBOV-GP IgG negative (red) and positive (blue) plasma sample with EBOV-GP-conjugated beads.*

3.3.2 Sample Selection and the Relationship of IgG/C1q Binding to *Ebolavirus* Glycoproteins

The complement system has many implications for pathogenesis and immunity, and the first steps of the classical pathway are IgG and C1q binding. This response can vary greatly between plasma samples which suggests that complement-mediated immune effector functions would also vary and could impact pathogenesis. We identified two cohorts (the LN and N cohorts) based on their relative neutralisation

and EBOV-GP IgG titres, and assessed their potential to mediate ADCD as a possible Fc-mediated function for survival.

The LN and N cohorts were identified from the correlation between neutralisation titres collected in the longitudinal study (372) and the EBOV-GP IgG titres also in the longitudinal study (**Figure 42**, **(A)**), or the flow cytometry data collected in this study (which included four additional plasma samples of interest) (**Appendix I**, **Figure 50**). Using flow cytometry, we observed IgG binding to the EBOV-GP (**Appendix I**, **Figure 51**, **(C)**), EBOV-sGP (**Appendix I**, **Figure 51**, **(D)**), and SUDV-GP (**Appendix I**, **Figure 51**, **(E)**) with all convalescent plasma samples. No binding was observed when using EBOV-GP IgG negative plasma.

The total IgG binding of plasma samples in the LN and N cohorts to EBOV-GP, EBOV-sGP, and SUDV-GP were compared after subtracting the negative plasma sample MFI from each plate (**Figure 42** , **(B)**). The total IgG binding of the LN and N cohorts to EBOV-GP (P = 0.673) and EBOV-sGP (P = 0.239) showed no significant difference using a Mann-Whitney test. However, the total IgG binding to SUDV-GP was significantly higher (P = 0.005) with a 1.4 log2-fold increase for the N cohort compared to the LN cohort. Linear regression analysis (GraphPad Prism software, version 9) was used to compare the titres for IgG binding in the LN and N cohorts to EBOV-GP, EBOV-sGP, and SUDV-GP (**Figure 42** , **(C)**). These parameters were correlated to identify possible variations in IgG binding to the *Ebolavirus* proteins. For the N cohort, there was a strong correlation between EBOV-GP and EBOV-sGP (R^2 = 0.734), a moderate correlation between SUDV-GP and EBOV-GP (R^2 = 0.429), and a weak correlation between SUDV-GP and EBOV-sGP (R^2 = 0.384). For the LN cohort, there was no correlation between any of the proteins tested: EBOV-GP and EBOV-sGP (R^2 = 0.036), SUDV-GP and EBOV-GP (R^2 = 0.007), and SUDV-GP and EBOV-sGP (R^2 = 0.009).

I then determined the potential for C1q to bind IgG in complex with the *Ebolavirus* proteins, and whether C1q could bind the viral antigens in absence of EBOV-GP IgG, as these are critical steps for the activation of the classical complement pathway

(**Figure 43**). Firstly, C1q binding was not observed with the use of EBOV-GP IgG negative plasma for any of the *Ebolavirus* proteins. Second, the detection of C1q binding to the EBOV-GP and EBOV-sGP was only observed with EBOV-GP IgG positive plasma and the addition of purified C1q, whilst C1q binding to the SUDV-GP was negative for all conditions tested. IgG binding to the EBOV-GP and EBOV-sGP was an essential preliminary step to detect C1q binding but a positive signal for SUDV-GP was not determined.

In summary, two cohorts (LN and N cohort) were identified based on their EBOV-GP IgG titres relative to their EBOV neutralisation titres (**Figure 42**, **(A)**). The LN cohort had a significantly lower IgG titre to the SUDV-GP compared to the N cohort, whilst EBOV-GP and EBOV-sGP IgG titres were similar for both cohorts (**Figure 42**, **(B)**). There was no clear relationship in these IgG titres between the *Ebolavirus* proteins for the LN cohort, whilst the N cohort correlated as expected (**Figure 42**, **(C)**). Lastly, the addition of EBOV-GP IgG positive plasma was essential for the detection of C1q binding to the EBOV-GP and EBOV-sGP, but no signal was detected for the SUDV-GP (**Figure 43**).

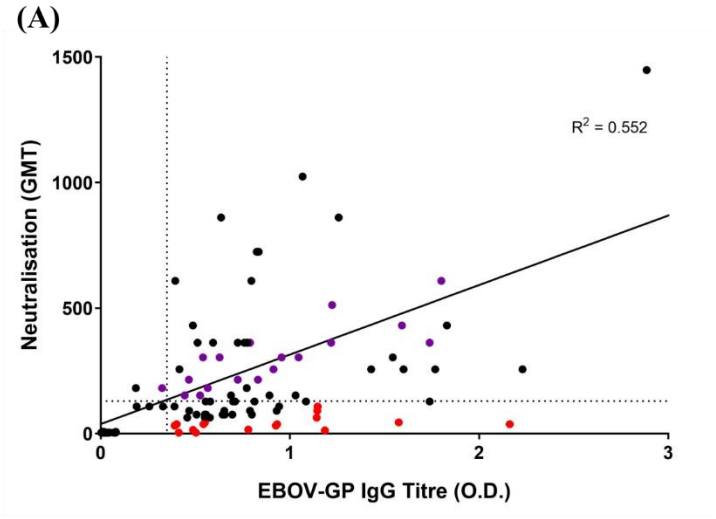
(A)
Neutralisation (GMT)
EBOV-GP IgG Titre (O.D.)
R2 = 0.552
1500
1000
500
0
0
1
2
3

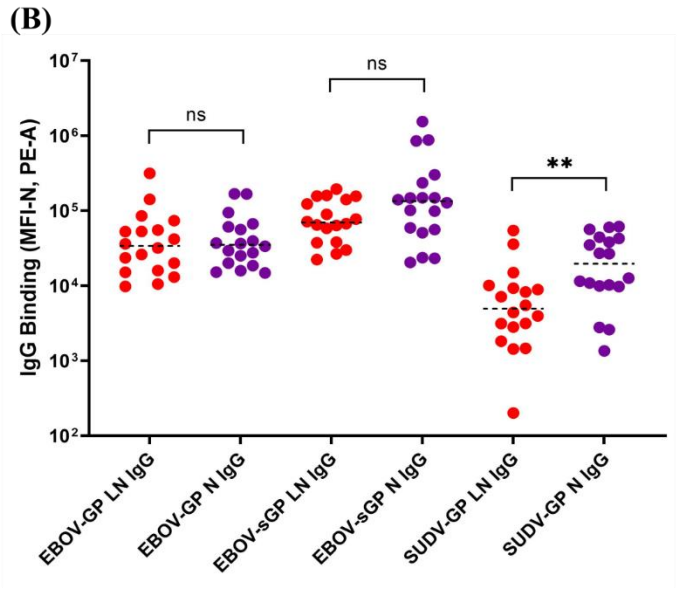
(B)
IgG Binding (MFI-N, PE-A)
ns
ns
**
EBOV-GP LN IgG
EBOV-GP N IgG
EBOV-sGP LN IgG
EBOV-sGP N IgG
SUDV-GP LN IgG
SUDV-GP N IgG

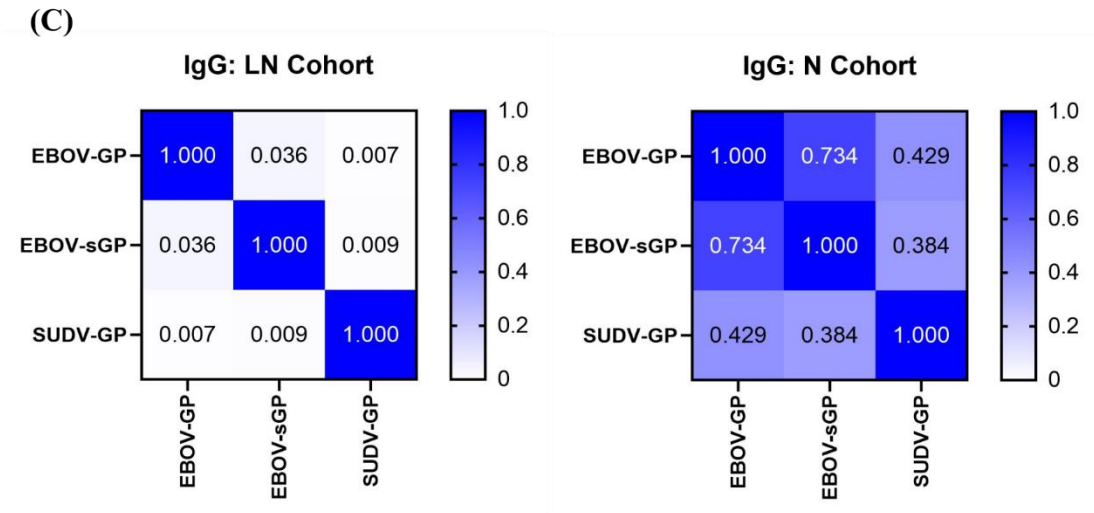
(C)
IgG: LN Cohort
EBOV-GP
EBOV-sGP
SUDV-GP
1.000
0.036
0.007
0.036
1.000
0.009
0.007
0.009
1.000
IgG: N Cohort
1.000
0.734
0.429
0.734
1.000
0.384
0.429
0.384
1.000
1.0
0.8
0.6
0.4
0.2
0

Figure 42: Selection of convalescent EVD plasma samples and their IgG binding to EBOV-GP, EBOV-sGP, and SUDV-GP

(A) *Historic EBOV neutralisation and EBOV-GP IgG ELISA data for 145 samples were correlated and analysed via linear regression. A neutralisation cut-off of < 130 GMT (horizontal dotted line), an IgG titre > 0.35 O.D. (vertical dotted line), and a maximum residual from the line of best fit (< -100 GMT) was used to select the LN cohort (red dots, n = 16). A neutralisation cut-off > 200 GMT and with the nearest possible residual to the line of best fit was used to select the N cohort.* ***(B)*** *Plasma from the LN (n = 18) or the N (n = 18) cohorts were incubated with EBOV-GP, EBOV-sGP, and SUDV-GP conjugated beads, and analysed via flow cytometry. Significant differences were determined by a Mann-Whitney test using the mean (dotted lines) values of each cohort.* ***(C)*** *Each bead conjugate incubated with LN (n = 18) and N (n = 18) plasma was analysed via a pairwise linear regression analysis and the R^2 values were represented as heatmaps. Abbreviations: median fluorescence intensity (MFI), negative (N), not significant (ns).*

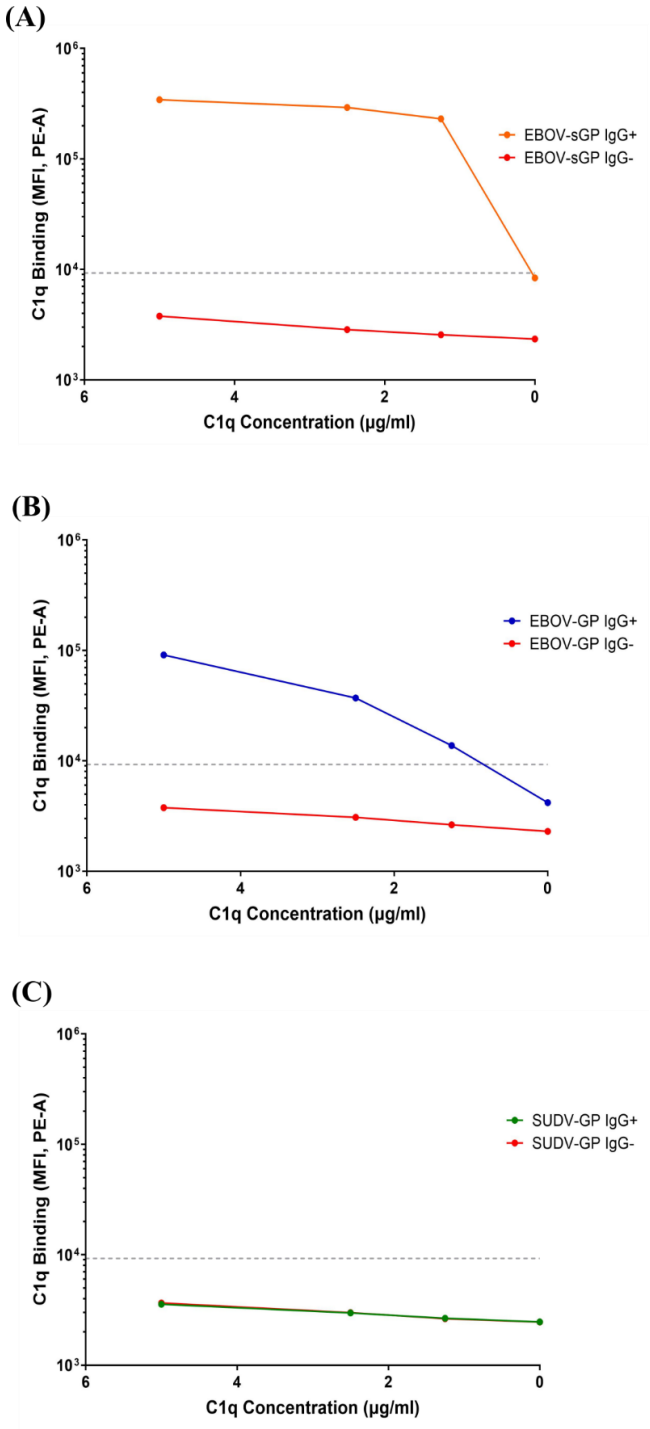

Figure 43: C1q binding to the EBOV-GP, EBOV-sGP, and SUDV-GP with EBOV-GP IgG positive plasma

*A titration of purified C1q protein was added to **(A)** EBOV-GP, **(B)** EBOV-sGP, and **(C)** SUDV-GP conjugated beads with EBOV-GP IgG positive or negative plasma. All samples were tested in duplicate and each dot represents the mean values calculated in GraphPad Prism software (version 9). Error bars were too small to be displayed. The negative cut-off (grey dotted line) was determined using the mean value of all control samples (n = 6) without the primary antibody, plus three standard deviations.*

3.3.3 Bead Validation with Heat-Inactivated PHP

We developed C3c and C5b-9 deposition assays to measure the ability of plasma samples to mediate ADCD in response to the *Ebolavirus* GPs. Complement is a heat-labile system and so the PHP was heat-inactivated and incubated with known positive controls to determine the background levels of each assay. The samples used would otherwise produce “low”, “medium”, or “high” levels of C3c (**Figure 44 (B)**, **(D)**, **(F)**) and C5b-9 deposition (**Figure 45 (B)**, **(D)**, **(F)**) when used with PHP. For the EBOV-GP and SUDV-GP assays, only minimal background signals were observed for C3c deposition (**Figure 44 (A)**, **(E)**) and C5b-9 deposition (**Figure 45 (A)**, **(E)**). For EBOV-sGP, C3c deposition with heat-inactivated PHP showed a slightly larger increase in both the background and the positive signals (**Figure 44 (C)**). The C5b-9 deposition with heat-inactivated PHP showed a low background except for the use of “high” plasma, where the signal remained constant throughout the titration (**Figure 45 (C)**).

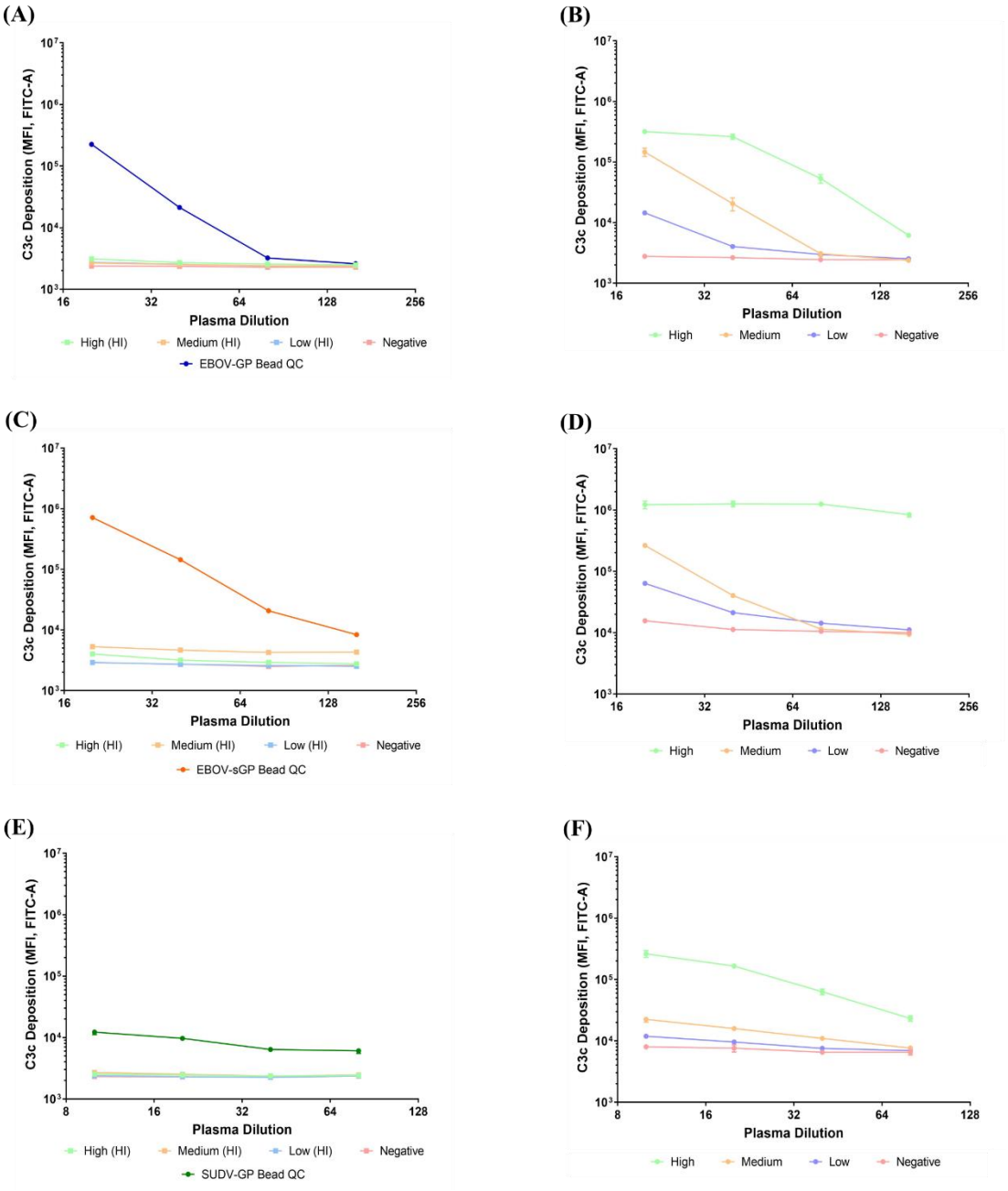

Figure 44: C3c deposition with heat-inactivated PHP

*EBOV-GP IgG positive samples that resulted in "high", "medium", and "low" levels of C3c deposition were incubated with heat-inactivated (HI) 10% PHP in assays with **(A)** EBOV-GP, **(C)** EBOV-sGP, and **(E)** SUDV-GP conjugated beads. The "high", "medium", and "low" samples were also incubated with the original PHP at a concentration of 10%, for **(B)** EBOV-GP, **(D)** EBOV-sGP, and **(F)** SUDV-GP conjugated beads. All samples were tested in duplicate and each dot/square represents the mean values calculated in GraphPad Prism software (version 9). Error bars show the variance from the mean. Abbreviations: HI = heat-inactivated; MFI = median fluorescence intensity; QC = quality control.*

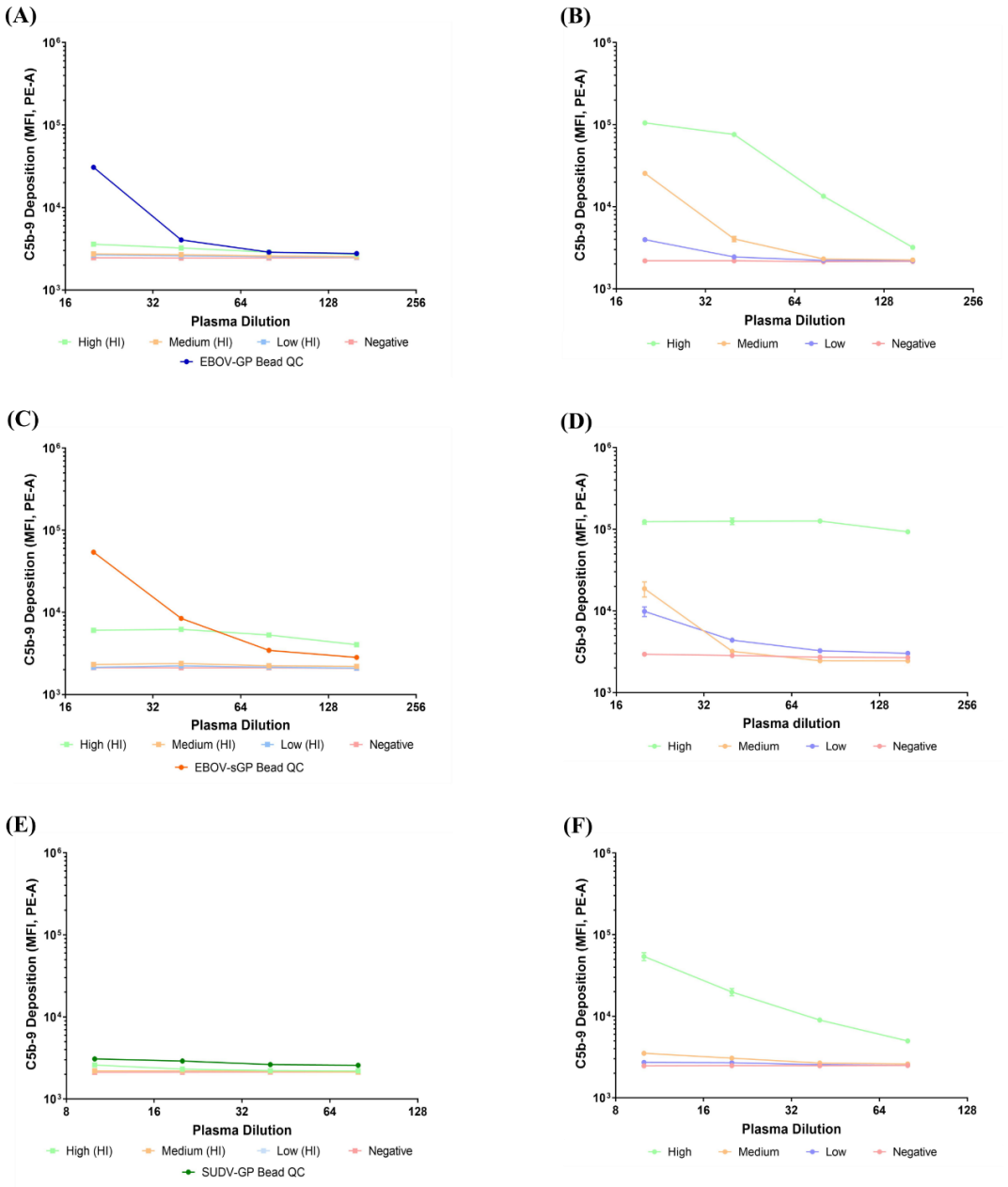

Figure 45: C5b-9 deposition with heat-inactivated PHP

*EBOV-GP IgG positive samples that resulted in "high", "medium", and "low" levels of C5b-9 deposition were incubated with heat-inactivated (HI) 10% PHP in assays with **(A)** EBOV-GP, **(C)** EBOV-sGP, and **(E)** SUDV-GP conjugated beads. The "high", "medium", and "low" samples were also incubated with the original PHP at a concentration of 10%, for **(B)** EBOV-GP, **(D)** EBOV-sGP, and **(F)** SUDV-GP conjugated beads. All samples were tested in duplicate and each dot/square represents the mean values calculated in GraphPad Prism software (version 9). Error bars show the variance from the mean. Abbreviations: HI = heat-inactivated; MFI = median fluorescence intensity; QC = quality control.*

3.3.4 Bead Validation with Negative Plasma

EBOV-GP IgG negative plasma samples were also used to determine the background levels of each assay. For the EBOV-GP and SUDV-GP, low background signals were observed for C3c (**Figure 46 (A)**, **(C)**) and C5b-9 deposition (**Figure 47 (A)**, **(C)**) with the use of all EBOV-GP IgG negative plasma samples. Some variation was observed between the negative samples for C3c deposition with SUDV-GP (**Figure 46 (C)**), however these negative samples are relative to a positive sample with a weak signal. For EBOV-sGP, the overall assay signal was higher again, and two negative samples in particular produced a higher signal than expected for both C3c deposition (**Figure 46 (B)**) and C5b-9 deposition (**Figure 47 (B)**).

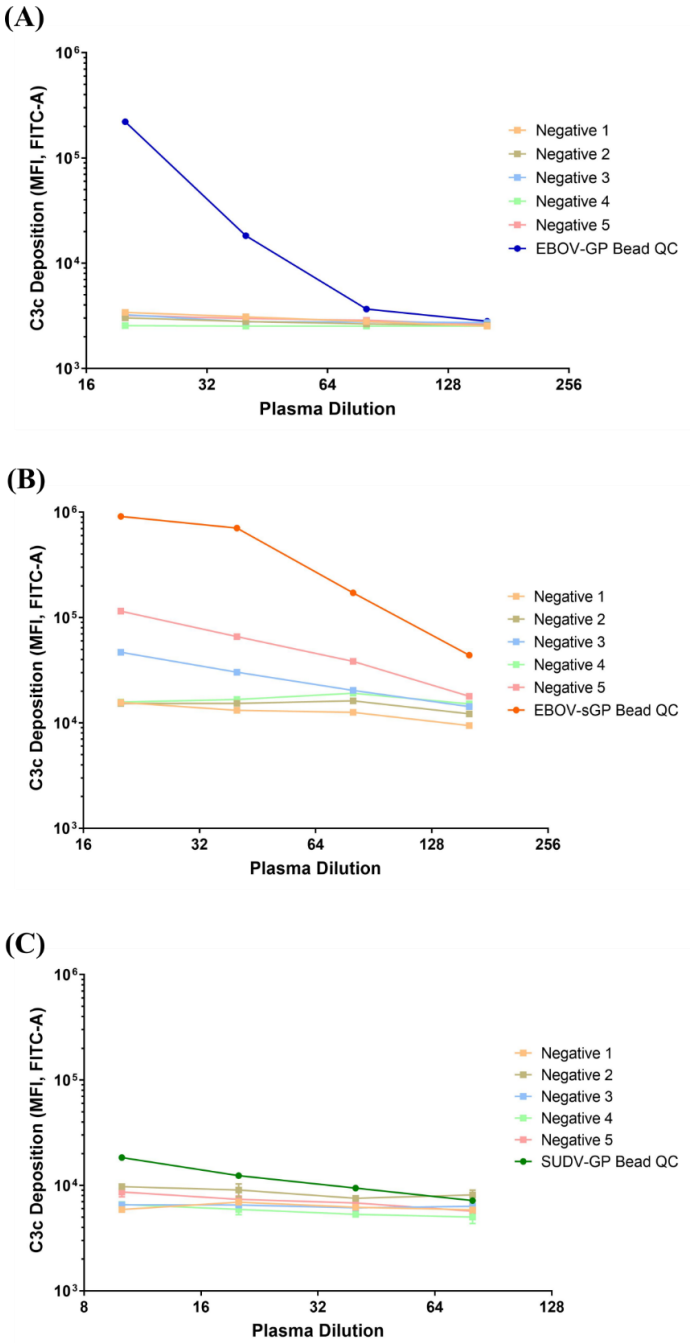

Figure 46: C3c deposition with negative plasma samples

*A selection of EBOV-GP IgG negative samples (as determined via ELISA in 2017) were incubated with **(A)** EBOV-GP, **(B)** EBOV-sGP, and **(C)** SUDV-GP conjugated beads to investigate the background levels of C3c deposition with 10% PHP. All samples were tested in duplicate and each dot/square represents the mean values calculated in GraphPad Prism software (version 9). Error bars show the variance from the mean. Abbreviations: MFI = median fluorescence intensity; QC = quality control.*

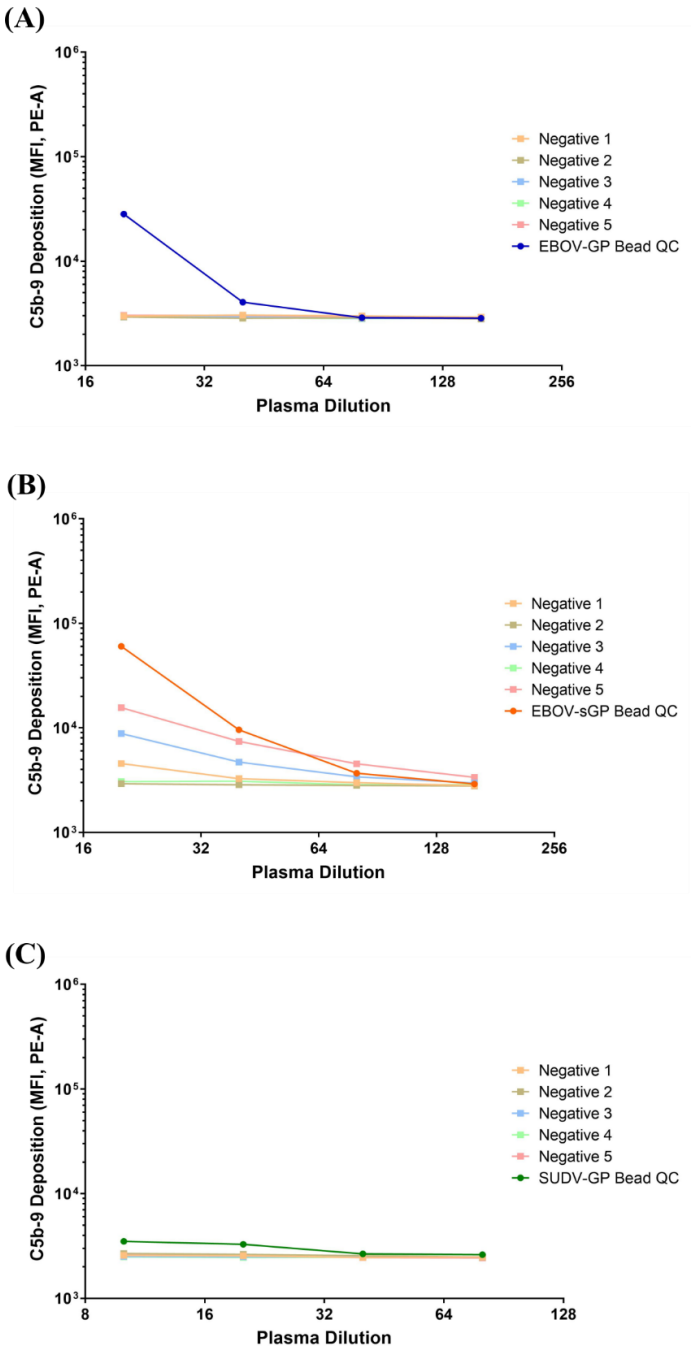

Figure 47: C5b-9 deposition with negative plasma samples

*A selection of EBOV-GP IgG negative samples (as determined via ELISA in 2017) were incubated with **(A)** EBOV-GP, **(B)** EBOV-sGP, and **(C)** SUDV-GP conjugated beads to investigate the background levels of C5b-9 deposition with 10% PHP. All samples were tested in duplicate and each dot/square represents the mean values calculated in GraphPad Prism software (version 9). Error bars show the variance from the mean. Abbreviations: MFI = median fluorescence intensity; QC = quality control.*

3.3.5 ADCD and its Relationship with IgG Binding

The binding of IgG and C1q to the *Ebolavirus* proteins showed the potential for classical complement pathway activation and ADCD. The extent of ADCD is influenced by antibody characteristics and can have both local and systemic effects on immunity, potentially influencing EBOV pathogenesis. ADCD was indirectly measured by the levels of C3c and C5b-9 deposition.

For EBOV-GP, there was no significant difference in IgG binding (P = 0.673) (previously shown in **Figure 42**, **(B)**), C3c deposition (P = 0.239), nor C5b-9 deposition (P = 0.181) between the LN and N cohorts using a Mann-Whitney test (**Figure 48**, **(A)**). The relationship between IgG titre, C3c deposition, and C5b-9 deposition was then analysed *via* linear regression for both cohorts. A strong correlation was observed for C3c deposition and C5b-9 deposition with $R^2 = 0.938$ and $R^2 = 0.914$ for the LN and N cohorts, respectively. Strong correlations were also observed for IgG titres and C3c deposition with the LN cohort ($R^2 = 0.788$) and N cohort ($R^2 = 0.856$), and again for C5b-9 deposition with the LN cohort ($R^2 = 0.881$) and N cohort ($R^2 = 0.940$) (**Figure 48**, **(B)**).

For EBOV-sGP, despite similar IgG titres (P = 0.239) between the LN and N cohorts (previously shown in **Figure 42**, **(B)**), the LN cohort had significantly lower levels of C3c deposition (P = 0.002) and C5b-9 deposition (P = 0.003) (**Figure 48**, **(C)**). As expected, there was a strong correlation in C3c and C5b-9 deposition with $R^2 = 0.969$ and $R^2 = 0.737$ for the LN and N cohorts, respectively. For the LN cohort, there was no correlation between C3c and IgG ($R^2 = 0.135$), and C5b-9 and IgG ($R^2 = 0.086$). For the N cohort, there was a strong correlation between C3c and IgG ($R^2 = 0.791$), and C5b-9 and IgG ($R^2 = 0.733$) (**Figure 48**, **(D)**).

For SUDV-GP, the LN cohort had significantly lower IgG titres (P = 0.005) (previously shown in **Figure 42**, **(B)**), C3c deposition (P = < 0.001), and C5b-9 deposition (P = 0.004) (**Figure 48**, **(E)**) compared to the N cohort. There was a moderate correlation

for C3c and C5b-9 deposition for the LN cohort (R^2 = 0.694), and a strong correlation (R^2 = 0.953) for the N cohort. For the LN cohort, no correlation was observed between C3c and IgG (R^2 = 0.189), and C5b-9 and IgG (R^2 = 0.202). For the N cohort, a weak correlation was observed between C3c and IgG (R^2 = 0.227), and no correlation between C5b-9 and IgG (R^2 = 0.144) (**Figure 48**, **(F)**).

In summary, significant differences ($P < 0.050$) were observed in the levels of ADCD depending on the LN and N cohorts and the *Ebolavirus* protein present (**Figure 48**). For EBOV-GP, similar levels of ADCD were observed for both cohorts and this response strongly correlated with IgG titres. For EBOV-sGP, IgG titres were similar between the two cohorts, but the LN cohort was less capable of mediating ADCD. Furthermore, ADCD was dependent on IgG titre in the N cohort, but these two parameters did not correlate for the LN cohort. For SUDV-GP, the LN cohort showed a significant reduction in all parameters tested compared to the N cohort, and ADCD did not correlate with IgG titre for either cohort.

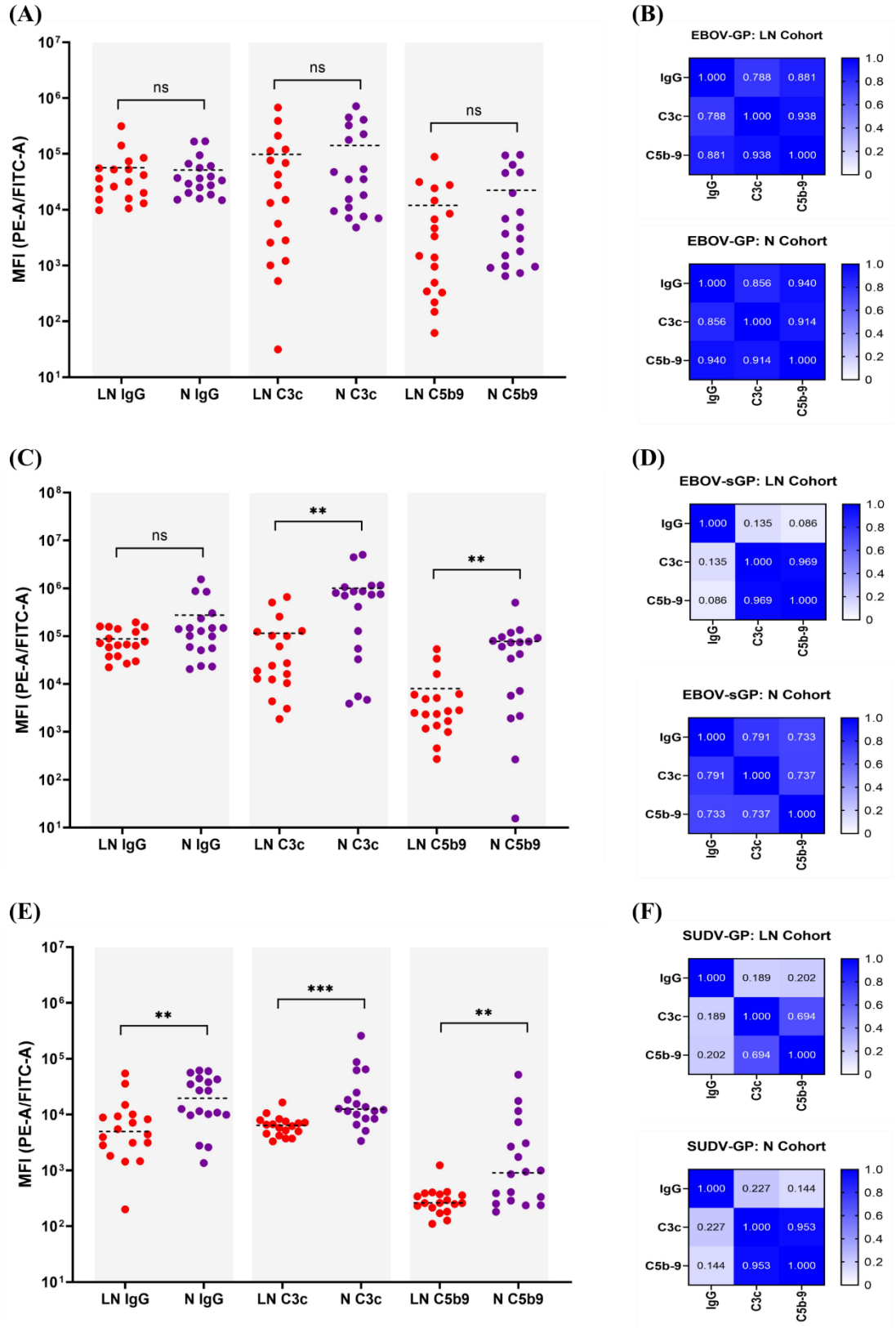

Figure 48: Comparison of IgG titres, C3c deposition, and C5b-9 deposition for EBOV-GP, EBOV-sGP, and SUDV-GP conjugated beads

IgG binding, C3c deposition, and C5b-9 deposition with LN cohort (red dots, n = 18) and N cohort (purple dots, n = 18) plasma samples were compared using a Mann-

*Whitney test with EBOV-GP **(A)**, EBOV-sGP **(C)**, and SUDV-GP **(E)**. The relationship for each parameter within the LN and N cohorts were then analysed via linear regression for EBOV-GP **(B)**, EBOV-sGP **(D)**, and SUDV-GP **(F)** with the R^2 values presented in the form of a heatmap. Assay types are distinguished by the grey shaded areas. All samples were analysed using GraphPad Prism (version 9).*

3.4 Discussion

This chapter describes the potential differences in ADCD between EBOV convalescent plasma samples in response to the EBOV-GP, EBOV-sGP, and SUDV-GP. The extent of ADCD could influence various aspects of immunity including neutralisation, opsonisation, agglutination, chemotaxis, and immune cell regulation. We found significant differences in the levels of ADCD depending on the level of neutralisation relative to the antibody titre (based on the LN and N cohorts) and the *Ebolavirus* protein present, which could help shape our understanding of EBOV immunity and pathogenesis.

The plasma samples from the LN cohort had a significantly lower capacity for cross-reacting with SUDV-GP despite similar IgG titres to the N cohort for the EBOV-GP and EBOV-sGP (**Figure 42**, **(B)**). The reduced IgG binding to the SUDV-GP could indicate that the epitopes recognised by IgG antibodies in the N cohort are better conserved amongst proteins, or that the LN cohort has less diversity in the IgG response. This may also explain the absence of correlation for IgG binding to SUDV-GP compared to EBOV-GP and EBOV-sGP for the LN cohort. Similarly, no correlation was observed for IgG binding to the EBOV-GP compared to the EBOV-sGP by the LN cohort, which may be explained by antibodies targeting various conformational epitopes on the EBOV-sGP or the whole EBOV-GP such that overall binding is not affected (565). It is possible that variations in antibody binding are caused by the bead conjugation process restricting certain epitopes. However, the conjugation method relies on free amine groups on the GPs which are abundant and regularly distributed, so this is unlikely to be an issue. Another cause of variation could be the source of the proteins, as discussed in **Chapter 2**. Whilst care was taken to ensure that all proteins were expressed in HEK 293 mammalian cell lines to reduce variation in glycosylation and

protein processing, different cell culture environments can cause minor variations in protein glycosylation (543). The use of antibody-dependent complement mechanisms in this section also mitigates concerns regarding variations in glycosylation.

As previously discussed, conventional activation of the classical pathway is dependent on prior engagement of antibodies to the target protein to facilitate C1q binding. In rare instances, C1q may directly bind viral antigens, or utilise acute phase proteins as substitutes for antibody binding, to activate the complement system (20,566,567). In our observations, C1q binding to the EBOV-GP and EBOV-sGP was dependent on the presence of EBOV-GP IgG, thus following the conventional classical pathway (**Figure 43**). C1q binding was not observed for the SUDV-GP, however this was likely a sensitivity issue with the reliance of cross-reactivity already producing lower signals for the SUDV-GP assays. The lower IgG titres and cross-reactivity would reduce the number of binding targets for the C1q protein and lower the epitope density, thus reducing the formation of antibody clusters required for efficient C1q binding (556) and any subsequent complement activation (554,555). Whilst C1q is also capable of binding IgM, based on previous studies regarding antibody kinetics following EBOV infection (568,569), these samples collected at least 1-year post-exposure are not anticipated to contain substantial levels of IgM. These results highlight some important functional differences in the initial stages of ADCD between convalescent EVD plasma samples.

For the EBOV-GP (**Figure 48**, **(A)**, **(B)**), IgG binding and ADCD levels were similar for the LN and N cohorts, with the level of ADCD dependent on the EBOV-GP IgG titre. In the context of EBOV pathogenesis, irrespective of neutralisation (as demonstrated with the LN cohort), Fc-mediated antibody functions could activate the complement system with implications for the upregulation of inflammation and chemotaxis (1,570), and a possible reduction of viral load (159,175,567,571). It is unclear whether this response would be beneficial or detrimental in the course of EBOV infection. I previously discussed the evidence for both the complement-mediated reduction and

enhancement of various viral infections. Whilst inflammation and chemotaxis help coordinate the immune response, sustained levels of inflammation can be detrimental. This is apparent in patients who succumb to EVD (350,371,393,520,546).

For the EBOV-sGP (**Figure 48**, **(C)**, **(D)**), IgG titres were similar for both the LN and N cohorts, yet the ability to mediate ADCD was significantly lower in the LN cohort. One possibility is that the isotype composition bound to the EBOV-sGP between the two cohorts differs, as IgG1 and IgG3 activate complement most efficiently, followed by IgG2, whilst IgG4 has no activity and may even be inhibitory (15,557,558). Again, the antibody recognition sites and epitope density could affect antibody clustering and thus affect the efficiency of C1q binding. This could also explain why there was no correlation between IgG titre and ADCD for the LN cohort. Acute-phase proteins are capable of mediating C1q binding and complement activation independent of antibodies (1). Such activity could explain the lack of correlation. However, the following reasons conflict with this: IgG titres and ADCD in the N cohort correlated as expected, we did not observe C1q binding to EBOV-sGP with EBOV-GP IgG negative plasma, the PHP-only controls were negative, and we did not observe a similar trend with EBOV-GP which might otherwise be expected. Whilst there was no significant difference ($P = 0.239$) in the IgG titres between cohorts for the EBOV-sGP, the LN cohort showed some reduction in IgG titre, and so the assay variation or the binding of other proteins in the cohort plasma may be more apparent at these lower levels. The significantly lower titres for C3c ($P = 0.002$) and C5b-9 deposition ($P = 0.003$) with the LN cohort could be impacted by the higher background signal observed for the EBOV-sGP assay, which would also influence the association of IgG titre with ADCD. Lastly, the origins of the EBOV-GP (Makona) and EBOV-sGP (Mayinga) may also account for some variation. The convalescent plasma from the Makona variant may not recognise some regions of the Mayinga variant, although IgG titres were similar to both proteins. Sequence analysis of the full-length genomes shows a 97% nucleotide sequence identity between the Makona and Mayinga variants used here (535).

As discussed in **Chapter 2**, the EBOV-sGP is the primary transcript of the *GP* gene (550) which is actively secreted from infected host cells during infection at levels detectable in the blood of acutely infected patients (551). We previously discussed the potential for the EBOV-sGP to function as a complement decoy molecule leading to the consumption of complement, which is partially driven by MBL binding. Here, we show that the known ability of the EBOV-sGP to divert the antibody response (550) would also divert the complement response from the EBOV virion. The EBOV-sGP may even contribute to more severe disease pathology in this way, as excessive complement activation has been associated with fatal EVD outcomes (546). The ADCD described in this chapter could provide some indication of the varying antibody responses to the EBOV-sGP, some of the characteristics which drive these responses, and how this influences ADCD.

For the SUDV-GP (**Figure 48**, **(E)**, **(F)**), IgG titres and the levels of C3c deposition and C5b-9 deposition were significantly lower in the LN cohort compared to the N cohort. C3c deposition and C5b-9 deposition correlated as expected for both cohorts, but the correlations of IgG titre to C3c deposition or C5b-9 deposition were either weak or not significant. Again, a possible explanation for this could be the IgG isotypes and/or the antibody epitopes available to enable efficient C1q binding. Based on the Sequence Manipulation Suite software and MUltiple Sequence Comparison by Log-Expectation (MUSCLE) software, the amino acid sequence similarity of the EBOV-GP and SUDV-GP used in this study is ~57%, which would support the explanation for reduced capacity to facilitate antibody clustering and C1q binding. The mechanism of ADCD mediated by cross-reactivity with EBOV-GP IgG positive plasma in response to SUDV-GP could have implications for cross-protection. While it is unclear how these results would translate *in vivo*, cross-reactive antibodies are likely to show a reduction in neutralisation, and so Fc-mediated mechanisms of protection could be an important consideration. Our results show that the levels of ADCD would vary in association with the neutralisation titres, as determined by the LN and N cohorts.

The endemicity of EBOV and SUDV covers neighbouring countries and the putative reservoir for EBOV overlaps all of these regions (279), which means there is the possibility for EBOV convalescent patients to be exposed to SUDV. EBOV has caused repeated outbreaks in DRC which have spilled over into neighbouring Uganda, whilst SUDV has caused multiple outbreaks in Uganda and South Sudan which borders both Uganda and DRC (572). The potential for overlap of these viruses is increased with factors such as: viral persistence in semen (573,574), ocular fluid (255), cerebrospinal fluid (258), and breast milk (259,575); the potential for recrudescence in humans (255,258) and NHPs (393); the high potential for human-to-human transmission (214); and a general lack of viral surveillance in endemic areas.

In summary, this is the first attempt at characterising antibodies in EBOV convalescent plasma by their ability to mediate ADCD in response to various *Ebolavirus* glycoproteins. We observed a large degree of variation in the ability to mediate ADCD between the LN and N cohorts, and highlighted factors associated with these differences including IgG titre, EBOV neutralisation titre, and the *Ebolavirus* protein present. One of our measurements of ADCD was the end-stage formation of the C5b-9 complex, which shows that the complement system was activated to completion. Therefore, in the context of EBOV pathogenesis, we would expect other complement-mediated immune functions such as inflammation and chemotaxis to become active. Our findings are assumed to be IgG-mediated, and this chapter would be most relevant to EBOV pathogenesis in the context of re-exposure, recrudescence, vaccinations, and cross-reactivity with SUDV. This work sets the foundations for investigating the complement system in the context of antibody-mediated virus neutralisation. The ability of antibodies to engage the complement system can also have significant implications for neutralisation, as previously discussed for EBOV (407) and other viruses (19,159,160,175).

The ADCD work for SARS-CoV-2 was a collaborative effort with other research projects to show multifunctional antibody responses to vaccination (504), the diversity of antibody responses to infection (563), and sex differences in response to

vaccination (manuscript submitted). However, the effect of this on neutralisation, as with EBOV, had not yet been investigated. These antibodies are capable of mediating ADCD, and the extent of ADCD is highly variable, therefore it is possible that the presence of complement could influence virus neutralisation and thus impact viral pathogenesis. In the next chapter, I set out to investigate the impact of both the antibody-independent and the antibody-dependent evidence collected in Chapter 2 and Chapter 3 on EBOV and SARS-CoV-2 neutralisation.

3.5 Appendix II

3.5.1 Optimisation of Plasma Titration for Complement Deposition Assays

EBOV convalescent plasma samples with a range of EBOV-GP IgG titres were used in C3c deposition assays with EBOV-GP conjugated beads to determine the optimal plasma dilutions for these assays. A dilution series of 1:2 starting from a 1:20 dilution was deemed optimal as it provided the clearest distinction between the weak positive ("low") and negative samples, whilst avoiding assay saturation with the strong positive sample ("high") (**Figure 49**). The same 1:2 dilution series was then applied to the C5b-9 deposition assays.

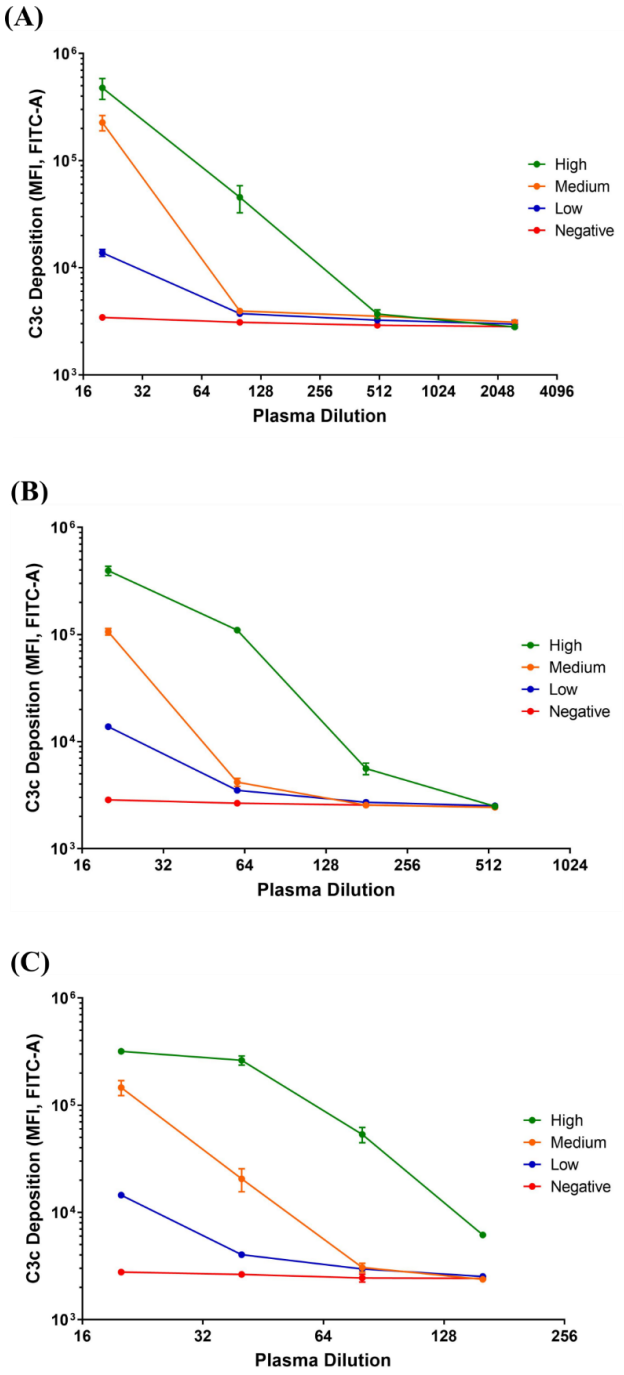

Figure 49: Titration of plasma with EBOV-GP conjugated beads for the C3c deposition assay

Various plasma titrations of EBOV convalescent plasma samples with "high", "medium", and "low" EBOV-GP IgG titres were used to determine optimal plasma concentrations. ***(A)*** *Plasma samples were diluted to 1:20, 1:100, 1:500, and 1:2500 for C3c deposition with EBOV-GP beads.* ***(B)*** *Plasma samples were diluted to 1:20, 1:60, 1:180, and 1:540 for C3c deposition with EBOV-GP beads.* ***(C)*** *Plasma samples were diluted to 1:20, 1:40, 1:80, and 1:160 for C3c deposition with EBOV-GP beads. All samples were tested in duplicate and presented with the mean value.*

3.5.2 Selection of Additional EBOV-GP IgG Positive Plasma Samples

The IgG titre of two low-neutralising plasma samples was not available within the historic data set. I determined their IgG titres using my flow cytometry IgG assay (**Figure 50**). They fit the criteria of the LN cohort and were included in this study, along with the selection of two additional samples for the N cohort to ensure matching cohort numbers (total n = 36).

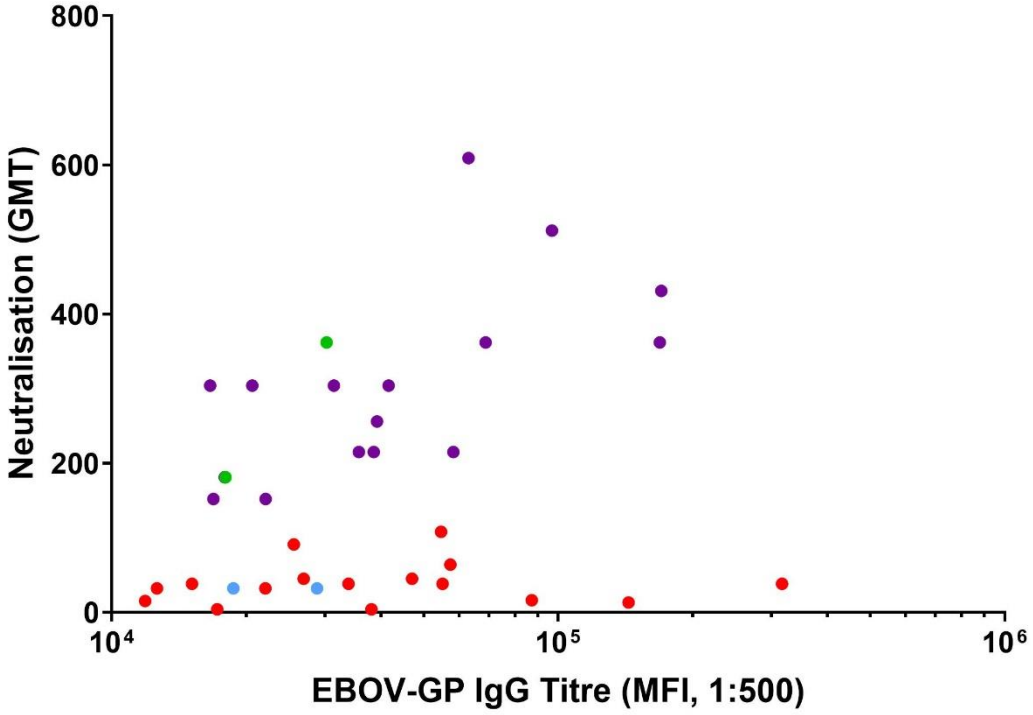

Figure 50: Selection of additional EBOV-GP IgG positive plasma samples using flow cytometry data

Four additional samples were selected for addition to the LN cohort (blue dots) or N cohort (green dots), using flow cytometry data collected in this study and historic neutralisation titres that were absent in the historic ELISA data from the year 2017. The remaining LN cohort samples (n = 16) are shown in red and the remaining N cohort samples (n = 16) are shown in purple.

3.5.3 Raw MFI and QC Data for IgG Assays

Inter-assay variation was monitored using a titration of EBOV-GP IgG positive plasma with EBOV-GP beads for every assay (**Figure 51 (A)**), with a maximum cut-off of 30% CV. EBOV-sGP and SUDV-GP beads were also used as an inter-assay QC with a fixed plasma dilution for each EBOV-sGP or SUDV-GP assay, respectively (**Figure 51 (B)**). All samples and QCs were then plotted on a single graph for EBOV-GP (**Figure 51 (C)**), EBOV-sGP (**Figure 51 (D)**), and SUDV-GP (**Figure 51 (E)**). The raw MFIs for all of my flow cytometry IgG assays were below 30% CV for intra-assay and inter-assay variation. Whilst the upper limit of 30% CV was accepted for intra-assay variation, the majority of these replicates were < 10% CV.

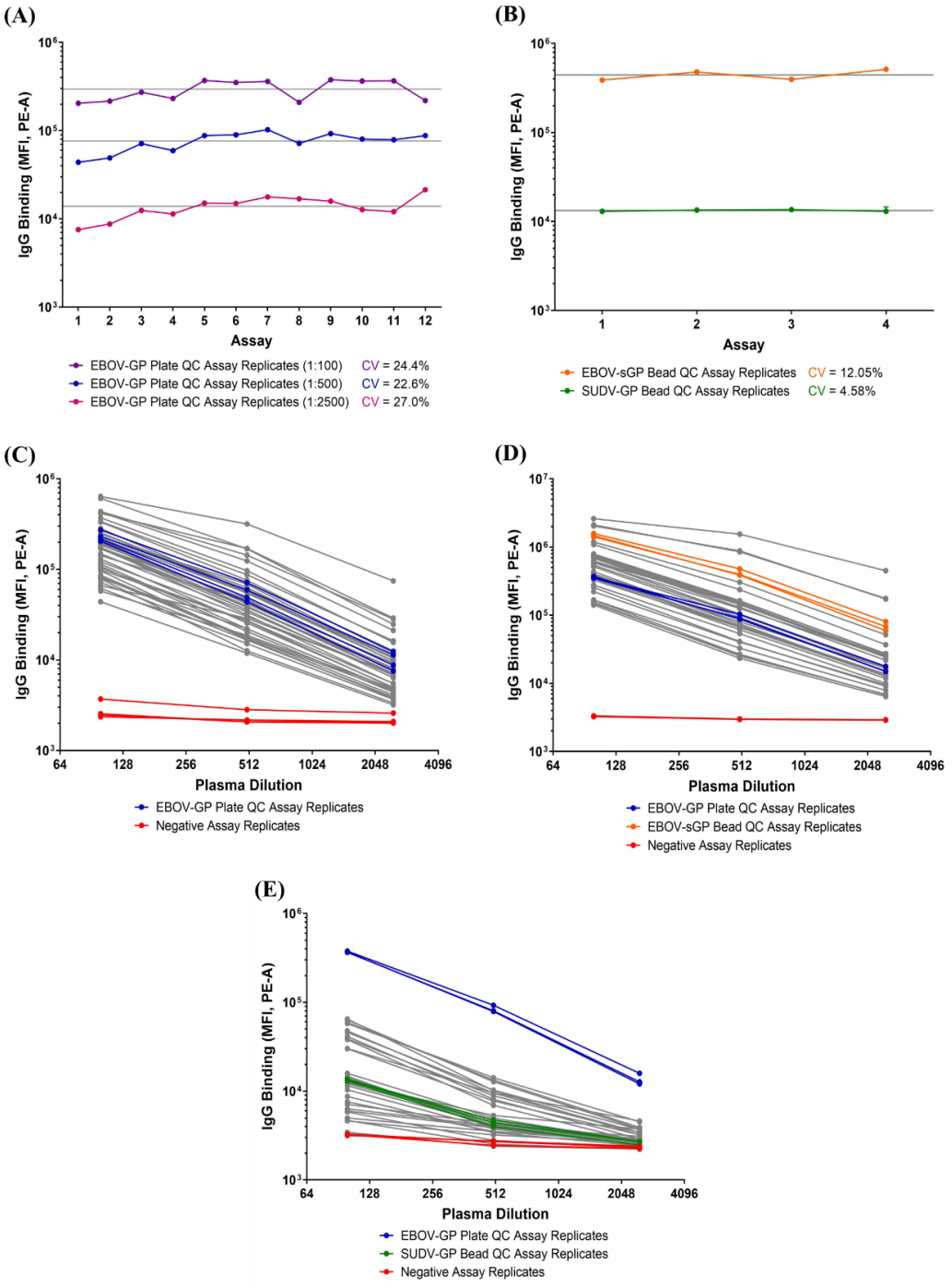

Figure 51: Raw MFI and QC data for all flow cytometry IgG assays with EBOV-GP, EBOV-sGP, and SUDV-GP

(A) *EBOV-GP beads with convalescent plasma at three dilutions (1:100, 1:500, 1:2500) were used as a QC for all plates, with a CV < 30%.* ***(B)*** *EBOV-sGP and SUDV-GP beads with convalescent plasma at three dilutions (1:100, 1:500, 1:2500) were included as additional QCs for their corresponding assays. The raw IgG titre MFIs of all plasma samples (grey dots/lines) against* ***(C)*** *EBOV-GP,* ***(D)*** *EBOV-sGP, and* ***(E)*** *SUDV-GP were determined using FlowJo software (Version 10.8.0) and presented using GraphPad Prism software (version 9).*

3.5.4 Raw MFI and QC Data for C3c and C5b-9 Deposition Assays

The raw MFIs for all of my flow cytometry C3c (**Figure 52 (A))** and C5b-9 (**Figure 53 (B))** deposition assays were below 30% CV for inter-assay variation. Whilst the upper limit of 30% CV was accepted for intra-assay variation, the majority of these replicates were < 10% CV. Similar to the IgG assay, I accepted a CV < 30% as inherent assay variation. I attempted to normalise the data based on the plate QCs or bead QCs, but adjusting for one parameter did not show an overall improvement. I attempted to use a standard curve for the interpolation of sample values, however the signal for some of the samples was too low for interpolation and would need to be excluded for analysis. Considering the small data set already, I did not proceed with this option although it did work well for the SARS-CoV-2 projects. I also attempted an end-point titration from the sample dilutions, but the signal titrated out too quickly. To overcome this, I would have needed a much smaller dilution factor and thus a much higher number of dilution points per sample to obtain accurate readings. Finally, it was concluded that subtracting the PHP-only control from the samples provided the most consistent results. The PHP-only control showed little variation between the plates, but subtracting this value was beneficial as it would minimise any possible effects of the lectin pathway. One of the C5b-9 EBOV assays (**Figure 53 (C)**) was repeated using a fresh bead conjugation which showed a considerably higher background. This assay otherwise showed high reproducibility. Subtracting the negative plasma background brought the QCs of this particular assay within the parameters of the original.

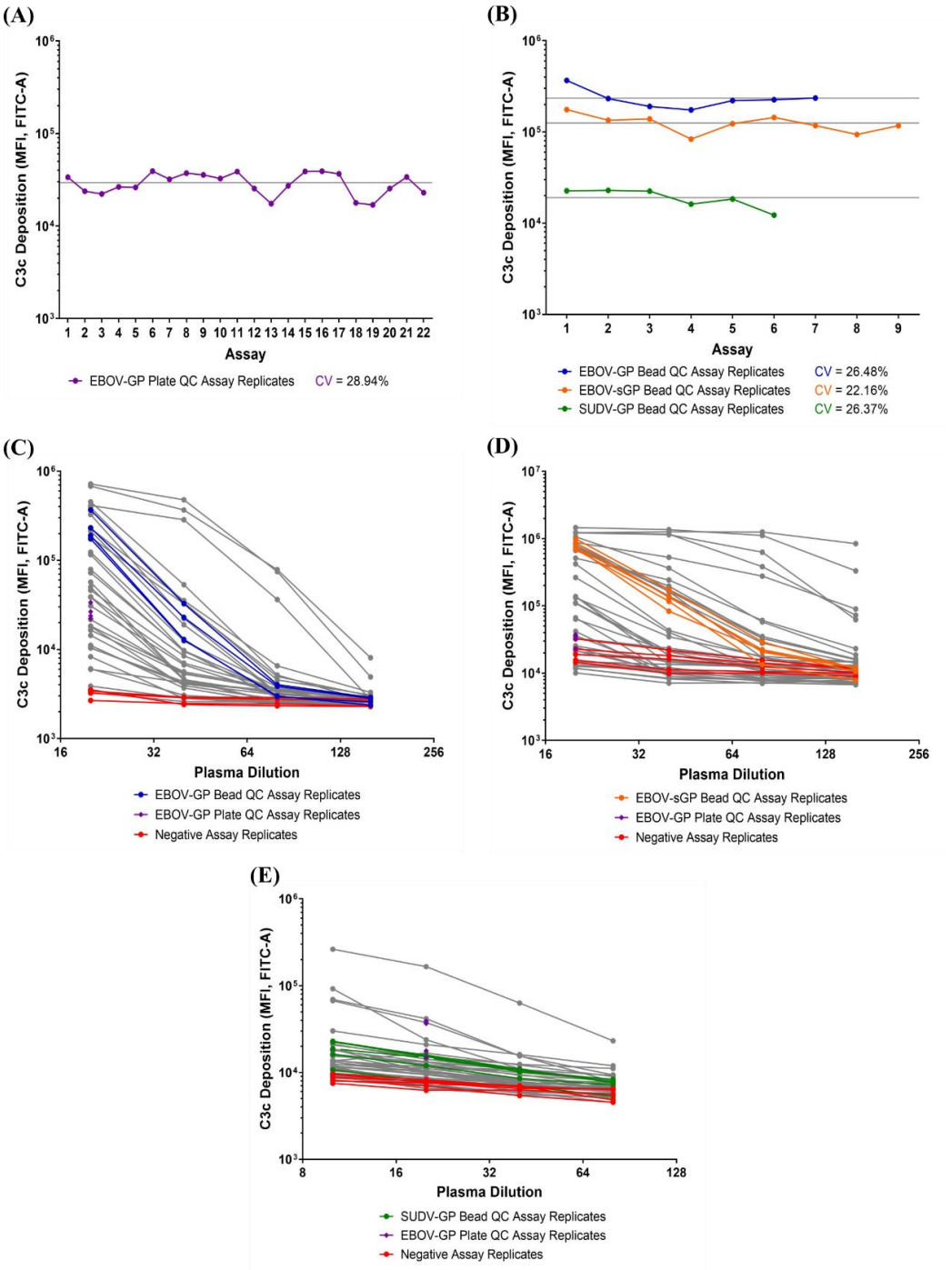

Figure 52: Raw MFI and QC data for all flow cytometry C3c deposition assays with EBOV-GP, EBOV-sGP, and SUDV-GP

(A) *EBOV-GP beads with convalescent plasma at a fixed 1:20 dilution were used as a QC for all plates, with a CV < 30%.* ***(B)*** *Each bead conjugate was also incubated with convalescent plasma at a 1:10 (SUDV-GP) or 1:20 dilution (EBOV-GP, EBOV-sGP) as additional QCs to monitor bead integrity. The raw C3c deposition MFIs of all plasma samples (grey dots/lines) against* ***(C)*** *EBOV-GP,* ***(D)*** *EBOV-sGP, and* ***(E)*** *SUDV-GP were determined using FlowJo software (Version 10.8.0) and presented using GraphPad software (version 9).*

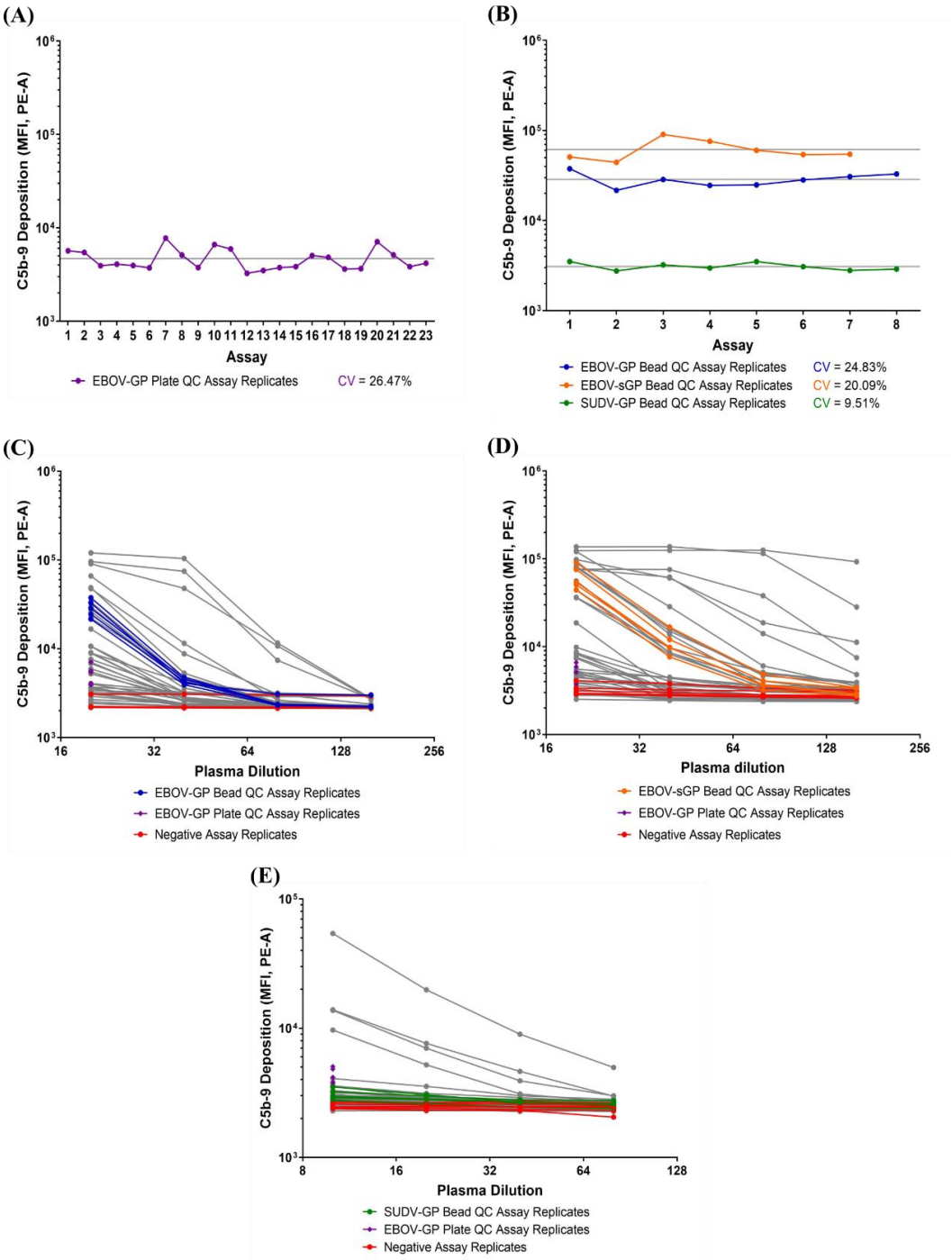

Figure 53: Raw MFI and QC data for all flow cytometry C5b-9 deposition assays with EBOV-GP, EBOV-sGP, and SUDV-GP

(A) *EBOV-GP beads with convalescent plasma at a fixed 1:20 dilution were used as a QC for all plates, with a CV < 30%.* ***(B)*** *Each bead conjugate was also incubated with convalescent plasma at a 1:10 (SUDV-GP) or 1:20 dilution (EBOV-GP, EBOV-sGP) as additional QCs to monitor bead integrity. The raw C5b-9 deposition MFIs of all plasma samples (grey dots/lines) against* ***(C)*** *EBOV-GP,* ***(D)*** *EBOV-sGP, and* ***(E)*** *SUDV-GP were determined using FlowJo software (Version 10.8.0) and presented using GraphPad software (version 9).*

Chapter 4: Complement-Mediated Neutralisation

4.1 Introduction

The complement system has the potential to enhance and enable virus neutralisation for low-neutralising and non-neutralising antibodies, respectively. In **Chapter 2**, we showed evidence for MBL-binding and formation of the membrane attack complex (MAC) in response to various *Ebolavirus* and *Coronavirus* glycoproteins (GPs), independent of antibodies. In **Chapter 3**, we found that low-neutralising, EBOV disease (EVD) convalescent plasma could mediate antibody-dependent complement deposition (ADCD) in response to the EBOV-GP and EBOV-sGP. In collaboration with the UKHSA and University of Oxford, we also found differential responses in the ability to mediate ADCD against the SARS-CoV-2 spike protein with the use of convalescent COVID-19, and ChAdOx1 nCoV-19 vaccinee, plasma. In this chapter, we investigated whether the antibody-independent complement interactions observed in **Chapter 2** could influence EBOV and SARS-CoV-2 neutralisation. Next, we assessed whether the antibody-dependent mechanisms observed in **Chapter 3** could enhance virus neutralisation of otherwise low-neutralising antibodies.

The antibody-independent mechanisms of the complement system form part of the early, innate response to viruses. This response can initiate a range of antiviral mechanisms, including agglutination, chemotaxis, neutralisation, opsonisation, and the lysis of virions and infected cells, as discussed previously in sections **1.1.5.1** to **1.1.5.4**. For EBOV, previous studies have demonstrated both antiviral (157,412,413) and viral-enhancing (7,8,403) effects of the lectin complement pathway. In **Chapter 2**, we demonstrated that MBL of the lectin pathway can bind to a range of *Ebolavirus* GPs, with the novel finding that MBL could also bind to the SUDV-GP. MBL binding to the SUDV-GP was significantly reduced compared to the EBOV-GP and EBOV-sGP. We also showed that the complement system could be activated to completion following stimulation with the *Ebolavirus* GPs, in the absence of EBOV-specific antibodies, which lead to the formation of the MAC. This was a novel observation which raised questions regarding the functional significance of this response. The MAC is capable of lysing virions and infected cells (19,159,160,175), which suggests that the

complement system could promote virus neutralisation. This aspect of immunity is commonly overlooked, as plasma samples used in conventional neutralisation assays are heat-inactivated or treated with EDTA, which inactivates the complement system (576–580). Formation of the end-stage MAC also indicates that other complement proteins would be deposited on the surface of the virion, and these proteins have the potential to both inhibit (6,20,167,168) or enhance (169,170) viral infections.

In **Chapter 2**, we also investigated MBL binding and antibody-independent complement deposition in response to the SARS-CoV-2 spike protein. During the course of this study, our observations of MBL binding and complement deposition in response to the SARS-CoV-2 spike protein have since been reported elsewhere (505,518), and their findings of MBL binding and MAC formation were in concordance with our own. One study by Stravalaci *et al* showed that MBL was capable of neutralising SARS-CoV-2 infection of Calu-3 cells and human bronchial epithelial cells, as well as reducing the production of IL-8 and CXCL5 (518). However, some of the published findings regarding interactions of the lectin pathway with SARS-CoV-2 proteins are conflicting. Stravalaci *et al* assessed the binding of recombinant C1q, collectins (CL-10/11/12), ficolins (FCN-1/2/3), MBL, pentraxins (serum amyloid P component [SAP], C-reactive protein [CRP], pentraxin 3 [PTX3]), and surfactant proteins (SP-A/D) to the SARS-CoV-2 spike protein and nucleoprotein. Only the long PTX3 and MBL bound to the nucleocapsid and spike protein, respectively. Investigations by Ali *et al* found that MBL could additionally bind to the nucleoprotein, and that FCN-2 and CL-11 could also bind the SARS-CoV-2 spike protein and nucleoprotein (505). Similarly, Hsieh *et al* found that SP-D could bind the SARS-CoV-2 spike protein (581). As highlighted by Stravalaci *et al*, their discrepancy with the findings by Ali *et al* could be their use of recombinant proteins instead of serum as a source of pattern recognition molecules (PRMs), as other components in serum could complex with the molecule of interest, for example MBL and MASP-2. Collectively, our evidence and the results published by others suggests a potential role of the lectin pathway in SARS-CoV-2 pathogenesis, but the effect of the

complement system in its entirety on SARS-CoV-2 neutralisation has not been investigated.

In **Chapter 3**, we considered the antibody-dependent effects of the complement system in the context of EBOV and SARS-CoV-2 infection. To determine which factors confer protection against a viral disease, one of the first considerations is often the presence and effectiveness of neutralising antibodies. These are typically identified *via* neutralisation assays with the use of heat-inactivated plasma; a process that inactivates the complement system. The complement system, and other Fc-mediated antibody functions, can be of equal importance to protection but are more complex to measure, and are thus less extensively studied (562). In **Chapter 3**, we observed a differential response of convalescent EVD survivor plasma in their ability to mediate complement deposition in response to a range of *Ebolavirus* GPs. In particular, we found that low-neutralising plasma (as determined by conventional neutralisation assays), could efficiently mediate ADCD in response to the EBOV-GP, but the ADCD response to the EBOV-sGP was significantly reduced. ADCD can promote complement-mediated neutralisation through virion aggregation (6,20,167,168), inhibition of protein interactions (77,155,157,165,166), and the lysis of virions and infected cells (19,159,160,175). These ADCD assays were also used to investigate various Fc-mediated antibody mechanisms in response to the SARS-CoV-2 spike protein, as part of a large collaborative research effort. In one study, ADCD was induced following vaccination with the ChAdOx1 nCoV-19 vaccine, and this response was increased in a dose-dependent response following a booster vaccination (504). In the second study, ADCD significantly increased in disease severity up to 180 days post-infection following SARS-CoV-2 natural infection, with those that experienced asymptomatic, mild, or severe illness (Kruskal-Wallis, $P = 0.0032$) (563). This chapter showed the differential ADCD responses to the EBOV and SARS-CoV-2 GPs, and provided the foundations for further investigations to determine the functional significance for protection and neutralisation.

For EVD, only two antibody therapeutics are approved by the FDA, one of which consists of a single monoclonal antibody (390). EBOV outbreaks are being reported more frequently over recent years and the constant threat of new variants could place a strain on the limited options of therapeutics. The importance of Fc-mediated antibody functions for EVD survival is demonstrated in the FDA-approved Inmazeb™ antibody cocktail (391). As our understanding of Fc-mediated functions in EVD progresses, these mechanisms could be further capitalised on for the development of therapeutics in the future (369). For COVID-19, complement is often described in the context of patients with severe disease and an elevated level of complement activation (490–497,499–501). ADCD has also been associated with disease severity (563). However, in some cases ADCD has been associated with protection (504,582,583). It is unclear whether ADCD is a causal factor in these associations, or whether its association with antibody titres are the reason for its relationship to disease. To help determine whether this is a causal relationship, a mechanistic understanding of ADCD, such as its role in neutralisation, could help address this discrepancy.

Therapeutic options for COVID-19 have also considered the use of complement inhibitors. Complement inhibitors have proven clinical safety but are typically only used to treat rare autoimmune diseases (584). For EVD, MBL was successfully used as a rescue therapy in mice infected with MA-EBOV *in vivo*, as previously discussed (412). Beyond this, complement therapeutics have not been used *in vivo* for the treatment of EVD, to our knowledge. For COVID-19, various C3 and C5 inhibitors are currently being used in phase 1/2 clinical trials: Zilucoplan® (complement C5 inhibitor, ClinicalTrial.gov Identifier: NCT04382755), AMY-101 (C3 inhibitor, ClinicalTrial.gov Identifier: NCT04395456), Ultomiris® (C5a inhibitor, ClinicalTrial.gov Identifier: NCT04570397), APL-9 (C3 inhibitor, ClinicalTrial.gov Identifier: NCT04402060). To improve the effectiveness of such treatments, it would be important to first understand which patients would benefit from its administration, and second, to determine when they should be administered. To understand this, it

is essential to further our understanding of the complement system in EVD and COVID-19 (1,584).

In this chapter, we hypothesised that the complement system would be able to influence EBOV and SARS-CoV-2 neutralisation, independent of antibodies. We also hypothesised that the complement system could enhance the neutralisation of low-neutralising antibodies against EBOV and SARS-CoV-2. We first supplemented wild-type EBOV neutralisation assays with exogenous pooled human plasma (PHP) to determine whether an enhancement of neutralisation could be conferred to the low-neutralising plasma described in **Chapter 3**. We also used exogenous PHP in the absence of EBOV-GP specific antibodies to determine whether the antibody-independent complement activation observed in **Chapter 2** could influence neutralisation. Next, we applied the same hypotheses to wild-type SARS-CoV-2 neutralisation assays, to determine whether the complement system could enhance antibody-mediated neutralisation and/or influence neutralisation in the absence of SARS-CoV-2 specific antibodies.

4.2 Methods

4.2.1 Sample Collection and Ethics

West African plasma was collected and processed as described in section **2.2.1**. PHP was collected as previously described by Alexander *et al* (521) and in section **2.2.1**. For the EBOV neutralisation assays, we used the PHP from 40 UK volunteers, collected and processed by the Pathogen Immunology Group at the UKHSA. For the SARS-CoV-2 neutralisation assays, we used the PHP from 5 UK volunteers, collected and processed by the High Consequence Emerging Viruses Group at the University of Oxford. The plasma containing antibodies to the SARS-CoV-2 spike protein were obtained as part of the OCTAVE trial (ISRCTN 12821688), which aims to assess the SARS-CoV-2 vaccine responses of immunocompromised individuals that were part of the UK national COVID-19 vaccination programme. The majority of subjects received either the COVID-19 mRNA vaccine BNT162b2 (Pfizer/BioNTech) or ChAdOx1 Vaccine (AstraZeneca formerly AZD1222) (585). In this chapter, we utilised 32 plasma samples

collected at two different time-points from 16 patients within the OCTAVE trial, with SARS-CoV-2 neutralisation titres and SARS-CoV-2-specific antibody titres (IgG, IgM, IgA) determined previously by the High Consequence Emerging Viruses Group at the University of Oxford.

Calu-3 cells (human lung epithelial cells) were generously provided by Michelle Hill at the Department of Biochemistry, University of Oxford, UK. Vero E6 cells (non-human primate kidney, Vero 76, clone E6, European Culture of Authenticated Cell Cultures (ECACC), Salisbury, UK, 85020206) were sourced from ECACC. The SARS-CoV-2 isolate (BetaCoV/Australia/VIC01/2020) was generously provided by The Doherty Institute, Melbourne, Australia (586).

4.2.2 Vero E6 Cell Viability with PHP

A Vero E6 cell monolayer was established using 100 µl of 4.5 x10^5 cells/ml in growth media (Gibco™ DMEM with 10% FCS and 1% Gibco™ Penicillin-Streptomycin (Fisher Scientific)). The plates were incubated at 37°C for 24 hrs and the media was replaced with dilution media (Gibco™ DMEM with 1% FCS and 1% Gibco™ Penicillin-Streptomycin (Fisher Scientific)) containing 40%, 20%, 10% or 0% PHP, in the presence or absence of 10mM EDTA. The plates were incubated at 37°C for 20 hrs and cell viability was determined using both microscopy and an MTT Assay Kit (Cell Proliferation) (abcam) according to the manufacturer's instructions. All samples were tested in duplicate and the data was analysed using GraphPad Prism software (version 9).

4.2.3 EBOV: Neutralisation Assay with PHP

We modified an existing EBOV (Makona isolate, GenBank accession No. KJ660347) neutralisation assay (587,588) to accommodate for the addition of PHP, which we have now published (589). Wild-type EBOV neutralisation assays were performed by Thomas Strecker and Sarah Katharina Fehling at the Institute of Virology, Philipps University of Marburg, Germany, in Biosafety Level (BSL)-4 laboratories. Eight plasma samples from the low-neutralising (LN) cohort in **Chapter 3** were randomly selected,

along with one control with high EBOV neutralisation. Plasma samples were serially diluted 1:2, from a 1:8 to 1:256 dilution, in 50 µl of DMEM with 100 U/ml penicillin, 100 mg/ml streptomycin, L-glutamine (2 mmol/L), and PHP at a final concentration of 20%, 10%, or 0%. Wild-type EBOV was diluted to 100 TCID50 units in DMEM with 2% FCS, and 50 µl was added to each plasma sample before incubating at 37^{o}C for 1 hr. Vero E6 cells were diluted in DMEM with 2% FCS, and added to each well at a final concentration of 9.4 x10^3 cells/ml. The plates were then incubated at 37^{o}C with 5% CO_2 for nine days. Cytopathic effects (CPE) were analysed on day nine and the geometric mean titres (GMT) of four replicates were used to calculate the final neutralisation titres.

Each plate included PHP at concentrations of 10% and 20% in the absence of convalescent EVD plasma, a cell-only control, and cells and virus with heat-inactivated PHP at 10% and 20% concentrations. We analysed the GMT of neutralisation by performing a Wilcoxon signed-rank test to compare neutralisation with plasma-only, with 10% PHP, and with 20% PHP, with a significance threshold of $P < 0.050$. Each sample was then analysed individually to compare the log2 fold-change of GMT with plasma-only, with 10% PHP, and with 20% PHP, using a significance threshold of plus or minus 1.5 the log2 fold-change. The data was analysed using GraphPad Prism software (version 9).

4.2.4 SARS-CoV-2: Neutralisation Assay with Native Plasma

The five native plasma samples that comprised the PHP used within this chapter were tested individually in neutralisation assays, in the absence of SARS-CoV-2 specific antibodies. Each individual plasma sample, the PHP, and heat-inactivated FCS were diluted in dilution media to achieve a 1:2 dilutions series, with final plasma concentrations from 20.00% to 0.16%. To each sample, 20 µl of the SARS-CoV-2 Victoria strain (10^3 PFU/ml) was added to obtain a final volume of 40 µl and incubated at 37^{o}C for 1 hr. Vero E6 cells were diluted in dilution media at a concentration of 4.5 x10^5 cells/ml and 100 µl of the cell suspension was added to each well. All conditions

were tested in duplicate and the neutralisation assay then proceeded according to section **4.2.8**.

4.2.5 SARS-CoV-2: Neutralisation Assay with MBL and FCN-1

Calu-3 cells were seeded with 1.0 x10^5 cells per well in Gibco™ DMEM/F-12 (supplemented with 1% Gibco™ Penicillin-Streptomycin (Fisher Scientific), 1% Gibco™ MEM Non-Essential Amino Acids Solution (Fisher Scientific), 1% 100mM sodium pyruvate (ThermoFisher Scientific), and 10% FBS (ThermoFisher Scientific)) and incubated for 24 hrs at 37°C. Vero E6 cells were prepared on the day of the assay and diluted into dilution media at a concentration of 4.5 x10^5 cells/ml. Recombinant MBL (R&D Systems) or FCN-1 (SinoBiological) was diluted in dilution media to achieve a 1:2 dilutions series, with the final protein concentrations from 20.00 µg/ml to 0.30 µg/ml. To each sample, 20 µl of the SARS-CoV-2 Victoria strain (10^3 PFU/ml) was added to obtain a final volume of 40 µl and incubated at 37°C for 1 hr. For the infection of Vero E6 cells, 100 µl of the cell suspension was added to each well. For the infection of Calu-3 cells, the growth media was replaced with 35 µl of the virus and MBL/FCN-1 mixture in 100 µl of dilution media. All conditions were tested in duplicate and the neutralisation assay then proceeded according to section **4.2.8**.

4.2.6 SARS-CoV-2: Selection of OCTAVE Plasma

OCTAVE plasma samples were used as a source of antibodies specific to the SARS-CoV-2 spike protein, to assess whether complement could enhance the antibody-mediated neutralisation of SARS-CoV-2. Neutralisation titres (determined *via* SARS-CoV-2 neutralisation assays) and IgG titres (determined *via* Meso Scale Discovery) of 32 OCTAVE plasma samples were determined by the High Consequence Emerging Viruses Group at the University of Oxford, prior to this study. We plotted the data on an XY scatter plot and selected three plasma samples with “high” (IC50: 3927), “medium” (IC50: 1336), and “low” (IC50: 154) neutralisation titres, and relatively high IgG titres (> 10^5 chemiluminescence).

4.2.7 SARS-CoV-2: Neutralisation Assay with OCTAVE Plasma and PHP

OCTAVE plasma samples were diluted into dilution media, to achieve a 1:2 dilution series with final concentrations from 1:10 – 1:640. All conditions were tested in duplicate, and each dilution series of OCTAVE plasma samples received either PHP or dilution media at a final concentration of 20%. To each sample, 20 µl of the SARS-CoV-2 Victoria strain (10^3 PFU/ml) was added to obtain a final volume of 40 µl and incubated at 37^{o}C for 1 hr. Vero E6 cells were diluted in dilution media at a concentration of 4.5 x10^5 cells/ml and 100 µl of cell suspension was added to each well. The neutralisation assay then proceeded according to section **4.2.8**.

4.2.8 SARS-CoV-2: Neutralisation Assay Method

The samples to be included in the SARS-CoV-2 neutralisation assays were prepared as described in each method section for using native plasma (section **4.2.4**), recombinant MBL and FCN-1 (section **4.2.5**), or PHP with OCTAVE sera (section **4.2.7**).

Following the addition of Vero E6 or Calu-3 cells, the neutralisation plates were incubated at 37^{o}C for 2 hrs before adding 100 µl of DMEM containing 1% FCS and 1.5% CMC, and returned to the incubator at 37^{o}C until 20 hrs post-infection. The CMC overlay was then aspirated and each well was washed in 200 µl of PBS and fixed in 100 µl of 4% paraformaldehyde (PFA) in PBS for 30 min. The samples were then aspirated and 100 µl of permeabilization buffer (2% Triton X-100 in PBS) was added. The plates were incubated at 37^{o}C for 30 min and washed three times in 100 µl of wash buffer (0.1% tween-20 in PBS). Anti-nucleocapsid monoclonal antibody (generously provided by Tiong Tan at the Radcliffe Department of Medicine, University of Oxford, UK) was diluted 1:5000 in PBS with 0.1% tween-20, and 50 µl was added to each well. The plates were incubated at RT for 1 hr whilst rotating at 500 rpm, then washed three times in 100 µl of wash buffer. Peroxidase-conjugated, anti-human IgG antibody (Merck) was diluted 1:5000 in PBS with 0.1% tween-20, and 50 µl was added to each well. The plates were incubated at RT for 1 hr whilst rotating at 500 rpm, then washed three times in 100 µl of wash buffer. 40 µl of TrueBlue^{TM} Peroxidase Substrate (Seracare) was then added to each well and incubated for 10

min at RT whilst shaking at 500 rpm. The staining solution was then aspirated and the plates were washed in 100 µl of ultrapure water and incubated for 5 min at RT, whilst shaking at 500 rpm. The plates were dried at RT for 45 min and the number of foci were counted using the ImmunoSpot® (Cellular Technology LTD). Mean values for the number of foci were calculated from duplicate samples at each plasma dilution, and fitted with a 4-parameter logistic (4PL) curve to calculate the half maximal inhibitory concentration (IC50) values using GraphPad Prism software (version 9).

4.3 Results

4.3.1 Vero E6 Cell Viability with PHP

The complement system is known to have potentially cytotoxic effects in cellular immunoassays, and so we determined the effect of our PHP on Vero E6 cells *via* microscopy and MTT assay. An MTT assay relies on the conversion of MTT into formazan by mitochondrial reductases as a direct measurement of cellular proliferation and viability. We also considered the use of EDTA before the addition of PHP to cells, as EDTA is a chelator of calcium and magnesium ions that are essential for complement activation. There was a significant reduction (Mann-Whitney, P = 0.028) in cell viability with the use of EDTA (**Figure 54**). The use of EDTA also caused the cells to detach, which was not suitable for our downstream analysis (**Figure 55**, **(E)**). The addition of PHP at all concentrations tested (40%, 20%, 10%, 0%) did not affect cell viability based on the MTT assay (**Figure 54**). However, our microscopy observations suggested that some cell integrity was lost with the use of PHP at a concentration of 40% (**Figure 55**, **(D)**).

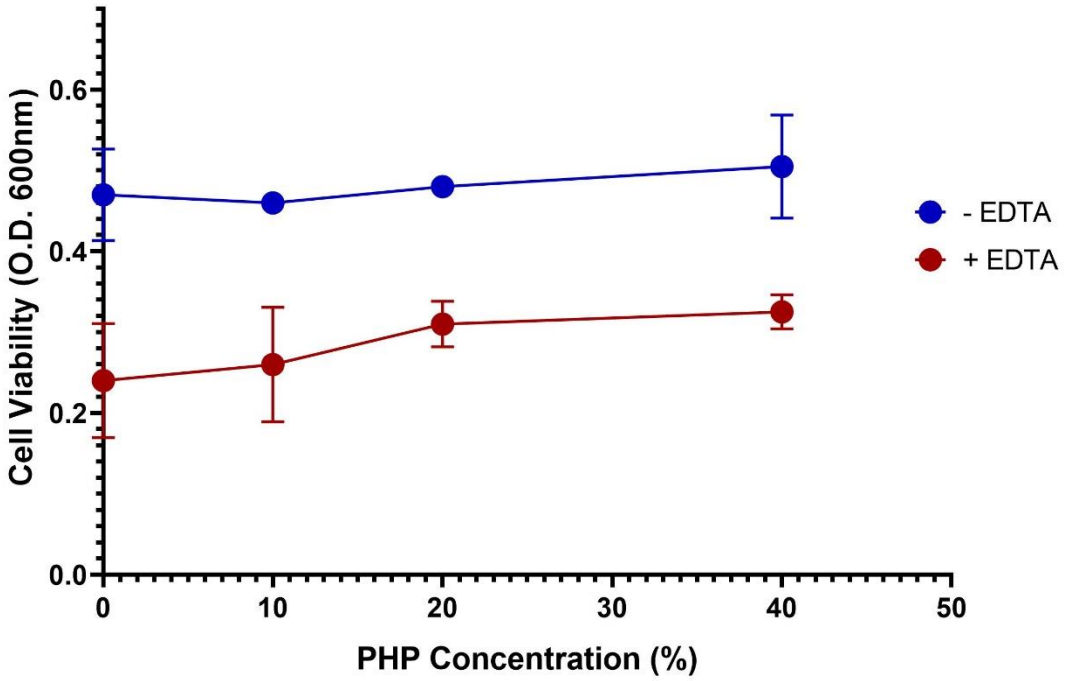

Figure 54: MTT assay of Vero E6 cells

Vero E6 cells were seeded at a concentration of 4.5 x10^5 cells/ml for 24 hrs and incubated with PHP for 20 hrs at a concentration of 40%, 20%, 10%, or media only, in the presence (red line) or absence (blue line) of 10 mM EDTA. Cell viability was then determined via MTT assay and a measurement of absorbance with a wavelength of 600 nm. Each sample was tested in duplicate and the data was analysed using GraphPad Prism software (version 9).

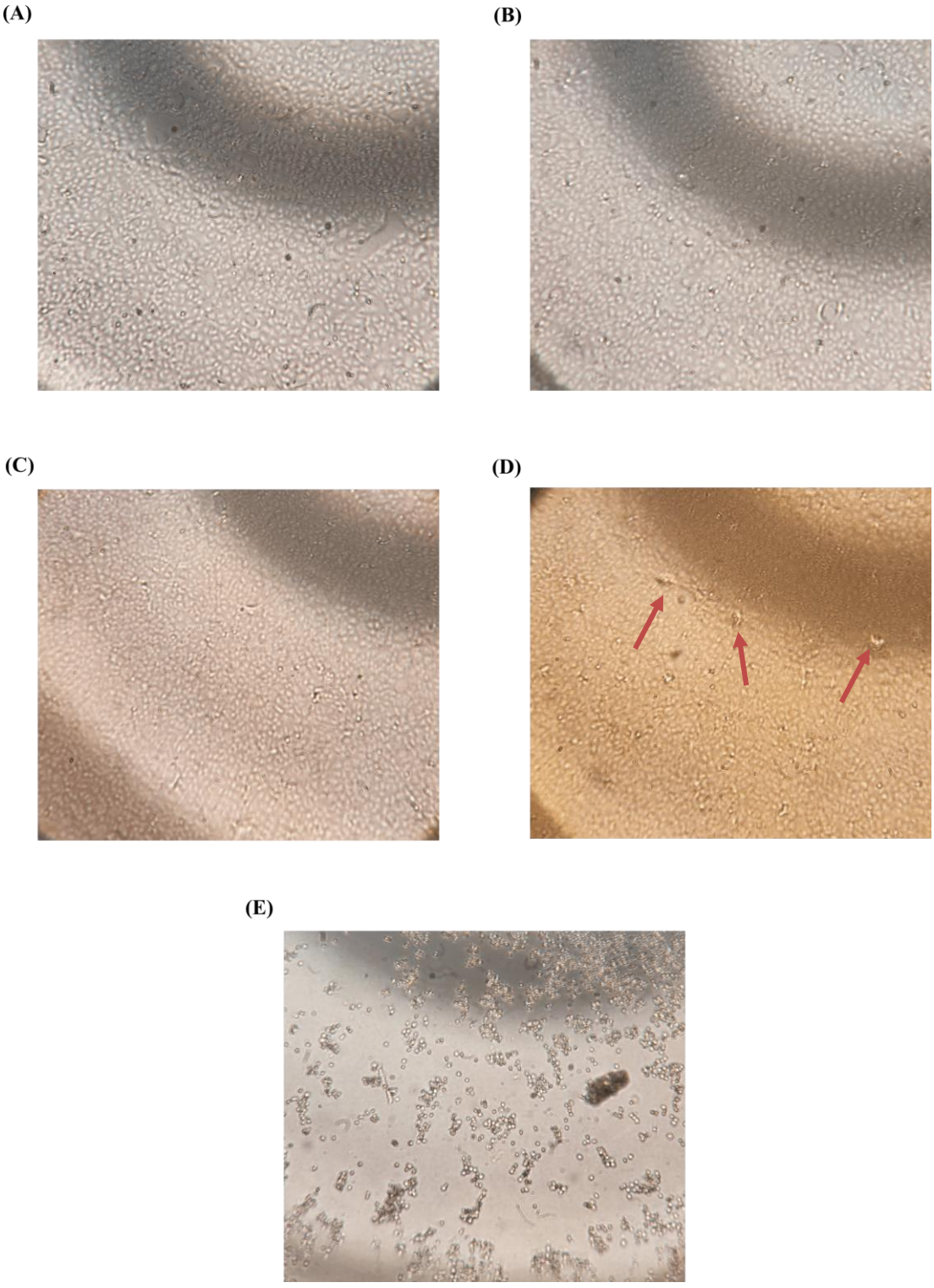

Figure 55: Microscopy of Vero E6 cells with PHP prior to MTT assay

Vero E6 cells were seeded at a concentration of 4.5 x10^5 cells/ml for 24 hrs and incubated with PHP for 20 hrs at a concentration of 40%, 20%, 10% or media only, in the presence or absence of 10 mM EDTA. The samples were then visualised via light microscopy. ***(A)*** *No PHP or EDTA was added to the cells and they remained healthy and attached to the flask.* ***(B)*** *PHP was added to the cells at a concentration of 10%*

and the cells remained healthy and attached to the flask. ***(C)*** *PHP was added to the cells at a concentration of 20%. The image has a slightly darker hue due to the plasma, but the cells remained attached with no clear changes to the structural integrity.* ***(D)*** *PHP was added to the cells at a concentration of 40%. Some of the cells had detached and there was some loss in structural integrity (red arrows).* ***(E)*** *EDTA was added to the cells at a concentration of 10 mM which caused the cells to detach and clump together.*

The EBOV neutralisation assays used a different neutralisation assay protocol and a different batch of PHP that was collected from 40 UK donors. The PHP was added to the Vero E6 cells at concentrations of 10%, 20%, 40%, or media only, and incubated at 37^{o}C for nine days to determine whether the complement system would have any adverse effects on the cells. Cell cytotoxicity became evident with the use of 40% PHP (**Figure 56**).

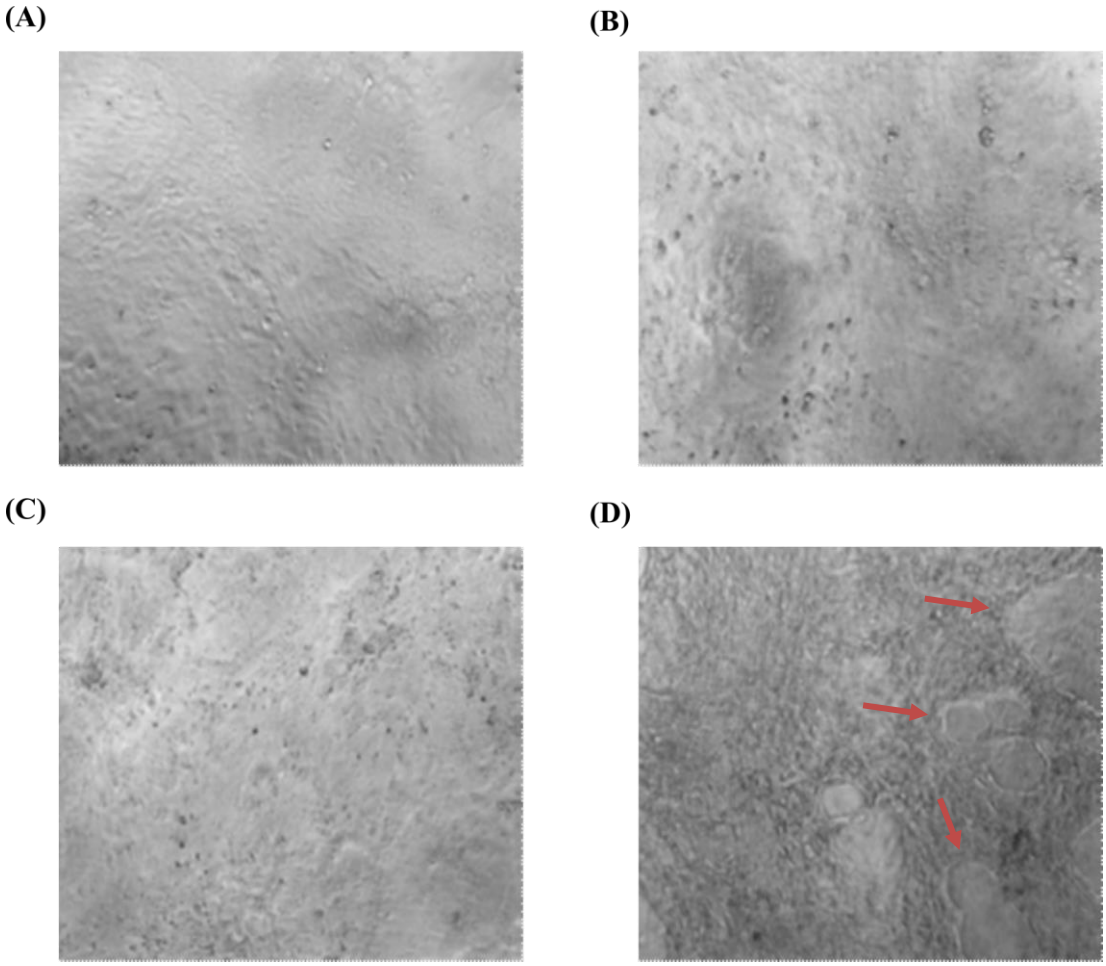

Figure 56: Microscopy of Vero E6 cells with PHP

Vero E6 cells at a final concentration of 9.4 x10^3 cells/ml were incubated with: ***(A)*** *media only,* ***(B)*** *10% PHP,* ***(C)*** *20% PHP, or* ***(D)*** *40% PHP, for 9 days at 37^{o}C. The cells were then visualised via light microscopy to determine whether the addition of PHP affected cell morphology. Cytotoxic effects towards the Vero E6 cells became apparent with the use of 40% PHP (red arrows).*

4.3.2 EBOV: Neutralisation Assay with PHP

One prior study has shown that the presence of complement is required for some monoclonal EBOV-GP antibodies to neutralise EBOV (407). Our results from **Chapter 2** and **Chapter 3** show that the complement system is activated in the presence of the EBOV-GP and EBOV-sGP, and that low-neutralising antibodies can mediate ADCD with similar potency to more strongly neutralising antibodies against the EBOV-GP, although this response was ameliorated in response to the EBOV-sGP. We wanted to

determine whether the ability of these low-neutralising antibodies to mediate ADCD could influence their neutralisation of EBOV.

In **Chapter 3**, we identified a cohort of convalescent EVD plasma samples with clearly defined EBOV-GP antibody titres that showed poor neutralisation. Eight samples from this cohort were chosen at random (**Figure 57**, **(A)**) to be used in wild-type EBOV neutralisation assays, in the presence or absence of exogenous PHP, along with a positive control that showed high neutralisation (sample C147). We found that the addition of 20% PHP resulted in a significant increase (Wilcoxon signed-rank, $P = 0.031$) in neutralisation compared to the antibody-only group (**Figure 57**, **(B)**). We also compared these two cohorts to the historic neutralisation data collected in 2017 when the convalescent EVD plasma samples were collected (372). There was no significant difference ($P > 0.050$) between the two antibody-only cohorts, whilst the cohort that received 20% PHP still showed a significant increase (Wilcoxon signed-rank, $P = 0.012$). We also compared the neutralisation titres of the group that received 20% PHP, to the median value of 132 survivor samples from the historic data set tested in 2017 (372), to understand how the new neutralisation titres might compare; the samples that received 20% PHP still remained below the median value of all EVD survivors (372).

We then analysed the log2 fold-change of each sample that received either 10% PHP or 20% PHP, compared to their antibody-only controls (**Figure 57**, **(C)**). One sample showed a significant increase (> 1.5 log2 fold-change) in neutralisation with 10% PHP (C067), and three samples significantly increased (> 1.5 log2 fold-change) with the addition of 20% PHP. No samples significantly decreased with the addition of PHP.

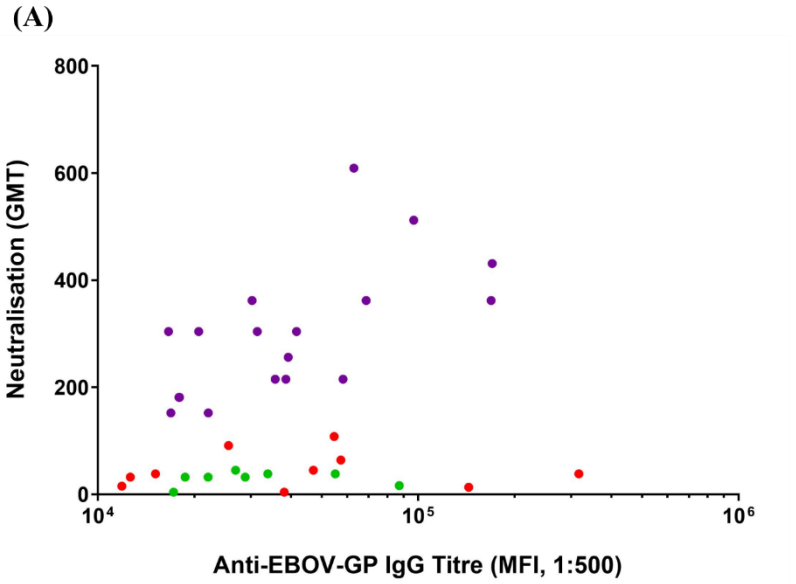
(A)
Neutralisation (GMT)
800
600
400
200
0
10^4
10^5
10^6
Anti-EBOV-GP IgG Titre (MFI, 1:500)

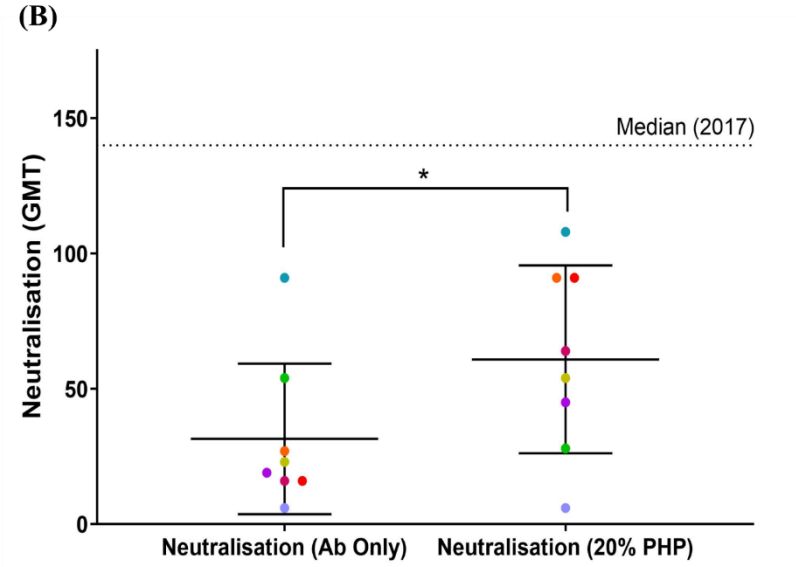
(B)
Neutralisation (GMT)
150
100
50
0
Median (2017)
*
Neutralisation (Ab Only)
Neutralisation (20% PHP)

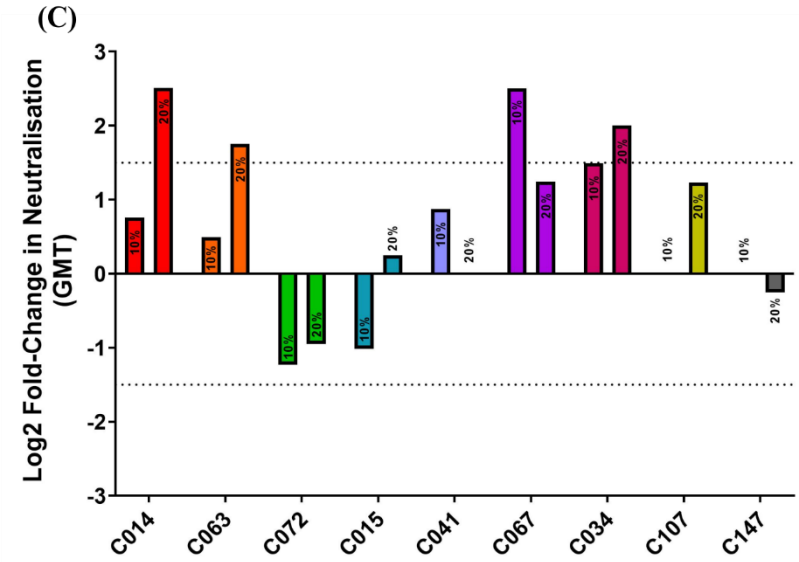
(C)
Log2 Fold-Change in Neutralisation (GMT)
3
2
1
0
-1
-2
-3
C014
C063
C072
C015
C041
C067
C034
C107
C147

Figure 57: Wild-type EBOV neutralisation assay with PHP

Wild-type EBOV neutralisation assays were supplemented with exogenous PHP to determine whether this would influence neutralisation. ***(A)*** *The neutralisation titres and EBOV-GP IgG titres of all samples from the LN (red dots) and N cohorts (purple dots) in* ***Chapter 3*** *were plotted on an XY scatter plot. Eight samples (green dots) were chosen at random from the LN cohort to be used in wild-type EBOV neutralisation assays.* ***(B)*** *There was a significant increase in neutralisation (Wilcoxon signed-rank, P = 0.031) with the addition of 20% PHP compared to the antibody (Ab) only cohort. The horizontal black lines show the mean value with SD for each cohort. All neutralisation titres remained below the median neutralisation titre of the 132 survivors from historical data collected in 2017 (horizontal dotted line).* ***(C)*** *Each sample was analysed individually, comparing the log2 fold-change with 10% PHP and 20% PHP from the antibody-only condition (horizontal black line). The dotted horizontal line shows the negative cut-off with a 1.5 log2 fold-change. The data was analysed using GraphPad Prism software (version 9).*

4.3.3 SARS-CoV-2: Neutralisation Assay with Native Plasma

The five individual plasma samples used to make the PHP were tested both individually and as a pool to determine whether the complement system could impact SARS-CoV-2 neutralisation, independent of antibodies. To test this hypothesis, SARS-CoV-2 neutralisation assays were supplemented with PHP, without the addition of COVID-19 convalescent plasma. Whilst there was an increase in the number of foci with the highest concentration of PHP at 20%, this difference was comparable to heat-inactivated FCS, which suggests this enhancement was an effect of supplementing the neutralisation assay with additional plasma rather than being complement-mediated (**Figure 58**, **(A)**). A similar effect was then observed for each of the individual plasma samples within the pool, showing an increase in foci from 1.7 to up to a 2.1-fold increase (**Figure 58, (B) – (F)**).

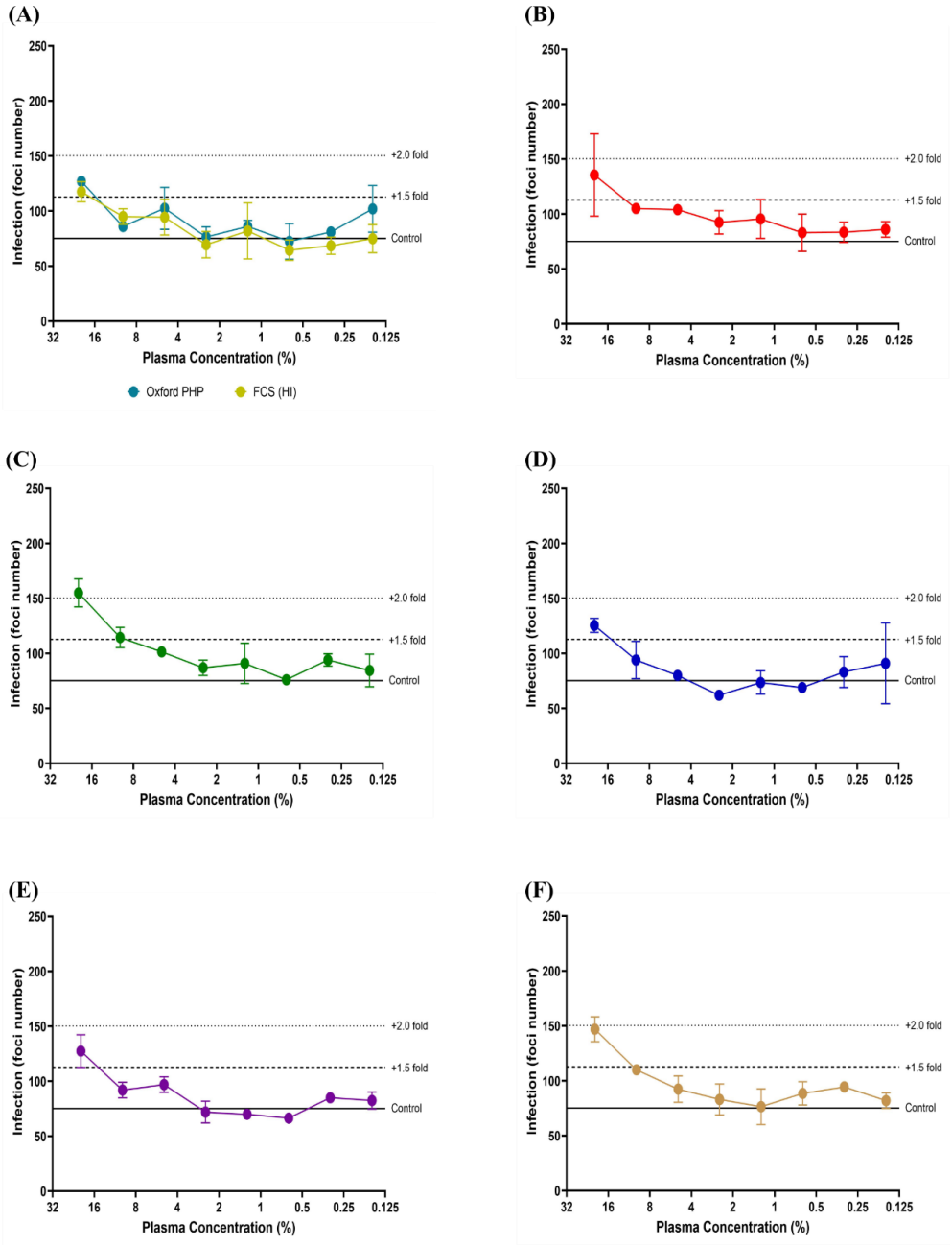

Figure 58: SARS-CoV-2: neutralisation assay with native plasma

PHP, heat-inactivated FCS, and the five individual plasma samples which make the PHP were incubated with SARS-CoV-2 to determine their impact on virus neutralisation. An increase in infection was observed with the use of 20% plasma or heat-inactivated FCS, which shows this effect is not complement-mediated. ***(A)*** *SARS-CoV-2 was incubated with FCS and PHP at various concentrations.* ***(B - F)*** *SARS-CoV-2 was incubated with individual plasma samples 1 – 5. The control line is the mean of all cells and virus control wells (n = 8), with either a plus 1.5-fold increase (dashed line) or 2.0-fold increase (dotted line). The foci number was determined using the ImmunoSpot® (Cellular Technology LTD) and the data was analysed using GraphPad Prism software (version 9).*

4.3.4 SARS-CoV-2: Neutralisation Assay with MBL and FCN-1

SARS-CoV-2 neutralisation assays were performed with recombinant MBL to determine whether its binding to the SARS-CoV-2 spike protein could influence the infection of Vero E6 and Calu-3 cells. FCN-1 does not reportedly bind to the SARS-CoV-2 spike protein (505,518) and was intended as a negative control. SARS-CoV-2 infection of Vero E6 cells showed a 1.8-fold increase in infection with the addition of 10 μg/ml of MBL, and a 2.7-fold increase in infection with the addition of 20 μg/ml of MBL, which was deemed significant (significance = fold-change > 2) (**Figure 59**, **(A)**). The addition of FCN-1 up to a concentration of 20 μg/ml did not increase SARS-CoV-2 infection of Vero E6 cells beyond the 2-fold cut-off for significance (**Figure 59**, **(B)**). SARS-CoV-2 infection of Calu-3 cells did not significantly increase with the addition of MBL up to a maximum concentration of 20 μg/ml, but was close to significance with a 1.9-fold increase at the highest concentration (**Figure 59**, **(C)**). SARS-CoV-2 infection of Calu-3 cells was increased by 2.5-fold with the addition FCN-1 at a concentration of 20 μg/ml, and by 1.8-fold with the addition of 10 μg/ml of FCN-1 (**Figure 59**, **(D)**).

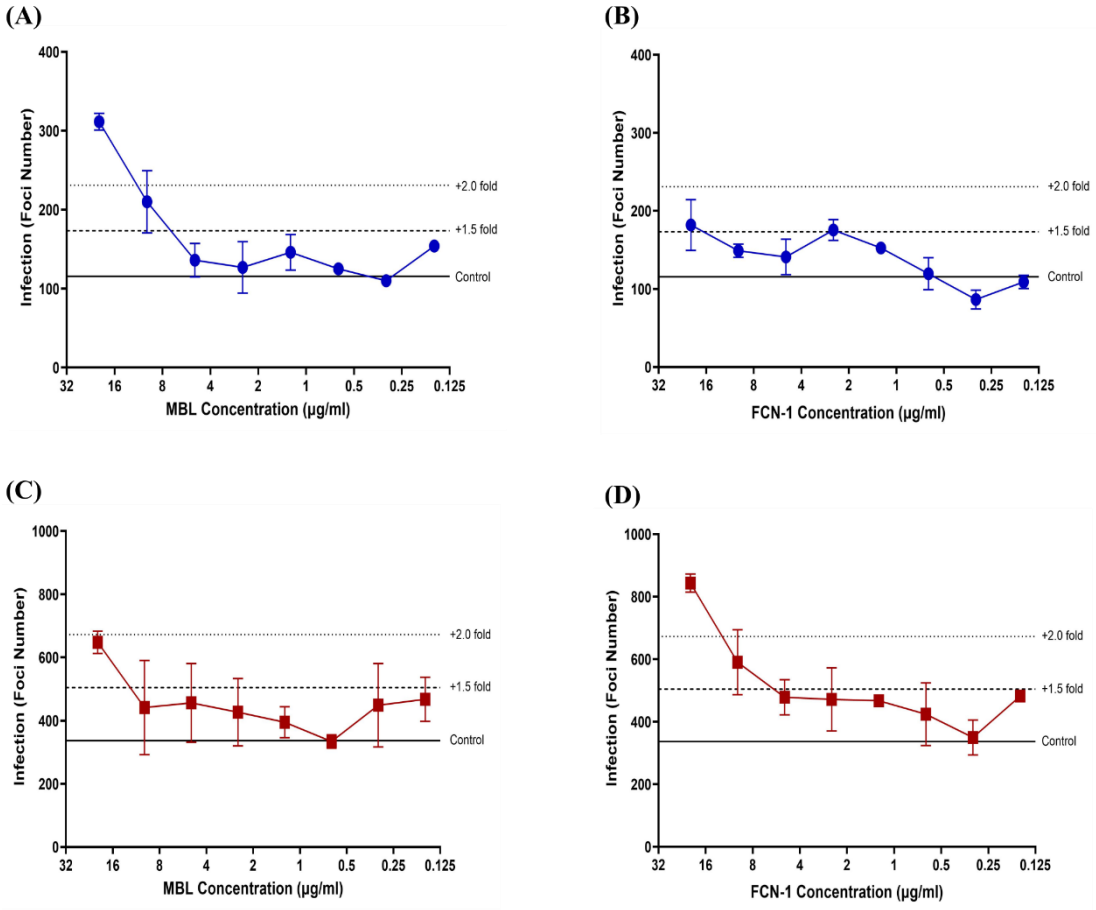

Figure 59: SARS-CoV-2: neutralisation assays with MBL and FCN-1

SARS-CoV-2 was incubated with various concentrations of MBL and FCN-1 prior to the infection of Vero E6 and Calu-3 cells. ***(A)*** *SARS-CoV-2 infection of Vero E6 cells following incubation with various concentrations of recombinant MBL from 20 µg/ml – 0.125 µg/ml.* ***(B)*** *SARS-CoV-2 infection of Vero E6 cells following incubation with various concentrations of recombinant FCN-1 from 20 µg/ml – 0.125 µg/ml.* ***(C)*** *SARS-CoV-2 infection of Calu-3 cells following incubation with various concentrations of recombinant MBL from 20 µg/ml – 0.125 µg/ml.* ***(D)*** *SARS-CoV-2 infection of Calu-3 cells following incubation with various concentrations of recombinant FCN-1 from 20 µg/ml – 0.125 µg/ml. The control line is the mean of all cells and virus control wells (n = 8), with either a plus 1.5-fold increase (dashed line) or 2.0-fold increase (dotted line). The foci number was determined using the ImmunoSpot® (Cellular Technology LTD) and the data was analysed using GraphPad Prism software (version 9).*

4.3.5 SARS-CoV-2: Neutralisation Assay with OCTAVE Plasma

Three plasma samples from the OCTAVE cohort were selected based on neutralisation titre and SARS-CoV-2 spike IgG titres, determined prior to this study. The samples we selected for use in SARS-CoV-2 neutralisation assays with the

addition of PHP, had a range in neutralisation titres (to see if a complement-mediated enhancement in neutralisation was limited to otherwise low-neutralising antibodies) and high IgG titres (to ensure the presence of SARS-CoV-2 spike-specific antibodies in the assay) (**Figure 60**).

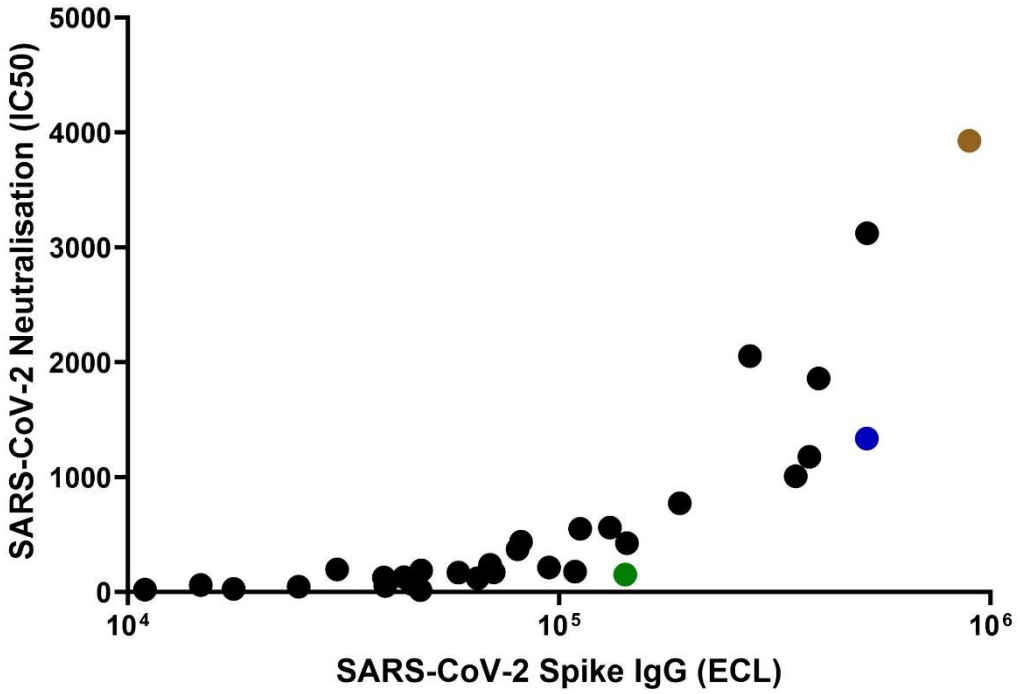

Figure 60: Selection of OCTAVE plasma for SARS-CoV-2 neutralisation assays

Historic neutralisation titres determined via SARS-CoV-2 (Victoria strain) neutralisation assays, and IgG titres determined via Meso Scale Discovery, were plotted on an XY scatter plot. Three plasma samples from the OCTAVE cohort were selected (green, blue, and brown dots) with high IgG titres > 10^5 electrochemiluminescence (ECL), and variable neutralisation titres. The data was plotted using GraphPad Prism software (version 9).

The "high", "medium", and "low" neutralising OCTAVE plasma samples followed the expected trend in IC50 values of > 640, 210.7, and 88.9, respectively. As demonstrated in **Figure 58**, the background signal of the assay was increased with the use of 20% PHP (Appendix III, **Figure 65**). To account for this signal variation when visualising the data, all values were normalised to a percentage between the minimum and maximum values for each sample. No infection was observed with the

dilution range for the “high” neutralising plasma, and so this data could not be normalised (Appendix III, **Figure 65**). We found that the addition of 20% PHP increased the IC50 values for both the “low” and “medium” neutralising OCTAVE plasma. In this example, an increase in IC50 shows that for SARS-CoV-2 to achieve 50% of maximal infection, less plasma is required to suppress infection and is therefore better at neutralising SARS-CoV-2 (**Figure 61**). Note that the normalisation does not affect the IC50 value.

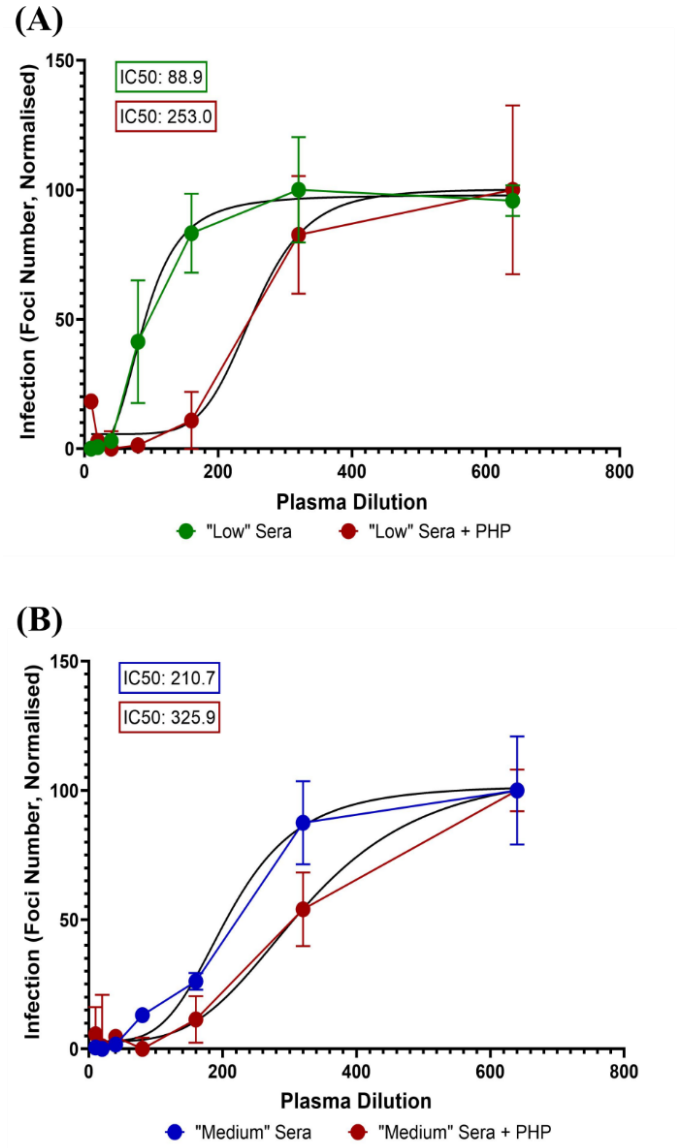

Figure 61: SARS-CoV-2: neutralisation with OCTAVE plasma and PHP (normalised)

The addition of PHP to the "low" and "medium" OCTAVE plasma samples resulted in an increase in IC50 values. In this example, an increase in IC50 shows that less plasma is required to reach the same level of protection. ***(A)*** *"Low" neutralising OCTAVE plasma (green dots) was supplemented with 20% PHP (red dots) which resulted in an increase in IC50 value.* ***(B)*** *"Medium" neutralising OCTAVE plasma (blue dots) was supplemented with 20% PHP (red dots) which resulted in an increase in IC50 value. Samples were fitted with a 4-parameter logistic curve (black line) to calculate the IC50 values. The foci number was determined using the ImmunoSpot® (Cellular Technology LTD) and the data was analysed using GraphPad Prism software (version 9).*

4.4 Discussion

In this chapter, we evaluated the antibody-independent and antibody-dependent effects of the complement system on wild-type EBOV and SARS-CoV-2 neutralisation, *in vitro*. For EBOV, we observed an enhancement to antibody-mediated neutralisation with the addition of PHP as a source of complement. The presence of PHP alone did not significantly affect EBOV neutralisation. For SARS-CoV-2, the addition of PHP and/or native plasma did not significantly influence neutralisation compared to the addition of heat-inactivated FCS. However, we did observe an enhancement of antibody-dependent neutralisation with the addition of 20% PHP in two vaccinee plasma samples. Interestingly, we also observed an enhancement of SARS-CoV-2 infection in Vero E6 cells with the addition of MBL, and enhanced infection into Calu-3 cells with the addition of FCN-1, with the use of each lectin at supraphysiological levels.

In **Chapter 2**, we showed that the EBOV-GP and EBOV-sGP were capable of mediating complement deposition and activating the complement system to completion. It was unclear whether this response could be beneficial or detrimental to protection. This response to the EBOV-GP could suggest antiviral complement-mediated mechanisms through the lysis of virions and infected cells, or neutralisation *via* agglutination or inhibition of host-receptor interactions. Conversely, complement activation has been shown to enhance infection of permissive cells for some viruses (169,170), and complement-mediated inflammation has been attributed to more severe disease pathologies (190–196). In our EBOV neutralisation assays within this chapter, the addition of 10% PHP or 20% PHP, in the absence of EVD survivor plasma, did not significantly impact EBOV neutralisation. Our findings of EBOV-GP-mediated lectin pathway activation, with no apparent antibody-independent effect on EBOV neutralisation, could have multiple explanations. Firstly, it is possible that the EBOV virion is capable of evading complement-mediated lysis through the acquisition of complement regulatory proteins in the budding stage of the virus lifecycle. This has been described previously for HIV-1, MuV, and SV5 (183,184) and could explain both the EBOV-GP-mediated complement deposition, and the lack of impact on

neutralisation. Secondly, it is possible that practical limitations of the neutralisation assays prevented the measurement of any significant effects. For example, the EBOV was incubated with PHP for 1 hr before being added to the Vero E6 cells, when it was then incubated for a further nine days. Unlike natural infection, the presence of complement would decrease over the course of our study. Another limitation of the neutralisation assay is that we were unable to ascertain the impact of other complement-mediated immune responses, such as inflammation and chemotaxis, which could influence EBOV pathogenesis.

In **Chapter 3**, we showed that low-neutralising, convalescent EVD survivor plasma was capable of mediating complement deposition in response to the EBOV-GP and the EBOV-sGP, with a differential in this response. The ability of these antibodies to engage the complement system could have implications for EBOV neutralisation, in the presence of complement. The complement-mediated enhancement of antibody-mediated EBOV neutralisation has been reported previously with the use of purified monoclonal antibodies (407). But the same effect was not observed in a separate study with the addition of guinea pig complement to EBOV convalescent human plasma (364). The use of guinea pig complement in the latter study could be an important distinction as it shows some functional differences from human complement (408–410). They also used historical plasma samples collected ~40 years post-infection. IgG isotype switching has been reported post-EBOV infection, where the IgG-4 isotype (which is unable to activate the complement system) starts to develop from 1–2 years post-EBOV infection (411). In our study, we observed a significant increase ($P = 0.031$) in the antibody-mediated neutralisation of wild-type EBOV with the addition of 20% PHP. Whilst the increase in neutralisation was still below the median neutralisation value reported for all 132 survivors in the historic data set (372), a further increase might be expected with higher concentrations of PHP, that would still be physiologically relevant to EBOV as it is a bloodborne pathogen, and plasma constitutes ~60% of total blood volume (590). One other study reported the use of complement from normal human serum (NHS) up to a concentration of 50% (567). In our study, attempts to increase the PHP concentration

to 40% resulted in cell cytotoxicity (**Figure 56**) which prohibited the interpretation of results. We observed a significant increase in EBOV neutralisation with sample C067 and the addition of 10% PHP, which dropped below the significance threshold with the addition of 20% PHP. This change was within the 1.5 log2 fold-change cut-off and could be the result of assay variance. It is possible that the use of 10% PHP with sample C067 led to assay saturation, although the majority of samples did show a positive trend between 10% and 20% PHP concentrations.

The neutralisation titre of each plasma sample was also analysed individually, as it was anticipated that only some plasma samples would show an increase in neutralisation with the addition of PHP, based on previous studies (159,167,405,406). This discrepancy has previously been attributed to the antibody isotype (407). In agreement with these studies, only 3/8 low-neutralising plasma samples showed a significant increase in neutralisation with 20% PHP (**Figure 57**). A previous study by Wilson *et al* found that all protective EBOV-GP monoclonal antibodies tested were of the IgG2a isotype (the most efficient complement-activating isotype in mice (407)). In our study, we were able to show neutralisation with native plasma which better recapitulates the natural polyclonal antibody response. The plasma samples will likely have a diverse antibody repertoire which targets a range of epitopes and consists of various isotype ratios. As discussed previously, these factors can influence their engagement of the complement system. These findings contribute to our understanding of EBOV neutralisation and could help inform future study designs and decisions for the development of EVD therapeutics.

In **Chapter 2**, we showed that the SARS-CoV-2 spike protein could mediate complement deposition in the absence of spike-specific antibodies. Similar to our discussion for EBOV, antibody-independent complement activation in response to the spike protein has the potential to mediate a range of antiviral or viral-enhancing effects, some of which can be determined *via* neutralisation assay. However, the presence of the complement system in our neutralisation assays did not significantly influence infection or neutralisation, in the absence of antibodies, when compared

to the addition of heat-inactivated FCS. Again, the complement system could still influence SARS-CoV-2 infection in response to the spike protein in ways beyond the scope of neutralisation assays, such as chemotaxis and inflammation.

In **Chapter 2**, we also observed the binding of MBL to the SARS-CoV-2 spike protein. In our SARS-CoV-2 neutralisation assays, the addition of 20 μg/ml of MBL showed a 2.7-fold increase in the SARS-CoV-2 infection of Vero E6 cells. We also observed an increase in infection of Calu-3 cells with an MBL concentration of 20 μg/ml, but this increase of 1.9-fold was below our significance threshold. Stravalaci *et al* previously showed that MBL inhibited SARS-CoV-2 infection of Calu-3 cells (518), and so our findings were unexpected. In Calu-3 cells, our use of 20 μg/ml of MBL was close to significance with a 1.9-fold increase, but the study by Stravalaci *et al* did not use MBL concentrations exceeding 10 μg/ml. MBL concentrations of 10 μg/ml are in the upper limit of MBL concentrations reported in the plasma of healthy individuals (we observed a maximum MBL concentration of ~7 μg/ml in our previous ELISAs: section **2.5.1**), and the concentration is highly variable during the acute phase responses, with the potential to increase further (591). The effect of MBL on SARS-CoV-2 infection of Vero E6 cells was not investigated by Stravalaci *et al*, and so our results may be explained by inherent differences in the intracellular signalling of Vero and Calu-3 cells during SARS-CoV-2 infection (592). A difference in virus neutralisation methods could also explain this discrepancy. We determined the potential for neutralisation based upon the presence of the nucleocapsid protein in the target cells, as an indication of infection. Stravalaci *et al* harvested the supernatant following virus incubation with Calu-3 cells for 48 to 72 hrs, and determined the impact of the addition of MBL on virus output using a plaque-forming assay in Vero E6 cells. They only observed significant changes in neutralisation with supernatant collected 72 hrs post-infection, using a multiplicity of infection of 0.1 and 1.0. Therefore, it is possible that we see a genuine increase in infection in our neutralisation assays with 20 μg/ml, but the virus is not capable of further infection. Another distinction between the two methods is that Stravalaci *et al* pre-incubated both virus and Calu-3 cells with MBL prior to infection, whilst we pre-incubated MBL with virus only. Pre-incubation of

cells with MBL could block certain receptors that would otherwise be bound by MBL in complex with SARS-CoV-2 that might facilitate uptake.

The FCN-1 protein was intended as a negative control as it does not reportedly bind to the SARS-CoV-2 spike protein (518). The addition of FCN-1 to SARS-CoV-2 neutralisation assays with Vero E6 cells had no effect on neutralisation. However, the addition of FCN-1 to neutralisation assays with Calu-3 cells showed a significant 2.5-fold increase in infection with FCN-1 at a concentration of 20 μg/ml, and an increase by 1.8-fold with 10 μg/ml of FCN-1 (**Figure 59**). This raises the question of whether FCN-1 is capable of binding to other proteins expressed on the virion surface such as the envelope protein, which could enhance viral infection. FCN-1 has also been shown to anchor onto the cell surface membranes of host cells (593,594). This could suggest that rather than cellular infection, we are observing cross-linking of the virus onto the surface of the cells. FCN-1 is expressed in the lung by neutrophils, monocytes, and type II alveolar epithelial cells (30,593). It would be important to confirm whether the protein is capable of influencing SARS-CoV-2 infection, and to identify a possible mechanism to explain this. However, we only observed a significant value with the use of 20 μg/ml of FCN-1 which far exceeds the levels of ~0.3 μg/ml reported in plasma (79), and of ~1.0 μg/ml in plasma within our own experiments (**Figure 23**). Lastly, whilst not all values were significant, a general upward trend in infection was observed in all conditions. This could suggest that our observations are simply an assay phenomenon with the use of high concentrations of protein, and so other means of experimentation would be required to confirm these findings.

In **Chapter 3**, we made reference to the application of the ADCD assays to various SARS-CoV-2 publications, which showed that ChAdOx1 nCoV-19 vaccine-induced antibodies could mediate ADCD, and this response was enhanced with a booster dose (504). Another collaborative study showed that ADCD was associated with disease severity in response to natural SARS-CoV-2 infection (563). In this chapter, we found that the addition of PHP as a source of complement was able to enhance the

neutralisation of otherwise “low” and “medium” neutralising plasma samples. For the “low”-neutralising plasma sample, we saw an increase in IC50 from 88.9 to 253.0 with the addition of 20% PHP. The difference was most apparent at a plasma dilution of 1:160, where 83.2% of maximal infection occurred in the absence of PHP, and the infection was reduced to 10.9% of maximal infection in the presence of PHP. For the “medium”-neutralising plasma sample, the IC50 increased from 210.7 to 325.9 with the addition of 20% PHP. The difference was most apparent at a plasma dilution of 1:320, where 87.5% of maximal infection occurred in the absence of PHP, and this was reduced to 54.0% in the presence of PHP. More samples would be required to accurately interpret trends within the data and to establish a reliable threshold for significance. However, the increase seen with the two samples tested is still noteworthy. As observed in our EBOV neutralisation assays (**Figure 57**), and as reported in other studies (405,407), not all plasma samples and/or antibodies show a change in neutralisation in the presence of complement. It is therefore promising to observe a positive change in the two samples tested. One limitation is the absence of a further control where the complement system in the 20% PHP has been inactivated. The use of EDTA to inactivate the complement system was not feasible, as EDTA caused the Vero E6 cells to detach and reduced their viability (**Figure 55**, **(E)**). We were also unable to use heat-inactivated PHP at 20%, as this created an artefact in the wells which prevented the accurate interpretation of foci (Appendix III, **Figure 63** and **Figure 64**). A suitable control could be the addition of heat-inactivated FCS which did not create artefacts in our assays at concentrations of 20%, and would be a suitable plasma substitute.

Our findings of complement-mediated enhancement of antibody-dependent SARS-CoV-2 neutralisation should be interpreted with caution until more samples can be tested along with an FCS-control. However, it is interesting to consider the potential significance of such findings. The complement system in COVID-19 is often reported in association with severe disease (490–497,499–501), which forms part of the rationale behind the use of complement inhibitors in clinical trials (ClinicalTrial.gov Identifier: NCT04382755; NCT04395456; NCT04570397; NCT04402060). Our findings

would suggest that the complement system could be beneficial in reducing viral titre in the presence of SARS-CoV-2-specific antibodies. Therefore, if complement inhibitors were to be used, the timing of their administration would be an important consideration. If complement assists viral clearance, but contributes to severe pathology post-viral clearance, then the optimal time to use the inhibitors would likely be post-viral clearance. It would also be important to understand the mechanism behind this complement-mediated enhancement of neutralisation, as this would give further validity to the results and could inform choices in therapeutics. For example, if the complement-mediated enhancement of neutralisation is mediated by the MAC, complement inhibitors targeting C5a rather than C5 may be more beneficial.

In summary, we did not observe any effect on neutralisation in the absence of virus-specific antibodies, despite previous evidence of complement activation for both EBOV and SARS-CoV-2. Our findings could be limited by the sensitivity of our assays, limitations in the methods, or it could indicate the existence of a viral mechanism to overcome the lectin pathway. Another possibility is that the complement system could still have antiviral activity beyond the measurements in neutralisation assays, i.e. chemotaxis and inflammation. We found that the addition of PHP as an exogenous source of complement could enhance the antibody-mediated neutralisation of EBOV and SARS-CoV-2. These are novel findings with the use of convalescent and vaccinee plasma for EBOV and SARS-CoV-2, respectively. This shows a beneficial role of the complement system in the pathogenesis of both viruses, where complement has been implicated in the disease severity of EVD and COVID-19. This work also highlights a limitation with conventional neutralisation assays that is often overlooked, and could be an important consideration when defining neutralisation, assessing vaccine-induced immune responses, measuring correlates of protection, and using neutralisation assays for the initial screening of therapeutic antibodies.

4.5 Appendix III

4.5.1 PHP C3c and C5b-9 Deposition Comparison

The two separate batches of PHP from either 5 UK donors (used in this chapter) or 40 UK donors (used in **Chapter 3**) were identical in their ability to mediate antibody-dependent C3c deposition and C5b-9 deposition in response to EBOV-GP conjugated beads (**Figure 62**). The PHP from 5 UK donors was further analysed using plasma samples with "high" and "low" EBOV-GP IgG titres, and five EBOV-GP IgG negative plasma samples. The level of complement deposition corresponded to the approximate IgG titres determined in **Chapter 3**.

Methods

Methods are as described in section **3.2.8** for EBOV-GP conjugated beads, using two batches of PHP: one from 5 UK donors and one from 40 UK donors. The two batches were directly compared using "medium" plasma with an intermediate IgG titre, to detect antibody-mediated C3c and C5b-9 deposition. The new PHP batch from 5 UK donors was scrutinised further using plasma samples with "high" and "low" IgG titres and five EBOV-GP IgG negative plasma samples.

Results

Both PHP batches were almost identical in the levels of C3c and C5b-9 deposition in response to EBOV-GP conjugated beads, as determined *via* flow cytometry (**Figure 62**). The PHP batch from five UK donors showed levels of ADCD relative to the IgG titre, as expected. Minimal background was observed with the use of EBOV-GP IgG negative plasma samples.

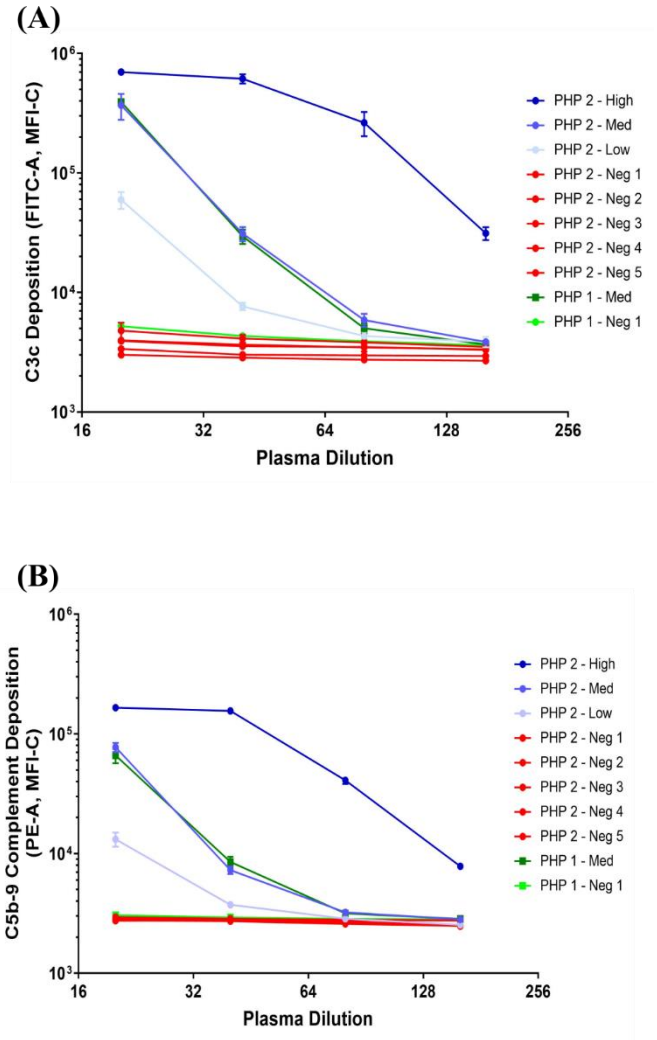

Figure 62: Comparison of C3c and C5b-9 deposition using two different PHP batches

Flow cytometry C3c and C5b-9 deposition assays were used to compare PHP from either 40 UK donors (PHP 1) or from 5 UK donors (PHP 2). ***(A)*** *Median fluorescence intensity (MFI) of C3c deposition against EBOV-GP conjugated beads using PHP1 and PHP2.* ***(B)*** *MFI of C5b-9 deposition against EBOV-GP conjugated beads using PHP1 and PHP2. All samples were tested in duplicate and each dot/square represents the mean values calculated in GraphPad Prism software (version 9).*

4.5.2 SARS-CoV-2: Neutralisation Assay with Heat-Inactivated PHP

Heat-inactivated PHP was intended for use as a negative control to determine whether a heat-labile component of plasma (indicative of the complement system) was responsible for the outcome of the SARS-CoV-2 neutralisation assays.

Methods

Methods were as described in section **4.2.4** and **4.2.8** with the use of heat-inactivated (56^{o}C for 30 min) PHP, native plasma samples, and heat-inactivated FCS.

Results

Based on the automated foci counting from the ImmunoSpot® (Cellular Technology LTD), there appeared to be a drastic increase in the number of foci for four out of the five plasma samples tested (**Figure 63**). However, visualisation of the wells with high automated foci counts suggests that these results are not genuine, and instead are an artefact being interpreted by the machine as foci (**Figure 64**).

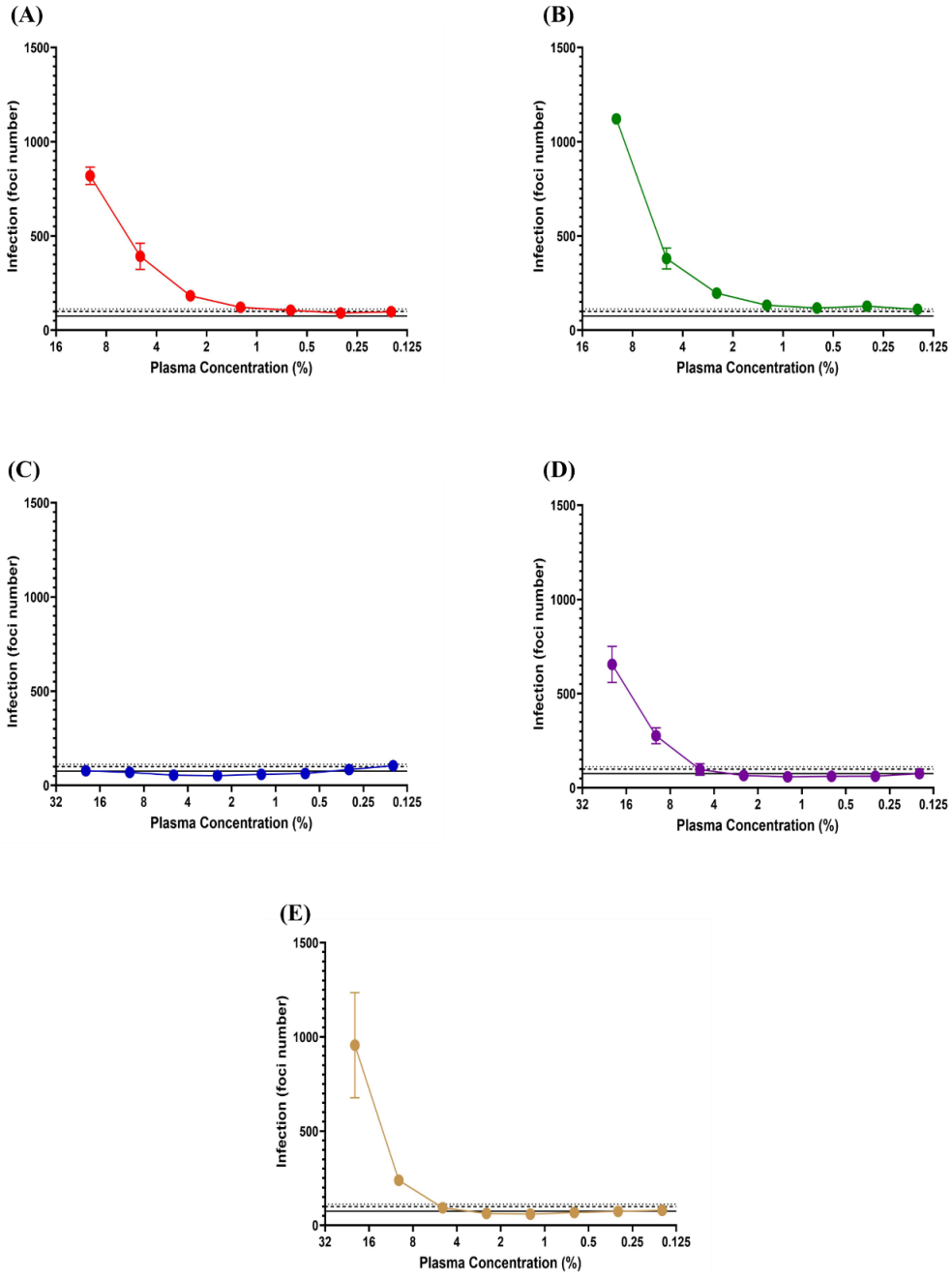

Figure 63: SARS-CoV-2: neutralisation assay with heat-inactivated native plasma

*Plasma samples 1 – 5 (**(A)** – **(E)**, respectively) that were used to make the human plasma pool, were heat-inactivated and tested individually in the SARS-CoV-2 neutralisation assays. Each dot represents the mean number of foci from duplicate samples with error bars to show the variance. The mean value of the cells and virus controls (n = 8) is represented with the black horizontal line, also showing plus two standard deviations (dashed line) and plus three standard deviations (dotted line). The number of foci were automatically determined by the ImmunoSpot (Cellular Technology LTD) and the data was analysed using GraphPad Prism software (version 9).*

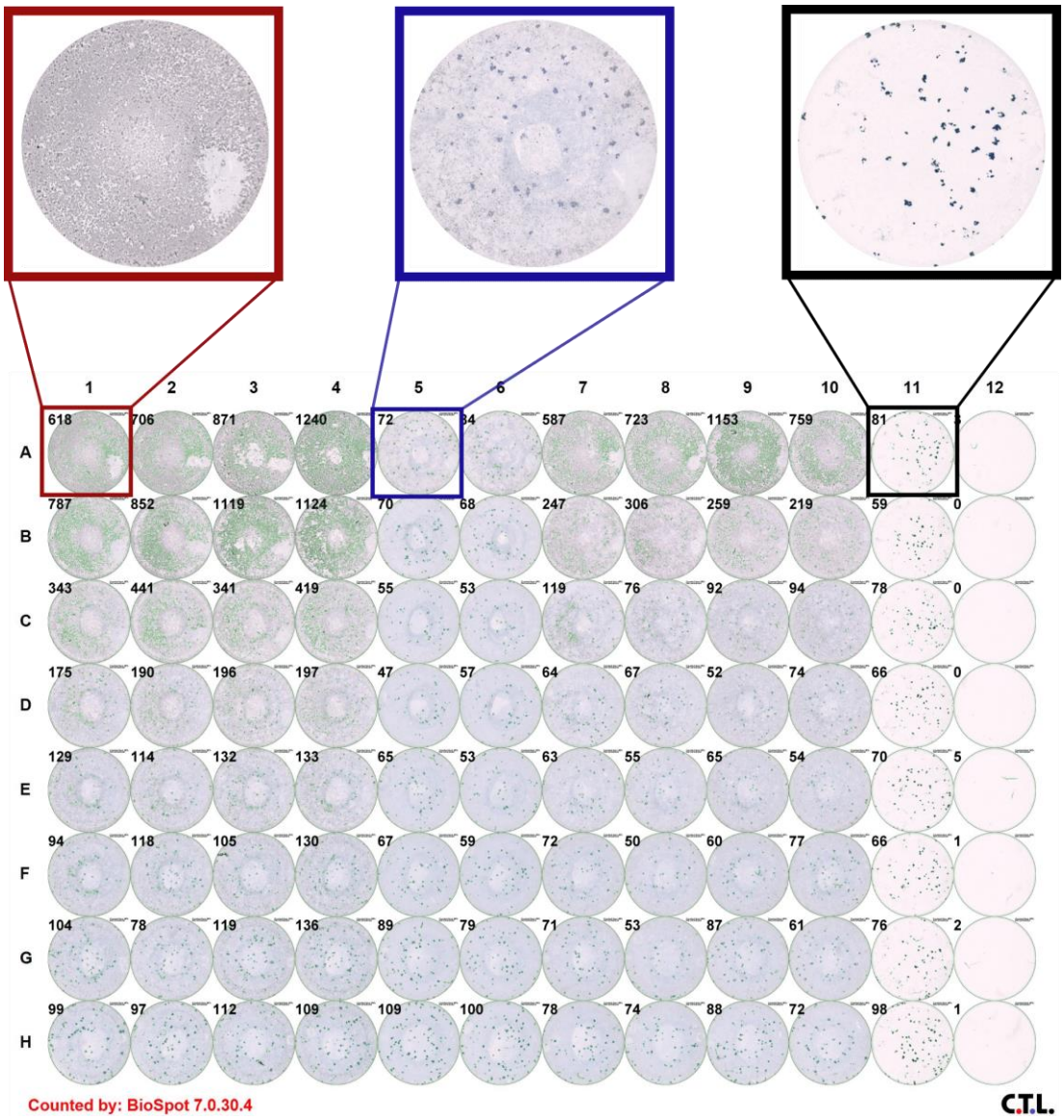

Figure 64: Well images of SARS-CoV-2 microneutralisation assay with heat-inactivated PHP

The 96-well plate shows the 1:2 dilution series of the individual plasma samples used to generate the PHP, from 20.000% (row A) to 0.156% (row H). Each sample was tested in duplicate: sample 1 (columns 1 – 2), sample 2 (columns 3 – 4), sample 3 (columns 5 – 6), sample 4 (columns 7 – 8), sample 5 (columns 9 – 10). Column 11 contained cells and virus only, and column 12 was left blank. Three example images are magnified to show the potential artefact with certain heat-inactivated (HI) samples at a PHP concentration of 20%. Foci are easily observed in the control well (black box). Foci are still clearly defined for sample 3 (blue box) although some background signal is evident. Sample 1 (red box) has no obvious foci. This image was captured by the ImmunoSpot® and annotated using InkScape software.

4.5.3 SARS-CoV-2: Neutralisation Assay with OCTAVE Plasma (Raw Values)

Three plasma samples from the OCTAVE cohort were selected with a range of neutralisation titres, and the final results were shown in section **4.3.5**. The data here shows the raw values prior to normalisation.

Methods

Methods are as described in sections **4.2.7** and **4.2.8**.

Results

The addition of PHP was found to increase the background signal of the SARS-CoV-2 neutralisation assays which is evident in the raw data (**Figure 65**). Despite the increase in background signal, the addition of PHP increased the IC50 values of the “low” and “medium” neutralising plasma samples.

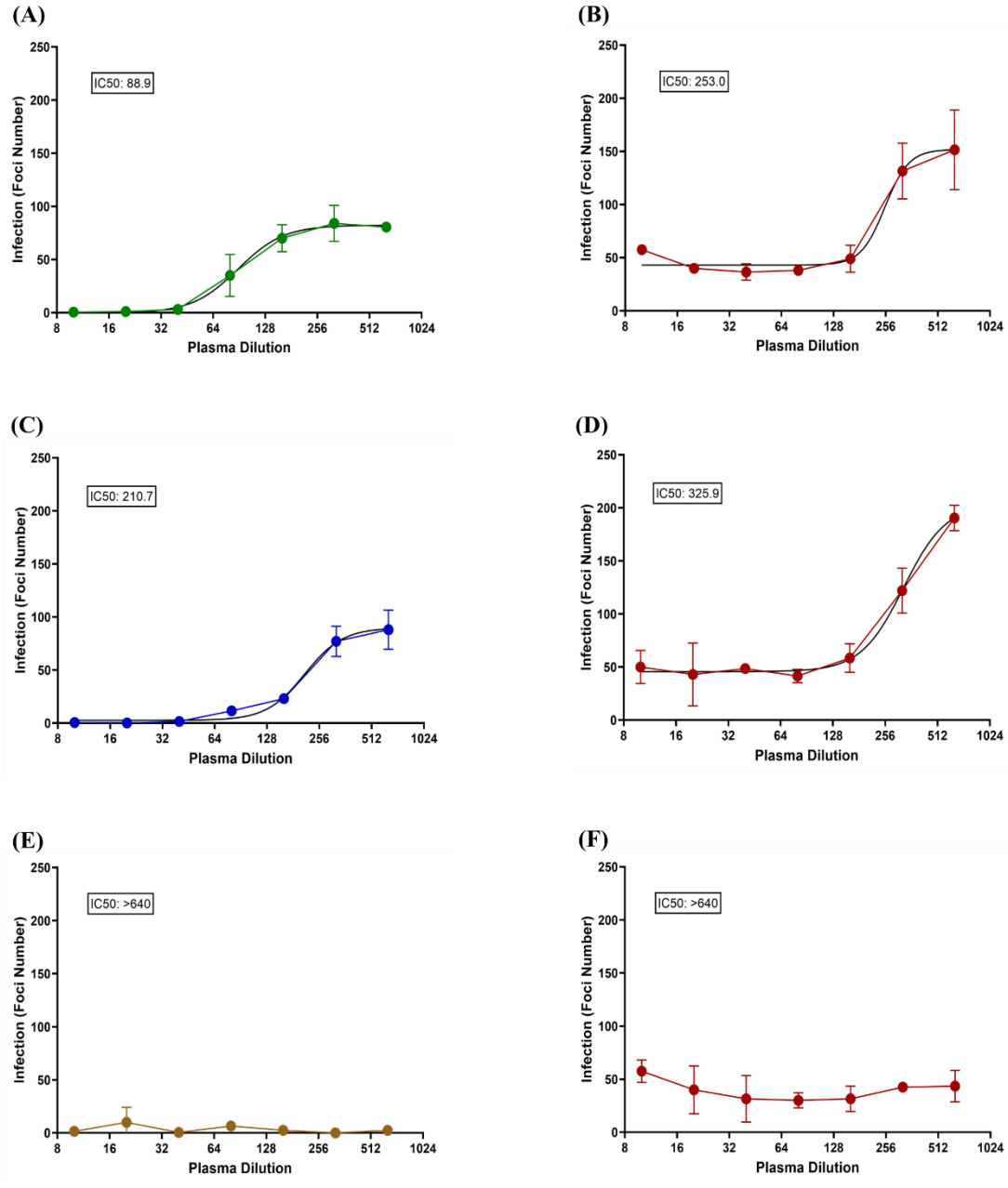

Figure 65: SARS-CoV-2: neutralisation assay with OCTAVE plasma and PHP (raw data)

(A) *"Low" neutralising plasma sample dilution.* ***(B)*** *"Low" neutralising plasma sample dilution with 20% PHP.* ***(C)*** *"Medium" neutralising plasma sample dilution.* ***(D)*** *"Medium" neutralising plasma sample dilution with 20% PHP.* ***(E)*** *"High" neutralising plasma sample dilution.* ***(F)*** *"High" neutralising plasma sample dilution with 20% PHP. A 4-parameter logistic curve (solid black line) was fitted to obtain IC50 values for each dilution series which showed a change in neutralisation. All samples were analysed using GraphPad Prism software (version 9).*

Chapter 5: Conclusion and Future Directions

The primary aim of this thesis was to investigate the role of the complement system in EBOV and SARS-CoV-2 pathogenesis. The complement system has been implicated in the progression and outcome of EVD and COVID-19, but explanations for the underlying mechanisms which explain these associations are not well-understood. We attempted to better understand both the antibody-dependent and antibody-independent mechanisms of the complement system, and to determine whether these mechanisms had any functional significance in the context of neutralisation for EBOV and SARS-CoV-2.

We first explored the antibody-independent mechanisms of the complement system in response to various *Ebolavirus* and *Coronavirus* glycoproteins (GPs), to determine whether the lectin/alternative (antibody-independent) complement pathways could influence EBOV and SARS-CoV-2 pathogenesis. For the *Ebolavirus* GPs, we made the novel observation that mannose-binding lectin (MBL) bound to the SUDV-GP, and the capacity to bind MBL was significantly reduced compared to the EBOV-GP and EBOV-sGP. We speculated that this could be influenced by the N-linked glycosylation patterns on these proteins. MBL can significantly influence EBOV infection *in vitro* and *in vivo* (7,157,412), and it is interesting to speculate whether the reduction in MBL binding (and complement deposition) to the SUDV-GP could be a contributing factor to the reduced mortality rates reported for SUDV (298). We next determined whether the *Ebolavirus* GPs could activate the complement system to completion, in the absence of GP-specific antibodies. We made the novel observation that the EBOV-GP, EBOV-sGP, and SUDV-GP could activate the complement system, leading to the end-stage formation of the MAC. The level of complement deposition strongly correlated with the level of MBL binding (Pearson correlation, $r = 0.9997$, $P < 0.0001$). These findings would be most relevant to the early stages of EBOV infection, before the development of an antibody response. The complement activation led to the formation of the MAC which has the potential to lyse virions and infected cells. Formation of the MAC also demonstrates complete activation of the complement

system, which can further influence viral pathogenesis *via* broader, more systemic immune responses such as inflammation, chemotaxis, and opsonisation.

For the *Coronavirus* GPs, we provided further evidence that MBL can bind to the SARS-CoV-1 spike protein, which had previously been disputed (77,166,532). We also found that MBL bound to the SARS-CoV-2 spike protein, and that the SARS-CoV-2 spike protein could activate the complement system to the eventual formation of the MAC, independent of SARS-CoV-2 spike-specific antibodies. During the course of this study, similar work was published which supported our findings (505,518). We made the novel observation that MBL binding (1.42-fold reduction (Mann Whitney test at 1 µg/ml MBL, P = 0.002)) and complement deposition (3.75-fold reduction (Mann Whitney test at 40% PHP, P = 0.002)) was significantly reduced in response to the SARS-CoV-2 spike protein, compared to the SARS-CoV-1 spike protein, used in this study. Similar to our comparison of SUDV and EBOV, the complement system has negative implications for SARS and severe cases of COVID-19. Thus, future investigations could consider whether this reduced capacity for complement activation is associated with reduced mortality. Our work augments the recent publications (505,518) that show potential mechanisms for activation of the complement system, which can ultimately help inform future therapeutic approaches.

Next, we investigated the ADCD response to *Ebolavirus* GPs with convalescent EVD plasma, using novel flow cytometry assays. Two cohorts were identified: one with low EBOV-neutralisation titres relative to EBOV-GP IgG titres (LN cohort), and the other with a direct linear relationship between EBOV-neutralisation and EBOV-GP IgG titres (N cohort). We found a differential response in the ability to mediate ADCD between plasma samples which was influenced by IgG titre, neutralisation titre, and the *Ebolavirus* antigen present (EBOV-GP, EBOV-sGP, or SUDV-GP). The LN and N cohorts were identical in their ability to mediate ADCD in response to the EBOV-GP, but this response was significantly reduced for the LN cohort in response to the EBOV-sGP and the SUDV-GP. For the low-neutralising antibodies in particular, the ability to

mediate ADCD could be an important Fc-mediated function for protection, which we later explored in the context of neutralisation, and it could have wider implications for inflammation, chemotaxis, and opsonisation. The ADCD response to the SUDV-GP was mediated by cross-reactive EBOV-GP antibodies and could contribute to immunity in the possible event of a subsequent infection with SUDV.

The ADCD assays were re-purposed for investigations into the Fc-mediated responses of convalescent and vaccinee plasma against the SARS-CoV-2 spike protein. This work was conducted in collaboration with the University of Oxford and the Pathogen Immunology Group at the UKHSA. The first research project demonstrated that antibodies induced by the ChAdOx1 nCoV-19 vaccine could mediate ADCD in response to the SARS-CoV-2 spike protein, and that this response was dose-dependent with the booster vaccine (504). The data collected in this study showed an array of Fc-mediated antibody responses that were induced following vaccination, and supported the use of a two-dose vaccine regime in the next stage of clinical trials. In the second research project, the ADCD response was associated with the severity of infection, for up to 180 days post-infection (563). This could be a consequence of antibody responses to the infection or it could indicate that a complement-mediated mechanism is responsible.

The findings reported in this thesis for the antibody-dependent and antibody-independent responses of the complement system to EBOV and SARS-CoV-2 were investigated further, in the context of neutralisation, to determine a functional significance. Our aims were to address whether the complement system could influence neutralisation in the absence of antibodies, and whether the presence of complement could enhance the neutralisation of otherwise low-neutralising antibodies. For both EBOV and SARS-CoV-2, we found that the addition of PHP, in the absence of virus-specific antibodies, was not sufficient to influence neutralisation in our *in vitro* assay. Other factors such as chemotaxis and opsonisation could still influence their pathogenesis, or the virus may have a mechanism to limit complement deposition that is only sufficient for the lower levels of lectin pathway activation.

However, in the presence of low-neutralising antibodies in plasma, we found that the addition of 20% PHP as an exogenous source of complement could significantly increase neutralisation potency. These findings were novel and demonstrated potential benefits of the complement system in EVD and COVID-19, where activation of the complement system often has negative associations with disease outcome. Our findings could be an important consideration for evaluating correlates of protection and vaccine-mediated immune responses for licensure, as neutralisation assays are common practice in the evaluation of vaccine effectiveness. These findings could also have important considerations for therapeutics, as the use of complement inhibitors are currently investigated in clinical trials for COVID-19. Understanding both the benefits and the detrimental effects of the complement system for COVID-19 could inform decisions on the type of complement inhibitor used, and the timing of administration. For EVD, only two therapeutics are FDA approved for use against the *Zaire* strain only. Future screening for therapeutic candidates might consider the effects that the complement system can have on antibody-mediated neutralisation, and how conventional neutralisation assays can neglect important immune components that would otherwise be present *in vivo*.

This thesis has provided the foundations for future studies to build upon. Of particular interest, would be to understand the complement-mediated mechanism responsible for the enhancement of antibody neutralisation of EBOV and SARS-CoV-2. This could be investigated with the use of C5-depleted plasma to determine whether the neutralisation is dependent on formation of the MAC, and therefore lysis, or whether virion aggregation is required instead. This would provide further evidence to support our observations of complement-mediated enhancement - along with testing a larger sample size - and would enable the dissection of which complement components may be beneficial to protection. This is an important consideration for the development and use of therapeutics, particularly the use of complement inhibitors. Another research question to arise from this thesis would be to address why the complement system does not influence EBOV or SARS-CoV-2 neutralisation in the absence of antibodies, despite complement activation *via* their GPs. One possibility is that the

complement system does influence neutralisation, just not within the conditions tested in this thesis for us to detect a significant result. A second possibility, for EBOV in particular, is that the virion may acquire host complement regulatory proteins (CD46, CD55, CD59) during the budding process from the cell-surface membrane (183,184). This explanation is less likely for SARS-CoV-2, as it leaves the cell *via* exocytosis and acquires its lipid envelope from the ERGIC membrane instead (415). A third possibility, for SARS-CoV-2, is that multiple viral proteins are expressed on the virion surface. The envelope protein has been shown to influence *Coronavirus* pathogenesis (443) and is expressed on the virion surface, but a potential role in mediating the complement system has not been reported. A complement regulatory role of surface-expressed viral or host-acquired proteins could explain the lack of effect of the complement system against SARS-CoV-2; the presence of spike-specific antibodies may then be sufficient to overcome this viral mechanism.

To conclude, this thesis furthers our understanding of the complement system in the pathogenesis of EBOV and SARS-CoV-2. This is a research area that is relatively neglected in the context of viral infections, but has gained increasing interest with the apparent involvement of the complement system in COVID-19. We add supporting and novel evidence to the existing literature regarding the response of the complement system to viral proteins, and demonstrate the significance of this for virus neutralisation. This research provides some of the foundations for future investigations of the complement system into EVD and COVID-19, whilst highlighting the areas that can be built upon. These findings could have significance for the optimisation of therapeutics with complement inhibitors for COVID-19, and the initial screening of antibodies for therapeutic use in EVD patients.

Bibliography

1. Mellors J, Tipton T, Longet S, Carroll M. Viral Evasion of the Complement System and Its Importance for Vaccines and Therapeutics. Front Immunol [Internet]. 2020 Jul 9 [cited 2021 Jan 26];11. Available from: https://www.ncbi.nlm.nih.gov/pmc/articles/PMC7363932/

2. Sarma JV, Ward PA. The Complement System. Cell Tissue Res. 2011 Jan;343(1):227–35.

3. Stoermer KA, Morrison TE. Complement and Viral Pathogenesis. Virology. 2011 Mar 15;411(2):362–73.

4. Male D, Brostoff J, Roth D, Roitt I. Immunology (8th edition). In: Immunology (8th Edition). 8th ed. Elsevier; 2012. p. 6–7.

5. Garcia BL, Zwarthoff SA, Rooijakkers SHM, Geisbrecht BV. Novel Evasion Mechanisms of the Classical Complement Pathway. Journal of immunology (Baltimore, Md : 1950). 2016 Sep 15;197(6):2051.

6. Fuchs A, Lin TY, Beasley DW, Stover CM, Schwaeble WJ, Pierson TC, et al. Direct complement restriction of flavivirus infection requires glycan recognition by mannose-binding lectin. Cell Host Microbe. 2010 Aug 19;8(2):186–95.

7. Brudner M, Karpel M, Lear C, Chen L, Yantosca LM, Scully C, et al. Lectin-Dependent Enhancement of Ebola Virus Infection via Soluble and Transmembrane C-type Lectin Receptors. PLoS One. 2013 Apr 2;8(4).

8. Favier AL, Gout E, Reynard O, Ferraris O, Kleman JP, Volchkov V, et al. Enhancement of Ebola Virus Infection via Ficolin-1 Interaction with the Mucin Domain of GP Glycoprotein. Journal of Virology. 2016 Jun 1;90(11):5256–69.

9. Avirutnan P, Fuchs A, Hauhart RE, Somnuke P, Youn S, Diamond MS, et al. Antagonism of the complement component C4 by flavivirus nonstructural

protein NS1. Journal of Experimental Medicine. 2010 Apr 12;207(4):793–806.

10. Kim H, Meyer K, Bisceglie AMD, Ray R. Hepatitis C Virus Suppresses C9 Complement Synthesis and Impairs Membrane Attack Complex Function. Journal of Virology. 2013 May 15;87(10):5858–67.

11. Conde JN, da Silva EM, Allonso D, Coelho DR, Andrade I da S, de Medeiros LN, et al. Inhibition of the Membrane Attack Complex by Dengue Virus NS1 through Interaction with Vitronectin and Terminal Complement Proteins. J Virol. 2016 01;90(21):9570–81.

12. Duncan AR, Winter G. The binding site for C1q on IgG. Nature. 1988 Apr 21;332(6166):738–40.

13. Bally I, Inforzato A, Dalonneau F, Stravalaci M, Bottazzi B, Gaboriaud C, et al. Interaction of C1q With Pentraxin 3 and IgM Revisited: Mutational Studies With Recombinant C1q Variants. Front Immunol [Internet]. 2019 [cited 2019 May 30];10. Available from: https://www.frontiersin.org/articles/10.3389/fimmu.2019.00461/full

14. Noris M, Remuzzi G. Overview of Complement Activation and Regulation. Semin Nephrol. 2013 Nov;33(6):479–92.

15. Kaul M, Loos M. Dissection of C1q Capability of Interacting with IgG Time-dependent formation of a tight and only partly reversible association. J Biol Chem. 1997 Dec 26;272(52):33234–44.

16. Nauta AJ, Trouw LA, Daha MR, Tijsma O, Nieuwland R, Schwaeble WJ, et al. Direct binding of C1q to apoptotic cells and cell blebs induces complement activation. European Journal of Immunology. 2002 Jun 1;32(6):1726–36.

17. Nauta AJ, Daha MR, Kooten C van, Roos A. Recognition and clearance of apoptotic cells: a role for complement and pentraxins. Trends in Immunology. 2003 Mar 1;24(3):148–54.

18. Ebenbichler CF, Thielens NM, Vornhagen R, Marschang P, Arlaud GJ, Dierich MP. Human immunodeficiency virus type 1 activates the classical pathway of

complement by direct C1 binding through specific sites in the transmembrane glycoprotein gp41. J Exp Med. 1991 Dec 1;174(6):1417–24.

19. Schiela B, Bernklau S, Malekshahi Z, Deutschmann D, Koske I, Banki Z, et al. Active Human Complement Reduces the Zika Virus Load via Formation of the Membrane-Attack Complex. Front Immunol. 2018 Oct 17;9.

20. Kunnakkadan U, Nag J, Kumar NA, Mukesh RK, Suma SM, Johnson JB. Complement-Mediated Neutralization of a Potent Neurotropic Human Pathogen, Chandipura Virus, Is Dependent on C1q. Journal of Virology [Internet]. 2019 Oct 1 [cited 2020 Jan 24];93(19). Available from: https://jvi.asm.org/content/93/19/e00994-19

21. McGrath FDG, Brouwer MC, Arlaud GJ, Daha MR, Hack CE, Roos A. Evidence That Complement Protein C1q Interacts with C-Reactive Protein through Its Globular Head Region. The Journal of Immunology. 2006 Mar 1;176(5):2950–7.

22. Nayak A, Pednekar L, Reid KB, Kishore U. Complement and non-complement activating functions of C1q: A prototypical innate immune molecule. Innate Immun. 2012 Apr 1;18(2):350–63.

23. Bing DH, Almeda S, Isliker H, Lahav J, Hynes RO. Fibronectin binds to the C1q component of complement. Proc Natl Acad Sci USA. 1982 Jul;79(13):4198–201.

24. Pearlstein E, Sorvillo J, Gigli I. The interaction of human plasma fibronectin with a subunit of the first component of complement, C1q. The Journal of Immunology. 1982 May 1;128(5):2036–9.

25. Krumdieck R, Höök M, Rosenberg LC, Volanakis JE. The proteoglycan decorin binds C1q and inhibits the activity of the C1 complex. J Immunol. 1992 Dec 1;149(11):3695–701.

26. Rainard P. Activation of the classical pathway of complement by binding of bovine lactoferrin to unencapsulated Streptococcus agalactiae. Immunology. 1993 Aug;79(4):648–52.

27. Sørensen IJ, Nielsen EH, Andersen O, Danielsen B, Svehag SE. Binding of complement proteins C1q and C4bp to serum amyloid P component (SAP) in solid contra liquid phase. Scand J Immunol. 1996 Oct;44(4):401–7.

28. Mortensen SA, Sander B, Jensen RK, Pedersen JS, Golas MM, Jensenius JC, et al. Structure and activation of C1, the complex initiating the classical pathway of the complement cascade. PNAS. 2017 Jan 31;114(5):986–91.

29. Serna M, Giles JL, Morgan BP, Bubeck D. Structural basis of complement membrane attack complex formation. Nat Commun. 2016 Feb 4;7.

30. Liu Y, Endo Y, Iwaki D, Nakata M, Matsushita M, Wada I, et al. Human M-Ficolin Is a Secretory Protein That Activates the Lectin Complement Pathway. The Journal of Immunology. 2005 Sep 1;175(5):3150–6.

31. Takahashi M, Iwaki D, Kanno K, Ishida Y, Xiong J, Matsushita M, et al. Mannose-binding lectin (MBL)-associated serine protease (MASP)-1 contributes to activation of the lectin complement pathway. J Immunol. 2008 May 1;180(9):6132–8.

32. Hansen S, Selman L, Palaniyar N, Ziegler K, Brandt J, Kliem A, et al. Collectin 11 (CL-11, CL-K1) Is a MASP-1/3-Associated Plasma Collectin with Microbial-Binding Activity. The Journal of Immunology. 2010 Nov 15;185(10):6096–104.

33. Nauser CL, Howard MC, Fanelli G, Farrar CA, Sacks S. Collectin-11 (CL-11) Is a Major Sentinel at Epithelial Surfaces and Key Pattern Recognition Molecule in Complement-Mediated Ischaemic Injury. Front Immunol [Internet]. 2018 Sep 6 [cited 2018 Nov 20];9. Available from: https://www.ncbi.nlm.nih.gov/pmc/articles/PMC6136055/

34. Teillet F, Dublet B, Andrieu JP, Gaboriaud C, Arlaud GJ, Thielens NM. The Two Major Oligomeric Forms of Human Mannan-Binding Lectin: Chemical Characterization, Carbohydrate-Binding Properties, and Interaction with MBL-Associated Serine Proteases. The Journal of Immunology. 2005 Mar 1;174(5):2870–7.

35. Tateishi K, Kanemoto T, Fujita T, Matsushita M. Characterization of the complex between mannose-binding lectin trimer and mannose-binding lectin-associated serine proteases. Microbiology and Immunology. 2011;55(6):427–33.

36. Weis WI, Drickamer K, Hendrickson WA. Structure of a C-type mannose-binding protein complexed with an oligosaccharide. Nature. 1992 Nov;360(6400):127–34.

37. Jensen PH, Weilguny D, Matthiesen F, McGuire KA, Shi L, Højrup P. Characterization of the Oligomer Structure of Recombinant Human Mannan-binding Lectin. J Biol Chem. 2005 Mar 25;280(12):11043–51.

38. Lu J, Le Y, Kon OL, Chan J, Lee SH. Biosynthesis of human ficolin, an Escherichia coli-binding protein, by monocytes: comparison with the synthesis of two macrophage-specific proteins, C1q and the mannose receptor. Immunology. 1996 Oct;89(2):289–94.

39. Garlatti V, Martin L, Lacroix M, Gout E, Arlaud GJ, Thielens NM, et al. Structural Insights into the Recognition Properties of Human Ficolins. Journal of Innate Immunity. 2010;2(1):17–23.

40. Runza VL, Schwaeble W, Männel DN. Ficolins: Novel pattern recognition molecules of the innate immune response. Immunobiology. 2008 May 14;213(3–4):297–306.

41. Kilpatrick DC, Chalmers JD. Human L-Ficolin (Ficolin-2) and Its Clinical Significance. BioMed Research International. 2012.

42. Swierzko A, Lukasiewicz J, Cedzynski M, Maciejewska A, Jachymek W, Niedziela T, et al. New functional ligands for ficolin-3 among lipopolysaccharides of Hafnia alvei. Glycobiology. 2012 Feb 1;22(2):267–80.

43. Henriksen ML, Brandt J, Andrieu JP, Nielsen C, Jensen PH, Holmskov U, et al. Heteromeric Complexes of Native Collectin Kidney 1 and Collectin Liver 1 Are Found in the Circulation with MASPs and Activate the Complement System. The Journal of Immunology. 2013 Dec 15;191(12):6117–27.

44. Nesargikar PN, Spiller B, Chavez R. The complement system: history, pathways, cascade and inhibitors. Eur J Microbiol Immunol (Bp). 2012 Jun;2(2):103–11.

45. Matsushita M, Thiel S, Jensenius JC, Terai I, Fujita T. Proteolytic activities of two types of mannose-binding lectin-associated serine protease. J Immunol. 2000 Sep 1;165(5):2637–42.

46. Ambrus G, Gál P, Kojima M, Szilágyi K, Balczer J, Antal J, et al. Natural Substrates and Inhibitors of Mannan-Binding Lectin-Associated Serine Protease-1 and -2: A Study on Recombinant Catalytic Fragments. The Journal of Immunology. 2003 Feb 1;170(3):1374–82.

47. Dahl MR, Thiel S, Matsushita M, Fujita T, Willis AC, Christensen T, et al. MASP-3 and its association with distinct complexes of the mannan-binding lectin complement activation pathway. Immunity. 2001 Jul;15(1):127–35.

48. Dobó J, Szakács D, Oroszlán G, Kortvely E, Kiss B, Boros E, et al. MASP-3 is the exclusive pro-factor D activator in resting blood: the lectin and the alternative complement pathways are fundamentally linked. Scientific Reports. 2016 Aug 18;6:31877.

49. Zewde N, Jr RDG, Dorado A, Morikis D. Quantitative Modeling of the Alternative Pathway of the Complement System. PLOS ONE. 2016 Mar 31;11(3):e0152337.

50. Thurman JM, Holers VM. The Central Role of the Alternative Complement Pathway in Human Disease. The Journal of Immunology. 2006 Feb 1;176(3):1305–10.

51. Tegla CA, Cudrici C, Patel S, Trippe R, Rus V, Niculescu F, et al. Membrane attack by complement: the assembly and biology of terminal complement complexes. Immunol Res. 2011 Oct;51(1):45–60.

52. Mueller-Ortiz SL, Drouin SM, Wetsel RA. The Alternative Activation Pathway and Complement Component C3 Are Critical for a Protective Immune

Response against Pseudomonas aeruginosa in a Murine Model of Pneumonia. Infection and Immunity. 2004 May 1;72(5):2899–906.

53. Bao L, Haas M, Boackle SA, Kraus DM, Cunningham PN, Park P, et al. Transgenic Expression of a Soluble Complement Inhibitor Protects Against Renal Disease and Promotes Survival in MRL/lpr Mice. The Journal of Immunology. 2002 Apr 1;168(7):3601–7.

54. Hietala MA, Jonsson IM, Tarkowski A, Kleinau S, Pekna M. Complement Deficiency Ameliorates Collagen-Induced Arthritis in Mice. The Journal of Immunology. 2002 Jul 1;169(1):454–9.

55. Spitzer D, Mitchell LM, Atkinson JP, Hourcade DE. Properdin Can Initiate Complement Activation by Binding Specific Target Surfaces and Providing a Platform for De Novo Convertase Assembly. The Journal of Immunology. 2007 Aug 15;179(4):2600–8.

56. Cortes C, Ferreira VP, Pangburn MK. Native Properdin Binds to Chlamydia pneumoniae and Promotes Complement Activation. Infection and Immunity. 2011 Feb 1;79(2):724–31.

57. Kemper C, Mitchell LM, Zhang L, Hourcade DE. The complement protein properdin binds apoptotic T cells and promotes complement activation and phagocytosis. Proc Natl Acad Sci U S A. 2008 Jul 1;105(26):9023–8.

58. Xu W, Berger SP, Trouw LA, de Boer HC, Schlagwein N, Mutsaers C, et al. Properdin binds to late apoptotic and necrotic cells independently of C3b and regulates alternative pathway complement activation. J Immunol. 2008 Jun 1;180(11):7613–21.

59. Strunk RC, Eidlen DM, Mason RJ. Pulmonary alveolar type II epithelial cells synthesize and secrete proteins of the classical and alternative complement pathways. J Clin Invest. 1988 May;81(5):1419–26.

60. Moutabarrik A, Nakanishi I, Matsumoto M, Zaid D, Seya T. Human glomerular epithelial cells synthesize and secrete the third component of complement. Nephron. 1995;70(1):55–61.

61. Andoh A, Kinoshita K, Rosenberg I, Podolsky DK. Intestinal Trefoil Factor Induces Decay-Accelerating Factor Expression and Enhances the Protective Activities Against Complement Activation in Intestinal Epithelial Cells. The Journal of Immunology. 2001 Oct 1;167(7):3887–93.

62. Langeggen H, Pausa M, Johnson E, Casarsa C, Tedesco F. The endothelium is an extrahepatic site of synthesis of the seventh component of the complement system. Clin Exp Immunol. 2000 Jul;121(1):69–76.

63. Turner NA, Moake J. Assembly and Activation of Alternative Complement Components on Endothelial Cell-Anchored Ultra-Large Von Willebrand Factor Links Complement and Hemostasis-Thrombosis. PLOS ONE. 2013 Mar 29;8(3):e59372.

64. Wittenborn T, Thiel S, Jensen L, Nielsen HJ, Jensenius JC. Characteristics and Biological Variations of M-Ficolin, a Pattern Recognition Molecule, in Plasma. JIN. 2010;2(2):167–80.

65. Lubbers R, van Essen MF, van Kooten C, Trouw LA. Production of complement components by cells of the immune system. Clin Exp Immunol. 2017 May;188(2):183–94.

66. Zhao J, Wu H, Khosravi M, Cui H, Qian X, Kelly JA, et al. Association of Genetic Variants in Complement Factor H and Factor H-Related Genes with Systemic Lupus Erythematosus Susceptibility. PLOS Genetics. 2011 May 26;7(5):e1002079.

67. Kim JS, Lee SY, Hahn HJ, Lee YB, Yu DS, Kim JW. Association of Single-Nucleotide Polymorphisms of the MBL2 with Atopic Dermatitis in Korean Patients. Ann Dermatol. 2017 Oct;29(5):571–7.

68. Gaya da Costa M, Poppelaars F, van Kooten C, Mollnes TE, Tedesco F, Würzner R, et al. Age and Sex-Associated Changes of Complement Activity and Complement Levels in a Healthy Caucasian Population. Front Immunol [Internet]. 2018 [cited 2019 May 3];9. Available from: https://www.frontiersin.org/articles/10.3389/fimmu.2018.02664/full

69. Avirutnan P, Hauhart RE, Marovich MA, Garred P, Atkinson JP, Diamond MS. Complement-mediated neutralization of dengue virus requires mannose-binding lectin. MBio. 2011;2(6).

70. Tu X, Chong WP, Zhai Y, Zhang H, Zhang F, Wang S, et al. Functional polymorphisms of the CCL2 and MBL genes cumulatively increase susceptibility to severe acute respiratory syndrome coronavirus infection. Journal of Infection. 2015 Jul 1;71(1):101–9.

71. Steffensen R, Thiel S, Varming K, Jersild C, Jensenius JC. Detection of structural gene mutations and promoter polymorphisms in the mannan-binding lectin (MBL) gene by polymerase chain reaction with sequence-specific primers. Journal of Immunological Methods. 2000 Jul 31;241(1):33–42.

72. Gupta A, Padh H. Frequency Distribution of Mannose Binding Lectin-2 and Vitamin D Receptor Gene Variants: Putative Markers for Tuberculosis. Genet Res Int [Internet]. 2015 [cited 2019 Jan 25];2015. Available from: https://www.ncbi.nlm.nih.gov/pmc/articles/PMC4674623/

73. Garred P, Madsen HO, Balslev U, Hofmann B, Pedersen C, Gerstoft J, et al. Susceptibility to HIV infection and progression of AIDS in relation to variant alleles of mannose-binding lectin. Lancet. 1997 Jan 25;349(9047):236–40.

74. Chen M, Liang Y, Li W, Wang M, Hu L, Abuaku BK, et al. Impact of MBL and MASP-2 gene polymorphism and its interaction on susceptibility to tuberculosis. BMC Infect Dis [Internet]. 2015 Mar 25 [cited 2018 Sep 11];15. Available from: https://www.ncbi.nlm.nih.gov/pmc/articles/PMC4399571/

75. Erdemir G, Ozkan TB, Ozgur T, Budak F, Kilic SS, Onay H. Mannose-binding lectin gene polymorphism and chronic hepatitis B infection in children. Saudi Journal of Gastroenterology. 2015 Mar 1;21(2):84.

76. Amiri A, Sabooteh T, Shahsavar F, Anbari K, Pouremadi F. Mannose-Binding Lectin (MBL) gene polymorphisms in susceptibility to pulmonary tuberculosis

among the Lur population of Lorestan Province of Iran. Genom Data. 2017 May 4;12:146–50.

77. Ip WKE, Chan KH, Law HKW, Tso GHW, Kong EKP, Wong WHS, et al. Mannose-binding lectin in severe acute respiratory syndrome coronavirus infection. J Infect Dis. 2005 May 15;191(10):1697–704.

78. Ammitzbøll CG, Kjær TR, Steffensen R, Stengaard-Pedersen K, Nielsen HJ, Thiel S, et al. Non-Synonymous Polymorphisms in the FCN1 Gene Determine Ligand-Binding Ability and Serum Levels of M-Ficolin. PLoS One [Internet]. 2012 Nov 28 [cited 2018 Sep 24];7(11). Available from: https://www.ncbi.nlm.nih.gov/pmc/articles/PMC3509001/

79. Munthe-Fog L, Hummelshoj T, Honoré C, Moller ME, Skjoedt MO, Palsgaard I, et al. Variation in FCN1 affects biosynthesis of ficolin-1 and is associated with outcome of systemic inflammation. Genes Immun. 2012 Oct;13(7):515–22.

80. Zimmer J, Hobkirk J, Mohamed F, Browning MJ, Stover CM. On the Functional Overlap between Complement and Anti-Microbial Peptides. Front Immunol. 2015;5.

81. Panda AK, Parida JR, Tripathy R, Pattanaik SS, Ravindran B, Das BK. Mannose binding lectin: a biomarker of systemic lupus erythematosus disease activity. Arthritis Res Ther. 2012;14(5):R218.

82. Goeldner I, Skare T, Boldt ABW, Nass FR, Messias-Reason IJ, Utiyama SR. Association of MASP-2 Levels and MASP2 Gene Polymorphisms with Rheumatoid Arthritis in Patients and Their Relatives. PLOS ONE. 2014 Mar 14;9(3):e90979.

83. Gandino IJ, Scolnik M, Bertiller E, Scaglioni V, Catoggio LJ, Soriano ER. Complement levels and risk of organ involvement in patients with systemic lupus erythematosus. Lupus Science & Medicine. 2017 Jun 1;4(1):e000209.

84. Winkelstein JA, Moxon ER. The Role of Complement in the Host's Defense against Haemophilus influenzae. J Infect Dis. 1992 Jun 1;165(Supplement_1):S62–5.

85. Garty BZ, Nitzan M, Danon YL. Systemic meningococcal infections in patients with acquired complement deficiency. Pediatr Allergy Immunol. 1993 Feb;4(1):6–9.

86. Yuste J, Sen A, Truedsson L, Jönsson G, Tay LS, Hyams C, et al. Impaired Opsonization with C3b and Phagocytosis of Streptococcus pneumoniae in Sera from Subjects with Defects in the Classical Complement Pathway. Infection and Immunity. 2008 Aug 1;76(8):3761–70.

87. Edelson BT, Stricker TP, Li Z, Dickeson SK, Shepherd VL, Santoro SA, et al. Novel collectin/C1q receptor mediates mast cell activation and innate immunity. Blood. 2006 Jan 1;107(1):143–50.

88. Stuart GR, Lynch NJ, Day AJ, Schwaeble WJ, Sim RB. The C1q and collectin binding site within C1 q receptor (cell surface calreticulin). Immunopharmacology. 1997 Dec 1;38(1):73–80.

89. Vandivier RW, Ogden CA, Fadok VA, Hoffmann PR, Brown KK, Botto M, et al. Role of Surfactant Proteins A, D, and C1q in the Clearance of Apoptotic Cells In Vivo and In Vitro: Calreticulin and CD91 as a Common Collectin Receptor Complex. The Journal of Immunology. 2002 Oct 1;169(7):3978–86.

90. Chao MP, Jaiswal S, Weissman-Tsukamoto R, Alizadeh AA, Gentles AJ, Volkmer J, et al. Calreticulin Is the Dominant Pro-Phagocytic Signal on Multiple Human Cancers and Is Counterbalanced by CD47. Science Translational Medicine. 2010 Dec 22;2(63):63ra94-63ra94.

91. Galvan MD, Greenlee-Wacker MC, Bohlson SS. C1q and phagocytosis: the perfect complement to a good meal. Journal of Leukocyte Biology. 2012;92(3):489–97.

92. Moestrup SK, Gliemann J, Pallesen G. Distribution of the α<Subscript>2</Subscript>-macroglobulin receptor/low density lipoprotein

receptor-related protein in human tissues. Cell Tissue Res. 1992 Sep 1;269(3):375–82.

93. Duus K, Hansen EW, Tacnet P, Frachet P, Arlaud GJ, Thielens NM, et al. Direct interaction between CD91 and C1q. FEBS J. 2010 Sep;277(17):3526–37.

94. Dedio J, Jahnen-Dechent W, Bachmann M, Müller-Esterl W. The Multiligand-Binding Protein gC1qR, Putative C1q Receptor, Is a Mitochondrial Protein. The Journal of Immunology. 1998 Apr 1;160(7):3534–42.

95. Leigh EAL, Ghebrehiwet B, Perera PST, Bird NI, Strong P, Kishore U, et al. C1q-mediated chemotaxis by human neutrophils: involvement of gClqR and G-protein signalling mechanisms. Biochemical Journal. 1998 Feb 15;330(1):247–54.

96. Vegh Z, Kew RR, Gruber BL, Ghebrehiwet B. Chemotaxis of human monocyte-derived dendritic cells to complement component C1q is mediated by the receptors gC1qR and cC1qR. Molecular Immunology. 2006 Mar 1;43(9):1402–7.

97. Steinberger P, Szekeres A, Wille S, Stöckl J, Selenko N, Prager E, et al. Identification of human CD93 as the phagocytic C1q receptor (C1qRp) by expression cloning. J Leukoc Biol. 2002 Jan;71(1):133–40.

98. Norsworthy PJ, Fossati-Jimack L, Cortes-Hernandez J, Taylor PR, Bygrave AE, Thompson RD, et al. Murine CD93 (C1qRp) Contributes to the Removal of Apoptotic Cells In Vivo but Is Not Required for C1q-Mediated Enhancement of Phagocytosis. The Journal of Immunology. 2004 Mar 15;172(6):3406–14.

99. Bohlson SS, Silva R, Fonseca MI, Tenner AJ. CD93 is rapidly shed from the surface of human myeloid cells and the soluble form is detected in human plasma. J Immunol. 2005 Jul 15;175(2):1239–47.

100. Wright SD, Silverstein SC. Tumor-promoting phorbol esters stimulate C3b and C3b' receptor-mediated phagocytosis in cultured human monocytes. J Exp Med. 1982 Oct 1;156(4):1149–64.

101. Berger M, Sorensen RU, Tosi MF, Dearborn DG, Döring G. Complement receptor expression on neutrophils at an inflammatory site, the Pseudomonas-infected lung in cystic fibrosis. J Clin Invest. 1989 Oct;84(4):1302–13.

102. Hivroz C, Fischer E, Kazatchkine MD, Grillot-Courvalin C. Differential effects of the stimulation of complement receptors CR1 (CD35) and CR2 (CD21) on cell proliferation and intracellular Ca2+ mobilization of chronic lymphocytic leukemia B cells. The Journal of Immunology. 1991 Mar 15;146(6):1766–72.

103. Rødgaard A, Christensen LD, Thomsen BS, Wiik A, Bendixen G. Complement receptor type 1 (CR1, CD35) expression on peripheral T lymphocytes: both CD4- and CD8-positive cells express CR1. Complement Inflamm. 1991;8(5–6):303–9.

104. Pascual M, Schifferli JA. The binding of immune complexes by the erythrocyte complement receptor 1 (CR1). Immunopharmacology. 1992 Oct;24(2):101–6.

105. Füreder W, Agis H, Willheim M, Bankl HC, Maier U, Kishi K, et al. Differential expression of complement receptors on human basophils and mast cells. Evidence for mast cell heterogeneity and CD88/C5aR expression on skin mast cells. J Immunol. 1995 Sep 15;155(6):3152–60.

106. Klickstein LB, Barbashov SF, Liu T, Jack RM, Nicholson-Weller A. Complement Receptor Type 1 (CR1, CD35) Is a Receptor for C1q. Immunity. 1997 Sep 1;7(3):345–55.

107. Fang Y, Xu C, Fu YX, Holers VM, Molina H. Expression of Complement Receptors 1 and 2 on Follicular Dendritic Cells Is Necessary for the Generation of a Strong Antigen-Specific IgG Response. The Journal of Immunology. 1998 Jun 1;160(11):5273–9.

108. Java A, Liszewski MK, Hourcade DE, Zhang F, Atkinson JP. Role of complement receptor 1 (CR1; CD35) on epithelial cells: A model for

understanding complement-mediated damage in the kidney. Mol Immunol. 2015 Oct;67(2 0 0):584–95.

109. Iida K, Nadler L, Nussenzweig V. Identification of the membrane receptor for the complement fragment C3d by means of a monoclonal antibody. J Exp Med. 1983 Oct 1;158(4):1021–33.

110. Levy E, Ambrus J, Kahl L, Molina H, Tung K, Holers VM. T lymphocyte expression of complement receptor 2 (CR2/CD21): a role in adhesive cell-cell interactions and dysregulation in a patient with systemic lupus erythematosus (SLE). Clin Exp Immunol. 1992 Nov;90(2):235–44.

111. Vorup-Jensen T, Jensen RK. Structural Immunology of Complement Receptors 3 and 4. Front Immunol. 2018;9.

112. Behrens EM, Sriram U, Shivers DK, Gallucci M, Ma Z, Finkel TH, et al. Complement Receptor 3 Ligation of Dendritic Cells Suppresses Their Stimulatory Capacity. The Journal of Immunology. 2007 May 15;178(10):6268–79.

113. Sándor N, Kristóf K, Paréj K, Pap D, Erdei A, Bajtay Z. CR3 is the dominant phagocytotic complement receptor on human dendritic cells. Immunobiology. 2013 Apr;218(4):652–63.

114. Bischoff SC, de Weck AL, Dahinden CA. Interleukin 3 and granulocyte/macrophage-colony-stimulating factor render human basophils responsive to low concentrations of complement component C3a. Proc Natl Acad Sci USA. 1990 Sep;87(17):6813–7.

115. Ehrengruber MU, Geiser T, Deranleau DA. Activation of human neutrophils by C3a and C5A. Comparison of the effects on shape changes, chemotaxis, secretion, and respiratory burst. FEBS Lett. 1994 Jun 13;346(2–3):181–4.

116. Nilsson G, Johnell M, Hammer CH, Tiffany HL, Nilsson K, Metcalfe DD, et al. C3a and C5a are chemotaxins for human mast cells and act through distinct receptors via a pertussis toxin-sensitive signal transduction pathway. J Immunol. 1996 Aug 15;157(4):1693–8.

117. Hartmann K, Henz BM, Krüger-Krasagakes S, Köhl J, Burger R, Guhl S, et al. C3a and C5a stimulate chemotaxis of human mast cells. Blood. 1997 Apr 15;89(8):2863–70.

118. Martin U, Bock D, Arseniev L, Tornetta MA, Ames RS, Bautsch W, et al. The human C3a receptor is expressed on neutrophils and monocytes, but not on B or T lymphocytes. J Exp Med. 1997 Jul 21;186(2):199–207.

119. Ischenko A, Sayah S, Patte C, Andreev S, Gasque P, Schouft MT, et al. Expression of a functional anaphylatoxin C3a receptor by astrocytes. J Neurochem. 1998 Dec;71(6):2487–96.

120. Peng Q, Li K, Anderson K, Farrar CA, Lu B, Smith RAG, et al. Local production and activation of complement up-regulates the allostimulatory function of dendritic cells through C3a-C3aR interaction. Blood. 2008 Feb 15;111(4):2452–61.

121. Weinmann O, Gutzmer R, Zwirner J, Wittmann M, Langer K, Lisewski M, et al. Up-regulation of C5a receptor expression and function on human monocyte derived dendritic cells by prostaglandin E2. Immunology. 2003 Dec;110(4):458–65.

122. Okinaga S, Slattery D, Humbles A, Zsengeller Z, Morteau O, Kinrade MB, et al. C5L2, a nonsignaling C5A binding protein. Biochemistry. 2003 Aug 12;42(31):9406–15.

123. Helmy KY, Katschke KJ, Gorgani NN, Kljavin NM, Elliott JM, Diehl L, et al. CRIg: a macrophage complement receptor required for phagocytosis of circulating pathogens. Cell. 2006 Mar 10;124(5):915–27.

124. McNearney T, Ballard L, Seya T, Atkinson JP. Membrane cofactor protein of complement is present on human fibroblast, epithelial, and endothelial cells. J Clin Invest. 1989 Aug;84(2):538–45.

125. Liszewski MK, Post TW, Atkinson JP. Membrane Cofactor Protein (MCP or CD46): Newest Member of the Regulators of Complement Activation Gene Cluster. Annual Review of Immunology. 1991;9(1):431–55.

126. Oglesby TJ, Allen CJ, Liszewski MK, White DJG, Atkinson JP. Membrane cofactor protein (CD46) protects cells from complement- mediated attack by an intrinsic mechanism. J Exp Med. 1992 Jun 1;175(6):1547–51.

127. Nicholson-Weller A, March JP, Rosen CE, Spicer DB, Austen KF. Surface membrane expression by human blood leukocytes and platelets of decay-accelerating factor, a regulatory protein of the complement system. Blood. 1985;65(5):1237–44.

128. Edward M, Walter EI, Rutgers JL, Knowles DM, Nussenzweig V. Identification of the complement Decay-Accelerating Factor (DAF) on epithelium and glandular cells and in body fluids. Journal of Experimental Medicine. 1987;165(3):848–64.

129. Medof ME, Walter EI, Rutgers JL, Knowles DM, Nussenzweig V. Identification of the complement decay-accelerating factor (DAF) on epithelium and glandular cells and in body fluids. J Exp Med. 1987 Mar 1;165(3):848–64.

130. Sun X, Funk CD, Deng C, Sahu A, Lambris JD, Song WC. Role of decay-accelerating factor in regulating complement activation on the erythrocyte surface as revealed by gene targeting. Proc Natl Acad Sci U S A. 1999 Jan 19;96(2):628–33.

131. Fang C, Miwa T, Song WC. Decay-accelerating factor regulates T-cell immunity in the context of inflammation by influencing costimulatory molecule expression on antigen-presenting cells. Blood. 2011 Jul 28;118(4):1008–14.

132. Meri S, Morgan BP, Davies A, Daniels RH, Olavesen MG, Waldmann H, et al. Human protectin (CD59), an 18,000-20,000 MW complement lysis restricting factor, inhibits C5b-8 catalysed insertion of C9 into lipid bilayers. Immunology. 1990 Sep;71(1):1–9.

133. Korty PE, Brando C, Shevach EM. CD59 functions as a signal-transducing molecule for human T cell activation. The Journal of Immunology. 1991 Jun 15;146(12):4092–8.

134. Meri S, Waldmann H, Lachmann PJ. Distribution of protectin (CD59), a complement membrane attack inhibitor, in normal human tissues. Lab Invest. 1991 Nov;65(5):532–7.

135. Rooney IA, Davies A, Griffiths D, Williams JD, Davies M, Meri S, et al. The complement-inhibiting protein, protectin (CD59 antigen), is present and functionally active on glomerular epithelial cells. Clin Exp Immunol. 1991 Feb;83(2):251–6.

136. Harris CL, Hanna SM, Mizuno M, Holt DS, Marchbank KJ, Morgan BP. Characterization of the mouse analogues of CD59 using novel monoclonal antibodies: tissue distribution and functional comparison. Immunology. 2003 May;109(1):117–26.

137. Xie XH, Gao MH, Zhang B, Wang MJ, Wang J. Post-transcriptional CD59 gene silencing by siRNAs induces enhanced human T lymphocyte response to tumor cell lysate-loaded DCs. Cellular Immunology. 2012 Jan 1;274(1–2):1–11.

138. Blaas-Mautner P, Filsinger S, Berger B, Roelcke D, Hänsch GM. C8 binding protein bears I antigenic determinants. Ann Hematol. 1991 Feb 1;62(2–3):64–7.

139. Jiang H, Wagner E, Zhang H, Frank MM. Complement 1 Inhibitor Is a Regulator of the Alternative Complement Pathway. J Exp Med. 2001 Dec 3;194(11):1609–16.

140. Seya T, Nakamura K, Masaki T, Ichihara-Itoh C, Matsumoto M, Nagasawa S. Human factor H and C4b-binding protein serve as factor I-cofactors both encompassing inactivation of C3b and C4b. Mol Immunol. 1995 Apr;32(5):355–60.

141. Barlow PN, Hageman GS, Lea SM. Complement Factor H: Using Atomic Resolution Structure to Illuminate Disease Mechanisms. Adv Exp Med Biol. 2008;632:117–42.

142. Bettoni S, Bresin E, Remuzzi G, Noris M, Donadelli R. Insights into the Effects of Complement Factor H on the Assembly and Decay of the Alternative Pathway C3 Proconvertase and C3 Convertase. J Biol Chem. 2016 Apr 8;291(15):8214–30.

143. Medicus RG, Melamed J, Arnaout MA. Role of human factor I and C3b receptor in the cleavage of surface-bound C3bi molecules. Eur J Immunol. 1983 Jun;13(6):465–70.

144. Masaki T, Matsumoto M, Nakanishi I, Yasuda R, Seya T. Factor I-dependent inactivation of human complement C4b of the classical pathway by C3b/C4b receptor (CR1, CD35) and membrane cofactor protein (MCP, CD46). J Biochem. 1992 May;111(5):573–8.

145. Hourcade DE. The role of properdin in the assembly of the alternative pathway C3 convertases of complement. J Biol Chem. 2006 Jan 27;281(4):2128–32.

146. Sjöberg AP, Trouw LA, McGrath FDG, Hack CE, Blom AM. Regulation of complement activation by C-reactive protein: targeting of the inhibitory activity of C4b-binding protein. J Immunol. 2006 Jun 15;176(12):7612–20.

147. Wenderfer SE, Soimo K, Wetsel RA, Braun MC. Analysis of C4 and the C4 binding protein in the MRL/lpr mouse. Arthritis Res Ther. 2007;9(5):R114.

148. Tschopp J, Chonn A, Hertig S, French LE. Clusterin, the human apolipoprotein and complement inhibitor, binds to complement C7, C8 beta, and the b domain of C9. J Immunol. 1993 Aug 15;151(4):2159–65.

149. Sheehan M, Morris CA, Pussell BA, Charlesworth JA. Complement inhibition by human vitronectin involves non-heparin binding domains. Clin Exp Immunol. 1995 Jul;101(1):136–41.

150. Arnold JN, Wallis R, Willis AC, Harvey DJ, Royle L, Dwek RA, et al. Interaction of Mannan Binding Lectin with α2 Macroglobulin via Exposed Oligomannose Glycans A CONSERVED FEATURE OF THE THIOL ESTER PROTEIN FAMILY? J Biol Chem. 2006 Mar 17;281(11):6955–63.

151. Campbell WD, Lazoura E, Okada N, Okada H. Inactivation of C3a and C5a octapeptides by carboxypeptidase R and carboxypeptidase N. Microbiol Immunol. 2002;46(2):131–4.

152. Heesterbeek DAC, Angelier ML, Harrison RA, Rooijakkers SHM. Complement and Bacterial Infections: From Molecular Mechanisms to Therapeutic Applications. JIN. 2018;10(5–6):455–64.

153. Kozel TR, Pfrommer GS. Activation of the complement system by Cryptococcus neoformans leads to binding of iC3b to the yeast. Infect Immun. 1986 Apr;52(1):1–5.

154. Mejia P, Diez-Silva M, Kamena F, Lu F, Fernandes SM, Seeberger PH, et al. Human C1-Inhibitor Suppresses Malaria Parasite Invasion and Cytoadhesion via Binding to Parasite Glycosylphosphatidylinositol and Host Cell Receptors. J Infect Dis. 2016 Jan 1;213(1):80–9.

155. Ezekowitz RA, Kuhlman M, Groopman JE, Byrn RA. A human serum mannose-binding protein inhibits in vitro infection by the human immunodeficiency virus. J Exp Med. 1989 Jan 1;169(1):185–96.

156. Jayasekera JP, Moseman EA, Carroll MC. Natural Antibody and Complement Mediate Neutralization of Influenza Virus in the Absence of Prior Immunity. Journal of Virology. 2007 Apr 1;81(7):3487–94.

157. Ji X, Olinger GG, Aris S, Chen Y, Gewurz H, Spear GT. Mannose-binding lectin binds to Ebola and Marburg envelope glycoproteins, resulting in blocking of virus interaction with DC-SIGN and complement-mediated virus neutralization. J Gen Virol. 2005 Sep;86(Pt 9):2535–42.

158. Tam JCH, Bidgood SR, McEwan WA, James LC. Intracellular sensing of complement C3 activates cell autonomous immunity. Science. 2014 Sep 5;345(6201):1256070.

159. Terajima M, Cruz J, Co MDT, Lee JH, Kaur K, Wilson PC, et al. Complement-Dependent Lysis of Influenza A Virus-Infected Cells by Broadly Cross-

Reactive Human Monoclonal Antibodies. Journal of Virology. 2011 Dec;85(24):13463.

160. Huber M, Fischer M, Misselwitz B, Manrique A, Kuster H, Niederöst B, et al. Complement Lysis Activity in Autologous Plasma Is Associated with Lower Viral Loads during the Acute Phase of HIV-1 Infection. PLoS Med. 2006 Nov;3(11).

161. Peng Q, Li K, Sacks SH, Zhou W. The role of anaphylatoxins C3a and C5a in regulating innate and adaptive immune responses. Inflamm Allergy Drug Targets. 2009 Jul;8(3):236–46.

162. Ghannam A, Fauquert JL, Thomas C, Kemper C, Drouet C. Human complement C3 deficiency: Th1 induction requires T cell-derived complement C3a and CD46 activation. Mol Immunol. 2014 Mar;58(1):98–107.

163. Weaver DJ, Reis ES, Pandey MK, Köhl G, Harris N, Gerard C, et al. C5a receptor-deficient dendritic cells promote induction of Treg and Th17. Eur J Immunol. 2010 Mar;40(3):710–21.

164. Barrington RA, Schneider TJ, Pitcher LA, Mempel TR, Ma M, Barteneva NS, et al. Uncoupling CD21 and CD19 of the B-cell coreceptor. PNAS. 2009 Aug 25;106(34):14490–5.

165. Ying H, Ji X, Hart ML, Gupta K, Saifuddin M, Zariffard MR, et al. Interaction of Mannose-Binding Lectin with HIV Type 1 Is Sufficient for Virus Opsonization But Not Neutralization. AIDS Research and Human Retroviruses. 2004 Mar 1;20(3):327–35.

166. Zhou Y, Lu K, Pfefferle S, Bertram S, Glowacka I, Drosten C, et al. A single asparagine-linked glycosylation site of the severe acute respiratory syndrome coronavirus spike glycoprotein facilitates inhibition by mannose-binding lectin through multiple mechanisms. J Virol. 2010 Sep;84(17):8753–64.

167. Johnson JB, Capraro GA, Parks GD. Differential mechanisms of complement-mediated neutralization of the closely related paramyxoviruses simian virus 5 and mumps virus. Virology. 2008 Jun 20;376(1):112–23.

168. Gupta P, Tripathy AS. Alternative pathway of complement activation has a beneficial role against Chandipura virus infection. Med Microbiol Immunol [Internet]. 2019 Nov 28 [cited 2020 Jan 24]; Available from: https://doi.org/10.1007/s00430-019-00648-z

169. Tjomsland V, Ellegård R, Che K, Hinkula J, Lifson JD, Larsson M. Complement Opsonization of HIV-1 Enhances the Uptake by Dendritic Cells and Involves the Endocytic Lectin and Integrin Receptor Families. PLOS ONE. 2011 Aug 11;6(8):e23542.

170. Crisci E, Ellegård R, Nyström S, Rondahl E, Serrander L, Bergström T, et al. Complement Opsonization Promotes Herpes Simplex Virus 2 Infection of Human Dendritic Cells. Journal of Virology. 2016 May 15;90(10):4939–50.

171. Mark L, Spiller OB, Villoutreix BO, Blom AM. Kaposi's sarcoma-associated herpes virus complement control protein: KCP – complement inhibition and more. Molecular Immunology. 2007 Jan 1;44(1):11–22.

172. Rosengard AM, Alonso LC, Korb LC, Baldwin WM, Sanfilippo F, Turka LA, et al. Functional characterization of soluble and membrane-bound forms of vaccinia virus complement control protein (VCP). Molecular Immunology. 1999 Jul 1;36(10):685–97.

173. Rosengard AM, Liu Y, Nie Z, Jimenez R. Variola virus immune evasion design: Expression of a highly efficient inhibitor of human complement. Proceedings of the National Academy of Sciences. 2002 Jun 25;99(13):8808–13.

174. Bottermann M, Foss S, Caddy SL, Clift D, van Tienen LM, Vaysburd M, et al. Complement C4 Prevents Viral Infection through Capsid Inactivation. Cell Host & Microbe. 2019 Apr 10;25(4):617-629.e7.

175. Harris SL, Frank I, Yee A, Cohen GH, Eisenberg RJ, Friedman HM. Glycoprotein C of herpes simplex virus type 1 prevents complement-

mediated cell lysis and virus neutralization. J Infect Dis. 1990 Aug;162(2):331–7.

176. Bayly-Jones C, Bubeck D, Dunstone MA. The mystery behind membrane insertion: a review of the complement membrane attack complex. Philosophical Transactions of the Royal Society B: Biological Sciences. 2017 Aug 5;372(1726):20160221.

177. Menny A, Serna M, Boyd CM, Gardner S, Joseph AP, Morgan BP, et al. CryoEM reveals how the complement membrane attack complex ruptures lipid bilayers. Nat Commun. 2018 Dec 14;9(1):5316.

178. Nakamura M, Okada H, Sasaki H, Yoshida K, Kamada M, Okada N, et al. Quantification of the CD55 and CD59, membrane inhibitors of complement on HIV-1 particles as a function of complement-mediated virolysis. Microbiol Immunol. 1996;40(8):561–7.

179. Avirutnan P, Hauhart RE, Somnuke P, Blom AM, Diamond MS, Atkinson JP. Binding of Flavivirus Nonstructural Protein NS1 to C4b Binding Protein Modulates Complement Activation. The Journal of Immunology. 2011 Jul 1;187(1):424–33.

180. Chung KM, Liszewski MK, Nybakken G, Davis AE, Townsend RR, Fremont DH, et al. West Nile virus nonstructural protein NS1 inhibits complement activation by binding the regulatory protein factor H. PNAS. 2006 Dec 12;103(50):19111–6.

181. Johnson JB, Borisevich V, Rockx B, Parks GD. A Novel Factor I Activity in Nipah Virus Inhibits Human Complement Pathways through Cleavage of C3b. Journal of Virology. 2015 Jan 15;89(2):989–98.

182. Nag J, Mukesh RK, Suma SM, Kunnakkadan U, Kumar NA, Johnson JB. A factor I-like activity associated with chikungunya virus contributes to its resistance to the human complement system. Journal of Virology [Internet]. 2020 Jan 15 [cited 2020 Jan 23]; Available from: https://jvi.asm.org/content/early/2020/01/09/JVI.02062-19

183. Saifuddin M, Hedayati T, Atkinson JP, Holguin MH, Parker CJ, Spear GT. Human immunodeficiency virus type 1 incorporates both glycosyl phosphatidylinositol-anchored CD55 and CD59 and integral membrane CD46 at levels that protect from complement-mediated destruction. J Gen Virol. 1997 Aug;78 (Pt 8):1907–11.

184. Johnson JB, Grant K, Parks GD. The paramyxoviruses simian virus 5 and mumps virus recruit host cell CD46 to evade complement-mediated neutralization. J Virol. 2009 Aug;83(15):7602–11.

185. Dufloo J, Guivel-Benhassine F, Buchrieser J, Lorin V, Grzelak L, Dupouy E, et al. Anti-HIV-1 antibodies trigger non-lytic complement deposition on infected cells. EMBO reports. 2019 Dec 12;n/a(n/a):e49351.

186. Kostavasili I, Sahu A, Friedman HM, Eisenberg RJ, Cohen GH, Lambris JD. Mechanism of complement inactivation by glycoprotein C of herpes simplex virus. J Immunol. 1997 Feb 15;158(4):1763–71.

187. Wetsel RA, Kildsgaard J, Haviland DL. Complement Anaphylatoxins (C3a, C4a, C5a) and Their Receptors (C3aR, C5aR/CD88) as Therapeutic Targets in Inflammation. In: Lambris JD, Holers VM, editors. Therapeutic Interventions in the Complement System [Internet]. Totowa, NJ: Humana Press; 2000 [cited 2019 Mar 3]. p. 113–53. (Contemporary Immunology). Available from: https://doi.org/10.1007/978-1-59259-017-9_5

188. Schwarze J, Mackenzie KJ. Novel insights into immune and inflammatory responses to respiratory viruses. Thorax. 2013 Jan 1;68(1):108–10.

189. Casanova JL, Abel L. Mechanisms of viral inflammation and disease in humans. Science. 2021 Nov 26;374(6571):1080–6.

190. Avirutnan P, Punyadee N, Noisakran S, Komoltri C, Thiemmeca S, Auethavornanan K, et al. Vascular leakage in severe dengue virus infections: a potential role for the nonstructural viral protein NS1 and complement. J Infect Dis. 2006 Apr 15;193(8):1078–88.

191. Morrison TE, Fraser RJ, Smith PN, Mahalingam S, Heise MT. Complement Contributes to Inflammatory Tissue Destruction in a Mouse Model of Ross River Virus-Induced Disease. Journal of Virology. 2007 May 15;81(10):5132–43.

192. Gunn BM, Morrison TE, Whitmore AC, Blevins LK, Hueston L, Fraser RJ, et al. Mannose Binding Lectin Is Required for Alphavirus-Induced Arthritis/Myositis. PLOS Pathogens. 2012 Mar 22;8(3):e1002586.

193. Cabezas S, Bracho G, Aloia AL, Adamson PJ, Bonder CS, Smith JR, et al. Dengue Virus Induces Increased Activity of the Complement Alternative Pathway in Infected Cells. Journal of Virology. 2018 Jul 15;92(14):e00633-18.

194. Gunn BM, Jones JE, Shabman RS, Whitmore AC, Sarkar S, Blevins LK, et al. Ross River virus envelope glycans contribute to disease through activation of the host complement system. Virology. 2018;515:250–60.

195. Gralinski LE, Sheahan TP, Morrison TE, Menachery VD, Jensen K, Leist SR, et al. Complement Activation Contributes to Severe Acute Respiratory Syndrome Coronavirus Pathogenesis. mBio [Internet]. 2018 Oct 9 [cited 2020 Feb 12];9(5). Available from: http://www.ncbi.nlm.nih.gov/pmc/articles/PMC6178621/

196. Jiang Y, Zhao G, Song N, Li P, Chen Y, Guo Y, et al. Blockade of the C5a–C5aR axis alleviates lung damage in hDPP4-transgenic mice infected with MERS-CoV. Emerg Microbes Infect [Internet]. 2018 Apr 24 [cited 2020 Mar 27];7. Available from: https://www.ncbi.nlm.nih.gov/pmc/articles/PMC5915580/

197. Pang RT, Poon TC, Chan KA, Lee NL, Chiu RW, Tong YK, et al. Serum Proteomic Fingerprints of Adult Patients with Severe Acute Respiratory Syndrome. Clin Chem. 2006 Mar 1;52(3):421–9.

198. Elvington M, Liszewski MK, Bertram P, Kulkarni HS, Atkinson JP. A C3(H20) recycling pathway is a component of the intracellular complement system. J Clin Invest. 2017;127(3):970–81.

199. Cardone J, Friec GL, Vantourout P, Roberts A, Fuchs A, Jackson I, et al. Complement regulator CD46 temporally regulates cytokine production by conventional and unconventional T cells. Nature Immunology. 2010 Sep;11(9):862–71.

200. Liszewski MK, Kolev M, Le Friec G, Leung M, Bertram PG, Fara AF, et al. Intracellular complement activation sustains T cell homeostasis and mediates effector differentiation. Immunity. 2013 Dec 12;39(6):1143–57.

201. Cravedi P, Leventhal J, Lakhani P, Ward SC, Donovan MJ, Heeger PS. Immune cell derived C3a and C5a costimulate human T cell alloimmunity. Am J Transplant [Internet]. 2013 Oct [cited 2020 Oct 8];13(10). Available from: https://www.ncbi.nlm.nih.gov/pmc/articles/PMC3809075/

202. Strainic MG, Shevach EM, An F, Lin F, Medof ME. Absence of signaling into $CD4^+$ cells via C3aR and C5aR enables autoinductive TGF-β1 signaling and induction of $Foxp3^+$ regulatory T cells. Nature Immunology. 2013 Feb;14(2):162–71.

203. Lalli PN, Strainic MG, Yang M, Lin F, Medof ME, Heeger PS. Locally produced C5a binds to T cell–expressed C5aR to enhance effector T-cell expansion by limiting antigen-induced apoptosis. Blood. 2008 Sep 1;112(5):1759–66.

204. Strainic MG, Liu J, Huang D, An F, Lalli PN, Muqim N, et al. Locally produced complement fragments C5a and C3a provide both costimulatory and survival signals to naive CD4+ T cells. Immunity. 2008 Mar;28(3):425–35.

205. Kopf M, Abel B, Gallimore A, Carroll M, Bachmann MF. Complement component C3 promotes T-cell priming and lung migration to control acute influenza virus infection. Nat Med. 2002 Apr;8(4):373–8.

206. Kim AHJ, Dimitriou ID, Holland MCH, Mastellos D, Mueller YM, Altman JD, et al. Complement C5a receptor is essential for the optimal generation of antiviral CD8+ T cell responses. J Immunol. 2004 Aug 15;173(4):2524–9.

207. Kittlesen DJ, Chianese-Bullock KA, Yao ZQ, Braciale TJ, Hahn YS. Interaction between complement receptor gC1qR and hepatitis C virus core protein

inhibits T-lymphocyte proliferation. Journal of Clinical Investigation. 2000 Nov 15;106(10):1239.

208. Fingeroth JD, Heath ME, Ambrosino DM. Proliferation of resting B cells is modulated by CR2 and CR1. Immunol Lett. 1989 Jun 15;21(4):291–301.

209. Aydar Y, Sukumar S, Szakal AK, Tew JG. The Influence of Immune Complex-Bearing Follicular Dendritic Cells on the IgM Response, Ig Class Switching, and Production of High Affinity IgG. The Journal of Immunology. 2005 May 1;174(9):5358–66.

210. Klaus GG, Humphrey JH. The generation of memory cells. I. The role of C3 in the generation of B memory cells. Immunology. 1977 Jul;33(1):31–40.

211. Waggoner SN, Hall CHT, Hahn YS. HCV core protein interaction with gC1q receptor inhibits Th1 differentiation of CD4+ T cells via suppression of dendritic cell IL-12 production. J Leukoc Biol. 2007 Dec;82(6):1407–19.

212. Kuhn JH. New filovirus disease classification and nomenclature. Nat Rev Microbiol. 2019 May;17(5):261–3.

213. Languon S, Quaye O. Filovirus Disease Outbreaks: A Chronological Overview. Virology (Auckl). 2019 Jun 21;10:1178122X19849927.

214. World Health Organization. Ebola virus disease [Internet]. 2021 [cited 2021 Oct 5]. Available from: https://www.who.int/westernpacific/health-topics/ebola

215. Centers for Disease Control and Prevention. Epidemiologic Notes and Reports Update: Filovirus Infection in Animal Handlers [Internet]. 1990 [cited 2022 Jan 20]. Available from: https://www.cdc.gov/mmwr/preview/mmwrhtml/00001593.htm

216. Centers for Disease Control and Prevention. Update: Filovirus Infections Among Persons with Occupational Exposure to Nonhuman Primates [Internet]. 1990 [cited 2022 Jan 20]. Available from: https://www.cdc.gov/mmwr/preview/mmwrhtml/00001608.htm

217. Miranda MaryEG, White MarkE, Dayrit ManuelM, Hayes CurtisG, Ksiazek ThomasG, Burans JamesP. Seroepidemiological study of filovirus related to Ebola in the Philippines. The Lancet. 1991 Feb 16;337(8738):425–6.

218. Goldstein T, Anthony SJ, Gbakima A, Bird BH, Bangura J, Tremeau-Bravard A, et al. Discovery of a new ebolavirus (Bombali virus) in molossid bats in Sierra Leone. Nat Microbiol. 2018 Oct;3(10):1084–9.

219. World Health Organization. Marburg virus disease [Internet]. 2021 [cited 2022 Feb 1]. Available from: https://www.who.int/news-room/fact-sheets/detail/marburg-virus-disease

220. Yang XL, Tan CW, Anderson DE, Jiang RD, Li B, Zhang W, et al. Characterization of a filovirus (Měnglà virus) from Rousettus bats in China. Nature Microbiology. 2019 Mar;4(3):390–5.

221. Negredo A, Palacios G, Vázquez-Morón S, González F, Dopazo H, Molero F, et al. Discovery of an Ebolavirus-Like Filovirus in Europe. PLOS Pathogens. 2011 Oct 20;7(10):e1002304.

222. Shi M, Lin XD, Chen X, Tian JH, Chen LJ, Li K, et al. The evolutionary history of vertebrate RNA viruses. Nature. 2018 Apr;556(7700):197–202.

223. Wamala JF, Lukwago L, Malimbo M, Nguku P, Yoti Z, Musenero M, et al. Ebola Hemorrhagic Fever Associated with Novel Virus Strain, Uganda, 2007–2008 - Volume 16, Number 7—July 2010 - Emerging Infectious Diseases journal - CDC. 2010 Jul [cited 2022 Jan 24]; Available from: https://wwwnc.cdc.gov/eid/article/16/7/09-1525_article

224. Jahrling PB, Geisbert TW, Johnson ED, Peters CJ, Dalgard DW, Hall WC. Preliminary report: isolation of Ebola virus from monkeys imported to USA. The Lancet. 1990 Mar 3;335(8688):502–5.

225. World Health Organization. Ebola haemorrhagic fever in Sudan, 1976. Bulletin of the World Health Organization. 1978;56(2):247.

226. Le Guenno B, Formenty P, Wyers M, Gounon P, Walker F, Boesch C. Isolation and partial characterisation of a new strain of Ebola virus. The Lancet. 1995 May 20;345(8960):1271–4.

227. World Health Organization. Ebola haemorrhagic fever in Zaire, 1976. Bull World Health Organ. 1978;56(2):271–93.

228. Centers for Disease Control and Prevention. About Marburg virus disease | Marburg (Marburg Virus Disease) | CDC [Internet]. 2021 [cited 2022 Mar 1]. Available from: https://www.cdc.gov/vhf/marburg/about.html

229. Nicholas VV, Rosenke R, Feldmann F, Long D, Thomas T, Scott DP, et al. Distinct Biological Phenotypes of Marburg and Ravn Virus Infection in Macaques. The Journal of Infectious Diseases. 2018 Nov 22;218(suppl_5):S458–65.

230. Martin B, Canard B, Decroly E. Filovirus proteins for antiviral drug discovery: Structure/function bases of the replication cycle. Antiviral Research. 2017 May 1;141:48–61.

231. Cantoni D, Rossman JS. Ebolaviruses: New roles for old proteins. PLOS Neglected Tropical Diseases. 2018 May 3;12(5):e0006349.

232. Mühlberger E, Weik M, Volchkov VE, Klenk HD, Becker S. Comparison of the Transcription and Replication Strategies of Marburg Virus and Ebola Virus by Using Artificial Replication Systems. J Virol. 1999 Mar;73(3):2333–42.

233. Mühlberger E. Filovirus replication and transcription. Future Virol. 2007 Mar;2(2):205–15.

234. Leung DW, Borek DM, Luthra P, Binning JM, Anantpadma M, Liu G, et al. An intrinsically disordered peptide from Ebola virus VP35 controls viral RNA synthesis by modulating nucleoprotein-RNA interactions. Cell Rep. 2015 Apr 21;11(3):376–89.

235. Huang Y, Xu L, Sun Y, Nabel GJ. The assembly of Ebola virus nucleocapsid requires virion-associated proteins 35 and 24 and posttranslational modification of nucleoprotein. Mol Cell. 2002 Aug;10(2):307–16.

236. Noda T, Aoyama K, Sagara H, Kida H, Kawaoka Y. Nucleocapsid-like structures of Ebola virus reconstructed using electron tomography. J Vet Med Sci. 2005 Mar;67(3):325–8.

237. Ito H, Watanabe S, Takada A, Kawaoka Y. Ebola virus glycoprotein: proteolytic processing, acylation, cell tropism, and detection of neutralizing antibodies. J Virol. 2001 Feb;75(3):1576–80.

238. Weik M, Modrof J, Klenk HD, Becker S, Mühlberger E. Ebola virus VP30-mediated transcription is regulated by RNA secondary structure formation. J Virol. 2002 Sep;76(17):8532–9.

239. Xu W, Luthra P, Wu C, Batra J, Leung DW, Basler CF, et al. Ebola virus VP30 and nucleoprotein interactions modulate viral RNA synthesis. Nat Commun. 2017 Jun 8;8(1):15576.

240. Basler CF, Mikulasova A, Martinez-Sobrido L, Paragas J, Mühlberger E, Bray M, et al. The Ebola Virus VP35 Protein Inhibits Activation of Interferon Regulatory Factor 3. J Virol. 2003 Jul;77(14):7945–56.

241. Haasnoot J, de Vries W, Geutjes EJ, Prins M, de Haan P, Berkhout B. The Ebola Virus VP35 Protein Is a Suppressor of RNA Silencing. PLoS Pathog [Internet]. 2007 Jun [cited 2018 Nov 12];3(6). Available from: https://www.ncbi.nlm.nih.gov/pmc/articles/PMC1894824/

242. Takamatsu Y, Kolesnikova L, Becker S. Ebola virus proteins NP, VP35, and VP24 are essential and sufficient to mediate nucleocapsid transport. PNAS. 2018 Jan 30;115(5):1075–80.

243. Ruigrok RW, Schoehn G, Dessen A, Forest E, Volchkov V, Dolnik O, et al. Structural characterization and membrane binding properties of the matrix protein VP40 of Ebola virus. J Mol Biol. 2000 Jun 30;300(1):103–12.

244. Fabozzi G, Nabel CS, Dolan MA, Sullivan NJ. Ebolavirus Proteins Suppress the Effects of Small Interfering RNA by Direct Interaction with the Mammalian RNA Interference Pathway. J Virol. 2011 Mar;85(6):2512–23.

245. Bornholdt ZA, Noda T, Abelson DM, Halfmann P, Wood MR, Kawaoka Y, et al. Structural rearrangement of ebola virus VP40 begets multiple functions in the virus life cycle. Cell. 2013 Aug 15;154(4):763–74.

246. Pleet ML, Mathiesen A, DeMarino C, Akpamagbo YA, Barclay RA, Schwab A, et al. Ebola VP40 in Exosomes Can Cause Immune Cell Dysfunction. Front Microbiol. 2016;7:1765.

247. Edri A, Shemesh A, Iraqi M, Matalon O, Brusilovsky M, Hadad U, et al. The Ebola-Glycoprotein Modulates the Function of Natural Killer Cells. Frontiers in Immunology [Internet]. 2018 [cited 2022 Feb 7];9. Available from: https://www.frontiersin.org/article/10.3389/fimmu.2018.01428

248. Jarahian M, Marstaller K, Banna N, Ahani R, Etemadzadeh MH, Boller LK, et al. Activating Natural Killer Cell Receptors, Selectins, and Inhibitory Siglecs Recognize Ebolavirus Glycoprotein. JIN. 2022;14(2):135–47.

249. de La Vega MA, Caleo G, Audet J, Qiu X, Kozak RA, Brooks JI, et al. Ebola viral load at diagnosis associates with patient outcome and outbreak evolution. J Clin Invest. 2015 Dec;125(12):4421–8.

250. Bradley JH, Shapiro L, Hitchcock C, Kulis D, Needell L, Henry N, et al. The effect of Ebola Virus secreted glycoprotein on activated macrophages. The Journal of Immunology. 2018 May 1;200(1 Supplement):168.15-168.15.

251. Zhu W, Banadyga L, Emeterio K, Wong G, Qiu X. The Roles of Ebola Virus Soluble Glycoprotein in Replication, Pathogenesis, and Countermeasure Development. Viruses. 2019 Oct 31;11(11):E999.

252. Radoshitzky SR, Warfield KL, Chi X, Dong L, Kota K, Bradfute SB, et al. Ebolavirus delta-peptide immunoadhesins inhibit marburgvirus and ebolavirus cell entry. J Virol. 2011 Sep;85(17):8502–13.

253. Smith DH, Isaacson M, Johnson KM, Bagshawe A, Johnson BK, Swanapoel R, et al. MARBURG-VIRUS DISEASE IN KENYA. The Lancet. 1982 Apr 10;319(8276):816–20.

254. Kuming BS, Kokoris N. Uveal involvement in Marburg virus disease. British Journal of Ophthalmology. 1977 Apr 1;61(4):265–6.

255. Varkey JB, Shantha JG, Crozier I, Kraft CS, Lyon GM, Mehta AK, et al. Persistence of Ebola Virus in Ocular Fluid during Convalescence [Internet]. http://dx.doi.org/10.1056/NEJMoa1500306. Massachusetts Medical Society; 2015 [cited 2021 Oct 5]. Available from: https://www.nejm.org/doi/10.1056/NEJMoa1500306

256. Diallo B, Sissoko D, Loman NJ, Bah HA, Bah H, Worrell MC, et al. Resurgence of Ebola Virus Disease in Guinea Linked to a Survivor With Virus Persistence in Seminal Fluid for More Than 500 Days. Clinical Infectious Diseases. 2016 Nov 15;63(10):1353–6.

257. Keita AK, Koundouno FR, Faye M, Düx A, Hinzmann J, Diallo H, et al. Resurgence of Ebola virus in 2021 in Guinea suggests a new paradigm for outbreaks. Nature. 2021 Sep;597(7877):539–43.

258. Jacobs M, Rodger A, Bell DJ, Bhagani S, Cropley I, Filipe A, et al. Late Ebola virus relapse causing meningoencephalitis: a case report. The Lancet. 2016 Jul 30;388(10043):498–503.

259. Sissoko D, Keïta M, Diallo B, Aliabadi N, Fitter DL, Dahl BA, et al. Ebola Virus Persistence in Breast Milk After No Reported Illness: A Likely Source of Virus Transmission From Mother to Child. Clin Infect Dis. 2017 Feb 15;64(4):513–6.

260. Formenty P, Hatz C, Le Guenno B, Stoll A, Rogenmoser P, Widmer A. Human Infection Due to Ebola Virus, Subtype Côte d'Ivoire: Clinical and Biologic Presentation. The Journal of Infectious Diseases. 1999 Feb 1;179(Supplement_1):S48–53.

261. Wendo C. Caring for the survivors of Uganda's Ebola epidemic one year on. The Lancet. 2001 Oct 20;358(9290):1350.

262. Clark DV, Kibuuka H, Millard M, Wakabi S, Lukwago L, Taylor A, et al. Long-term sequelae after Ebola virus disease in Bundibugyo, Uganda: a

retrospective cohort study. The Lancet Infectious Diseases. 2015 Aug 1;15(8):905–12.

263. Epstein L, Wong KK, Kallen AJ, Uyeki TM. Post-Ebola Signs and Symptoms in U.S. Survivors [Internet]. http://dx.doi.org/10.1056/NEJMc1506576. Massachusetts Medical Society; 2015 [cited 2022 Feb 2]. Available from: https://www.nejm.org/doi/10.1056/NEJMc1506576

264. Diallo MSK, Toure A, Sow MS, Kpamou C, Keita AK, Taverne B, et al. Understanding Long-term Evolution and Predictors of Sequelae of Ebola Virus Disease Survivors in Guinea: A 48-Month Prospective, Longitudinal Cohort Study (PostEboGui). Clin Infect Dis. 2021 Feb 23;73(12):2166–74.

265. LaVergne SM, Sakabe S, Kanneh L, Momoh M, Al-Hassan F, Yilah M, et al. Ebola-Specific CD8+ and CD4+ T-Cell Responses in Sierra Leonean Ebola Virus Survivors With or Without Post-Ebola Sequelae. J Infect Dis. 2020 Oct 1;222(9):1488–97.

266. Howlett PJ, Walder AR, Lisk DR, Fitzgerald F, Sevalie S, Lado M, et al. Case Series of Severe Neurologic Sequelae of Ebola Virus Disease during Epidemic, Sierra Leone. Emerg Infect Dis. 2018 Aug;24(8):1412–21.

267. Paquin-Proulx D, Gunn BM, Alrubayyi A, Clark DV, Creegan M, Kim D, et al. Associations Between Antibody Fc-Mediated Effector Functions and Long-Term Sequelae in Ebola Virus Survivors. Frontiers in Immunology. 2021;12:1917.

268. Wiedemann A, Foucat E, Hocini H, Lefebvre C, Hejblum BP, Durand M, et al. Long-lasting severe immune dysfunction in Ebola virus disease survivors. Nat Commun. 2020 Jul 24;11(1):3730.

269. Mehedi M, Groseth A, Feldmann H, Ebihara H. Clinical aspects of Marburg hemorrhagic fever. Future Virol. 2011 Sep;6(9):1091–106.

270. Kemenesi G, Kurucz K, Dallos B, Zana B, Földes F, Boldogh S, et al. Re-emergence of Lloviu virus in Miniopterus schreibersii bats, Hungary, 2016.

Emerg Microbes Infect [Internet]. 2018 Apr 18 [cited 2018 Oct 15];7. Available from: https://www.ncbi.nlm.nih.gov/pmc/articles/PMC5906664/

271. Towner JS, Amman BR, Sealy TK, Carroll SAR, Comer JA, Kemp A, et al. Isolation of Genetically Diverse Marburg Viruses from Egyptian Fruit Bats. PLOS Pathogens. 2009 Jul 31;5(7):e1000536.

272. Amman BR, Bird BH, Bakarr IA, Bangura J, Schuh AJ, Johnny J, et al. Isolation of Angola-like Marburg virus from Egyptian rousette bats from West Africa. Nat Commun. 2020 Jan 24;11(1):510.

273. Fischer K, Suluku R, Fehling SK, Jabaty J, Koroma B, Strecker T, et al. Ebola Virus Neutralizing Antibodies in Dogs from Sierra Leone, 2017. Emerg Infect Dis. 2020 Apr;26(4):760–3.

274. Centers for Disease Control and Prevention. What is Ebola Virus Disease? | Ebola (Ebola Virus Disease) | CDC [Internet]. 2021 [cited 2022 Mar 20]. Available from: https://www.cdc.gov/vhf/ebola/about.html

275. Nakayama E, Saijo M. Animal models for Ebola and Marburg virus infections. Frontiers in Microbiology [Internet]. 2013 [cited 2022 Feb 3];4. Available from: https://www.frontiersin.org/article/10.3389/fmicb.2013.00267

276. Longet S, Mellors J, Carroll MW, Tipton T. Ebolavirus: Comparison of Survivor Immunology and Animal Models in the Search for a Correlate of Protection. Frontiers in Immunology. 2021;11:3871.

277. Leroy EM, Kumulungui B, Pourrut X, Rouquet P, Hassanin A, Yaba P, et al. Fruit bats as reservoirs of Ebola virus. Nature. 2005 Dec;438(7068):575–6.

278. Schuh AJ, Amman BR, Towner JS. Filoviruses and bats. Microbiology Australia. 2017 Mar;38(1):12–6.

279. Koch LK, Cunze S, Kochmann J, Klimpel S. Bats as putative Zaire ebolavirus reservoir hosts and their habitat suitability in Africa. Sci Rep. 2020 Aug 31;10(1):14268.

280. Barrette RW, Metwally SA, Rowland JM, Xu L, Zaki SR, Nichol ST, et al. Discovery of Swine as a Host for the Reston ebolavirus. Science. 2009 Jul 10;325(5937):204–6.

281. Pan Y, Zhang W, Cui L, Hua X, Wang M, Zeng Q. Reston virus in domestic pigs in China. Arch Virol. 2014 May;159(5):1129–32.

282. Pourrut X, Délicat A, Rollin PE, Ksiazek TG, Gonzalez JP, Leroy EM. Spatial and temporal patterns of Zaire ebolavirus antibody prevalence in the possible reservoir bat species. J Infect Dis. 2007 Nov 15;196 Suppl 2:S176-183.

283. Hayman DTS, Yu M, Crameri G, Wang LF, Suu-Ire R, Wood JLN, et al. Ebola Virus Antibodies in Fruit Bats, Ghana, West Africa. Emerg Infect Dis. 2012 Jul;18(7):1207–9.

284. Yuan J, Zhang Y, Li J, Zhang Y, Wang LF, Shi Z. Serological evidence of ebolavirus infection in bats, China. Virol J. 2012 Oct 13;9:236.

285. Jayme SI, Field HE, de Jong C, Olival KJ, Marsh G, Tagtag AM, et al. Molecular evidence of Ebola Reston virus infection in Philippine bats. Virol J. 2015 Jul 17;12:107.

286. Lacroix A, Mbala Kingebeni P, Ndimbo Kumugo SP, Lempu G, Butel C, Serrano L, et al. Investigating the Circulation of Ebola Viruses in Bats during the Ebola Virus Disease Outbreaks in the Equateur and North Kivu Provinces of the Democratic Republic of Congo from 2018. Pathogens. 2021 May 4;10(5):557.

287. Swanepoel R, Leman PA, Burt FJ, Zachariades NA, Braack LE, Ksiazek TG, et al. Experimental inoculation of plants and animals with Ebola virus. Emerging Infect Dis. 1996 Dec;2(4):321–5.

288. Fedewa G, Radoshitzky SR, Chī X, Dǒng L, Zeng X, Spear M, et al. Ebola virus, but not Marburg virus, replicates efficiently and without required adaptation in snake cells. Virus Evolution. 2018 Jul 1;4(2):vey034.

289. Cross RW, Mire CE, Borisevich V, Geisbert JB, Fenton KA, Geisbert TW. The Domestic Ferret (Mustela putorius furo) as a Lethal Infection Model for 3 Species of Ebolavirus. J Infect Dis. 2016 Aug 15;214(4):565–9.

290. Bray M, Davis K, Geisbert T, Schmaljohn C, Huggins J. A mouse model for evaluation of prophylaxis and therapy of Ebola hemorrhagic fever. J Infect Dis. 1998 Sep;178(3):651–61.

291. Ebihara H, Takada A, Kobasa D, Jones S, Neumann G, Theriault S, et al. Molecular determinants of Ebola virus virulence in mice. PLoS Pathog. 2006 Jul;2(7):e73.

292. Wahl-Jensen V, Bollinger L, Safronetz D, de Kok-Mercado F, Scott DP, Ebihara H. Use of the Syrian Hamster as a New Model of Ebola Virus Disease and Other Viral Hemorrhagic Fevers. Viruses. 2012 Dec 14;4(12):3754–84.

293. Connolly BM, Steele KE, Davis KJ, Geisbert TW, Kell WM, Jaax NK, et al. Pathogenesis of experimental Ebola virus infection in guinea pigs. J Infect Dis. 1999 Feb;179 Suppl 1:S203-217.

294. Centers for Disease Control and Prevention. Transmission | Ebola Hemorrhagic Fever | CDC [Internet]. 2021 [cited 2022 Mar 20]. Available from: https://www.cdc.gov/vhf/ebola/transmission/index.html

295. Ordaz-Németh I, Arandjelovic M, Boesch L, Gatiso T, Grimes T, Kuehl HS, et al. The socio-economic drivers of bushmeat consumption during the West African Ebola crisis. PLoS Negl Trop Dis [Internet]. 2017 Mar 10 [cited 2019 Aug 14];11(3). Available from: https://www.ncbi.nlm.nih.gov/pmc/articles/PMC5362244/

296. Manguvo A, Mafuvadze B. The impact of traditional and religious practices on the spread of Ebola in West Africa: time for a strategic shift. Pan Afr Med J [Internet]. 2015 Oct 10 [cited 2019 Aug 14];22(Suppl 1). Available from: https://www.ncbi.nlm.nih.gov/pmc/articles/PMC4709130/

297. Breman JG, Heymann DL, Lloyd G, McCormick JB, Miatudila M, Murphy FA, et al. Discovery and Description of Ebola Zaire Virus in 1976 and Relevance

to the West African Epidemic During 2013–2016. The Journal of Infectious Diseases. 2016 Oct 15;214(Suppl 3):S93.

298. Centers for Disease Control and Prevention. History of Ebola Virus Disease (EVD) Outbreaks | History | Ebola (Ebola Virus Disease) | CDC [Internet]. 2022 [cited 2022 Mar 17]. Available from: https://www.cdc.gov/vhf/ebola/history/chronology.html

299. Wickham H. ggplot2: Elegant Graphics for Data Analysis [Internet]. Springer-Verlag New York; 2016. Available from: https://ggplot2.tidyverse.org

300. South A. rnaturalearth: World Map Data from Natural Earth [Internet]. 2017 [cited 2022 May 2]. Available from: https://CRAN.R-project.org/package=rnaturalearth

301. South A. rnaturalearthdata: World Vector Map Data from Natural Earth Used in "rnaturalearth" [Internet]. 2017 [cited 2022 May 2]. Available from: https://CRAN.R-project.org/package=rnaturalearthdata

302. Pebesma E. Simple Features for R: Standardized Support for Spatial Vector Data. The R Journal. 2018;10(1):439–46.

303. Dunnington D, Thorne B. ggspatial: Spatial Data Framework for ggplot2 [Internet]. 2021 [cited 2022 May 2]. Available from: https://CRAN.R-project.org/package=ggspatial

304. Centers for Disease Control and Prevention. Marburg Hemorrhagic Fever | CDC [Internet]. 2014 [cited 2018 Oct 10]. Available from: https://www.cdc.gov/vhf/marburg/resources/outbreak-table.html

305. Towner JS, Khristova ML, Sealy TK, Vincent MJ, Erickson BR, Bawiec DA, et al. Marburgvirus Genomics and Association with a Large Hemorrhagic Fever Outbreak in Angola. J Virol. 2006 Jul;80(13):6497–516.

306. Hayes CG, Burans JP, Ksiazek TG, Del Rosario RA, Miranda ME, Manaloto CR, et al. Outbreak of fatal illness among captive macaques in the Philippines caused by an Ebola-related filovirus. Am J Trop Med Hyg. 1992 Jun;46(6):664–71.

307. Rollin PE, Williams RJ, Bressler DS, Pearson S, Cottingham M, Pucak G, et al. Ebola (Subtype Reston) Virus among Quarantined Nonhuman Primates Recently Imported from the Philippines to the United States. J Infect Dis. 1999 Feb 1;179(Supplement_1):S108–14.

308. Ramírez de Arellano E, Sanchez-Lockhart M, Perteguer MJ, Bartlett M, Ortiz M, Campioli P, et al. First Evidence of Antibodies Against Lloviu Virus in Schreiber's Bent-Winged Insectivorous Bats Demonstrate a Wide Circulation of the Virus in Spain. Viruses. 2019 Apr;11(4):360.

309. Hume AJ, Heiden B, Olejnik J, Suder EL, Ross S, Scoon WA, et al. Recombinant Lloviu virus as a tool to study viral replication and host responses. PLOS Pathogens. 2022 Feb 4;18(2):e1010268.

310. Kemenesi G, Tóth GE, Mayora-Neto M, Scott S, Temperton N, Wright E, et al. Isolation of infectious Lloviu virus from Schreiber's bats in Hungary. Nat Commun. 2022 Mar 31;13(1):1706.

311. Towner JS, Sealy TK, Khristova ML, Albariño CG, Conlan S, Reeder SA, et al. Newly Discovered Ebola Virus Associated with Hemorrhagic Fever Outbreak in Uganda. PLoS Pathog. 2008 Nov 21;4(11):e1000212.

312. MacNeil A, Farnon EC, Wamala J, Okware S, Cannon DL, Reed Z, et al. Proportion of Deaths and Clinical Features in Bundibugyo Ebola Virus Infection, Uganda. Emerg Infect Dis. 2010 Dec;16(12):1969–72.

313. Kratz T, Roddy P, Oloma AT, Jeffs B, Ciruelo DP, Rosa O de la, et al. Ebola Virus Disease Outbreak in Isiro, Democratic Republic of the Congo, 2012: Signs and Symptoms, Management and Outcomes. PLOS ONE. 2015 Jun 24;10(6):e0129333.

314. Hulseberg CE, Kumar R, Di Paola N, Larson P, Nagle ER, Richardson J, et al. Molecular analysis of the 2012 Bundibugyo virus disease outbreak. Cell Reports Medicine. 2021 Aug;2(8):100351.

315. Karan LS, Makenov MT, Korneev MG, Sacko N, Boumbaly S, Yakovlev SA, et al. Bombali Virus in Mops condylurus Bats, Guinea. Emerg Infect Dis. 2019 Sep;25(9):1774–5.

316. Forbes KM, Webala PW, Jääskeläinen AJ, Abdurahman S, Ogola J, Masika MM, et al. Bombali Virus in Mops condylurus Bat, Kenya - Volume 25, Number 5—May 2019 - Emerging Infectious Diseases journal - CDC. 2019 May [cited 2022 Jan 25]; Available from: https://wwwnc.cdc.gov/eid/article/25/5/18-1666_article

317. Baize S, Pannetier D, Oestereich L, Rieger T, Koivogui L, Magassouba N, et al. Emergence of Zaire Ebola Virus Disease in Guinea. N Engl J Med. 2014 Oct 9;371(15):1418–25.

318. World Health Organization. Origins of the Ebola epidemic [Internet]. 2015 [cited 2022 Feb 22]. Available from: https://www.who.int/news-room/spotlight/one-year-into-the-ebola-epidemic/origins-of-the-2014-ebola-epidemic

319. Holmes EC, Dudas G, Rambaut A, Andersen KG. The Evolution of Ebola virus: Insights from the 2013–2016 Epidemic. Nature. 2016 Oct 13;538(7624):193–200.

320. Timothy JWS, Hall Y, Akoi-Boré J, Diallo B, Tipton TRW, Bower H, et al. Early transmission and case fatality of Ebola virus at the index site of the 2013–16 west African Ebola outbreak: a cross-sectional seroprevalence survey. The Lancet Infectious Diseases. 2019 Apr 1;19(4):429–38.

321. Centers for Disease Control and Prevention. 2014-2016 Ebola Outbreak in West Africa | Ebola Hemorrhagic Fever | CDC.

322. Quick J, Loman NJ, Duraffour S, Simpson JT, Severi E, Cowley L, et al. Real-time, portable genome sequencing for Ebola surveillance. Nature. 2016 Feb;530(7589):228–32.

323. EMA. First vaccine to protect against Ebola [Internet]. European Medicines Agency. 2019 [cited 2022 Mar 1]. Available from: https://www.ema.europa.eu/en/news/first-vaccine-protect-against-ebola

324. Geisbert TW, Hensley LE, Larsen T, Young HA, Reed DS, Geisbert JB, et al. Pathogenesis of Ebola Hemorrhagic Fever in Cynomolgus Macaques. Am J Pathol. 2003 Dec;163(6):2347–70.

325. Wahl-Jensen V, Kurz SK, Hazelton PR, Schnittler HJ, Ströher U, Burton DR, et al. Role of Ebola virus secreted glycoproteins and virus-like particles in activation of human macrophages. J Virol. 2005 Feb;79(4):2413–9.

326. Centers for Disease Control and Prevention. Ebola virus disease Information for Clinicians in U.S. Healthcare Settings | For Clinicians | Ebola (Ebola Virus Disease) | Ebola Hemorrhagic Fever | CDC [Internet]. 2021 [cited 2022 Feb 4]. Available from: https://www.cdc.gov/vhf/ebola/clinicians/evd/clinicians.html

327. Hoenen T, Groseth A, Feldmann H. Therapeutic strategies to target the Ebola virus life cycle. Nat Rev Microbiol. 2019 Oct;17(10):593–606.

328. Aleksandrowicz P, Marzi A, Biedenkopf N, Beimforde N, Becker S, Hoenen T, et al. Ebola virus enters host cells by macropinocytosis and clathrin-mediated endocytosis. J Infect Dis. 2011 Nov;204 Suppl 3:S957-967.

329. Moller-Tank S, Maury W. Ebola Virus Entry: A Curious and Complex Series of Events. PLOS Pathogens. 2015 Apr 30;11(4):e1004731.

330. Adu-Gyamfi E, Digman MA, Gratton E, Stahelin RV. Single-particle tracking demonstrates that actin coordinates the movement of the Ebola virus matrix protein. Biophys J. 2012 Nov 7;103(9):L41-43.

331. Han Z, Harty RN. Packaging of actin into Ebola virus VLPs. Virol J. 2005 Dec 20;2:92.

332. Ruthel G, Demmin GL, Kallstrom G, Javid MP, Badie SS, Will AB, et al. Association of ebola virus matrix protein VP40 with microtubules. J Virol. 2005 Apr;79(8):4709–19.

333. Lu J, Qu Y, Liu Y, Jambusaria R, Han Z, Ruthel G, et al. Host IQGAP1 and Ebola virus VP40 interactions facilitate virus-like particle egress. J Virol. 2013 Jul;87(13):7777–80.

334. Yamayoshi S, Noda T, Ebihara H, Goto H, Morikawa Y, Lukashevich IS, et al. Ebola Virus Matrix VP40 Protein Uses the COPII Transport System for Its Intracellular Transport. Cell Host Microbe. 2008 Mar 13;3(3):168–77.

335. Geisbert TW, Hensley LE, Gibb TR, Steele KE, Jaax NK, Jahrling PB. Apoptosis Induced In Vitro and In Vivo During Infection by Ebola and Marburg Viruses. Laboratory Investigation. 2000 Feb;80(2):171–86.

336. Gupta M, Mahanty S, Ahmed R, Rollin PE. Monocyte-Derived Human Macrophages and Peripheral Blood Mononuclear Cells Infected with Ebola Virus Secrete MIP-1α and TNF-α and Inhibit Poly-IC-Induced IFN-α in Vitro. Virology. 2001 May 25;284(1):20–5.

337. Ströher U, West E, Bugany H, Klenk HD, Schnittler HJ, Feldmann H. Infection and Activation of Monocytes by Marburg and Ebola Viruses. J Virol. 2001 Nov 15;75(22):11025–33.

338. Hensley LE, Young HA, Jahrling PB, Geisbert TW. Proinflammatory response during Ebola virus infection of primate models: possible involvement of the tumor necrosis factor receptor superfamily. Immunology Letters. 2002 Mar 1;80(3):169–79.

339. Gupta M, Spiropoulou C, Rollin PE. Ebola virus infection of human PBMCs causes massive death of macrophages, CD4 and CD8 T cell sub-populations in vitro. Virology. 2007 Jul 20;364(1):45–54.

340. Geisbert TW, Young HA, Jahrling PB, Davis KJ, Kagan E, Hensley LE. Mechanisms Underlying Coagulation Abnormalities in Ebola Hemorrhagic Fever: Overexpression of Tissue Factor in Primate Monocytes/Macrophages Is a Key Event. J INFECT DIS. 2003 Dec;188(11):1618–29.

341. Bosio CM, Aman MJ, Grogan C, Hogan R, Ruthel G, Negley D, et al. Ebola and Marburg Viruses Replicate in Monocyte-Derived Dendritic Cells without

Inducing the Production of Cytokines and Full Maturation. J INFECT DIS. 2003 Dec;188(11):1630–8.

342. Mahanty S, Hutchinson K, Agarwal S, Mcrae M, Rollin PE, Pulendran B. Cutting Edge: Impairment of Dendritic Cells and Adaptive Immunity by Ebola and Lassa Viruses. J Immunol. 2003 Mar 15;170(6):2797–801.

343. McElroy AK, Harmon JR, Flietstra TD, Campbell S, Mehta AK, Kraft CS, et al. Kinetic Analysis of Biomarkers in a Cohort of US Patients With Ebola Virus Disease. Clin Infect Dis. 2016 Aug 15;63(4):460–7.

344. Lanini S, Portella G, Vairo F, Kobinger GP, Pesenti A, Langer M, et al. Relationship Between Viremia and Specific Organ Damage in Ebola Patients: A Cohort Study. Clinical Infectious Diseases. 2018 Jan 6;66(1):36–44.

345. Liu X, Speranza E, Muñoz-Fontela C, Haldenby S, Rickett NY, Garcia-Dorival I, et al. Transcriptomic signatures differentiate survival from fatal outcomes in humans infected with Ebola virus. Genome Biol [Internet]. 2017 Jan 19 [cited 2019 Jan 25];18. Available from: https://www.ncbi.nlm.nih.gov/pmc/articles/PMC5244546/

346. Feldmann H, Geisbert TW. Ebola haemorrhagic fever. Lancet. 2011 Mar 5;377(9768):849–62.

347. Cimini E, Viola D, Cabeza-Cabrerizo M, Romanelli A, Tumino N, Sacchi A, et al. Different features of Vδ2 T and NK cells in fatal and non-fatal human Ebola infections. PLOS Neglected Tropical Diseases. 2017 May 30;11(5):e0005645.

348. Ellis DS, Simpson IH, Francis DP, Knobloch J, Bowen ET, Lolik P, et al. Ultrastructure of Ebola virus particles in human liver. Journal of Clinical Pathology. 1978 Mar 1;31(3):201–8.

349. Hunt L, Gupta-Wright A, Simms V, Tamba F, Knott V, Tamba K, et al. Clinical presentation, biochemical, and haematological parameters and their association with outcome in patients with Ebola virus disease: an observational cohort study. Lancet Infect Dis. 2015 Nov;15(11):1292–9.

350. Vernet MA, Reynard S, Fizet A, Schaeffer J, Pannetier D, Guedj J, et al. Clinical, virological, and biological parameters associated with outcomes of Ebola virus infection in Macenta, Guinea. JCI Insight. 2017 Mar;2(6):e88864.

351. Kash JC, Mühlberger E, Carter V, Grosch M, Perwitasari O, Proll SC, et al. Global Suppression of the Host Antiviral Response by Ebola- and Marburgviruses: Increased Antagonism of the Type I Interferon Response Is Associated with Enhanced Virulence. Journal of Virology. 2006 Mar 15;80(6):3009–20.

352. Kindrachuk J, Wahl-Jensen V, Safronetz D, Trost B, Hoenen T, Arsenault R, et al. Ebola Virus Modulates Transforming Growth Factor β Signaling and Cellular Markers of Mesenchyme-Like Transition in Hepatocytes. J Virol. 2014 Sep;88(17):9877–92.

353. Petrosillo N, Nicastri E, Lanini S, Capobianchi MR, Di Caro A, Antonini M, et al. Ebola virus disease complicated with viral interstitial pneumonia: a case report. BMC Infect Dis. 2015 Oct 16;15:432.

354. Chughtai AA, Barnes M, Macintyre CR. Persistence of Ebola virus in various body fluids during convalescence: evidence and implications for disease transmission and control. Epidemiol Infect. 2016 Jun;144(8):1652–60.

355. Reisler RB, Zeng X, Schellhase CW, Bearss JJ, Warren TK, Trefry JC, et al. Ebola Virus Causes Intestinal Tract Architectural Disruption and Bacterial Invasion in Non-Human Primates. Viruses. 2018 Sep 20;10(10):513.

356. Cournac JM, Karkowski L, Bordes J, Aletti M, Duron S, Janvier F, et al. Rhabdomyolysis in Ebola Virus Disease. Results of an Observational Study in a Treatment Center in Guinea. Clinical Infectious Diseases. 2016 Jan 1;62(1):19–23.

357. Larsen T, Stevens EL, Davis KJ, Geisbert JB, Daddario-DiCaprio KM, Jahrling PB, et al. Pathologic Findings Associated with Delayed Death in Nonhuman Primates Experimentally Infected with Zaire Ebola Virus. The Journal of Infectious Diseases. 2007 Nov 15;196(Supplement_2):S323–8.

358. Twenhafel NA, Mattix ME, Johnson JC, Robinson CG, Pratt WD, Cashman KA, et al. Pathology of Experimental Aerosol Zaire Ebolavirus Infection in Rhesus Macaques. Vet Pathol. 2013 May 1;50(3):514–29.

359. Jankeel A, Menicucci AR, Woolsey C, Fenton KA, Mendoza N, Versteeg K, et al. Early Transcriptional Changes within Liver, Adrenal Gland, and Lymphoid Tissues Significantly Contribute to Ebola Virus Pathogenesis in Cynomolgus Macaques. J Virol. 2020 May 18;94(11):e00250-20.

360. Bradfute SB, Warfield KL, Bavari S. Functional CD8+ T cell responses in lethal Ebola virus infection. J Immunol. 2008 Mar 15;180(6):4058–66.

361. Baize S, Leroy EM, Georges-Courbot MC, Capron M, Lansoud-Soukate J, Debré P, et al. Defective humoral responses and extensive intravascular apoptosis are associated with fatal outcome in Ebola virus-infected patients. Nature Medicine. 1999 Apr;5(4):423–6.

362. Ksiazek TG, Rollin PE, Williams AJ, Bressler DS, Martin ML, Swanepoel R, et al. Clinical virology of Ebola hemorrhagic fever (EHF): virus, virus antigen, and IgG and IgM antibody findings among EHF patients in Kikwit, Democratic Republic of the Congo, 1995. J Infect Dis. 1999 Feb;179 Suppl 1:S177-187.

363. McElroy AK, Akondy RS, Davis CW, Ellebedy AH, Mehta AK, Kraft CS, et al. Human Ebola virus infection results in substantial immune activation. Proc Natl Acad Sci U S A. 2015 Apr 14;112(15):4719–24.

364. Rimoin AW, Lu K, Bramble MS, Steffen I, Doshi RH, Hoff NA, et al. Ebola Virus Neutralizing Antibodies Detectable in Survivors of theYambuku, Zaire Outbreak 40 Years after Infection. The Journal of Infectious Diseases. 2018 Jan 4;217(2):223–31.

365. Bornholdt ZA, Turner HL, Murin CD, Li W, Sok D, Souders CA, et al. Isolation of potent neutralizing antibodies from a survivor of the 2014 Ebola virus outbreak. Science. 2016 Mar 4;351(6277):1078–83.

366. Warfield KL, Howell KA, Vu H, Geisbert J, Wong G, Shulenin S, et al. Role of Antibodies in Protection Against Ebola Virus in Nonhuman Primates

Immunized With Three Vaccine Platforms. The Journal of Infectious Diseases. 2018 Nov 22;218(suppl_5):S553–64.

367. Rijal P, Elias SC, Machado SR, Xiao J, Schimanski L, O'Dowd V, et al. Therapeutic Monoclonal Antibodies for Ebola Virus Infection Derived from Vaccinated Humans. Cell Reports. 2019 Apr 2;27(1):172-186.e7.

368. Fuentes S, Ravichandran S, Coyle EM, Klenow L, Khurana S. Human Antibody Repertoire following Ebola Virus Infection and Vaccination. iScience. 2020 Mar 27;23(3):100920.

369. Saphire EO, Schendel SL, Gunn BM, Milligan JC, Alter G. Antibody-mediated protection against Ebola virus. Nat Immunol. 2018 Nov;19(11):1169–78.

370. Agrati C, Castilletti C, Casetti R, Sacchi A, Falasca L, Turchi F, et al. Longitudinal characterization of dysfunctional T cell-activation during human acute Ebola infection. Cell Death & Disease. 2016 Mar;7(3):e2164–e2164.

371. Ruibal P, Oestereich L, Lüdtke A, Becker-Ziaja B, Wozniak DM, Kerber R, et al. Unique human immune signature of Ebola virus disease in Guinea. Nature. 2016 May;533(7601):100–4.

372. Thom R, Tipton T, Strecker T, Hall Y, Akoi Bore J, Maes P, et al. Longitudinal antibody and T cell responses in Ebola virus disease survivors and contacts: an observational cohort study. The Lancet Infectious Diseases. 2021 Apr;21(4):507–16.

373. Williams KJN, Qiu X, Fernando L, Jones SM, Alimonti JB. VSVΔG/EBOV GP-induced innate protection enhances natural killer cell activity to increase survival in a lethal mouse adapted Ebola virus infection. Viral Immunol. 2015 Feb;28(1):51–61.

374. Sanchez A, Lukwiya M, Bausch D, Mahanty S, Sanchez AJ, Wagoner KD, et al. Analysis of Human Peripheral Blood Samples from Fatal and Nonfatal Cases of Ebola (Sudan) Hemorrhagic Fever: Cellular Responses, Virus Load, and Nitric Oxide Levels. Journal of Virology [Internet]. 2004 Oct 1 [cited 2022 Feb

7]; Available from: https://journals.asm.org/doi/abs/10.1128/JVI.78.19.10370-10377.2004

375. Wauquier N, Becquart P, Padilla C, Baize S, Leroy EM. Human Fatal Zaire Ebola Virus Infection Is Associated with an Aberrant Innate Immunity and with Massive Lymphocyte Apoptosis. PLOS Neglected Tropical Diseases. 2010 Oct 5;4(10):e837.

376. Wagstaffe HR, Clutterbuck EA, Bockstal V, Stoop JN, Luhn K, Douoguih M, et al. Ebola virus glycoprotein stimulates IL-18–dependent natural killer cell responses. J Clin Invest. 2020 Jul 1;130(7):3936–46.

377. Fausther-Bovendo H, Qiu X, He S, Bello A, Audet J, Ippolito G, et al. NK Cells Accumulate in Infected Tissues and Contribute to Pathogenicity of Ebola Virus in Mice. Journal of Virology [Internet]. 2019 May 15 [cited 2020 Aug 20];93(10). Available from: https://jvi.asm.org/content/93/10/e01703-18

378. Rubins KH, Hensley LE, Wahl-Jensen V, Daddario DiCaprio KM, Young HA, Reed DS, et al. The temporal program of peripheral blood gene expression in the response of nonhuman primates to Ebola hemorrhagic fever. Genome Biol. 2007;8(8):R174.

379. Colavita F, Biava M, Castilletti C, Lanini S, Miccio R, Portella G, et al. Inflammatory and Humoral Immune Response during Ebola Virus Infection in Survivor and Fatal Cases Occurred in Sierra Leone during the 2014–2016 Outbreak in West Africa. Viruses [Internet]. 2019 Apr [cited 2022 Apr 9];11(4). Available from: https://www.ncbi.nlm.nih.gov/pmc/articles/PMC6520887/

380. Dye JM, Herbert AS, Kuehne AI, Barth JF, Muhammad MA, Zak SE, et al. Postexposure antibody prophylaxis protects nonhuman primates from filovirus disease. Proc Natl Acad Sci U S A. 2012 Mar 27;109(13):5034–9.

381. Lee JE, Fusco ML, Hessell AJ, Oswald WB, Burton DR, Saphire EO. Structure of the Ebola virus glycoprotein bound to an antibody from a human survivor. Nature. 2008 Jul 10;454(7201):177–82.

382. Parren PWHI, Geisbert TW, Maruyama T, Jahrling PB, Burton DR. Pre- and Postexposure Prophylaxis of Ebola Virus Infection in an Animal Model by Passive Transfer of a Neutralizing Human Antibody. Journal of Virology. 2002 Jun 15;76(12):6408–12.

383. Oswald WB, Geisbert TW, Davis KJ, Geisbert JB, Sullivan NJ, Jahrling PB, et al. Neutralizing antibody fails to impact the course of Ebola virus infection in monkeys. PLoS Pathog. 2007 Jan;3(1):e9.

384. Qiu X, Fernando L, Melito PL, Audet J, Feldmann H, Kobinger G, et al. Ebola GP-specific monoclonal antibodies protect mice and guinea pigs from lethal Ebola virus infection. PLoS Negl Trop Dis. 2012;6(3):e1575.

385. Qiu X, Audet J, Wong G, Pillet S, Bello A, Cabral T, et al. Successful treatment of ebola virus-infected cynomolgus macaques with monoclonal antibodies. Sci Transl Med. 2012 Jun 13;4(138):138ra81.

386. Olinger GG, Pettitt J, Kim D, Working C, Bohorov O, Bratcher B, et al. Delayed treatment of Ebola virus infection with plant-derived monoclonal antibodies provides protection in rhesus macaques. Proc Natl Acad Sci U S A. 2012 Oct 30;109(44):18030–5.

387. Pettitt J, Zeitlin L, Kim DH, Working C, Johnson JC, Bohorov O, et al. Therapeutic Intervention of Ebola Virus Infection in Rhesus Macaques with the MB-003 Monoclonal Antibody Cocktail. Science Translational Medicine. 2013 Aug 21;5(199):199ra113-199ra113.

388. Qiu X, Wong G, Audet J, Bello A, Fernando L, Alimonti JB, et al. Reversion of advanced Ebola virus disease in nonhuman primates with ZMapp. Nature. 2014 Oct 2;514(7520):47–53.

389. PREVAIL II Writing Group, Multi-National PREVAIL II Study Team, Davey RT, Dodd L, Proschan MA, Neaton J, et al. A Randomized, Controlled Trial of ZMapp for Ebola Virus Infection. N Engl J Med. 2016 Oct 13;375(15):1448–56.

390. Centers for Disease Control and Prevention. Treatment | Ebola (Ebola Virus Disease) | CDC [Internet]. 2021 [cited 2021 Mar 17]. Available from: https://www.cdc.gov/vhf/ebola/treatment/index.html

391. Regeneron Pharmaceuticals. Inmazeb™ (atoltivimab, maftivimab and odesivimab-ebgn) Injection [Internet]. 2020 [cited 2022 Mar 12]. Available from: https://www.inmazeb.com

392. Clinical Trials Arena. Ebanga (ansuvimab-zykl) for the Treatment of Zaire Ebolavirus Infection [Internet]. Clinical Trials Arena. 2021 [cited 2022 Mar 12]. Available from: https://www.clinicaltrialsarena.com/projects/ebanga-ansuvimab-zykl/

393. Liu J, Trefry JC, Babka AM, Schellhase CW, Coffin KM, Williams JA, et al. Ebola virus persistence and disease recrudescence in the brains of antibody-treated nonhuman primate survivors. Science Translational Medicine. 2022;14(631):eabi5229.

394. Marzi A, Engelmann F, Feldmann F, Haberthur K, Shupert WL, Brining D, et al. Antibodies are necessary for rVSV/ZEBOV-GP–mediated protection against lethal Ebola virus challenge in nonhuman primates. Proc Natl Acad Sci U S A. 2013 Jan 29;110(5):1893–8.

395. Jones SM, Ströher U, Fernando L, Qiu X, Alimonti J, Melito P, et al. Assessment of a Vesicular Stomatitis Virus-Based Vaccine by Use of the Mouse Model of Ebola Virus Hemorrhagic Fever. J Infect Dis. 2007 Nov 15;196(Supplement_2):S404–12.

396. Lai L, Davey R, Beck A, Xu Y, Suffredini AF, Palmore T, et al. Emergency postexposure vaccination with vesicular stomatitis virus-vectored Ebola vaccine after needlestick. JAMA. 2015 Mar 24;313(12):1249–55.

397. Davis C, Tipton T, Sabir S, Aitken C, Bennett S, Becker S, et al. Postexposure Prophylaxis With rVSV-ZEBOV Following Exposure to a Patient With Ebola Virus Disease Relapse in the United Kingdom: An Operational, Safety, and

Immunogenicity Report. Clinical Infectious Diseases. 2020 Dec 1;71(11):2872–9.

398. Henao-Restrepo AM, Camacho A, Longini IM, Watson CH, Edmunds WJ, Egger M, et al. Efficacy and effectiveness of an rVSV-vectored vaccine in preventing Ebola virus disease: final results from the Guinea ring vaccination, open-label, cluster-randomised trial (Ebola Ça Suffit!). The Lancet. 2017 Feb 4;389(10068):505–18.

399. Metzger WG, Vivas-Martínez S. Questionable efficacy of the rVSV-ZEBOV Ebola vaccine. The Lancet. 2018 Mar 17;391(10125):1021.

400. Ishola D, Manno D, Afolabi MO, Keshinro B, Bockstal V, Rogers B, et al. Safety and long-term immunogenicity of the two-dose heterologous Ad26.ZEBOV and MVA-BN-Filo Ebola vaccine regimen in adults in Sierra Leone: a combined open-label, non-randomised stage 1, and a randomised, double-blind, controlled stage 2 trial. The Lancet Infectious Diseases. 2022 Jan 1;22(1):97–109.

401. Afolabi MO, Ishola D, Manno D, Keshinro B, Bockstal V, Rogers B, et al. Safety and immunogenicity of the two-dose heterologous Ad26.ZEBOV and MVA-BN-Filo Ebola vaccine regimen in children in Sierra Leone: a randomised, double-blind, controlled trial. The Lancet Infectious Diseases. 2022 Jan 1;22(1):110–22.

402. Takada A, Watanabe S, Okazaki K, Kida H, Kawaoka Y. Infectivity-Enhancing Antibodies to Ebola Virus Glycoprotein. Journal of Virology. 2001 Mar 1;75(5):2324–30.

403. Takada A, Feldmann H, Ksiazek TG, Kawaoka Y. Antibody-Dependent Enhancement of Ebola Virus Infection. J Virol. 2003 Jul;77(13):7539–44.

404. Takada A, Ebihara H, Feldmann H, Geisbert TW, Kawaoka Y. Epitopes Required for Antibody-Dependent Enhancement of Ebola Virus Infection. J Infect Dis. 2007 Nov 15;196(Supplement_2):S347–56.

405. Li F, Freed DC, Tang A, Rustandi RR, Troutman MC, Espeseth AS, et al. Complement enhances in vitro neutralizing potency of antibodies to human cytomegalovirus glycoprotein B (gB) and immune sera induced by gB/MF59 vaccination. NPJ Vaccines [Internet]. 2017 Dec 14 [cited 2019 Nov 23];2. Available from: https://www.ncbi.nlm.nih.gov/pmc/articles/PMC5730571/

406. Golden JW, Shoemaker CJ, Lindquist ME, Zeng X, Daye SP, Williams JA, et al. GP38-targeting monoclonal antibodies protect adult mice against lethal Crimean-Congo hemorrhagic fever virus infection. Science Advances. 2019 Jul 1;5(7):eaaw9535.

407. Wilson JA, Hevey M, Bakken R, Guest S, Bray M, Schmaljohn AL, et al. Epitopes Involved in Antibody-Mediated Protection from Ebola Virus. Science. 2000 Mar 3;287(5458):1664–6.

408. Bartholomew RM, Esser AF. Differences in Activation of Human and Guinea Pig Complement by Retroviruses. The Journal of Immunology. 1978 Nov 1;121(5):1748–51.

409. van der Zee JS, Beuvery EC, van Ree R, Aalberse RC. Human IgM antibodies do not activate guinea-pig complement after interaction with soluble antigen. Molecular Immunology. 1986 Jun 1;23(6):669–73.

410. Collins C, Tsui FWL, Shulman MJ. Differential activation of human and guinea pig complement by pentameric and hexameric IgM. Eur J Immunol. 2002 Jun;32(6):1802–10.

411. Davis CW, Jackson KJL, McElroy AK, Halfmann P, Huang J, Chennareddy C, et al. Longitudinal Analysis of the Human B Cell Response to Ebola Virus Infection. Cell. 2019 30;177(6):1566-1582.e17.

412. Michelow IC, Lear C, Scully C, Prugar LI, Longley CB, Yantosca LM, et al. High-Dose Mannose-Binding Lectin Therapy for Ebola Virus Infection. J Infect Dis. 2011 Jan 15;203(2):175–9.

413. Escudero-Pérez B, Volchkova VA, Dolnik O, Lawrence P, Volchkov VE. Shed GP of Ebola Virus Triggers Immune Activation and Increased Vascular Permeability. PLOS Pathogens. 2014 Nov 20;10(11):e1004509.

414. Kuzmina NA, Younan P, Gilchuk P, Santos RI, Flyak AI, Ilinykh PA, et al. Antibody-Dependent Enhancement of Ebola Virus Infection by Human Antibodies Isolated from Survivors. Cell Reports. 2018 Aug 14;24(7):1802-1815.e5.

415. Fehr AR, Perlman S. Coronaviruses: An Overview of Their Replication and Pathogenesis. Coronaviruses. 2015 Feb 12;1282:1–23.

416. Naqvi AAT, Fatima K, Mohammad T, Fatima U, Singh IK, Singh A, et al. Insights into SARS-CoV-2 genome, structure, evolution, pathogenesis and therapies: Structural genomics approach. Biochim Biophys Acta Mol Basis Dis. 2020 Oct 1;1866(10):165878.

417. V'kovski P, Kratzel A, Steiner S, Stalder H, Thiel V. Coronavirus biology and replication: implications for SARS-CoV-2. Nat Rev Microbiol. 2021 Mar;19(3):155–70.

418. Tang T, Bidon M, Jaimes JA, Whittaker GR, Daniel S. Coronavirus membrane fusion mechanism offers a potential target for antiviral development. Antiviral Res. 2020 Jun;178:104792.

419. Knyazev E, Nersisyan S, Tonevitsky A. Endocytosis and Transcytosis of SARS-CoV-2 Across the Intestinal Epithelium and Other Tissue Barriers. Frontiers in Immunology [Internet]. 2021 [cited 2022 Apr 10];12. Available from: https://www.frontiersin.org/article/10.3389/fimmu.2021.636966

420. Tyrrell DAJ, Bynoe ML. Cultivation of a Novel Type of Common-cold Virus in Organ Cultures. Br Med J. 1965 Jun 5;1(5448):1467–70.

421. Bradburne AF, Bynoe ML, Tyrrell DA. Effects of a "new" human respiratory virus in volunteers. Br Med J. 1967 Sep 23;3(5568):767–9.

422. Jean A, Quach C, Yung A, Semret M. Severity and outcome associated with human coronavirus OC43 infections among children. Pediatr Infect Dis J. 2013 Apr;32(4):325–9.

423. Woo PCY, Lau SKP, Chu C ming, Chan K hung, Tsoi H wah, Huang Y, et al. Characterization and Complete Genome Sequence of a Novel Coronavirus, Coronavirus HKU1, from Patients with Pneumonia. Journal of Virology. 2005 Jan 15;79(2):884–95.

424. Sechan F, Grobben M, Edridge AWD, Jebbink MF, Loens K, Ieven M, et al. Atypical Antibody Dynamics During Human Coronavirus HKU1 Infections. Frontiers in Microbiology [Internet]. 2022 [cited 2022 Jul 29];13. Available from: https://www.frontiersin.org/articles/10.3389/fmicb.2022.853410

425. Cherry JamesD. The chronology of the 2002–2003 SARS mini pandemic. Paediatr Respir Rev. 2004 Dec;5(4):262–9.

426. Cherry JD, Krogstad P. SARS: The First Pandemic of the 21st Century. Pediatr Res. 2004 Jul;56(1):1–5.

427. World Health Organization. Severe acute respiratory syndrome (SARS) [Internet]. 2004 [cited 2022 Jan 25]. Available from: https://www.who.int/publications-detail-redirect/severe-acute-respiratory-syndrome-(sars)-executive-board-113

428. Guan Y, Zheng BJ, He YQ, Liu XL, Zhuang ZX, Cheung CL, et al. Isolation and Characterization of Viruses Related to the SARS Coronavirus from Animals in Southern China. Science [Internet]. 2003 Oct 10 [cited 2022 Jan 27]; Available from: https://www.science.org/doi/abs/10.1126/science.1087139

429. Wu D, Tu C, Xin C, Xuan H, Meng Q, Liu Y, et al. Civets are equally susceptible to experimental infection by two different severe acute respiratory syndrome coronavirus isolates. J Virol. 2005 Feb;79(4):2620–5.

430. Tu C, Crameri G, Kong X, Chen J, Sun Y, Yu M, et al. Antibodies to SARS Coronavirus in Civets. Emerg Infect Dis. 2004 Dec;10(12):2244–8.

431. World Health Organization. Summary of probable SARS cases with onset of illness from 1 November 2002 to 31 July 2003 [Internet]. 2015 [cited 2022 Jan 27]. Available from: https://www.who.int/publications/m/item/summary-of-probable-sars-cases-with-onset-of-illness-from-1-november-2002-to-31-july-2003

432. Centers for Disease Control and Prevention. CDC SARS Response Timeline | About | CDC [Internet]. 2021 [cited 2022 Jan 27]. Available from: https://www.cdc.gov/about/history/sars/timeline.htm

433. CDC. About MERS [Internet]. Centers for Disease Control and Prevention. 2019 [cited 2022 Mar 7]. Available from: https://www.cdc.gov/coronavirus/mers/about/index.html

434. European Centre for Disease Prevention and Control. MERS-CoV worldwide overview [Internet]. European Centre for Disease Prevention and Control. 2022 [cited 2022 Mar 7]. Available from: https://www.ecdc.europa.eu/en/middle-east-respiratory-syndrome-coronavirus-mers-cov-situation-update

435. World Health Organization. Middle East respiratory syndrome coronavirus (MERS-CoV) [Internet]. 2022 [cited 2022 Mar 7]. Available from: https://www.who.int/westernpacific/health-topics/middle-east-respiratory-syndrome-coronavirus-mers

436. Al-Omari A, Rabaan AA, Salih S, Al-Tawfiq JA, Memish ZA. MERS coronavirus outbreak: Implications for emerging viral infections. Diagn Microbiol Infect Dis. 2019 Mar;93(3):265–85.

437. Valencia DN. Brief Review on COVID-19: The 2020 Pandemic Caused by SARS-CoV-2. Cureus [Internet]. 2020 Mar 24 [cited 2021 Jan 7];12(3). Available from: https://www.ncbi.nlm.nih.gov/pmc/articles/PMC7179986/

438. World Health Organization. WHO Coronavirus (COVID-19) Dashboard [Internet]. 2022 [cited 2022 Mar 17]. Available from: https://covid19.who.int

439. Zhou P, Yang XL, Wang XG, Hu B, Zhang L, Zhang W, et al. A pneumonia outbreak associated with a new coronavirus of probable bat origin. Nature. 2020 Mar;579(7798):270–3.

440. Holmes EC, Goldstein SA, Rasmussen AL, Robertson DL, Crits-Christoph A, Wertheim JO, et al. The origins of SARS-CoV-2: A critical review. Cell. 2021 Sep 16;184(19):4848–56.

441. Shahhosseini N, Wong G, Kobinger GP, Chinikar S. SARS-CoV-2 spillover transmission due to recombination event. Gene Reports. 2021 Jun 1;23:101045.

442. Wang MY, Zhao R, Gao LJ, Gao XF, Wang DP, Cao JM. SARS-CoV-2: Structure, Biology, and Structure-Based Therapeutics Development. Frontiers in Cellular and Infection Microbiology [Internet]. 2020 [cited 2022 Feb 28];10. Available from: https://www.frontiersin.org/article/10.3389/fcimb.2020.587269

443. Schoeman D, Fielding BC. Coronavirus envelope protein: current knowledge. Virology Journal. 2019 May 27;16(1):69.

444. Bestle D, Heindl MR, Limburg H, Van TVL, Pilgram O, Moulton H, et al. TMPRSS2 and furin are both essential for proteolytic activation of SARS-CoV-2 in human airway cells. Life Science Alliance [Internet]. 2020 Sep 1 [cited 2022 Mar 17];3(9). Available from: https://www.life-science-alliance.org/content/3/9/e202000786

445. Mandala VS, McKay MJ, Shcherbakov AA, Dregni AJ, Kolocouris A, Hong M. Structure and drug binding of the SARS-CoV-2 envelope protein transmembrane domain in lipid bilayers. Nat Struct Mol Biol. 2020 Dec;27(12):1202–8.

446. Boson B, Legros V, Zhou B, Siret E, Mathieu C, Cosset FL, et al. The SARS-CoV-2 envelope and membrane proteins modulate maturation and retention of the spike protein, allowing assembly of virus-like particles. Journal of Biological Chemistry. 2021 Jan 1;296:100111.

447. Sui L, Zhao Y, Wang W, Wu P, Wang Z, Yu Y, et al. SARS-CoV-2 Membrane Protein Inhibits Type I Interferon Production Through Ubiquitin-Mediated Degradation of TBK1. Frontiers in Immunology [Internet]. 2021 [cited 2022 Feb 28];12. Available from: https://www.frontiersin.org/article/10.3389/fimmu.2021.662989

448. McBride R, van Zyl M, Fielding BC. The Coronavirus Nucleocapsid Is a Multifunctional Protein. Viruses. 2014 Aug 7;6(8):2991–3018.

449. Carlson CR, Asfaha JB, Ghent CM, Howard CJ, Hartooni N, Safari M, et al. Phosphoregulation of Phase Separation by the SARS-CoV-2 N Protein Suggests a Biophysical Basis for its Dual Functions. Molecular Cell. 2020 Dec 17;80(6):1092-1103.e4.

450. Yang M, He S, Chen X, Huang Z, Zhou Z, Zhou Z, et al. Structural Insight Into the SARS-CoV-2 Nucleocapsid Protein C-Terminal Domain Reveals a Novel Recognition Mechanism for Viral Transcriptional Regulatory Sequences. Frontiers in Chemistry [Internet]. 2021 [cited 2022 Mar 17];8. Available from: https://www.frontiersin.org/article/10.3389/fchem.2020.624765

451. CDC. Coronavirus Disease 2019 (COVID-19) – Symptoms [Internet]. Centers for Disease Control and Prevention. 2021 [cited 2022 Feb 14]. Available from: https://www.cdc.gov/coronavirus/2019-ncov/symptoms-testing/symptoms.html

452. CDC. Omicron Variant: What You Need to Know [Internet]. Centers for Disease Control and Prevention. 2022 [cited 2022 Feb 14]. Available from: https://www.cdc.gov/coronavirus/2019-ncov/variants/omicron-variant.html

453. Jeffery-Smith A, Rowland TAJ, Patel M, Whitaker H, Iyanger N, Williams SV, et al. Reinfection with new variants of SARS-CoV-2 after natural infection: a prospective observational cohort in 13 care homes in England. The Lancet Healthy Longevity. 2021 Dec 1;2(12):e811–9.

454. Davis HE, Assaf GS, McCorkell L, Wei H, Low RJ, Re'em Y, et al. Characterizing long COVID in an international cohort: 7 months of symptoms and their

impact. eClinicalMedicine [Internet]. 2021 Aug 1 [cited 2022 Feb 14];38. Available from: https://www.thelancet.com/journals/eclinm/article/PIIS2589-5370(21)00299-6/fulltext

455. Crook H, Raza S, Nowell J, Young M, Edison P. Long covid-mechanisms, risk factors, and management. BMJ. 2021 Jul 26;374:n1648.

456. Berlin DA, Gulick RM, Martinez FJ. Severe Covid-19. New England Journal of Medicine. 2020 Dec 17;383(25):2451–60.

457. Zhu N, Wang W, Liu Z, Liang C, Wang W, Ye F, et al. Morphogenesis and cytopathic effect of SARS-CoV-2 infection in human airway epithelial cells. Nat Commun. 2020 Aug 6;11(1):3910.

458. Ravindra NG, Alfajaro MM, Gasque V, Huston NC, Wan H, Szigeti-Buck K, et al. Single-cell longitudinal analysis of SARS-CoV-2 infection in human airway epithelium identifies target cells, alterations in gene expression, and cell state changes. PLOS Biology. 2021 Mar 17;19(3):e3001143.

459. Fiege JK, Thiede JM, Nanda HA, Matchett WE, Moore PJ, Montanari NR, et al. Single cell resolution of SARS-CoV-2 tropism, antiviral responses, and susceptibility to therapies in primary human airway epithelium. PLOS Pathogens. 2021 Jan 28;17(1):e1009292.

460. Chua RL, Lukassen S, Trump S, Hennig BP, Wendisch D, Pott F, et al. COVID-19 severity correlates with airway epithelium–immune cell interactions identified by single-cell analysis. Nat Biotechnol. 2020 Aug;38(8):970–9.

461. Mulay A, Konda B, Garcia G, Yao C, Beil S, Villalba JM, et al. SARS-CoV-2 infection of primary human lung epithelium for COVID-19 modeling and drug discovery. Cell Reports. 2021 May;35(5):109055.

462. Bridges JP, Vladar EK, Huang H, Mason RJ. Respiratory epithelial cell responses to SARS-CoV-2 in COVID-19. Thorax. 2022 Feb 1;77(2):203–9.

463. Zhang H, Kang Z, Gong H, Xu D, Wang J, Li Z, et al. Digestive system is a potential route of COVID-19: an analysis of single-cell coexpression pattern of key proteins in viral entry process. Gut. 2020 Jun 1;69(6):1010–8.

464. Lamers MM, Beumer J, van der Vaart J, Knoops K, Puschhof J, Breugem TI, et al. SARS-CoV-2 productively infects human gut enterocytes. Science. 2020 Jul 3;369(6499):50–4.

465. Lehmann M, Allers K, Heldt C, Meinhardt J, Schmidt F, Rodriguez-Sillke Y, et al. Human small intestinal infection by SARS-CoV-2 is characterized by a mucosal infiltration with activated CD8+ T cells. Mucosal Immunol. 2021 Nov;14(6):1381–92.

466. Chen L, Li X, Chen M, Feng Y, Xiong C. The ACE2 expression in human heart indicates new potential mechanism of heart injury among patients infected with SARS-CoV-2. Cardiovascular Research. 2020 May 1;116(6):1097–100.

467. Sakamoto A, Kawakami R, Kawai K, Gianatti A, Pellegrini D, Kutys R, et al. ACE2 (Angiotensin-Converting Enzyme 2) and TMPRSS2 (Transmembrane Serine Protease 2) Expression and Localization of SARS-CoV-2 Infection in the Human Heart. Arteriosclerosis, Thrombosis, and Vascular Biology. 2021 Jan;41(1):542–4.

468. Monteil V, Kwon H, Prado P, Hagelkrüys A, Wimmer RA, Stahl M, et al. Inhibition of SARS-CoV-2 Infections in Engineered Human Tissues Using Clinical-Grade Soluble Human ACE2. Cell. 2020 May 14;181(4):905-913.e7.

469. Jansen J, Reimer KC, Nagai JS, Varghese FS, Overheul GJ, de Beer M, et al. SARS-CoV-2 infects the human kidney and drives fibrosis in kidney organoids. Cell Stem Cell. 2022 Feb 3;29(2):217-231.e8.

470. Jing Y, Run-Qian L, Hao-Ran W, Hao-Ran C, Ya-Bin L, Yang G, et al. Potential influence of COVID-19/ACE2 on the female reproductive system. Molecular Human Reproduction. 2020 Jun 1;26(6):367–73.

471. Huang Y, Yang C, Xu X feng, Xu W, Liu S wen. Structural and functional properties of SARS-CoV-2 spike protein: potential antivirus drug development for COVID-19. Acta Pharmacol Sin. 2020 Sep;41(9):1141–9.

472. da Costa VG, Moreli ML, Saivish MV. The emergence of SARS, MERS and novel SARS-2 coronaviruses in the 21st century. Arch Virol. 2020 Apr 22;1–10.

473. Petersen OH, Gerasimenko OV, Gerasimenko JV. Endocytic uptake of SARS-CoV-2: the critical roles of pH, Ca2+, and NAADP. Function [Internet]. 2020 Jan 1 [cited 2021 Jan 8];1(1). Available from: https://academic.oup.com/function/article/1/1/zqaa003/5851680

474. Dan JM, Mateus J, Kato Y, Hastie KM, Yu ED, Faliti CE, et al. Immunological memory to SARS-CoV-2 assessed for up to 8 months after infection. Science. 2021 Feb 5;371(6529):eabf4063.

475. Doria-Rose N, Suthar MS, Makowski M, O'Connell S, McDermott AB, Flach B, et al. Antibody Persistence through 6 Months after the Second Dose of mRNA-1273 Vaccine for Covid-19. N Engl J Med. 2021 Jun 10;384(23):2259–61.

476. Earle KA, Ambrosino DM, Fiore-Gartland A, Goldblatt D, Gilbert PB, Siber GR, et al. Evidence for antibody as a protective correlate for COVID-19 vaccines. Vaccine. 2021 Jul 22;39(32):4423–8.

477. Feng S, Phillips DJ, White T, Sayal H, Aley PK, Bibi S, et al. Correlates of protection against symptomatic and asymptomatic SARS-CoV-2 infection. Nat Med. 2021 Nov;27(11):2032–40.

478. Hansen CH, Michlmayr D, Gubbels SM, Mølbak K, Ethelberg S. Assessment of protection against reinfection with SARS-CoV-2 among 4 million PCR-tested individuals in Denmark in 2020: a population-level observational study. The Lancet. 2021 Mar 27;397(10280):1204–12.

479. Khoury DS, Cromer D, Reynaldi A, Schlub TE, Wheatley AK, Juno JA, et al. Neutralizing antibody levels are highly predictive of immune protection from symptomatic SARS-CoV-2 infection. Nat Med. 2021 Jul;27(7):1205–11.

480. Pilz S, Chakeri A, Ioannidis JP, Richter L, Theiler-Schwetz V, Trummer C, et al. SARS-CoV-2 re-infection risk in Austria. Eur J Clin Invest. 2021 Apr;51(4):e13520.

481. Dimeglio C, Herin F, Martin-Blondel G, Miedougé M, Izopet J. Antibody titers and protection against a SARS-CoV-2 infection. Journal of Infection. 2022 Feb 1;84(2):248–88.

482. Finch E, Lowe R, Fischinger S, Aubin M de S, Siddiqui SM, Dayal D, et al. SARS-CoV-2 antibodies protect against reinfection for at least 6 months in a multicentre seroepidemiological workplace cohort. PLOS Biology. 2022 Feb 10;20(2):e3001531.

483. Gilbert PB, Montefiori DC, McDermott AB, Fong Y, Benkeser D, Deng W, et al. Immune correlates analysis of the mRNA-1273 COVID-19 vaccine efficacy clinical trial. Science. 2022 Jan 7;375(6576):43–50.

484. Grifoni A, Weiskopf D, Ramirez SI, Mateus J, Dan JM, Moderbacher CR, et al. Targets of T Cell Responses to SARS-CoV-2 Coronavirus in Humans with COVID-19 Disease and Unexposed Individuals. Cell. 2020 Jun 25;181(7):1489-1501.e15.

485. Tan AT, Linster M, Tan CW, Le Bert N, Chia WN, Kunasegaran K, et al. Early induction of functional SARS-CoV-2-specific T cells associates with rapid viral clearance and mild disease in COVID-19 patients. Cell Reports. 2021 Feb 9;34(6):108728.

486. Le Bert N, Clapham HE, Tan AT, Chia WN, Tham CYL, Lim JM, et al. Highly functional virus-specific cellular immune response in asymptomatic SARS-CoV-2 infection. J Exp Med. 2021 May 3;218(5):e20202617.

487. Stephenson E, Reynolds G, Botting RA, Calero-Nieto FJ, Morgan MD, Tuong ZK, et al. Single-cell multi-omics analysis of the immune response in COVID-19. Nat Med. 2021 May;27(5):904–16.

488. Urra JM, Cabrera CM, Porras L, Ródenas I. Selective CD8 cell reduction by SARS-CoV-2 is associated with a worse prognosis and systemic inflammation in COVID-19 patients. Clin Immunol. 2020 Aug;217:108486.

489. Skelly DT, Harding AC, Gilbert-Jaramillo J, Knight ML, Longet S, Brown A, et al. Two doses of SARS-CoV-2 vaccination induce robust immune responses to emerging SARS-CoV-2 variants of concern. Nat Commun. 2021 Aug 17;12(1):5061.

490. Kurtovic L, Beeson JG. Complement Factors in COVID-19 Therapeutics and Vaccines. Trends Immunol [Internet]. 2020 Dec 13 [cited 2021 Jan 12]; Available from: https://www.ncbi.nlm.nih.gov/pmc/articles/PMC7733687/

491. Li L, Chen C. Contribution of acute-phase reaction proteins to the diagnosis and treatment of 2019 novel coronavirus disease (COVID-19). Epidemiol Infect. 2020 Jul 27;148:e164.

492. Fang S, Wang H, Lu L, Jia Y, Xia Z. Decreased complement C3 levels are associated with poor prognosis in patients with COVID-19: A retrospective cohort study. Int Immunopharmacol. 2020 Dec;89(Pt A):107070.

493. Zhao Y, Nie HX, Hu K, Wu XJ, Zhang YT, Wang MM, et al. Abnormal immunity of non-survivors with COVID-19: predictors for mortality. Infect Dis Poverty. 2020 Aug 3;9(1):108.

494. Prendecki M, Clarke C, Medjeral-Thomas N, McAdoo SP, Sandhu E, Peters JE, et al. Temporal changes in complement activation in haemodialysis patients with COVID-19 as a predictor of disease progression. Clin Kidney J. 2020 Oct;13(5):889–96.

495. de Nooijer AH, Grondman I, Janssen NAF, Netea MG, Willems L, van de Veerdonk FL, et al. Complement Activation in the Disease Course of

Coronavirus Disease 2019 and Its Effects on Clinical Outcomes. J Infect Dis. 2021 Feb 3;223(2):214–24.

496. Busch MH, Timmermans SAMEG, Nagy M, Visser M, Huckriede J, Aendekerk JP, et al. Neutrophils and Contact Activation of Coagulation as Potential Drivers of COVID-19. Circulation. 2020 Nov 3;142(18):1787–90.

497. Cugno M, Meroni PL, Gualtierotti R, Griffini S, Grovetti E, Torri A, et al. Complement activation and endothelial perturbation parallel COVID-19 severity and activity. J Autoimmun. 2021 Jan;116:102560.

498. Magro C, Mulvey JJ, Berlin D, Nuovo G, Salvatore S, Harp J, et al. Complement associated microvascular injury and thrombosis in the pathogenesis of severe COVID-19 infection: A report of five cases. Transl Res. 2020 Jun;220:1–13.

499. Ma L, Sahu SK, Cano M, Kuppuswamy V, Bajwa J, McPhatter J, et al. Increased complement activation is a distinctive feature of severe SARS-CoV-2 infection. Science Immunology. 2021 May 13;6(59):eabh2259.

500. Charitos P, Heijnen IAFM, Egli A, Bassetti S, Trendelenburg M, Osthoff M. Functional Activity of the Complement System in Hospitalized COVID-19 Patients: A Prospective Cohort Study. Frontiers in Immunology [Internet]. 2021 [cited 2022 Mar 11];12. Available from: https://www.frontiersin.org/article/10.3389/fimmu.2021.765330

501. Sinkovits G, Mező B, Réti M, Müller V, Iványi Z, Gál J, et al. Complement Overactivation and Consumption Predicts In-Hospital Mortality in SARS-CoV-2 Infection. Frontiers in Immunology [Internet]. 2021 [cited 2022 Mar 12];12. Available from: https://www.frontiersin.org/article/10.3389/fimmu.2021.663187

502. Ramlall V, Thangaraj PM, Meydan C, Foox J, Butler D, Kim J, et al. Immune complement and coagulation dysfunction in adverse outcomes of SARS-CoV-2 infection. Nat Med. 2020;26(10):1609–15.

503. Jarlhelt I, Nielsen SK, Jahn CXH, Hansen CB, Pérez-Alós L, Rosbjerg A, et al. SARS-CoV-2 Antibodies Mediate Complement and Cellular Driven Inflammation. Frontiers in Immunology [Internet]. 2021 [cited 2022 Mar 12];12. Available from: https://www.frontiersin.org/article/10.3389/fimmu.2021.767981

504. Barrett JR, Belij-Rammerstorfer S, Dold C, Ewer KJ, Folegatti PM, Gilbride C, et al. Phase 1/2 trial of SARS-CoV-2 vaccine ChAdOx1 nCoV-19 with a booster dose induces multifunctional antibody responses. Nature Medicine. 2020 Dec 17;27(2):1–10.

505. Ali YM, Ferrari M, Lynch NJ, Yaseen S, Dudler T, Gragerov S, et al. Lectin Pathway Mediates Complement Activation by SARS-CoV-2 Proteins. Frontiers in Immunology [Internet]. 2021 [cited 2022 Mar 12];12. Available from: https://www.frontiersin.org/article/10.3389/fimmu.2021.714511

506. Yu J, Yuan X, Chen H, Chaturvedi S, Braunstein EM, Brodsky RA. Direct activation of the alternative complement pathway by SARS-CoV-2 spike proteins is blocked by factor D inhibition. Blood. 2020 Oct 29;136(18):2080–9.

507. Moore MS, Reichard JD, Murtha TD, Zahedi B, Fallier RM, Kunz TH. Specific Alterations in Complement Protein Activity of Little Brown Myotis (Myotis lucifugus) Hibernating in White-Nose Syndrome Affected Sites. PLOS ONE. 2011 Nov 30;6(11):e27430.

508. Rainard P. The complement in milk and defense of the bovine mammary gland against infections. Vet Res. 2003 Oct;34(5):647–70.

509. Isogai E, Kamewaka Y, Isogai H, Kimura K, Fujii N, Nishikawa T. Complement-mediated killing of Borrelia garinii--bactericidal activity of wild deer serum. Microbiol Immunol. 1994;38(9):753–6.

510. Khoa DVA, Wimmers K. Genetic Association of the Porcine C9 Complement Component with Hemolytic Complement Activity. Asian-Australas J Anim Sci. 2015 Sep;28(9):1354–61.

511. Lewis LA, Vu DM, Granoff DM, Ram S. Inhibition of the Alternative Pathway of Nonhuman Infant Complement by Porin B2 Contributes to Virulence of Neisseria meningitidis in the Infant Rat Model. Infection and Immunity. 2014 Jun 1;82(6):2574–84.

512. Sumiya M, Tabona P, Arai T, Summerfield JA, Super M, Levinsky RJ, et al. Molecular basis of opsonic defect in immunodeficient children. The Lancet. 1991 Jun 29;337(8757):1569–70.

513. Madsen HO, Garred P, Kurtzhals JAL, Lamm LU, Ryder LP, Thiel S, et al. A new frequent allele is the missing link in the structural polymorphism of the human mannan-binding protein. Immunogenetics. 1994 Jan 1;40(1):37–44.

514. Madsen HO, Garred P, Thiel S, Kurtzhals JA, Lamm LU, Ryder LP, et al. Interplay between promoter and structural gene variants control basal serum level of mannan-binding protein. The Journal of Immunology. 1995 Sep 15;155(6):3013–20.

515. Martens HA, Zuurman MW, de Lange AHM, Nolte IM, van der Steege G, Navis GJ, et al. Analysis of C1q polymorphisms suggests association with systemic lupus erythematosus, serum C1q and CH50 levels and disease severity. Ann Rheum Dis. 2009 May;68(5):715–20.

516. Lipscombe RJ, Sumiya M, Hill AVS, Lau YL, Levinsky RJ, Summerfield JA, et al. High frequencies in African and non-African populations of independent mutations in the mannose binding protein gene. Human Molecular Genetics. 1992 Dec 1;1(9):709–15.

517. Pieczarka C, Andrade FA, Catarino SJ, Lidani KCF, Bavia L, Tizzot R, et al. Ficolin-1 and ficolin-3 polymorphisms and susceptibility to rheumatoid arthritis. Autoimmunity. 2020 Nov;53(7):400–7.

518. Stravalaci M, Pagani I, Paraboschi EM, Pedotti M, Doni A, Scavello F, et al. Recognition and inhibition of SARS-CoV-2 by humoral innate immunity pattern recognition molecules. Nat Immunol. 2022 Feb;23(2):275–86.

519. McElroy AK, Erickson BR, Flietstra TD, Rollin PE, Nichol ST, Towner JS, et al. Ebola Hemorrhagic Fever: Novel Biomarker Correlates of Clinical Outcome. The Journal of Infectious Diseases. 2014 Aug 15;210(4):558–66.

520. Baize S, Leroy EM, Georges AJ, Georges-Courbot MC, Capron M, Bedjabaga I, et al. Inflammatory responses in Ebola virus-infected patients. Clinical and Experimental Immunology. 2002 Apr 1;128(1):163–8.

521. Alexander F, Brunt E, Humphries H, Cavell B, Leung S, Allen L, et al. Generation of a Universal Human Complement Source by Large-Scale Depletion of IgG and IgM from Pooled Human Plasma. Methods Mol Biol. 2022;2414:341–62.

522. Tipton TRW, Hall Y, Bore JA, White A, Sibley LS, Sarfas C, et al. Characterisation of the T-cell response to Ebola virus glycoprotein amongst survivors of the 2013–16 West Africa epidemic. Nat Commun. 2021 Feb 19;12(1):1153.

523. Kalia N, Singh J, Sharma S, Arora H, Kaur M. Genetic and Phenotypic Screening of Mannose-Binding Lectin in Relation to Risk of Recurrent Vulvovaginal Infections in Women of North India: A Prospective Cohort Study. Front Microbiol. 2017 Jan 31;8.

524. Chow SC, Wang H, Shao J. Sample Size Calculations in Clinical Research. 2nd ed. New York: Chapman and Hall/CRC; 2007. 480 p.

525. Ma B, Zhang K, Hendrie C, Liang C, Li M, Doherty-Kirby A, et al. PEAKS: powerful software for peptide de novo sequencing by tandem mass spectrometry. Rapid Commun Mass Spectrom. 2003;17(20):2337–42.

526. Aljabr W, Armstrong S, Rickett NY, Pollakis G, Touzelet O, Cloutman-Green E, et al. High Resolution Analysis of Respiratory Syncytial Virus Infection In Vivo. Viruses. 2019 Oct 10;11(10):926.

527. Wickham H, Averick M, Bryan J, Chang W, McGowan LD, François R, et al. Welcome to the Tidyverse. Journal of Open Source Software. 2019 Nov 21;4(43):1686.

528. Wickham H, Bryan J, attribution) Rs (Copyright holder of all R code and all C code without explicit copyright, code) MK (Author of included R, code) KV (Author of included libxls, code) CL (Author of included libxls, et al. readxl: Read Excel Files [Internet]. 2022 [cited 2022 May 2]. Available from: https://CRAN.R-project.org/package=readxl

529. Lê S, Josse J, Husson F. FactoMineR: An R Package for Multivariate Analysis. Journal of Statistical Software. 2008 Mar 18;25:1–18.

530. Kassambara A, Mundt F. factoextra: Extract and Visualize the Results of Multivariate Data Analyses [Internet]. 2020 [cited 2022 May 2]. Available from: https://CRAN.R-project.org/package=factoextra

531. Maechler M, original) PR (Fortran, original) AS (S, original) MH (S, Hornik [trl K, maintenance(1999-2000)) ctb] (port to R, et al. cluster: "Finding Groups in Data": Cluster Analysis Extended Rousseeuw et al. [Internet]. 2022 [cited 2022 May 2]. Available from: https://CRAN.R-project.org/package=cluster

532. Leth-Larsen R, Zhong F, Chow VTK, Holmskov U, Lu J. The SARS coronavirus spike glycoprotein is selectively recognized by lung surfactant protein D and activates macrophages. Immunobiology. 2007;212(3):201–11.

533. Gupta A, Gupta GS. Status of mannose-binding lectin (MBL) and complement system in COVID-19 patients and therapeutic applications of antiviral plant MBLs. Mol Cell Biochem. 2021;476(8):2917–42.

534. Viodé A, Smolen KK, Fatou B, Wurie Z, Van Zalm P, Konde MK, et al. Plasma Proteomic Analysis Distinguishes Severity Outcomes of Human Ebola Virus Disease. mBio. 2022;0(0):e00567-22.

535. Albariño CG, Wiggleton Guerrero L, Lo MK, Nichol ST, Towner JS. Development of a reverse genetics system to generate a recombinant Ebola virus Makona expressing a green fluorescent protein. Virology. 2015 Oct 1;484:259–64.

536. Pitti T, Chen CT, Lin HN, Choong WK, Hsu WL, Sung TY. N-GlyDE: a two-stage N-linked glycosylation site prediction incorporating gapped dipeptides and pattern-based encoding. Sci Rep. 2019 Nov 4;9(1):15975.

537. Wang B, Wang Y, Frabutt DA, Zhang X, Yao X, Hu D, et al. Mechanistic understanding of N-glycosylation in Ebola virus glycoprotein maturation and function. J Biol Chem. 2017 Apr 7;292(14):5860–70.

538. Reily C, Stewart TJ, Renfrow MB, Novak J. Glycosylation in health and disease. Nat Rev Nephrol. 2019 Jun;15(6):346–66.

539. Zheng J, Yamada Y, Fung TS, Huang M, Chia R, Liu DX. Identification of N-linked glycosylation sites in the spike protein and their functional impact on the replication and infectivity of coronavirus infectious bronchitis virus in cell culture. Virology. 2018 Jan 1;513:65–74.

540. Zhao P, Praissman JL, Grant OC, Cai Y, Xiao T, Rosenbalm KE, et al. Virus-Receptor Interactions of Glycosylated SARS-CoV-2 Spike and Human ACE2 Receptor. Cell Host & Microbe. 2020 Oct 7;28(4):586-601.e6.

541. Bonomelli C, Doores KJ, Dunlop DC, Thaney V, Dwek RA, Burton DR, et al. The Glycan Shield of HIV Is Predominantly Oligomannose Independently of Production System or Viral Clade. PLoS One. 2011 Aug 16;6(8):e23521.

542. Mathys L, Balzarini J. Several N-Glycans on the HIV Envelope Glycoprotein gp120 Preferentially Locate Near Disulphide Bridges and Are Required for Efficient Infectivity and Virus Transmission. PLoS One. 2015 Jun 29;10(6):e0130621.

543. Croset A, Delafosse L, Gaudry JP, Arod C, Glez L, Losberger C, et al. Differences in the glycosylation of recombinant proteins expressed in HEK and CHO cells. Journal of Biotechnology. 2012 Oct 31;161(3):336–48.

544. Barnum SR, Bubeck D, Schein TN. Soluble Membrane Attack Complex: Biochemistry and Immunobiology. Frontiers in Immunology [Internet]. 2020 [cited 2022 Jul 29];11. Available from: https://www.frontiersin.org/articles/10.3389/fimmu.2020.585108

545. Menny A, Lukassen MV, Couves EC, Franc V, Heck AJR, Bubeck D. Structural basis of soluble membrane attack complex packaging for clearance. Nat Commun. 2021 Oct 19;12(1):6086.

546. Liu X, Speranza E, Muñoz-Fontela C, Haldenby S, Rickett NY, Garcia-Dorival I, et al. Transcriptomic signatures differentiate survival from fatal outcomes in humans infected with Ebola virus. Genome Biol [Internet]. 2017 Jan 19 [cited 2019 Jan 25];18. Available from: https://www.ncbi.nlm.nih.gov/pmc/articles/PMC5244546/

547. Reynard O, Reid StP, Page A, Mateo M, Alazard-Dany N, Raoul H, et al. Unconventional Secretion of Ebola Virus Matrix Protein VP40. J Infect Dis. 2011 Nov 1;204(Suppl 3):S833–9.

548. Hovingh ES, Broek B van den, Kuipers B, Pinelli E, Rooijakkers SHM, Jongerius I. Acquisition of C1 inhibitor by Bordetella pertussis virulence associated gene 8 results in C2 and C4 consumption away from the bacterial surface. PLOS Pathogens. 2017 Jul 24;13(7):e1006531.

549. Thiemmeca S, Tamdet C, Punyadee N, Prommool T, Songjaeng A, Noisakran S, et al. Secreted NS1 Protects Dengue Virus from Mannose-Binding Lectin-Mediated Neutralization. J Immunol. 2016 Nov 15;197(10):4053–65.

550. de La Vega MA, Wong G, Kobinger GP, Qiu X. The Multiple Roles of sGP in Ebola Pathogenesis. Viral Immunol. 2015 Feb 1;28(1):3–9.

551. Sanchez A, Trappier SG, Mahy BW, Peters CJ, Nichol ST. The virion glycoproteins of Ebola viruses are encoded in two reading frames and are expressed through transcriptional editing. Proc Natl Acad Sci U S A. 1996 Apr 16;93(8):3602–7.

552. Mohan GS, Li W, Ye L, Compans RW, Yang C. Antigenic subversion: a novel mechanism of host immune evasion by Ebola virus. PLoS Pathog. 2012;8(12):e1003065.

553. Markham A. REGN-EB3: First Approval. Drugs. 2021 Jan 11;1–4.

554. Garred P, Michaelsen TE, Aase A. The IgG subclass pattern of complement activation depends on epitope density and antibody and complement concentration. Scand J Immunol. 1989 Sep;30(3):379–82.

555. Michaelsen TE, Garred P, Aase A. Human IgG subclass pattern of inducing complement-mediated cytolysis depends on antigen concentration and to a lesser extent on epitope patchiness, antibody affinity and complement concentration. Eur J Immunol. 1991 Jan;21(1):11–6.

556. Diebolder CA, Beurskens FJ, Jong RN de, Koning RI, Strumane K, Lindorfer MA, et al. Complement Is Activated by IgG Hexamers Assembled at the Cell Surface. Science. 2014 Mar 14;343(6176):1260–3.

557. Bindon CI, Hale G, Brüggemann M, Waldmann H. Human monoclonal IgG isotypes differ in complement activating function at the level of C4 as well as C1q. J Exp Med. 1988 Jul 1;168(1):127–42.

558. Lilienthal GM, Rahmöller J, Petry J, Bartsch YC, Leliavski A, Ehlers M. Potential of Murine IgG1 and Human IgG4 to Inhibit the Classical Complement and Fcγ Receptor Activation Pathways. Front Immunol. 2018 May 9;9:958.

559. Gunn BM, Lu R, Slein MD, Ilinykh PA, Huang K, Atyeo C, et al. A Fc engineering approach to define functional humoral correlates of immunity against Ebola virus. Immunity. 2021 Apr 13;54(4):815-828.e5.

560. Takada A, Ebihara H, Jones S, Feldmann H, Kawaoka Y. Protective efficacy of neutralizing antibodies against Ebola virus infection. Vaccine. 2007 Jan 22;25(6):993–9.

561. Liu Q, Fan C, Li Q, Zhou S, Huang W, Wang L, et al. Antibody-dependent-cellular-cytotoxicity-inducing antibodies significantly affect the post-exposure treatment of Ebola virus infection. Sci Rep. 2017 Mar 30;7:45552.

562. Saphire EO, Schendel SL, Fusco ML, Gangavarapu K, Gunn BM, Wec AZ, et al. Systematic analysis of monoclonal antibodies against Ebola virus GP defines features that contribute to protection. Cell. 2018 Aug 9;174(4):938-952.e13.

563. Tomic A, Skelly DT, Ogbe A, O'Connor D, Pace M, Adland E, et al. Divergent trajectories of antiviral memory after SARS-CoV-2 infection. Nat Commun. 2022 Mar 10;13(1):1251.

564. Brown EP, Licht AF, Dugast AS, Choi I, Bailey-Kellogg C, Alter G, et al. High-throughput, multiplexed IgG subclassing of antigen-specific antibodies from clinical samples. J Immunol Methods. 2012 Dec 14;386(1–2):117–23.

565. Pallesen J, Murin CD, de Val N, Cottrell CA, Hastie KM, Turner HL, et al. Structures of Ebola virus GP and sGP in complex with therapeutic antibodies. Nat Microbiol. 2016 Aug 8;1(9):1–9.

566. Ebenbichler CF, Thielens NM, Vornhagen R, Marschang P, Arlaud GJ, Dierich MP. Human immunodeficiency virus type 1 activates the classical pathway of complement by direct C1 binding through specific sites in the transmembrane glycoprotein gp41. J Exp Med. 1991 Dec 1;174(6):1417–24.

567. Schiela B, Bernklau S, Malekshahi Z, Deutschmann D, Koske I, Banki Z, et al. Active Human Complement Reduces the Zika Virus Load via Formation of the Membrane-Attack Complex. Front Immunol [Internet]. 2018 [cited 2019 Apr 11];9. Available from: https://www.frontiersin.org/articles/10.3389/fimmu.2018.02177/full

568. Ksiazek TG, West CP, Rollin PE, Jahrling PB, Peters CJ. ELISA for the Detection of Antibodies to Ebola Viruses. The Journal of Infectious Diseases. 1999 Feb 1;179(Supplement_1):S192–8.

569. Liu Y, Sun Y, Wu W, Li Aq, Yang X, Zhang S, et al. Serological Investigation of Laboratory-Confirmed and Suspected Ebola Virus Disease Patients During the Late Phase of the Ebola Outbreak in Sierra Leone. Virol Sin. 2018 Jul 31;33(4):323–34.

570. Markiewski MM, Lambris JD. The Role of Complement in Inflammatory Diseases From Behind the Scenes into the Spotlight. Am J Pathol. 2007 Sep;171(3):715–27.

571. Huber M, Fischer M, Misselwitz B, Manrique A, Kuster H, Niederöst B, et al. Complement lysis activity in autologous plasma is associated with lower viral loads during the acute phase of HIV-1 infection. PLoS Med. 2006 Nov;3(11):e441.

572. Centers for Disease Control and Prevention. Ebola Virus Disease Distribution Map: Cases of Ebola Virus Disease in Africa Since 1976 [Internet]. 2021 [cited 2021 Oct 5]. Available from: https://www.cdc.gov/vhf/ebola/history/distribution-map.html

573. Deen GF, Broutet N, Xu W, Knust B, Sesay FR, McDonald SLR, et al. Ebola RNA Persistence in Semen of Ebola Virus Disease Survivors — Final Report [Internet]. https://doi.org/10.1056/NEJMoa1511410. Massachusetts Medical Society; 2015 [cited 2021 Oct 5]. Available from: https://www.nejm.org/doi/10.1056/NEJMoa1511410

574. Thorson AE, Deen GF, Bernstein KT, Liu WJ, Yamba F, Habib N, et al. Persistence of Ebola virus in semen among Ebola virus disease survivors in Sierra Leone: A cohort study of frequency, duration, and risk factors. PLoS Med. 2021 Feb;18(2):e1003273.

575. Bausch DG, Towner JS, Dowell SF, Kaducu F, Lukwiya M, Sanchez A, et al. Assessment of the Risk of Ebola Virus Transmission from Bodily Fluids and Fomites. The Journal of Infectious Diseases. 2007 Nov 15;196(Supplement_2):S142–7.

576. Tuck MK, Chan DW, Chia D, Godwin AK, Grizzle WE, Krueger KE, et al. Standard Operating Procedures for Serum and Plasma Collection: Early Detection Research Network Consensus Statement Standard Operating Procedure Integration Working Group. J Proteome Res. 2009 Jan;8(1):113–7.

577. Namekar M, Kumar M, O'Connell M, Nerurkar VR. Effect of Serum Heat-Inactivation and Dilution on Detection of Anti-WNV Antibodies in Mice by West Nile Virus E-protein Microsphere Immunoassay. PLoS One. 2012 Sep 25;7(9):e45851.

578. Pastorino B, Touret F, Gilles M, de Lamballerie X, Charrel RN. Heat Inactivation of Different Types of SARS-CoV-2 Samples: What Protocols for Biosafety, Molecular Detection and Serological Diagnostics? Viruses. 2020 Jul 7;12(7):735.

579. Bewley KR, Coombes NS, Gagnon L, McInroy L, Baker N, Shaik I, et al. Quantification of SARS-CoV-2 neutralizing antibody by wild-type plaque reduction neutralization, microneutralization and pseudotyped virus neutralization assays. Nat Protoc. 2021 Jun;16(6):3114–40.

580. Sotelo-Orozco J, Chen SY, Hertz-Picciotto I, Slupsky CM. A Comparison of Serum and Plasma Blood Collection Tubes for the Integration of Epidemiological and Metabolomics Data. Frontiers in Molecular Biosciences. 2021;8:650.

581. Hsieh MH, Beirag N, Murugaiah V, Chou YC, Kuo WS, Kao HF, et al. Human Surfactant Protein D Binds Spike Protein and Acts as an Entry Inhibitor of SARS-CoV-2 Pseudotyped Viral Particles. Front Immunol. 2021;12:641360.

582. Mercado NB, Zahn R, Wegmann F, Loos C, Chandrashekar A, Yu J, et al. Single-shot Ad26 vaccine protects against SARS-CoV-2 in rhesus macaques. Nature. 2020 Oct;586(7830):583–8.

583. Yu J, Tostanoski LH, Peter L, Mercado NB, McMahan K, Mahrokhian SH, et al. DNA vaccine protection against SARS-CoV-2 in rhesus macaques. Science. 2020 Aug 14;369(6505):806–11.

584. Risitano AM, Mastellos DC, Huber-Lang M, Yancopoulou D, Garlanda C, Ciceri F, et al. Complement as a target in COVID-19? Nat Rev Immunol. 2020 Apr 23;1–2.

585. Kearns P, Siebert S, Willicombe M, Gaskell C, Kirkham A, Pirrie S, et al. Examining the Immunological Effects of COVID-19 Vaccination in Patients with Conditions Potentially Leading to Diminished Immune Response Capacity – The OCTAVE Trial [Internet]. Rochester, NY: Social Science

Research Network; 2021 Aug [cited 2022 May 18]. Report No.: 3910058. Available from: https://papers.ssrn.com/abstract=3910058

586. Caly L, Druce J, Roberts J, Bond K, Tran T, Kostecki R, et al. Isolation and rapid sharing of the 2019 novel coronavirus (SARS-CoV-2) from the first patient diagnosed with COVID-19 in Australia. Medical Journal of Australia. 2020;212(10):459–62.

587. Agnandji ST, Huttner A, Zinser ME, Njuguna P, Dahlke C, Fernandes JF, et al. Phase 1 Trials of rVSV Ebola Vaccine in Africa and Europe. N Engl J Med. 2016 Apr 28;374(17):1647–60.

588. Dowall SD, Callan J, Zeltina A, Al-Abdulla I, Strecker T, Fehling SK, et al. Development of a Cost-effective Ovine Polyclonal Antibody-Based Product, EBOTAb, to Treat Ebola Virus Infection. J Infect Dis. 2016 Apr 1;213(7):1124–33.

589. Mellors J, Tipton T, Fehling SK, Akoi Bore J, Koundouno FR, Hall Y, et al. Complement-Mediated Neutralisation Identified in Ebola Virus Disease Survivor Plasma: Implications for Protection and Pathogenesis. Frontiers in Immunology [Internet]. 2022 [cited 2022 Apr 14];13. Available from: https://www.frontiersin.org/article/10.3389/fimmu.2022.857481

590. Sharma R, Sharma S. Physiology, Blood Volume. In: StatPearls [Internet]. Treasure Island (FL): StatPearls Publishing; 2022 [cited 2022 May 19]. Available from: http://www.ncbi.nlm.nih.gov/books/NBK526077/

591. Dean MM, Minchinton RM, Heatley S, Eisen DP. Mannose binding lectin acute phase activity in patients with severe infection. J Clin Immunol. 2005 Jul;25(4):346–52.

592. Park BK, Kim D, Park S, Maharjan S, Kim J, Choi JK, et al. Differential Signaling and Virus Production in Calu-3 Cells and Vero Cells upon SARS-CoV-2 Infection. Biomol Ther (Seoul). 2021 May 1;29(3):273–81.

593. Rørvig S, Honore C, Larsson LI, Ohlsson S, Pedersen CC, Jacobsen LC, et al. Ficolin-1 is present in a highly mobilizable subset of human neutrophil

granules and associates with the cell surface after stimulation with fMLP. J Leukoc Biol. 2009 Dec;86(6):1439–49.

594. Zhang J, Yang L, Ang Z, Yoong SL, Tran TTT, Anand GS, et al. Secreted M-Ficolin Anchors onto Monocyte Transmembrane G Protein-Coupled Receptor 43 and Cross Talks with Plasma C-Reactive Protein to Mediate Immune Signaling and Regulate Host Defense. The Journal of Immunology. 2010 Dec 1;185(11):6899–910.